TUNNELLING IN ROCK
WITH ROCKBOLTS AND SHOTCRETE

By

Chikaosa TANIMOTO

Department of Civil Engineering
Kyoto University
Kyoto, Japan
October, 1980

TUNNELLING IN ROCK
WITH ROCKBOLTS AND SHOTCRETE

By

Chikaosa TANIMOTO

Department of Civil Engineering
Kyoto University
Kyoto, Japan
October, 1980

SUMMARY

This dissertation is devoted to investigation of rational tunnelling method with rockbolts and shotcrete, based on fundamentals of rock mechanics through numerical simulations, theoretical analyses, laboratory tests and field measurement.

No two tunnels are alike as to driving conditions, therefore the details of procedure will vary to meet each different situation. In recognition of these varying conditions, this dissertation gives several variations of fundamental procedure, such as ground support and blasting.

Rockbolts and shotcrete have great advantages in construction, for without any alternation of construction procedure and sectional area to be excavated they can supply flexible confinement effect to rock if deformation of tunnels is monitored adequately.

The face has an important role as a temporary support. The rock mass near the face is stabilized by the half-dome action in the profile and the ring action in the cross section. When advancing the face, it is required to place the artificial support to substitute for the half-dome action within the span length from the face so as to mobilize the bearing capacity of the rock mass as fully as possible. The interaction between rock and support is analyzed theoretically, numerically and practically through laboratory experiment, computation and field measurement specially from the point of view standing on construction engineering.

The fundamental behavior of rock in the vicinity of mining face is confirmed clearly in the both of theory and practice. By replacing the effect of rockbolting and shotcreting by equivalent inner pressure acting onto the wall, when the allowable plastic strain is determined, fundamental concept of tunnel support is proposed with the consideration on the advance of the face, and practical indication is suggested by carrying out laboratory test and field measurement.

In most of cases blasting is quite essential for the excavation of rock, but practice is too empirical to be controlled from the engineering side. In the dissertation, dynamic strength of rock, propagation behavior of stress wave generated blasting are clarified experimentally and numerically, and the result can be reflected to construction planning and method.

Finite Element Method is very powerful tool for the author to analize rock with uncertainty in tunnelling. By employing Gauss–Seidel iteration successive over relaxation factor, computation is executed so good even to three-dimensional problem with several thousands nodal points.

The application of the author's proposal to tunnel design is quite acceptable to practical field, and some actual behaviors of tunnels under difficult conditions can be simulated in accordance with the concept given by the author.

ACKNOWLEDGEMENT

The author wishes to express his sincere gratitude to Professor Shojiro Hata of Kyoto University for constant encouragement and valuable suggestions during his research days at Department of Civil Engineering, Kyoto University and also for critical reading of the manuscript.

His special gratitude is extended to Dr. Ichiro Ito, Professor Emeritus of Kyoto University, Professors Makoto Terada and Koichi Sassa – Kyoto University, and Dr. D.F. Coates, Head of Canadian Mining Research Laboratory, Ottawa in completing the dissertation. He is further indebted to his colleagues of Professor Hata's laboratory for their profitable discussions, dedication in field measurements and daily research activities. He is also thankful for valuable discussions and hearty encouragement from Professors Shoichi Kobayashi, Toshihisa Adachi and Yuzo Ohnishi – Kyoto University; Professor Toshikazu Kawamoto – Nagoya University; Professor Shunsuke Sakurai – Kobe University; Professor Shunji Murai – Tokyo University; and Professor Ryoki Nakano – Gifu University.

Grateful acknowledgements are made to Drs. L. Müller, H. Habenichit and G. Sauer in Salzburg; Professor R.E. Goodman, University of California; Prof. E.J. Cording, University of Illinois; Dr. P. Egger, Lausanne Polytechnic; Messrs. K. Hama, A. Yokoyama, M. Ohtsuka and K. Kimura, Japan Railway Construction Authority; Messrs. H. Yoshimura and T. Katase, Japan National Railways; Mr. S. Nagatomo, Japan Highway Public Corporation; Mr. I. Kitamura, Japan Tunnelling Association; Drs. S. Kitahara and K. Fujita – Tokyo; Dr. Y. Iwasaki, Osaka Geotechnical Institute; Dr. M. Teramoto, Kansai Data Processing Centre; Messrs. T. Azuma and K. Yoshimura – Tokyo, for their stimulating discussions and constructive criticisms. Messrs. K. Tateyama, K. Kariya and A. Nishihara, graduate students of Kyoto University, are also thanked for their help in the calculations and drawings in the manuscript.

The author thanks Junko, his wife, for supporting his research life.

CONTENTS

Chapter 1

INTRODUCTION

1.1 General Remarks

In building structures, if we can say the esthetics of convex to a dam, a skyscraper, or a bridge, a 'tunnel' is expressed the esthetics of concave. Namely, removing some portion of underground intentionally means 'building' in tunnelling, and there exists no site which has the same condition. Each one is an 'art'.

Site investigations for most kinds of construction are restricted to relatively small areas at the earth's surface, and, allowing reasonable costs of construction, detailed investigations are not only feasible but indicated. In addition, excavation uncovers unforeseen conditions that can be appraised and, if undesirable, remedied before construction of the designed facility. In contrast, a tunnel is the designed facility, and, as construction proceeds, adjustments must be made and construction procedures modified to maintain and protect the opening, as anticipated or unanticipated rock conditions are encountered. Also, because of prohibitive costs, site investigations yielding the detailed quantitative information expected from site investigations of localized heavy structures commonly cannot be made, and recourse must be made to geological and geophysical investigations which, at best, yield predictions based on qualitative or semiquantitative empiricism and, perhaps, on information from always too few exploratory drill holes. Cost estimates for tunnels prior to construction, especially for long tunnels in regions of geological complexity, are made with great uncertainty because of inability exactly to assess underground conditions. It is not uncommon for an initial cost estimate to be greatly exceeded because of difficulties encountered in sections comprising only a small per cent of the total length of a tunnel.

It is the function of those who plan and design tunnels to make every reasonable effort based on geological, geophysical, and rock-mechanics studies to anticipate undesirable underground conditions and, if possible, to locate tunnels so as to avoid or at least minimize hazardous geological conditions that, from past experience, can be expected to create excessively high costs of tunneiiing.

The modern technology of underground excavation has reached an advanced stage of development in both theory and practice. Rock-mechanics investigations have provided a vast reservoir of knowledge concerning the behavior of rocks under stress, and this knowledge can be applied to the planning and design of tunnels to the extent that underground geological conditions can be predicted. Unfortunately, underground rock-mechanics studies can be made only after the excavation of a tunnel, and serve their most useful immediately practical purpose in determination of the kinds and amounts of supports and tunnel lining that should be installed to prevent

short term or long term structural failure of a tunnel.

The ability to anticipate underground geologic conditions is directly related to the simplicity of the geological conditions and the extent to which these conditions are known. For example, tunnels driven in a horizontally-layered massive, well-cemented, relatively unjointed sandstone, through a layer of coal, or through monolithic, relatively unfractured bodies of granite pose no special problems in design and preparation of cost estimates. In contrast, design and cost estimates for tunnels in geologically complex areas, where surface rock exposures may be few in number because of extensive cover, must be based to a large extent on intelligent guesswork, and the planning and design of such tunnels is skilled art rather than quantitative science. It is not surprising that one of the most comprehensive and authoritative treatises on tunnelling is entitled The Art of Tunnelling (Széchy, 1967). [1]

HISTORY OF TUNNELING ([1] – [5])

The beginnings of man's efforts to go underground by means of subterranean excavations are lost in the haze of antiquity, but there is abundant archeological evidence that in Europe Stone Age man sank shafts and drove tunnels to recover flint for the fabrication of sharp-edged implements such as knives, axes, arrowheads, and scrapers. Later, as an elementary knowledge of metallurgy was acquired by primitive people, possible for the first time in central Asia, underground mining became necessary to supply the increasing demands for metals and alloys in technologically and culturally advancing civilizations. Very early underground excavations for metal-bearing ores have been identified in Caucasia, between the Black and Caspian Seas, and date back to approximately 3500 B.C. From this center and others of unknown location and through ever-expanding communication and trade, knowledge of mining and metallurgical techniques spread in all directions throughout the civilized world.

Many tunnels were built in ancient times by the Babylonians, by the Aztecs and Incas in the search for precious metals, and by the peoples of India, Persia, and Egypt. The Romans, superb planners and engineers, built many tunnels, some connecting with still-standing aqueducts and others as integral parts of highway systems or military operations.

Stone Age man used very primitive tools in underground excavation. Particularly useful to him were picks made of deer antlers, flint axes, and hammers, and wedges made of bone and wood. The discovery of smelting and the production of metals and alloys, first bronze, and later iron and steel, provided materials for increasingly efficient rock excavation. However, even with metal tools and until the first underground use of explosives in the seventeenth and, especially in the eighteenth centuries, mining of hard rocks was a difficult challenge that could be overcome only by fire-setting. For hundreds and perhaps thousands of years underground workings in hard rocks, especially those containing few fractures and fissures, were advanced by building fires against rock faces to cause expansion and spalling. In some operations spalling of the heated rock was accelerated by dowsing it with water. The fractured rock was then sepa-

rated from the working face with picks, gads, and wedges.

Hand-in-hand with the increasing use of explosives, first "black powder" and later nitroglycerine and dynamite, steel tempering techniques were perfected and permitted efficient and economical hand-drilling of holes for explosives in the hardest of rocks. Near the middle of the nineteenth century steampowered piston drills, and, later, pneumatic percussion drills, powered by compressed air, made their appearance; and at about the same time, but with less than notable success, several tunnelling machines (moles) were invented and given field tests. Without exception, all of the early tunnelling machines were dismal failures, but the pneumatic rock drills proved their worth and have played a major role in the development of the modern technology of rock excavation. Again, after more than a century, tunnelling machines are being given increasing attention, and, because of many notable successes in rapid and economical driving of tunnels, must be considered as offering a reasonable and competitive alternative to driving tunnels by conventional methods employing pneumatic drills and explosives.

TUNNEL SUPPORTS AND LINING [1]

In mining operations where it is expected that tunnels and other underground workings eventually will be abandoned, no attempt is made to install permanent supports and lining in sections or incompetent rock except, perhaps, in major haulways. The main purpose of installing supports is to provide relatively short-term safety in the excavation. In contrast, in a tunnel that is built to serve a long-time function, such as a traffic tunnel or a water tunnel, efforts must be made during construction to ensure service that will not be interrupted by structural failure within the projected lifetime of the facility.

Until rather recent times many tunnels in incompetent rock were supported by heavy timber which subsequently were removed as masonry walls and arches built from carefully shaped blocks of rock were installed. Modern tunnelling makes full use of a variety of supports, such as steel beams and reinforced concrete, and very recently rockbolting and shotcreting have been employed reasonably.

ROCK PRESSURE [6]

The determination of the magnitude of rock pressure is one of the most intricate problems in engineering science. This complexity is due not only to the inherent difficulty of predicting the stress conditions (primary stresses) prevailing in the interior of the non-uniform rock mass, but also to the fact that in addition to the strength properties of the rock the magnitude of secondary pressures developing after excavation around the cavity is governed by a variety of factors, such as the size of the cavity, the method of its excavation, rigidity of its support and the length of the period during which the cavity is left unsupported.

Within any particular rock the pressures to which it was exposed during its history are best indicated by the pattern of folds, joints and fissures, but it would be extremely difficult to

determine how far these pressures are still latent. There is, in addition, a significant difference between the internal stress condition of rocks and soils. Soils – particularly gravel and sand – were deposited uninterruptedly and uniformly and this regular sedimentation and stratification was but rarely disturbed by external forces. (The probability of external disturbance increases with the age of the formation.) In soil mechanics only vertical stresses due to the weight of the overlying layers, and horizontal stresses resulting form lateral deformation – determined with the help of Poisson's number – are taken into consideration. According to Talobre this approach cannot be accepted in rock mechanics. At first a similar differentiation of internal stresses according to the orientation of layers would be unimaginable there. Yet even in this case groundwater conditions, settlement and plastic properties ought to be considered as these all tend to bring about an equalization between vertical and horizontal stresses. In rocks, similar effects need not be considered. In sedimentary limestones or in rocks crystallized from the molten state, for example, there are frequent indications from which the existence of an initial hydrostatic, rather than an oriented stress distribution may be concluded. The enormous changes produced by tectonic effects act in the same stress field. Tectonic effects act in a sense opposite to gravitational ones. The rock joints and fissures are seldom vertical and bear signs of the numerous changes which they have undergone in the course of time as a result of various external effects even within the same block of rock.

In soils, especially in clays, it may frequently be observed that lateral pressures do not develop in accordance with lateral deformations but undergo a gradual transition from this initial stage to hydrostatic stress conditions. This process is stimulated and aided by repeated seismic movements which contribute over a lengthy period to the equalization of stratification, fissuration and the effects of other irregularities.

In the hydrostatic state, however, the principal stresses are of equal magnitude and perpendicular to each other, i.e. shear stresses are zero. This assumption was made by Heim as early as 1878 for stress conditions prevailing at great depths. Tunnelling practice was unable to furnish even general support for this theory because of the wide variety of factors involved.

There is a further difference between rocks and soils, especially granular soils, in their stress-strain curves; those of the former being dependent on three variable, i.e. load and deformation and also time.

According to Terzaghi secondary rock pressure in general, should be understood as the weight of a rock mass of a certain height above the tunnel, which when left unsupported would gradually drop out of the roof, and the only consequence of installing no propping would be that this rock mass would fall into the cavity. Successive displacements would result in the gradual development of an irregular natural arch above the cavity without necessarily involving the complete collapse of the tunnel itself. Earth pressure, on the other hand, would denote the pressure exerted by cohesionless, or plastic masses on the tunnel supports, without any pressure relief which would – in the absence of supports – sooner or later completely fill the cavity leading to its complete dis-

appearance.

The magnitude of earth pressure is, in general, independent of the strength and installation time of the supporting structure and it is only its distribution which is affected by the deformation of the latter. The magnitude of rock pressures, on the other hand, is influenced decisively by the strength and time of installation of props. This is because the deformation following the excavation of the cavity in rock masses surrounding the tunnel is of a plastic nature and extends over a period of time. This period required for the final deformations and, thus, for the pressures to develop, generally increases with the plasticity of the rock and with the depth and dimensions of its cross-section. The magnitude of deformations and consequently that of stresses can, therefore, be limited by sufficiently strong propping installed at the proper time. It should be remembered, however, that the intensity of plastic pressures shows a tendency to decrease with increasing deformations. Furthermore the loads are carried both by the tunnelling and the surrounding rock and every attempt should be made to utilize this co-operation.

According to one of the authorities on tunnelling, Professor Ržiha, "The true art in tunnelling lies in the anticipation of the development of large rock pressures, which is far more effective than to find the means of resisting rock pressures which have already developed. This contrast is similar to that existing between mental work and physical labour." This remark holds however mainly for rock, whereas in soils with plastic deformation qualities, the acting pressure will be rather reduced by the yield of supports.

PRESENT STATUS OF TUNNELS IN JAPAN

Japan is composed of mainlands and other small islands with a large portion of mountainous area and difficult topographical conditions, and there is a increasing need for construction of railway and road tunnels to set up efficient transportation networks accordingly.

Fig. 1.1 shows geomorphological classification in Japan.

At the same time, it can not be overlooked the fact that the tunnelling structures are almost free from such the natural disasters as land slides, land falls or snow avalanches which are due to the severe meteorological, topographical and geological conditions, and are not vulnerable to earthquake.

Table 1.1 shows the present situations of various categories of tunnels under construction in Japan as of December 1979. Japan imports almost all the petroleums, and it is expected that the underground development would contribute to the energy savings. The future tunnel construction program includes 4,000 kilometers of railway tunnels, 7,000 kilometers of highway tunnels and 850 kilometers of subways. Sewage tunnels are being constructed at the annual rate of 100 kilometers.

The demand for tunnelling construction will be much more increased when the technical innovations are more developed concerning the rational design, cost and time reduction, improvement of working conditions, safety, and environmental preservation.

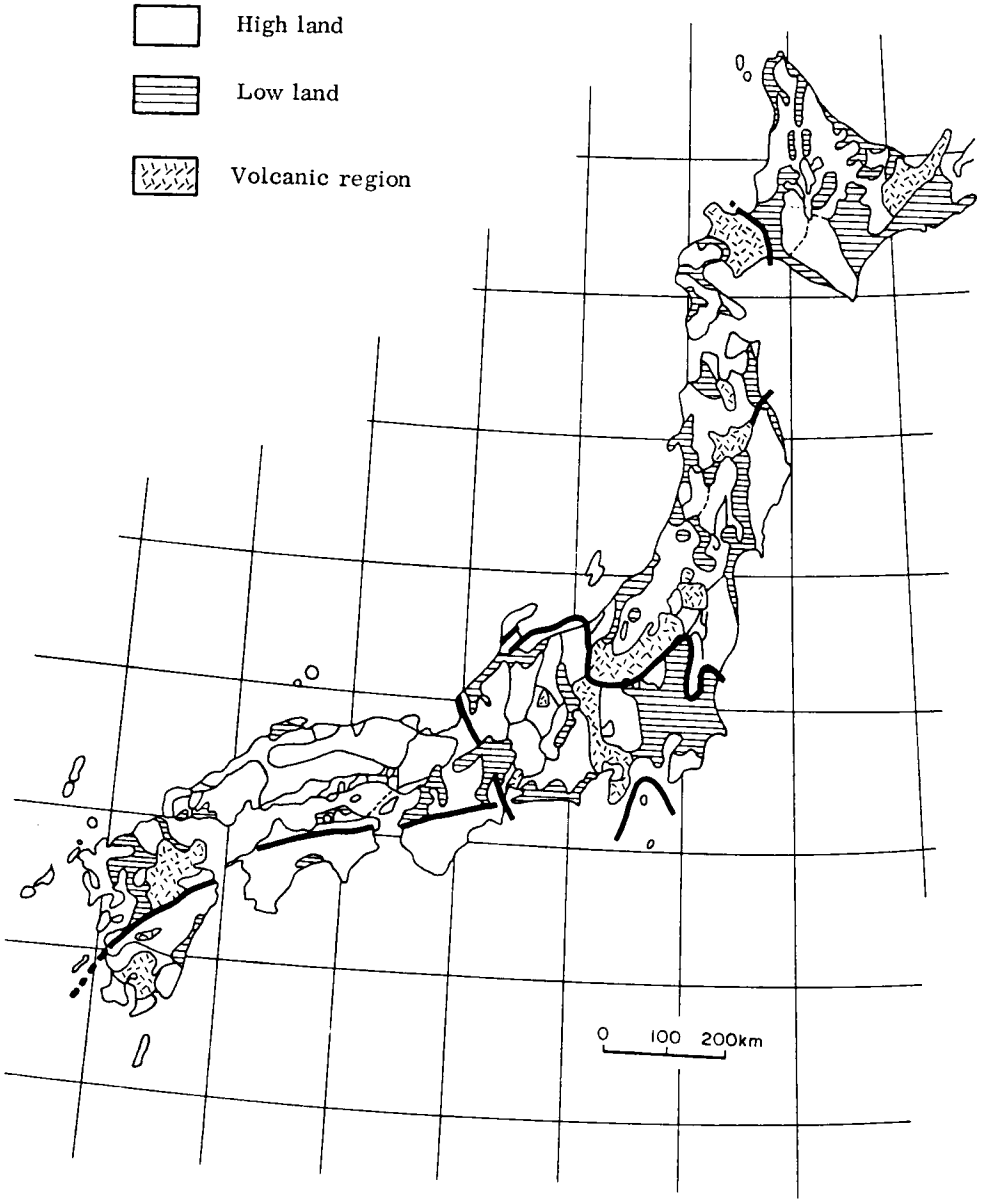

Fig. 1.1 Geomorphological Classification in Japan and Geomorphological Region (after M. Watanabe)

Table 1.1 The Tunnels Under Construction in December 1979

Classification	Number of Contractual Lots	Length (kilometer)	Cost (million Yen)
- RAILWAY TUNNEL	252	269.2	594,302
National Railway	115	211.0	239,302
Public Railway	130	54.4	347,461
Private Railway	7	3.8	7,539
- ROAD TUNNEL	256	211.7	334,140
- WATERWAY TUNNEL	1,085	862.1	794,582
Water Supply	79	74.7	71,732
Sewage	704	516.2	423,693
Hydroelectric Waterway	136	127.2	205,750
Dual Purpose Canal	166	144.0	93,407
- DUCT TUNNEL	100	48.7	93,216
- OTHERS	17	32.1	42,076
TOTAL	1,710	1,423.8	1,858,316

Note: Railway tunnel includes subway.

RECENT TOPICS ([7] – [19])

L. V. Rabcewicz presented his papers, entitled "New Austrian Tunnelling Method", on the Journals of Water Power (Nov. 1964–Jan. 1965) concerning his new concept of tunnelling. He explained the interaction between rock/earth pressure and lining support, and proposed that it is possible to support a tunnel economically with rockbolts and shotcrete by means of installing supports so as to mobilize a ring consisting of rock and support system. Hitherto, whatever it may be intentional or unintentional, tunnelers have been driving by utilizing natural rock arching around an opening, but there did not have been available so quantitative approach to designing tunnels with concrete consideration of rock arch effect before his proposal. His mechanical consideration on the relation between rock pressure and support reaction has been known widely. Then, he presented another paper to the same Journal, based on practical results, which pointed out the existence of minimum point for reaction of support on Pacher–Fenner characteristic curve when support system to be installed, including lining, has an appropriate stiffness to rock deformation. Additionally, the concrete designing method, regarding shotcrete and rockbolts, was presented on the same journal in March, 1973. About these papers, Y. Oka tried to explain the contents and what it meant in his way, based on the experimental results. Making it a turning point, many tunnel engineers have begun to watch the advantage of this method in Japan.

Without any usage of the expression of New Austrian Tunnelling Method (abbreviated "NATM"), rockbolting and shotcreting had drawn many engineers' attention for a long time. For example, the author can pick up the noticeable activities of tunnelling committee entrusted by Highway Research Institute, which gathered many informations regarding theories of tunnel statics, supporting methods (including above mentioned ones) and machineries.

As well as the discussion based on the informations, the members of the committee carried out several field measurements from their practical point of view. (The author also acted as one of managing staffs of the committee in 1970–1975.) Besides their activities, rockbolts were employed at several construction sites in Sanyo–Shinkansen Project between Okayama and Hakata, 60% of which was occupied by underground works. And also practical engineers and researchers carried out some tests for the investigation of rockbolting and shotcreting techniques.

However, the proposal by Rabcewicz, which developed only fundamentals of designing concept, could not satisfied increasing interest in the theory of NATM among practical designers, who are required to analyze the behavior of actual tunnels in detail numerically, and among practical engineers, who must determine the construction procedure and must confirm stability. It is well known that the actual behavior of rock has many unknown factors, and it is quite difficult to find out homogeneous rock without any discontinuity, which is typical assumption in ordinary calculation. The behavior of rock is much subjected to respective conditions specified by geological and tectonic condition, construction method, employed support system, capability of works etc. It is a common problem in rock engineering, and also it is one of reasons for the choice that empirical judgment is considered much reliable than analysis in tunnelling.

Nevertheless, so long as we try to get much reliable information through field measurement, laboratory tests, monitoring etc. than limited experiences in the past, NATM should be evaluated as more reasonable method than conventional method with steel ribs.

NATM can be defined the tunnelling method aiming at the objective of activating a supporting hollow-cylindrical structure within the surrounding mass of an underground excavation in rock or soil. To that purpose some principles are to be applied as follow:

- Taking into account of the geomechanical behavior of the underground,
- Avoidance of adverse states of stress and strain by the application of suitable supports at the due moment,
- Particularly by the closing of the sole vault in order to perform a statically efficient structure having the stability of a hollow-cylindrical support.
- Optimization of the means of supports in reference to the admissible deformation, as well as
- Supervising by measurement, also as an expedient for the control of the optimization

During the excavation works of an underground cavity the existing, primary state of equilibrium within the natural ground has to be transformed into a new, stable secondary equilibrium, at which the passage from the primary state to the secondary state is composed of an infinite succession of unstable intermediate states that are characterized by transitions of strains and stresses. The objective of NATM is the steering of these transformations as much as possible in an economical and technically safe manner. Therefore the proportioning of the deformations is aspired after becoming

a) on the one hand as small as possible, so that the underground will not suffer more or less of its primary strength as it is inevitable, and
b) on the other hand as large as it is indispensable, to activate the underground in forming a supporting hollow-cylinder and in optimizing the cost of supporting materials versus the cost of excavation.

Among many experienced tunnelers in other countries than Austria, there may exist some hesitation against the expression or naming "New Austrian Tunnelling Method". The expressions such as Characteristic Line Method, Convergence Confinement Method or European Method are sometimes used depending on occasion. The basic concept is not different in respective expressions.

Fig. 1.2 shows various factors, regarding NATM, which should be considered in order to get successful result.

Regarding necessity of tunnel project, the application of NATM is developed due to its cost and man power. On the other hand, it is necessary to make closer contact between client and contractor in order to correspond to the variable behavior of ground. Estimation system and specification should be modified to be much more flexible. By understanding better the actual behavior of tunnel, based on the relation between the results by laboratory tests and the one by field measurement / monitoring, not only qualitatively but also quantitatively, optimization of construction should be prospected.

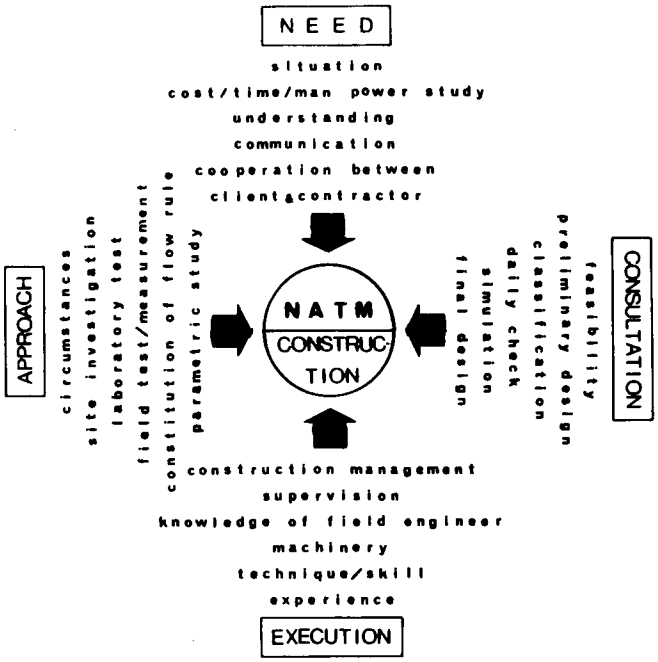

Fig. 1.2 Factors for Successful NATM.

Now in Japan more than 50 sites are under construction by applying NATM.

For example, Enrei T. in mudstone and tuff; 1st Hiraishi T. in weathered granite; Mukaiyama T. in rhyolite; Nakayama T. in green tuff; Shin–Usami T. in andesite and basalt; Nabetachiyama T. in mudstone; Takakurayama T. in slate; Najio T. in rhyolite; Hijirigaoka T. in shale and so on.

Table 1.2 shows the list of tunnels in foreign countries in accordance with NATM.

The largest railway tunnel in Japan is the Seikan Undersea Tunnel under construction which will connect the island of Hokkaido with the main land of Japan. The tunnel length is 53.8 kilometers and the maximum sea depth is 140 meters with minimum overburden thickness of 100 meters. It is estimated that the two pilot tunnels would be connected each other in 1981, and the whole tunnel project would be completed in 1983.

1.2 Outline of the Dissertation

Tunnelling technique is the most empirical in the field of civil engineering. It means that there has still remained so wide and deep gap between theory and practice, and also both of theorists and practicians are not apt to stand on the same stage. It seems to the author that they live in quite different world each other. In order to make tunnelling real engineering which can be dealt with by aid of not only qualitative, but also quantitative approach, it is required to advance research from the both sides of theory and practice based on field measurement.

From the view point of construction engineering, this dissertation aimed at supplying practical

Table 1.2 List of Tunnels Supported in Accordance with New Austrian Tunnelling Method (after H. Nussbaum, 1973)

Country (1)	Type of tunnel (2)	Location, name (3)	Length, in meters (4)	Cross section, in square meters (5)
Austria	Water conduits	various locations in Eastern Alps—TIWAG, KELAG, Illwerke hydro-power projects	together approx. 400,000	10 to 40
	Hydropower caverns	Kops	70	600
	Highways	Massenberg	~400	80
		Peggau	~400	80
		Bergisel	2 × 460	80
		Wolfsberg	675 + 880	70
		Assingberg (project)	2 × 2,100	85
		Tauern	2 × 6,400	100
		Katschberg	2 × 5,400	95
		Ofenauer	2 × 1,400	75
		Hiefler	2 × 2,000	75
		Hallstatt	1,400	70
		Lend	no record	no record
		Sonnenburghof	no record	no record
		Gleinalm (project)	2 × 8,000	no record
		Arlberg (project)	8,000	no record
	Military	Information restricted	several 1,000	information restricted
Germany	Water conduits	alpine locations similar as in Austria	perhaps 1/10 of Austrian	10 to 40
	Hydropower caverns	Säckingen	no record	no record
		Waldeck	105	1,100
	Highway	Pfaffenstein	2 × 1,100	80
	Railroad	Schwaikheim	400	85
	Subway	Frankfurt	no record	no record
	Miltary	information restricted	information restricted	15 to 200
Switzer-land	Water conduits	alpine locations similar as in Austria	perhaps 1/2 of Austrian	10 to 40
	Hydropower caverns	Veytaux Hongrin	137	680
	Highway	Belchen	2 × 4,500	80
		Glion	2 × 2,500	80
		Reussport	2 × 600	100
		several others	no record	no record
	Military	information restricted	information restricted	information restricted
Italy	Water conduits	alpine locations similar as in Austria	no records	no records
	Highway	several on Autostrada del sol	no records	90
		Gran Sesso	2 × 12,000	80
Luxem-bourg	Water supply	City of Luxembourg	2,500	14
	Hydropower caverns	Vianden (partly)	500	650
Vene-zuela	Highway	Cabrera	2 × 500	75
		El Valle	2 × 1,300	80
		El Cementerio (project)	2 × 800	75
		Paraiso (project)	2 × 800	75
Hong Kong	Water supply	Plover Cove	12,000	40
Pakistan	Water conduits	Tarbela Dam	4 × 800	230 to 470

information to the rational design and construction of tunnel which can follow actual behavior of rock associated with tunnel driving through field measurement and/or monitoring. Therefore, the dissertation corresponds with the practical sequence of tunnelling works, and the respective items are analyzed and discussed in following chapters.

That is,

for construction:

Drilling – Blasting – Mucking – Supporting – Lining

for design and supervision:

Field Measurement – Interpretation – Design – Monitoring – Confirmation of Stability

The objectives to be discussed are:

Regarding **blasting** – the relation between dynamic strength of rock and characteristics of explosives, propagation of stress wave, breakage mechanism of controlled blasting and so on.

Regarding **supporting** – supporting mechanism of rockbolt and shotcrete, stress rearrangement and deformation of surrounding rock with supports.

Regarding **field measurement** – correlation among different types of loading test, the application of newly developed deformation meter, calibration of pressure cell, interpretation of result, feeding back to actual design, meaning of convergence survey.

Regarding **tunnel stability** – rock behavior in the vicinity of mining face, role of face as a significant temporary support (half-dome effect), ground-support interaction and so on.

Regarding **environmental assessment** – vibration caused by blasting, relation among particle velocity, frequency and damage, empirical propagation equation of blasting vibration.

Regarding **construction method** – rockbolting, shotcrete, machinery, examples of actual status of tunnelling through squeezing and swelling rock (mudstone distributed Hokuriku Region), decomposed weathered rock (Izumi Formation), typical medium hard rock (rhyolite) and so on.

Fig. 1.3 shows the relations among the chapters in the dissertation and sequence of tunnelling.

The summaries of respective chapters are:

Chapter 2

The Finite Element Method has been developed so rapidly and highly in the field of rock-mechanics, confronting with many uncertainties. Analyses based on numerical approach should be reliable enough to satisfy practical problems. Researchers and engineers in the field of rock mechanics, occasionally whatever the real solution may be, are forced to be involved in computational works. This comes from the fact that computer engineers (sometimes, called system engineers in computer field) and civil engineers in rock-mechanical field are apt to pass by each other without mutual exchange of sufficient information, and also the interpretation of actual behavior of rock by means of qualitative and quantitative representations is heavy burden to practical engineers.

To determine appropriate constitutive equations, mechanical properties of rock in actual

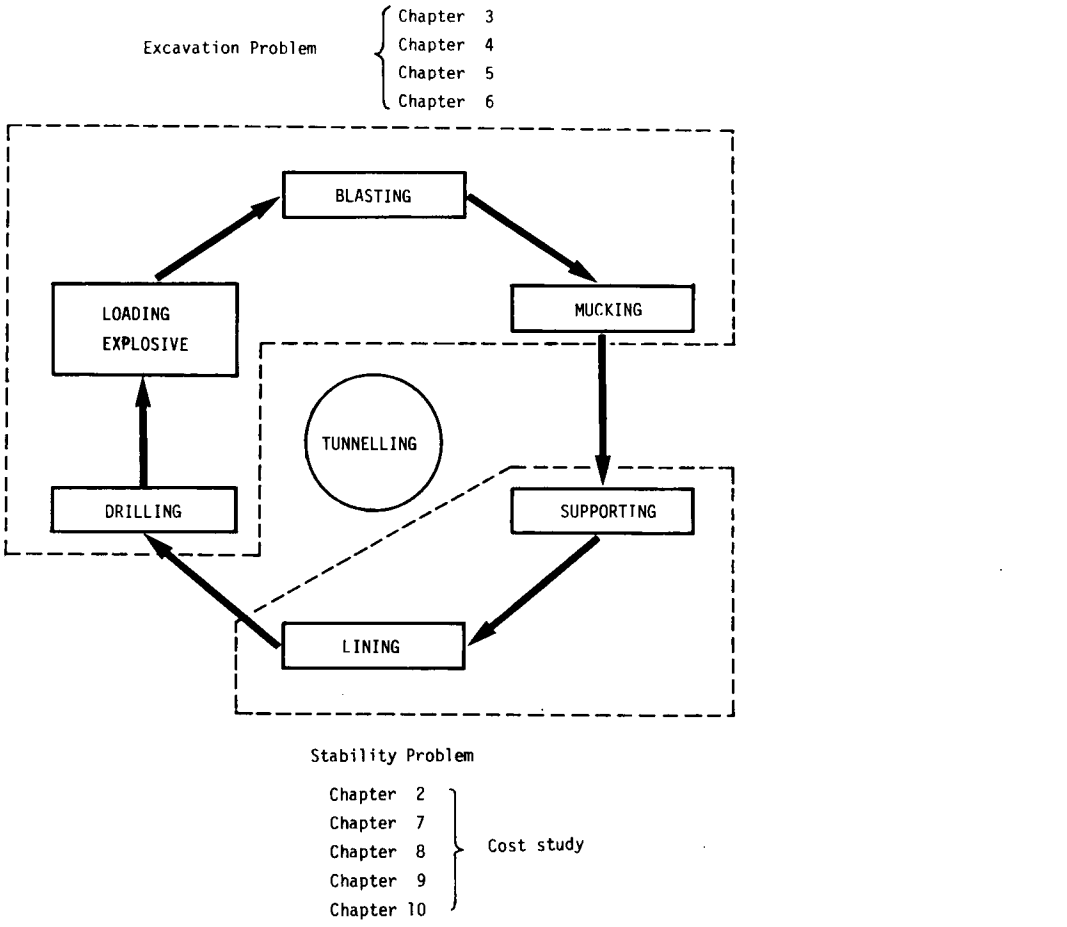

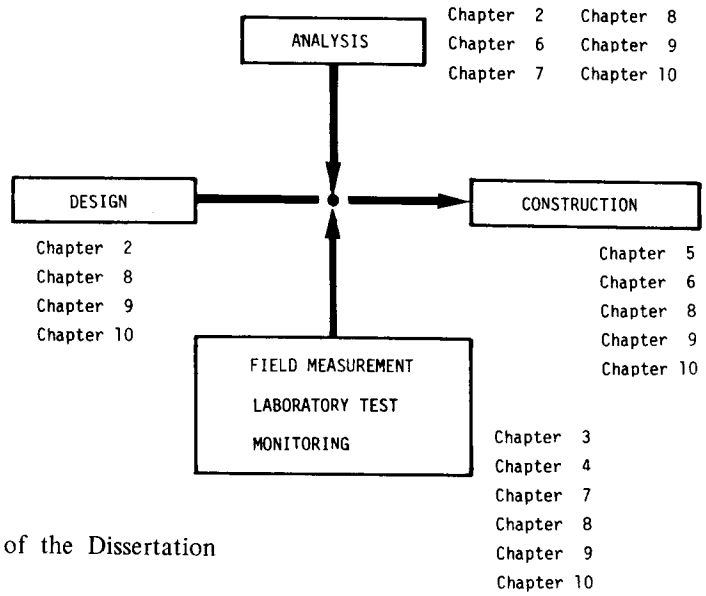

Fig. 1.3 The Contents of the Dissertation

scale and loading condition including primary stress field are very important works ahead of computation by FEM.

However, in order not to make the computational procedure too much unknown "Black Box", practical engineers and researchers should have knowledges on FEM enough to evaluate the appropriateness of computer OUTPUT.

Solving method is also the key-point of FEM analysis. In the dissertation, the appropriateness of assumed displacement functions is verified, and the applicability of Gauss–Seidel interative method with "Successive Over–Relaxation Procedure" is clarified through parametric study, investigation and mathematical theory. For practice optimum value of over-relaxation-factor is suggested in the range of 1.70 – 1.85.

Chapter 3

This experimental study was conducted in order to obtain the information on the dynamic tensile strength of rocks as a part of a blasting research project.

One end of the cylindrical rock specimen was impacted by the attack of a No. 8 cap and the spalling phenomenon was observed near the other end of the specimen.

At the same time, the stress wave shape induced and propagated in and through the rock specimen was measured at the free end of the specimen by using the capacitance gauge system.

From the observed stress wave shape, the attenuation of stress wave induced in the rock specimen was expressed by a decreasing exponential function of the distance from the shot point, and the dynamic tensile strength of rock was determined by analyzing the spalling phenomenon.

In this study, the dynamic tensile strength of rock was determined under the considerations of the decay of the stress wave with its propagation and the influence of the dynamic loading time to its strength.

It was found that the shorter the dynamic loading time was, acting at the place under consideration, the stronger was the dynamic tensile strength of rock.

In order to solve the problems in actual rock blasting, it seemed to be reasonable that 1 – 5 times the strength obtained by the conventional tension test was used for the dynamic tensile strength of rock.

Incidentally, the dynamic compressive strength of rock, which was nearly equal to 5 – 7 times the strength obtained by the static conventional compression test, was also observed in this experiment.

Chapter 4

In this study, when a spherical explosive charge is detonated in the infinite ground which is regarded to be an elastic, isotropic and homogeneous material, the radial stress of the spherical wave induced in and propagated through the ground is analyzed by a theory of elasticity.

From this results, the attenuation of the spherical stress wave with the distance from the

shot point is derived theoretically and compared with the actual attenuation of the spherical stress wave induced in the rock, which was measured in the experiment carried out previously.

Finally, it is found that about 90% of the stress amplitude of the wave theoretically induced is lost in the actual rock at the distance of 10 times the radius of the spherical charge. For this reason, it is considered that the lost stress amplitude is not only due to the energy loss with the propagation of the stress wave, but also due to the increasing of its wave length.

Chapter 5

In tunnel driving through hard or soft rocks, the usage of blasting has been conventional and typical excavation method, and still more efficient and economical. With the demands of tunnels and the development of rock blasting technique the question of ground vibrations has become increasingly important, and it has become more or less routine to excavate rocks close to or below houses and buildings.

Blasting is carried out for the purpose to fragment and to demolish rocks for removal by utilizing vast energy which the explosion of explosive generates. Near the explosive charge, the high amplitude stress wave and borehole gases produced by the detonation process create a crushed and fractured zones. Beyond these zones, where the amplitude of the stress wave does not exceed the strength of rock, the wave is propagated elastically. The elastic stress waves spread out in all directions and cause the surface of the underground opening to oscillate as a free surface. If the amplitudes of the wall vibrations, and particularly of the roof vibrations, are sufficiently high, loose blocks of rock may be dislodged or fractures in rock may be extended, further weakening the tunnel.

The empirical equation for propagation is discussed with the consideration of followings : a) particle velocity, b) distance from blasting point, c) types of explosive, d) quantity of charge, e) method of initiation, f) drilling pattern, g) path of propagation, h) tamping condition, i) characteristics of ground and j) states of ground formation.

In the relation between magnitude of damage regarding nearby structures and particle velocity, the allowable limit of vibration to buildings can be specified by the particle velocity in the range of 3 – 5 cm/s.

Chapter 6

Through the observation of a face created by smooth blasting, it can be recognized that a line of major crack is created from hole to hole and the cracks in the other directions are few. The crack pattern shown above is obvious in practice, but it seems that the reason why the major crack from hole to hole is created without cracks in the other directions has not been clarified completely. Therefore, in order to clarify the mechanism of rock breakage by smooth blasting and to find out a better technique which can be used more satisfactory to the purpose, both the state of the dynamic stress caused by the stress wave and the quasi-static stress distribution

caused by the pressure of the explosion gases have been analyzed for the typical pattern of smooth blasting. It is recognized that the pattern of the breakage of the material deduced from the above stress analyses coincided fairly well with that obtained in practice. This means that the mechanism of rock breakage by smooth blasting deduced from this study is reasonable.

Chapter 7

In designing the substructure of a bridge having a long span and being subjected to heavy loads, it is very important to determine the appropriate moduli of deformability of its foundation rock. The Izumi–layers ground on which two huge anchorage blocks and three ganged pipe piers are planned to be built up under the Ohnaruto Bridge project is so called compound soft rock ground consisting of 10 – 50 cm thick and remarkably fissured alternative layers of sandstone, shale, mudstone and their decomposed zones. It is anticipated that the rock ground behaves in quite different ways governed by local conditions and stress levels.

Several attempts have been carried out to evaluate the deformation modulus of a huge mass of the Izumi–layers, and plate loading test and borehole loading test have therefore been applied conveniently so far. Judging from practical knowledges and considerations, however, it seems that the result obtained throughout plate loading test or borehole loading test is strongly affected by the local geological conditions, particularly in the specific region which is subjected to the load. Therefore, field measurements and tests on large scale should be undertaken in order to promote better understanding with respect to the behaviors of the rockground.

This chapter deals with the methods and results of the displacement measurement undertaken at the various locations during the operation of the transportation tunnel of which excavation caused some change of stress distribution in the ground. Following the excavation of the tunnel which was initiated from the landside portal, the aluminium pipe, of 6 cm dia. and 50 m long on the inside of which 48 strain gauges had been attached in axial direction, was accommodated into the horizontal borehole of 9 cm dia. drilled at the position of 2 m higher above the tunnel crown from the seaside portal. Grouting has then been performed in the borehole to fix the pipe in the position and to make the pipe deform together with the surrounding rock mass. At the site the deformation of the rock due to the progress of the mining face was investigated by two different methods, i.e. measuring the deformation of the aluminium pipe and surveying the convergence of the tunnel section. The values of displacement measured by two different ways showed very good agreement. In addition to the field measurement, a few representative cases have been preliminarily analyzed with different deformation modulus and the results of the field measurement are fitted to the analytical result to find actual global modulus. As a result, it is found to be 2240 kgf/cm^2 (2.24 x 10^5 kN/m^2) for C-ranked ground having the deformation modulus of 4560 kgf/cm^2 (4.56 x 10^5 kN/m^2) which has been determined by the plate load test.

Chapter 8

The rapid increase in tunnelling projects requires better design methods which can deal with post-peak behavior of soft rock subjected to heavy loads. The analytical solution for strain softening behavior of rock around a circular opening is derived from the strain energy theorem employing Coulomb's yield criterion. Using a simplified stress-strain relation it is possible to obtain uniquely the magnitudes of stress, strain and displacement in elastic, softening and flow states by using only 10 input data: radius of a circular opening, hydro-static initial stress field, equivalent inner pressure to reaction of supports, elastic modulus, Poisson's ratio, negative gradient of deformation coefficient, and peak and residual strengths (uniaxial compressive strengths and angles of internal friction). Case studies conclude that a small increase of inner pressure has a large influence on the width of the plastic zone in rock which has induced softening, and that there is a big difference between the strain softening model and a conventional bi-linear elasto-plastic model, for the case of rock having a low competence factor. Herein, the author discussed a procedure to design a support system, including rockbolts and shotcrete, by replacing supports by an inner pressure acting on the surface of the tunnel wall.

Chapter 9

Recently, rockbolt support has been one of the most essential and practical method for tunnelling in rock. The author has been discussing the fundamental mechanism of tunnel driving from the point of view that, when advancing the face, it is necessary to place artificial supports to substitute for half-dome action within a span length from the face, so as to mobilize the bearing capacity of the rock mass as fully as possible. Also it is proposed that the supporting effect can be expressed by an equivalent inner pressure acting on the inner wall. However, the interaction between rockbolts and the ground occurs not only on the wall, but is distributed in the region outside the wall face. Here, axial force in and shear force along bolts fully bonded were analyzed by the finite element method for the case of weak rock showing strain softening behavior, and the optimum length of rockbolts through plasticized zone, and how to evaluate the effect of rockbolt support, were discussed. It is also concluded that an appropriate length of bolts can be determined from a ratio of supporting (pick-up) length to anchor length which is observed at the construction site, and that an equivalent inner pressure given by bolts can be calculated from the observed reduction of displacement.

Chapter 10

Shotcrete in tunnelling is considered as the most flexible and reliable support, and it works so as to maintain confining pressure in surrounding rock.

In accordance with the investigations through experimental study, theoretical analyses, numerical simulation and field measurement, it is pointed out that supporting effect of shotcrete does highly depend on techniques and efficiency of workers at tunnelling sites. Considering the

behavior of rock in the vicinity of mining face, practical designing method is proposed by means of replacing the supporting capacity of shotcrete by a sort of an equivalent inner pressure, and it is based on the common fundamental concept as the design of rock bolt support. To spray shotcrete without any void between shotcrete layer and rock surface is extraordinarily successful, and closing the excavated surface, with shotcrete as early as possible, mobilizes high confinement effect without any noticeable cracking in shotcrete layer, that means the breakage of shotcrete layer is subjected mainly to shear stress.

The difference on stability between shotcreting at full face and shotcreting partially is discussed, and objective procedure for shotcrete design is proposed by considering the interaction between rock and shotcrete with the deformation associated with the rearrangement of stress field near the face.

REFERENCES for Chapter 1

[1] Wahlstrom, E.: Tunnelling in rock, Elsevier Scientific Publishing Co., 1973.

[2] Agricola, G. (George Bauer): De Re Metallica (in Latin), 1556. Translated into English by Herbert C. and L.H. Hoover, The Mining Magazine, London, 1912. Reprinted by Dover, New York, 1950.

[3] Murray, D.: Man against Earth, J.B. Lippincott Co., Philadelphia, N.J., pp. 176, 1961.

[4] Sandström, G.E.: History of Tunnelling, Barrie and Rockcliff, London, pp. 427, 1963.

[5] Sandström, G.E.: Tunnels, Holt, Rinehart and Winston, New York, N.Y., pp. 427, 1963.

[6] Széchy, K.: The Art of Tunnelling, Akademiai Kiado, Budapest, 1967.

[7] Rabcewicz, L.v.: The New Austrian Tunnelling Method, Water Power, Nov. 1964 – Jan. 1965.

[8] Rabcewicz, L.v.: Stability of tunnels under rock load, Water Power, Jun. – Aug. 1969.

[9] Rabcewicz, L.v. and Golser, J.: Principles of dimensioning the supporting system for the "New Austrian tunnelling method", Water Power, Mar. 1973.

[10] Oka, Y.: Theory of tunnelling with rockbolts and shotcrete, 3rd Tunnel Sympo., JTA, 1974. (in Japanese)

[11] Committee on tunnelling research: Guide for rockbolting, Highway Research Association, 1973. (in Japanese)

[12] Committee on tunnelling research: Investigation of researches on shotcrete, Highway Research Association, 1973. (in Japanese)

[13] Austrian Society for Geomechanics: Definition of NATM, 1980.

[14] Kastner, H.: Statik des Tunnel und Stollenbaues, Berlin – Göttingen, Germany, 1962.

[15] Lauffer, H.: Gebirgsklassifizierung für den Stollenbau, Geologie und Bauwesen, Heft. 1, No. 24, 1958.

[16] Lombardi, G.: The influence of rock characteristics on the stability of rock cavities, Tunnels

and Tunnelling, Jan., 1970.

[17] Müller, L.: Der Felsbau, Enke Verlag, Stuttgart, Germany.

[18] Owen, S.C.: Shotcrete support in rock tunnels in Scandinavia, Civil Engineering, ASCE, Vol. 40, No. 1, Jan. 1970, pp. 74–79.

[19] Pacher, F.: Tunnelbauten im Zuge der österreichischen Autobahnen, Öst, Ingenieur Zeitschrift, Nov., 1970.

Chapter 2

PROGRAMMING OF FINITE ELEMENT METHOD AND ITS APPLICATION TO GEOMECHANICAL PROBLEMS

2.1 Introduction

During his stay at the Mining Research Laboratory, the governmental institute belonging to Department of Energy, Mines and Resources, Ottawa, Canada in 1966 ~ 1967, the author had been initiated to deal with the Finite Element Method (in the following occasionally abbreviated to FEM). At that time there was no computer programme available in the vicinity of the author, and there was very few practical information about the programming of FEM. Relying upon the limited information, the author tried to start understanding and programming of FEM, and the most important and troublesome matter in programming was to employ feasible method for solving simultaneous linear equations, which needed so numerous memory devices comparing with the capability of a computer developed in the middle of 1960s. (For example, it is picked up as one of the representative computers IBM 7090 with the storages of 32 kilowords.) Then, the application of Gauss–Seidel iterative method with an optimum over-relaxation factor was the best for the author, and still the basic idea for programming has been alive whatever a computer may be.

In Japan, it was when the First Congress of ISRM was held in Lisbon in September of 1966 that many researchers in the field of rock mechanics watched the applicability of FEM to their problems, for several remarkable papers (e.g. [1] - [5]), based on the numerical approach done through quite new concept, were presented. It is considered as the opening of the development of FEM among Japanese engineers belonging to geomechanical field.

After his return to Kyoto University, he had devoted two full years to the development of general purposed program (entitled GEOFEM), in which it is possible to deal with two dimensional (plane stress; plane strain), axi-symmetric and three dimensional problems with the consideration of elastic and elasto-plastic behavior for rocklike material. In the both fields of researches and practical designs, GEOFEM was employed to approximately 500 cases with respect to following problems :

For research

- stress concentration due to the variation of shape for underground openings ;
- deformation of inhomogeneous rock mass ;
- multiple holes problem ;
- slope stability ;
- stress distribution of rock specimen subjected to uni-axial loading ;
- crack problem around an opening ;
- breakage mechanism by smooth blasting ;

– heat conduction in rock specimen ;
– deformability of jointed rock ;
– tunnelling (rock-support interaction, deformation of rock in the vicinity of mining face, analysis of stress and strain distribution along a fully bonded rock bolts, stress rearrangement accompanied by excavation process, stress in lining, parametric study on anisotropy of rock, interpretation of convergence survey, etc.) ;
– stress concentration of a lipper tip attached to a bulldozer ;
– to simulate deformation behavior of a huge anchorage block with 120,000 m^3 for the large suspension bridge

and so on.

For design

– slope stability during and after construction (Kinki Highway – Wakayama, Chugoku Highway – Yamaguchi and Niimi, Funakira Dam along Tenryu River, construction site of Ohnaruto Bridge, etc.) ;
– dam foundation (Takarazuka, Shin-Nagano, Ogochi, etc.) ;
– foundation of bridge (Hirado Bridge, Ohnaruto Bridge, etc.) ;
– foundation of multi-floored apartment house on soft rock formation ;
– tunnels (Bingo T. and Hosaka T. – Sanyo Shinkansen, Kameura T. – Naruto, Ogoto T. – Kosei Line, Nabetachiyama T. – Matsudai, Urasa T. – Joetsu Shinkansen, several tunnels constructed by NATM) ;
– heat conduction problem (design of cooling system in massive concrete body)

and so on. (The author should add that he had been engaged in practical works as the practical designer and the supervisor at construction sites during 1970 ~ 1976.)

Here, for the application of FEM to geomechanical problems, the author wishes to sympathize strongly with the following comment of Prof. R.H. Gallagher's of Cornell University at the US – Japan jointed Seminar on the application of FEM in Tokyo, which was held by Japanese Society of Steel Construction in 1969 :

– Both practicing designers and theorists are prone to adopt disparate philosophies which promote negative attitudes towards the necessary directions of progress in finite element analysis. The practitioner, on his part, tends to view the remarkable advances in analysis as accomplishments which remove " sound engineering " from the design cycle. An objective of this paper has been to demonstrate that the need for such judgment is in fact more clearly delineated in the methodology that has been solidly established to date. Furthermore, the established methodology falls far short of furnishing a complete definition of response to overall design environment. Efforts must be continued in the latter direction.

– The theorist has been known to lose sight of the requirement to obtain acceptable solutions at minimum cost. Often, formidable exercises are launched in attempts to accomplished marginal

improvement of existing analysis capability, with no clear identification of the significance of the results in practical application. In common with all other numerical methods, the raison d'etre of finite element analysis derives from application in practice.

– The above brief thoughts issue implicitly from the aggregate of papers at the Symposium/ Seminar. A valid measure of success in these meetings will be the extent to which the respective participants will establish more meaningful operational philosophies and avenues of research activity based upon their own professional responsibilities. Since this measure can be defined only in the future, it is hoped that this same forum for the interchange of information and experience of U.S. and Japanese engineers and scientists in finite element analysis will again be furnished.

2.2 General Description of the Method [6]

The finite element method has developed simultaneously with the increasing use of high-speed electronic digital computers and with the growing emphasis on numerical methods for engineering analysis. Although the method was originally developed for structural analysis, the general nature of the theory on which it is based has also made possible its successful application for solutions of problems in other fields of engineering.

It is not possible to obtain analytical mathematical solutions for many engineering problems. An analytical solution is a mathematical expression that gives the values of the desired unknown quantity at any location in a body, and as a consequence it is valid for an infinite number of locations in the body. Analytical solutions can be obtained only for certain simplified situations. For problems involving complex material properties and boundary conditions, the engineer resorts to numerical methods that provide approximate, but acceptable, solutions. In most of the numerical methods, the solutions yield approximate values of the unknown quantities only at a discrete number of points in the body. The process of selecting only a certain number of discrete points in the body can be termed discretization. One of the ways to discretize a body or a structure is to divide it into an equivalent system of smaller bodies, or units. The assemblage of such units then represents the original body. Instead of solving the problem for the entire body in one operation, the solutions are formulated for each constituent unit and combined to obtain the solution for the original body or structure. This approach is known as going from part to whole. Although the analysis procedure is thereby considerably simplified, the amount of data to be handled is dependent upon the number of smaller bodies into which the original body is divided. For a large number of subdivisions it is a formidable task to handle the volume of data manually, and recourse must be made to automatic electronic computation.

In brief, the basis of the finite element method is the representation of a body or a structure by an assemblage of subdivisions called finite elements, Fig. 2.1. These elements are considered interconnected at joints which are called nodes or nodal points. Simple functions are chosen to approximate the distribution or variation of the actual displacements over each finite element.

Such assumed functions are called displacement functions or displacement models. The unknown magnitudes or amplitudes of the displacement functions are the displacements (or the derivatives of the displacements) at the nodal points, Fig. 2.2. Hence, the final solution will yield the approximate displacements at discrete locations in the body, the nodal points. A displacement model can be expressed in various simple forms, such as polynomials and trigonometric functions. Since polynomials offer ease in mathematical manipulations, they have been employed commonly in finite element applications.

A variational principle of mechanics, such as the principle of minimum potential energy, is usually employed to obtain the set of equilibrium equations for each element. The potential energy of a loaded elastic body or structure is represented by the sum of the internal energy stored as a result of the deformations and the potential energy of the external loads. If the body is in a state of equilibrium, this energy is a minimum. This is a simple statement of the principle of minimum potential energy.

To illustrate the concept of the potential energy, we consider an elementary example. Fig. 2.3 shows a linear spring, with spring constant s [kgf/cm], under a load of P kgf. The spring deflects by the amount u [cm] under the load. The internal strain energy stored in the spring is given by

$$\begin{aligned} U &= 1/2 \cdot (\text{Force in the spring}) \cdot (\text{Displacement}) \\ &= 1/2 \cdot (su)\,(u) \\ &= 1/2 \cdot su^2 \end{aligned} \tag{2.1}$$

The potential energy of the external load P is

$$\begin{aligned} W_p &= (\text{Load})\,(\text{Displacement from zero potential state}) \\ &= -P \cdot u \end{aligned} \tag{2.2}$$

where the zero potential state corresponds to $u = 0$. Hence the total potential energy π is

$$\pi = U + W_p = 1/2 \cdot su^2 - P \cdot u \tag{2.3}$$

The minimum of π can be obtained by differentiating it with respect to u, and equating the result to zero :

$$\frac{\partial \pi}{\partial u} = su - P = 0 \tag{2.4}$$

or

$$su = P$$

Equation (2.4) is the equilibrium equation or load-displacement relation for the loaded spring.

The equilibrium equations for the entire body are then obtained by combining the equations for the individual elements in such a way that continuity of displacements is preserved at the inter-

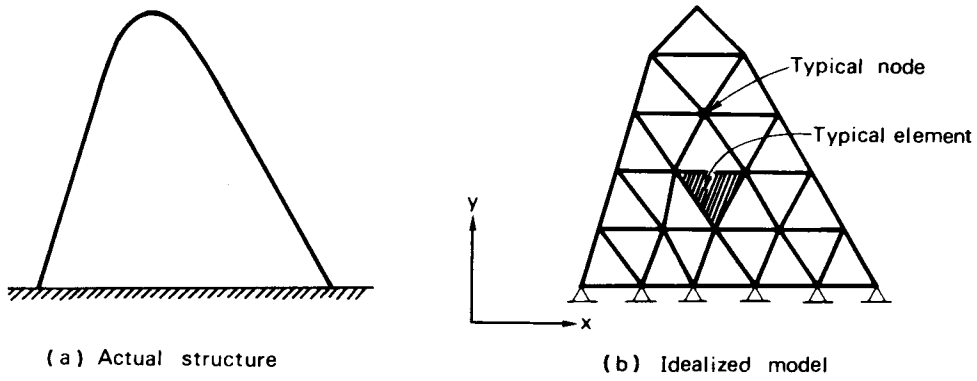

Fig. 2.1 Two-dimensional Region Represented as an Assemblage of Triangular Elements [6]

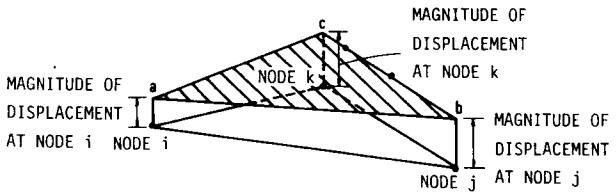

Fig. 2.2 Isometric View of Triangular Element with Linear Displacement Model Plotted in the Third Dimensions. [6]

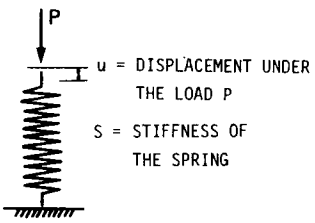

Fig. 2.3 Linear Spring [6]

connecting nodes. These equations are modified for the given displacement boundary conditions and then solved to obtain the unknown displacement. In many types of problems, the desired solution is in terms of the strains or stresses rather than the displacements, so additional manipulations or calculations may be necessary.

Nevertheless, it is apparent that the theory of the finite element method may be divided into two phases. The first phase consists of the study of the individual element. The second phase is the study of the assemblage of elements representing the entire body.

The initial development of the finite element method for aerospace and structural engineering was soon followed by application of the method to problems in soil and rock mechanics. The nature of soils and rocks, however, is highly complex and requires different considerations from the materials used in structures. A realistic appraisal of the complexities imposed by such natural causes as joints and other discontinuities would often require that soils and rocks be treated as a discontinua. Nevertheless, approximate but acceptable solutions can be obtained by considering them as continuous masses. In most applications of the finite element method, the continuum approach is used; hence, we shall restrict our attention to this idealization. Furthermore, we shall consider only those aspects of rock mechanics directly related to the applications of the finite element method.

The uncertainties inherent in the behavior of rocks require experimental or field verification for any analytical technique before it can be used for practical design analysis. For certain problems, such as the analyses of slopes, dams and foundations, and some rock-structure interaction problems, sufficient experimental verifications have been obtained. Additional experimental correlation, however, is desirable for such topics as the complex shapes of dams, jointed rocks, group foundations, multiple wheel loads on pavements, post-cracking phenomena, work softening behavior, and very soft materials. Table 2.1 shows various topics for which the finite element method has been successfully employed. Other topics such as seepage and creep effects are included.

Deformation behavior of rocks is influenced by a number of factors, such as the physical structure, porosity, density, stress history, loading characteristics, existence and movement of fluids in the pores, and time-dependent or viscous effects in the solid and the pore fluids. In addition, such geologic features as faults, joints, seams, crushed zones, veins, fissures, folds, and other tectonic effects produce behavior significantly different from that derived on the assumption of continuous mass. These factors render the stress-deformation behavior highly complex and nonlinear. No available analytical solution scheme can handle them all. Numerical methods, such as the finite element method, have proved successful in approximating the effects of many of these factors, and they show promise of incorporating a number of others. Moreover, the initial success of the finite element method has indicated that some of these factors have a more significant effect than had been expected.

Table 2.1 Topics in Rock Mechanics [6]

Topics	Typical Applications
I Stress-deformation and stability analyses	Stress analysis of slopes, excavations.
II Structures	Dams, tunnels, mines, pits, cavities, boreholes
III Geologic features	Joints, fissures, fractures, layers
IV Constitutive laws	Intact rocks, discontinuous rocks

2.3 Summary of the Analysis Procedure [6]

The following six steps summary FEM procedure

(1) Discretization of the continuum

The continuum is the physical body, structure, or solid being analyzed. Discretization may be simply described as the process in which the given body is subdivided into an equivalent system of finite elements. The finite elements may be triangles, groups of triangles, or quadrilaterals for a two-dimensional continuum. Fig. 2.1 shows an arbitrary two-dimensional body discretized into a system of triangular finite elements. For three-dimensional analysis, the finite elements may be tetrahedra, rectangular prisms, or hexahedra. Although some efforts have been made to automate the process of subdivision, it remains essentially a judgmental process on the part of the engineer. He must decide what number, size, and arrangement of finite elements will give an effective representation of the given continuum for the particular problem considered.

Only a significant portion of such a continuum need be considered and discretized. Indeed, practical limitations require that one include only the significant portion of any large continuum in the finite element analysis.

(2) Selection of the displacement model

The assumed displacement functions or models represent only approximately the actual or

exact distribution of the displacements. For example, a displacement function is commonly assumed in a polynomial form, and practical considerations limit the number of terms that can be retained in the polynomial. The simplest displacement model that is commonly employed is a linear polynomial. The shaded portion abc over the triangular finite element ijk in Fig. 2.2 is a typical example of linear variation of displacement given by a linear polynomial. Obviously, it is generally not possible to select a displacement function that can represent exactly the actual variation of displacement in the element. Hence, the basic approximation of the finite element method is introduced at this stage.

There are three interrelated factors which influence the selection of a displacement model. First, the type and the degree of the displacement model must be chosen. (Usually, since a polynomial is chosen, only the degree of the polynomial is open to decision.) Second, the particular displacement magnitudes that describe the model must be selected. These are usually the displacements of the nodal points, but they may also include derivatives of the displacements at some or all of the nodes. Third, the model should satisfy certain requirements which ensure that the numerical results approach the correct solution.

(3) Derivation of the element stiffness matrix using a variational principle.

The stiffness matrix consists of the coefficients of the equilibrium equations derived from the material and geometric properties of an element and obtained by use of the principle of minimum potential energy. The stiffness relates the displacements at the nodal points (the nodal displacements) to the applied forces at the nodal points (the nodal forces). The distributed forces applied to the structure are converted into equivalent concentrated forces at the nodes. The equilibrium relation between the stiffness matrix [k], nodal force vector $\{f\}$, and nodal displacement vector $\{u\}$ is expressed as a set of simultaneous linear algebraic equations,

$$[k]\ \{u\} = \{f\} \tag{2.5}$$

The elements of the stiffness matrix are the influence coefficients. Recall that a stiffness of a structure is an influence coefficient that gives the force at one point on a structure associated with a unit displacement of the same or a different point.

(4) Assembly of the algebraic equations for the overall discretized continuum.

This process includes the assembly of the overall or global stiffness matrix for the entire body from the individual element stiffness matrices, and the overall or global force or load vector from the element nodal force vectors. The most common assembly technique is known as the direct stiffness method. In general, the basis for an assembly method is that the nodal interconnections require the displacements at a node to be the same for all elements adjacent to that node. The overall equilibrium relations between the total stiffness matrix [K], the total load vector $\{R\}$, and the nodal displacement vector for the entire body $\{r\}$ will again be expressed as a set of simultaneous equations.

$$[K]\{r\}=\{R\} \tag{2.6}$$

These equations cannot be solved until the geometric boundary conditions are taken into account by appropriate modification of the equations. A geometric boundary condition arises from the fact that displacement may be prescribed at the boundaries or edges of the body or structure.

(5) Solutions for the unknown displacements.

The algebraic equations assembled in step (4) are solved for the unknown displacements. In linear equilibrium problems, this is a relatively straightforward application of matrix algebra techniques. However, for nonlinear problems the desired solutions are obtained by a sequence of steps, each step involving the modification of the stiffness matrix and/or load vector.

(6) Computation of the element strains and stresses from the nodal displacements.

In certain cases the magnitudes of the primary unknowns, that is the nodal displacements, will be all that are required for an engineering solution. More often, however, other quantities derived from the primary unknowns, such as strains and/or stresses, must be computed.

In general, the stresses and strains are proportional to the derivatives of the displacements; and in the domain of each element meaningful values of the required quantities are calculated. These " meaningful values " are usually taken as some average value of the stress or strain at the center of the element.

2.4 General Derivation of Stiffness Matrix

The relation between nodal force $\{R\}$ and nodal displacement $\{r\}$ is

$$\{R\} = [K]\{r\} \tag{2.7}$$

where [K] is stiffness matrix.

As it is considered as the main part of procedure in FEM to solve simultaneous linear equations as shown by Eq. (2.7), it is required to employ appropriate stiffness matrix and to discretize to elements as many as possible in order to get results with reliable accuracy. Hence, let us talk about how to derive Stiffness Matrix [K] generally. The case for two dimensional problem may be explainable for general explanation, and it is very easy to enlarge this fundamental concept to three dimensional problems.

(1) To express displacement of an arbitrary point P (x, y) in an element in terms of displacement function:

$$\{V(x, y)\} = [M(x, y)]\{\alpha\} \tag{2.8}$$

where, M (x, y) is displacement function which should be defined so as to satisfy condition of compatibility not only in an element, but also on its boundary. For example, denoting nodal points, i, j and k; and displacements of nodal points (i, j and k) as shown in Fig. 2.4, the displacement (u, v) of an arbitrary point P (x, y) in two dimensional coordinate (x, y) can be defined in the forms

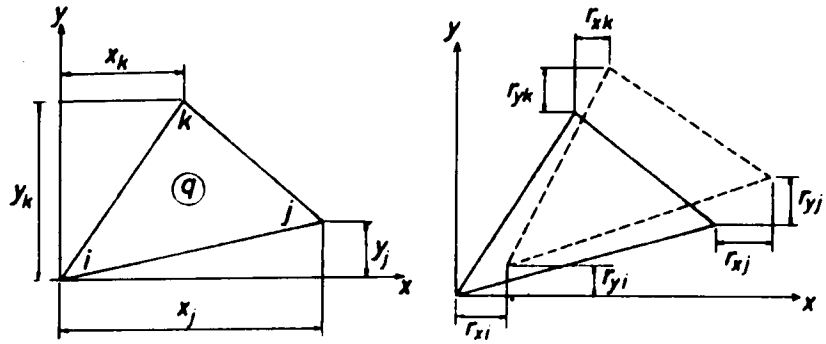

Fig. 2.4 Coordinates of Nodal Points and Displacements at Nodes

of

$$\left.\begin{aligned} u &= \alpha_1 + \alpha_2 \cdot x + \alpha_3 \cdot y \\ v &= \alpha_4 + \alpha_5 \cdot x + \alpha_6 \cdot y \end{aligned}\right\} \tag{2.9}$$

or in matrix form as

$$\begin{Bmatrix} u \\ v \end{Bmatrix} = \begin{bmatrix} 1 & x & y & 0 & 0 & 0 \\ 0 & 0 & 0 & 1 & x & y \end{bmatrix} \begin{Bmatrix} \alpha_1 \\ \alpha_2 \\ \vdots \\ \alpha_6 \end{Bmatrix} = [N]\{\alpha\} \tag{2.10}$$

(2) To express nodal displacement component r_i as the function of generalized coordinate α :

$$\{r_i\} = [A]\ \{\alpha\} \tag{2.11}$$

Matrix [A] is obtaining by substituting coordinates of nodal points into displacement function [M (x, y)], and when number of coefficients α is equal to total number of displacement components, v_i, [A] is square matrix.

For two dimensional problem,

$$\{r\} = \begin{Bmatrix} r_{xi} \\ r_{yi} \\ r_{xj} \\ r_{yj} \\ r_{xk} \\ r_{yk} \end{Bmatrix} = \begin{bmatrix} 1 & x_i & y_j & 0 & 0 & 0 \\ 0 & 0 & 0 & 1 & x_i & y_i \\ 1 & x_j & y_j & 0 & 0 & 0 \\ 0 & 0 & 0 & 1 & x_j & y_j \\ 1 & x_k & y_k & 0 & 0 & 0 \\ 0 & 0 & 0 & 1 & x_k & y_k \end{bmatrix} \begin{Bmatrix} \alpha_1 \\ \alpha_2 \\ \alpha_3 \\ \alpha_4 \\ \alpha_5 \\ \alpha_6 \end{Bmatrix} = [A]\{\alpha\} \tag{2.12}$$

(3) To express generalized coordinates α as the function of nodal displacements:

$$\{\alpha\}=[A]^{-1}\{r\} \tag{2.13}$$

(4) To form the relation between strain and α :

$$\left\{\epsilon\ (x, y)\right\} = [\ B\ (x, y)\ ]\ \left\{\alpha\right\} \tag{2.14}$$

Namely, in two dimensional problems strain $\left\{\epsilon\right\}$ at a point can be defined as follows

$$\varepsilon_x=\frac{\partial u}{\partial x}=\alpha_2,\quad \varepsilon_y=\frac{\partial v}{\partial y}=\alpha_6,\quad \gamma_{xy}=\frac{\partial v}{\partial x}+\frac{\partial u}{\partial y}=\alpha_5+\alpha_3 \tag{2.15}$$

Hence, in matrix form

$$\{\varepsilon\}=\begin{Bmatrix}\varepsilon_x\\ \varepsilon_y\\ \gamma_{xy}\end{Bmatrix}=\begin{bmatrix}0&1&0&0&0&0\\ 0&0&0&0&0&1\\ 0&0&1&0&1&0\end{bmatrix}\begin{Bmatrix}\alpha_1\\ \alpha_2\\ \vdots\\ \alpha_6\end{Bmatrix}=[B]\{\alpha\} \tag{2.16}$$

By substituting Eq. (2.13) into Eq. (2.16), we obtain

$$\{\varepsilon\}=[B][A]^{-1}\{r\} \tag{2.17}$$

(5) The relation between stress and strain is

$$\begin{aligned}\left\{\sigma\ (x, y)\right\} &= [D]\ \left\{\epsilon\ (x, y)\right\}\\ &= [D]\ [\ B\ (x, y)\ ]\ \left\{\alpha\right\}\end{aligned} \tag{2.18}$$

where Matrix [D] is the matrix for each element, specified by physical properties of material, and it is determined by such condition as isotropy, anisotropy, elastic, elasto-plastic, etc.
For example, in the case of plane stress, it is

$$\begin{Bmatrix}\sigma_x\\ \sigma_y\\ \tau_{xy}\end{Bmatrix}=\frac{E}{1-\nu^2}\begin{bmatrix}1&\nu&0\\ \nu&1&0\\ 0&0&\dfrac{1-\nu}{2}\end{bmatrix}\begin{Bmatrix}\varepsilon_x\\ \varepsilon_y\\ \gamma_{xy}\end{Bmatrix} \tag{2.19}$$

where E and ν are Elastic constant and Poisson's ratio.

Then, in the case of plane strain it takes the form of

$$\begin{Bmatrix}\sigma_x\\ \sigma_y\\ \tau_{xy}\end{Bmatrix}=\frac{E(1-\nu)}{(1+\nu)(1-2\nu)}\begin{bmatrix}1&\dfrac{\nu}{1-\nu}&0\\ \dfrac{\nu}{1-\nu}&1&0\\ 0&0&\dfrac{1-2\nu}{2(1-\nu)}\end{bmatrix}\begin{Bmatrix}\varepsilon_x\\ \varepsilon_y\\ \gamma_{xy}\end{Bmatrix} \tag{2.20}$$

Namely,

$$\{\sigma\}=[D]\{\varepsilon\}=[D][B][A]^{-1}\{r\} \tag{2.21}$$

It is clear that strain in an element as shown by Eq. (2.16) is uniform when the displacement function is defined by the form of Eq. (2.9), and consequently that stress in the form of Eq. (2.21) becomes constant.

(6) To obtain element stiffness $[K]^q$:

According to the principle of virtual works, virtual internal work, dW_I, to infinitesimal volume, dV, with respect to element is defined by the product of actual stress σ and virtual strain $\bar{\epsilon}$:

$$d\bar{W}_I = \bar{\epsilon}^T \sigma \, d\bar{V} \tag{2.22}$$

By substituting Eq. (2.14) and Eq. (2.18) into Eq. (2.22), we obtain

$$d\bar{W}_I = \bar{\alpha}^T B^T D B \alpha \, dV \tag{2.23}$$

where $\bar{\alpha}$ expresses virtual displacement associated with $\bar{\epsilon}$. Hence, the total virtual internal work, W_I, can be determined by integrating dW_I over the whole volume:

$$\bar{W}_I = \bar{\alpha}^T [\int_{vol} B^T D B \, dV] \alpha \tag{2.24}$$

Then, the external work associated displacement component $\bar{\alpha}$ in general coordinates is

$$\bar{W}_E = \bar{\alpha}^T \beta \tag{2.25}$$

where, β expresses generalized force corresponding to displacement.

Now, by giving virtual unit displacement one by one (i.e. $\bar{\alpha} \equiv I$), let us make the internal work equal to the external work. Thus,

$$\beta = [\int_{vol} B^T D B \, dV] \alpha \tag{2.26}$$

According to the definition of stiffness matrix, the term in brackets express stiffness matrix in generalized coordinates.

Otherwise, in symbolic form they become as follows :

$$\begin{aligned} W_I &= \int_{(vol)} \{\varepsilon\}^T \{\sigma\} d(vol) \\ &= (vol) \cdot \{r\}^T \cdot ([A]^{-1})^T [B]^T [D] [B] [A]^{-1} \{r\} \end{aligned} \tag{2.27}$$

where (vol) corresponds with the area of triangular element in two dimensional problem.

$$W_B = \{r\}^T \{f\}^q \tag{2.28}$$

Because $W_I = W_E$,

$$\begin{aligned} \{f\}^q &= (vol) ([A]^{-1})^T [B]^T [D] [B] [A]^{-1} \{r\} \\ &= [K]^q \{r\} \end{aligned} \tag{2.29}$$

where $[K]^q$ is element stiffness regarding to Element q, which can be determined by giving coordinates of Nodal points, (i, j, k) and physical properties of Element q.

For better understanding, when we denote as shown in Fig. 2.5, Eq. (2.29) is expressed in the detailed form

$$\begin{Bmatrix} f_{xi} \\ f_{yi} \\ f_{xj} \\ f_{yj} \\ f_{xk} \\ f_{yk} \end{Bmatrix} = \begin{bmatrix} k_{xi,xi} & k_{xi,yi} & k_{xi,xj} & k_{xi,yj} & k_{xi,xk} & k_{xi,yk} \\ k_{yi,xi} & k_{yi,yi} & k_{yi,xj} & k_{yi,yj} & k_{yi,xk} & k_{yi,yk} \\ k_{xj,xi} & \cdots & \cdots & \cdots & \cdots & \cdots \\ k_{yj,xi} & \cdots & \cdots & \cdots & \cdots & \cdots \\ k_{xk,xi} & \cdots & \cdots & \cdots & \cdots & \cdots \\ k_{yk,xi} & \cdots & \cdots & \cdots & \cdots & \cdots \end{bmatrix} \times \begin{Bmatrix} r_{xi} \\ r_{yi} \\ r_{xj} \\ r_{yj} \\ r_{xk} \\ r_{yk} \end{Bmatrix} \tag{2.30}$$

In the former matrix, for example, the notation of $k_{xi,\,yk}$ represents the force in x-direction, developed on element q, at nodal point x due to unit displacement in y-direction at nodal point k.

To denote with respect to arbitrary nodal points, l and m,

$$f_l \equiv \begin{Bmatrix} f_{xl} \\ f_{yl} \end{Bmatrix}, \quad k_{lm} \equiv \begin{bmatrix} k_{xl,xm} & k_{xl,ym} \\ k_{yl,xm} & k_{yl,ym} \end{bmatrix}, \quad r_l \equiv \begin{Bmatrix} r_{xl} \\ r_{yl} \end{Bmatrix}$$

as Eq. (2.30) is the equation with respect to element q, let us denote upper subscript, q.

$$\begin{Bmatrix} f_i^q \\ f_j^q \\ f_k^q \end{Bmatrix} = \begin{bmatrix} k_{ii}^q & k_{ij}^q & k_{ik}^q \\ k_{ji}^q & k_{jj}^q & k_{jk}^q \\ k_{ki}^q & k_{kj}^q & k_{kk}^q \end{bmatrix} \begin{Bmatrix} r_i \\ r_j \\ r_k \end{Bmatrix} \tag{2.31}$$

Consequently, $[K]^q$ is determined in the following form by Eq. (2.29) :

$$[K]^q = (vol)([A]^{-1})^T[B]^T[D][B][A]^{-1} \tag{2.32}$$

(7) To form nodal stiffness [K] with respect to node n, by summing element stiffnesses adjacent to nodal point n :

In stead of the above mentioned general description, it can give better understanding to explain by using two dimensional problem as follows :

Now, let us assume that elements, q_1, q_2, $\cdots\cdots$, q_5, surround node, n, and each element consists of three nodes as shown in Fig. 2.6.

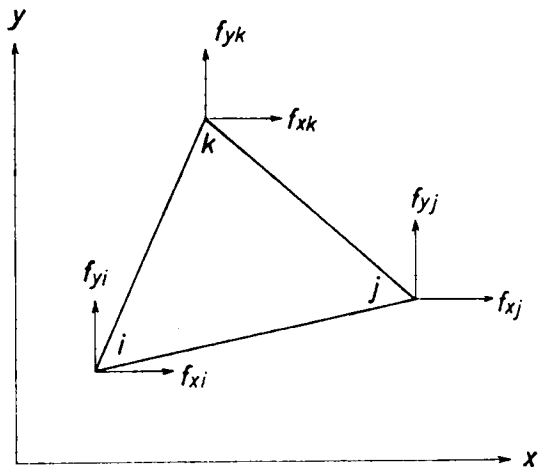

Fig. 2.5 Nodal Forces

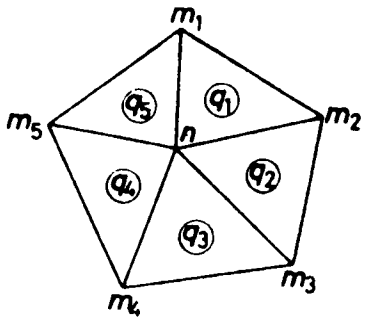

Fig. 2.6 Elements Surrounding a Node

Under this assumption, when we pick up terms which are located on the row of (2n – 1) and (2n), the equilibrium at Node n is expressed in terms of

$$\{P_n\}=\begin{Bmatrix}P_{xn}\\P_{yn}\end{Bmatrix}=\{f_n\}^{q_1}+\{f_n\}^{q_2}+\cdots+\{f_n\}^{q_5} \tag{2.33}$$

By replacing Eq. (2.31) to Eq. (2.33),

$$\begin{aligned}\{P_n\}&=[k_{nn}{}^{q_1}]\{r_n\}+[k_{nm_1}{}^{q_1}]\{r_{m1}\}+[k_{nm2}{}^{q_1}]\{r_{m2}\}\\&+[k_{nn}{}^{q_2}]\{r_n\}+[k_{nm2}{}^{q_2}]\{r_{m2}\}+[k_{nm_3}{}^{q_2}]\{r_{m3}\}\\&+\cdots\cdots\cdots\\&+[k_{nn}{}^{q_5}]\{r_n\}+[k_{nm_5}{}^{q_5}]\{r_{m5}\}+[k_{nm_1}{}^{q_5}]\{r_{m1}\}\\&=[k_{nn}{}^{q_1}+k_{nn}{}^{q_2}+k_{nn}{}^{q_3}+k_{nn}{}^{q_4}+k_{nn}{}^{q_5}]\{r_n\}\\&+[k_{nm_1}{}^{q_1}+k_{nm_1}{}^{q_5}]\{r_{m1}\}+[k_{nm2}{}^{q_1}+k_{nm2}{}^{q_2}]\{r_{m2}\}\\&+[k_{nm2}{}^{q_2}+k_{nm_3}{}^{q_3}]\{r_{m3}\}+[k_{nm_4}{}^{q_3}+k_{nm_4}{}^{q_4}]\{r_{m4}\}\\&+[k_{nm_5}{}^{q_4}+k_{nm_5}{}^{q_5}]\{r_{m5}\}\end{aligned} \tag{2.34}$$

As shown in the former equation, Eq. (2.34), 1st, 2nd · · · · · , and 6th terms on right side correspond to matrix elements which are situated at columns of (2n – 1) and (2n) ; ($2m_1$ – 1) and ($2m_1$) ; · · · · and ($2m_5$ – 1) and ($2m_5$) in rows (2n – 1) and (2n), respectively.

2.5 Fundamentals of FEM

2.5.1 Problem in Small Displacement Theory [8]

Let us deal with the small displacement theory of elasticity and derive the principle of virtual work and related variational principles for the problem of an elastic body in static equilibrium under body forces and prescribed boundary conditions. Rectangular Cartesian coordinates (x, y, z) will be employed for defining the three-dimensional space containing the body. In the small displacement theory of elasticity displacement components, u, v, w, of a point of the body are assumed so small that we are justified in linearizing equations governing the problem. The linearized governing equations may be summarized as follows :

(a) Stress. The state of internal force at a point of the body is defined by nine components of stress :

$$\begin{matrix}\sigma_x & \tau_{yx} & \tau_{zx},\\ \tau_{xy} & \sigma_y & \tau_{zy},\\ \tau_{xz} & \tau_{yz} & \sigma_z,\end{matrix} \tag{2.35}$$

which should satisfy the equations of equilibrium :

$$\begin{aligned}\frac{\partial\sigma_x}{\partial x}+\frac{\partial\tau_{yx}}{\partial y}+\frac{\partial\tau_{zx}}{\partial z}+\bar{X}=0,\\ \frac{\partial\tau_{xy}}{\partial x}+\frac{\partial\sigma_y}{\partial y}+\frac{\partial\tau_{zy}}{\partial z}+\bar{Y}=0,\\ \frac{\partial\tau_{xz}}{\partial x}+\frac{\partial\tau_{yz}}{\partial y}+\frac{\partial\sigma_z}{\partial z}+\bar{Z}=0,\end{aligned} \tag{2.36}$$

and

$$\tau_{yz} = \tau_{zy}, \quad \tau_{zx} = \tau_{xz}, \quad \tau_{xy} = \tau_{yx}, \tag{2.37}$$

where $\bar{X}$, $\bar{Y}$ and $\bar{Z}$ are components of the body forces per unit volume. We shall eliminate τ_{zy}, τ_{xz} and τ_{yx} by the use of Eqs. (2.37), and specify the state of stress at a point of the body with six components (σ_x, σ_y, σ_z, τ_{yz}, τ_{zx}, τ_{xy}).
Then, Eqs. (2.36) become :

$$\begin{aligned}
&\frac{\partial \sigma_x}{\partial x} + \frac{\partial \tau_{xy}}{\partial y} + \frac{\partial \tau_{zx}}{\partial z} + \bar{X} = 0, \\
&\frac{\partial \tau_{xy}}{\partial x} + \frac{\partial \sigma_y}{\partial y} + \frac{\partial \tau_{yz}}{\partial z} + \bar{Y} = 0, \\
&\frac{\partial \tau_{zx}}{\partial x} + \frac{\partial \tau_{yz}}{\partial y} + \frac{\partial \sigma_z}{\partial z} + \bar{Z} = 0.
\end{aligned} \tag{2.38}$$

(b) Strain. The state of strain at a point of the body is defined by six components of strain (ϵ_x, ϵ_y, ϵ_z, γ_{yz}, γ_{zx}, γ_{xy}).

(c) Strain-displacement relations. In small displacement theory the strain-displacement relations are given as follows :

$$\begin{aligned}
&\varepsilon_x = \frac{\partial u}{\partial x}, \quad \varepsilon_y = \frac{\partial v}{\partial y}, \quad \varepsilon_z = \frac{\partial w}{\partial z}, \\
&\gamma_{yz} = \frac{\partial w}{\partial y} + \frac{\partial v}{\partial z}, \quad \gamma_{zx} = \frac{\partial u}{\partial z} + \frac{\partial w}{\partial x}, \quad \gamma_{xy} = \frac{\partial v}{\partial x} + \frac{\partial u}{\partial y}.
\end{aligned} \tag{2.39}$$

We observe from Eqs. (2.39) that when a continuum deforms, the six strain components (ϵ_x, ϵ_y, ϵ_z,γ_{yz}, γ_{zx}, γ_{xy}) cannot behave independently, but must be derived from three functions, u, v and w as shown.

The necessary and sufficient conditions that the six strain components can be derived from three single-valued function as given in Eqs. (2.39) are called the conditions of compatibility. It is shown, for example, that the conditions of compatibility are given in a matrix form as,

$$[R] = \begin{bmatrix} R_x & U_z & U_y \\ U_z & R_y & U_x \\ U_y & U_x & R_z \end{bmatrix} = 0, \tag{2.40}$$

where

$$\begin{aligned}
R_x &= \frac{\partial^2 \varepsilon_z}{\partial y^2} + \frac{\partial^2 \varepsilon_y}{\partial z^2} - \frac{\partial^2 \gamma_{yz}}{\partial y \, \partial z}, \\
R_y &= \frac{\partial^2 \varepsilon_x}{\partial z^2} + \frac{\partial^2 \varepsilon_z}{\partial x^2} - \frac{\partial^2 \gamma_{zx}}{\partial z \, \partial x}, \\
R_z &= \frac{\partial^2 \varepsilon_y}{\partial x^2} + \frac{\partial^2 \varepsilon_x}{\partial y^2} - \frac{\partial^2 \gamma_{xy}}{\partial x \, \partial y},
\end{aligned} \tag{2.41}$$

$$
\begin{aligned}
U_x &= -\frac{\partial^2 \varepsilon_x}{\partial y\,\partial z} + \frac{1}{2}\frac{\partial}{\partial x}\left(-\frac{\partial \gamma_{yz}}{\partial x} + \frac{\partial \gamma_{zx}}{\partial y} + \frac{\partial \gamma_{xy}}{\partial z}\right), \\
U_y &= -\frac{\partial^2 \varepsilon_y}{\partial z\,\partial x} + \frac{1}{2}\frac{\partial}{\partial y}\left(\frac{\partial \gamma_{yz}}{\partial x} - \frac{\partial \gamma_{zx}}{\partial y} + \frac{\partial \gamma_{xy}}{\partial z}\right), \\
U_z &= -\frac{\partial^2 \varepsilon_z}{\partial x\,\partial y} + \frac{1}{2}\frac{\partial}{\partial z}\left(\frac{\partial \gamma_{yz}}{\partial x} + \frac{\partial \gamma_{zx}}{\partial y} - \frac{\partial \gamma_{xy}}{\partial z}\right).
\end{aligned}
\qquad \text{(2.41, continued)}
$$

(d) Stress-strain relations. In small displacement theory, the stress-strain relations are given in linear, homogeneous form :

$$
\begin{bmatrix} \sigma_x \\ \sigma_y \\ \sigma_z \\ \tau_{yz} \\ \tau_{zx} \\ \tau_{xy} \end{bmatrix} = \begin{bmatrix} a_{11} & a_{12} & a_{13} & a_{14} & a_{15} & a_{16} \\ a_{21} & a_{22} & a_{23} & a_{24} & a_{25} & a_{26} \\ a_{31} & a_{32} & a_{33} & a_{34} & a_{35} & a_{36} \\ a_{41} & a_{42} & a_{43} & a_{44} & a_{45} & a_{46} \\ a_{51} & a_{52} & a_{53} & a_{54} & a_{55} & a_{56} \\ a_{61} & a_{62} & a_{63} & a_{64} & a_{65} & a_{66} \end{bmatrix} \begin{bmatrix} \varepsilon_x \\ \varepsilon_y \\ \varepsilon_z \\ \gamma_{yz} \\ \gamma_{zx} \\ \gamma_{xy} \end{bmatrix}. \qquad (2.42)
$$

The coefficients of these equations are called elastic constants. Among them, there exist relations of the form :

$$
a_{rs} = a_{sr}, \quad (r, s = 1, 2, \ldots, 6). \qquad (2.43)
$$

Eqs. (2.42) may be inverted to yield :

$$
\begin{bmatrix} \varepsilon_x \\ \varepsilon_y \\ \varepsilon_z \\ \gamma_{yz} \\ \gamma_{zx} \\ \gamma_{xy} \end{bmatrix} = \begin{bmatrix} b_{11} & b_{12} & b_{13} & b_{14} & b_{15} & b_{16} \\ b_{21} & b_{22} & b_{23} & b_{24} & b_{25} & b_{26} \\ b_{31} & b_{32} & b_{33} & b_{34} & b_{35} & b_{36} \\ b_{41} & b_{42} & b_{43} & b_{44} & b_{45} & b_{46} \\ b_{51} & b_{52} & b_{53} & b_{54} & b_{55} & b_{56} \\ b_{61} & b_{62} & b_{63} & b_{64} & b_{65} & b_{66} \end{bmatrix} \begin{bmatrix} \sigma_x \\ \sigma_y \\ \sigma_z \\ \tau_{yz} \\ \tau_{zx} \\ \tau_{xy} \end{bmatrix}, \qquad (2.44)
$$

where

$$
b_{rs} = b_{sr}, \quad (r, s = 1, 2, \ldots, 6), \qquad (2.45)
$$

are commonly called the stiffness coefficients.

For an isotropic material, the number of the independent elastic constants reduces to 2, and the stress-strain relations are given by :

$$
\begin{aligned}
\sigma_x &= 2G\left[\varepsilon_x + \frac{\nu}{1-2\nu}(\varepsilon_x + \varepsilon_y + \varepsilon_z)\right], \quad \tau_{yz} = G\gamma_{yz}, \\
\sigma_y &= 2G\left[\varepsilon_y + \frac{\nu}{1-2\nu}(\varepsilon_x + \varepsilon_y + \varepsilon_z)\right], \quad \tau_{zx} = G\gamma_{zx}, \\
\sigma_z &= 2G\left[\varepsilon_z + \frac{\nu}{1-2\nu}(\varepsilon_x + \varepsilon_y + \varepsilon_z)\right], \quad \tau_{xy} = G\gamma_{xy},
\end{aligned}
\qquad (2.46)
$$

or, inversely,

$$\begin{aligned} E\varepsilon_x &= \sigma_x - \nu(\sigma_y + \sigma_z), \quad G\gamma_{yz} = \tau_{yz}, \\ E\varepsilon_y &= \sigma_y - \nu(\sigma_z + \sigma_x), \quad G\gamma_{zx} = \tau_{zx}, \\ E\varepsilon_z &= \sigma_z - \nu(\sigma_x + \sigma_y), \quad G\gamma_{xy} = \tau_{xy}. \end{aligned} \tag{2.47}$$

(e) Boundary conditions. The surface of the body can be divided into two parts from the viewpoint of the boundary conditions : the part S_1 over which boundary conditions are prescribed in terms of external forces and the part S_2 over which boundary conditions are prescribed in terms of displacements. Obviously $S = S_1 + S_2$. Denoting the components of the prescribed external forces per unit area of the boundary surface by $\bar{X}_\nu$, $\bar{Y}_\nu$ and $\bar{Z}_\nu$, the mechanical boundary conditions are given by

$$X_\nu = \bar{X}_\nu, \quad Y_\nu = \bar{Y}_\nu, \quad Z_\nu = \bar{Z}_\nu \quad \text{on} \quad S_1, \tag{2.48}$$

where

$$\begin{aligned} X_\nu &= \sigma_x l + \tau_{xy} m + \tau_{zx} n, \\ Y_\nu &= \tau_{xy} l + \sigma_y m + \tau_{yz} n, \\ Z_\nu &= \tau_{zx} l + \tau_{yz} m + \sigma_z n, \end{aligned} \tag{2.49}$$

l, m, n being the direction cosines of the unit normal ν drawn outwards on the boundary : $l = \cos(x, \nu)$, $m = \cos(y, \nu)$ and $n = \cos(z, \nu)$. On the other hand, denoting the components of the prescribed displacements by u, v and w, the geometrical conditions are given by

$$u = \bar{u}, \quad v = \bar{v}, \quad w = \bar{w} \quad \text{on} \quad S_2. \tag{2.50}$$

Thus, we obtain all the governing equations of the elasticity problem in small displacement theory : the equations of equilibrium (2.38), the strain-displacement relation (2.39) and the stress-strain relations (2.42) in the interior V of the body, and the mechanical and geometrical boundary conditions, (2.48) and (2.50), on the surface S of the body. These conditions show that we have 15 unknowns, namely, 6 stress components, 6 strain components and 3 displacement components in the 15 equations (2.38), (2.39) and (2.42). Our problem is then to solve these 15 equations under the boundary conditions (2.48) and (2.50). Since all the governing equations have linear forms, the law of superposition can be applied in solving the problem. Thus, we obtain linear relationships between the prescribed quantities such as the applied load on S_1 and resulting quantities such as stress and displacement caused in the body.

2.5.2 Principle of Minimum Potential Energy [8]

First, it is observed that we can derive a state function $A(\epsilon_x, \epsilon_y, \cdots, \gamma_{xy})$ from the stress-strain relation (2.42), such that

$$\delta A = \sigma_x \delta\varepsilon_x + \sigma_y \delta\varepsilon_y + \cdots + \tau_{xy} \delta\gamma_{xy}, \tag{2.51}$$

where

$$2A = (a_{11}\varepsilon_x + a_{12}\varepsilon_y + \cdots + a_{16}\gamma_{xy})\,\varepsilon_x + \cdots + (a_{61}\varepsilon_x + a_{62}\varepsilon_y + \cdots + a_{66}\gamma_{xy})\,\gamma_{xy}. \tag{2.52}$$

For the stress-strain relations of an isotropic material, namely Eqs. (2.42), we have

$$A = \frac{Ev}{2(1+\nu)(1-2\nu)}(\varepsilon_x + \varepsilon_y + \varepsilon_z)^2 + G(\varepsilon_x^2 + \varepsilon_y^2 + \varepsilon_z^2) + \frac{G}{2}(\gamma_{yz}^2 + \gamma_{zx}^2 + \gamma_{xy}^2). \tag{2.53}$$

We shall refer to A as the strain energy function. (The quantity A is also called the strain energy per unit volume or the strain energy density.) We may assume the strain energy function to be a positive definite function of the strain components. This assumption involves some relations of inequality among the elastic constants. [9]

We have a variational principle called the principle of minimum potential energy : Among all the admissible displacement functions, the actual displacements make the total potential energy

$$\Pi = \iiint_V A(u, v, w)\,dV - \iiint_V (\bar{X}u + \bar{Y}v + \bar{Z}w)\,dV - \iint_{S_1} (\bar{X}_s u + \bar{Y}_s v + \bar{Z}_s w)\,dS, \tag{2.54}$$

an absolute minimum.

2.5.3 Principle of Minimum Complementary Energy [8]

We observe that a state function B (σ_x, σ_y, $\cdots$, τ_{xy}) may be derived from the stress-strain relations (2.44), such that

$$\delta B = \varepsilon_x\,\delta\sigma_x + \varepsilon_y\,\delta\sigma_y + \cdots + \gamma_{xy}\,\delta\tau_{xy}, \tag{2.55}$$

where

$$2B = (b_{11}\sigma_x + b_{12}\sigma_y + \cdots + b_{16}\tau_{xy})\,\sigma_x + \cdots + (b_{61}\sigma_x + b_{62}\sigma_y + \cdots + b_{66}\tau_{xy})\,\tau_{xy}. \tag{2.56}$$

For the stress-strain relations of an isotropic material, namely Eqs. (2.47), we have

$$B = \frac{1}{2E}\{(\sigma_x + \sigma_y + \sigma_z)^2 + 2(1+\nu)(\tau_{yz}^2 + \tau_{zx}^2 + \tau_{xy}^2 - \sigma_y\sigma_z - \sigma_z\sigma_x - \sigma_x\sigma_y)\}. \tag{2.57}$$

We shall refer to B as the complementary energy function. (The quantity B is also called the complementary energy per unit volume, complementary energy density or the stress energy per unit volume.) It is obvious that, the strain energy function A defined by Eq. (2.52) is equal to the complementary energy function B defined by Eq. (2.56) and that, if the former is positive definite, so is the latter. When the existence of the complementary energy function is thus assured, the principle of complementary virtual work can be transformed into :

$$\delta \iiint_V B(\sigma_x, \sigma_y, \ldots, \tau_{xy})\, dV - \iint_{S_2} (\bar{u}\, \delta X_\nu + \bar{v}\, \delta Y_\nu + \bar{w}\, \delta Z_\nu)\, dS = 0. \tag{2.58}$$

Employing the assumption that the quantities u, v and w are kept unchanged during variation, we can derive from Eq. (2.58) a variational principle called the principle of minimum complementary energy : Among all the sets of admissible stresses σ_x, σ_y, $\cdots$, and τ_{xy}, which satisfy the equations of equilibrium and the prescribed mechanical boundary conditions on S_1, the set of actual stress components makes the total complementary energy π_c defined by

$$\Pi_c = \iiint_V B(\sigma_x, \sigma_y, \ldots, \tau_{xy})\, dV - \iint_{S_2} (\bar{u}X_\nu + \bar{v}Y_\nu + \bar{w}Z_\nu)\, dS, \tag{2.59}$$

an absolute minimum.

We observe that the arguments of A are strain components, while those of B are stress components. For the linear stress-strain relations, Eqs. (2.42) and (2.44), B is equal to A and has the same physical meaning : The strain energy stored in a unit volume of the elastic body. It should be noted, however, that when stress-strain relations are nonlinear, B defined by Eq. (2.55) is different from A defined by Eq. (2.51). For example, in the simple case of a bar in tension, we have

$$\sigma_x = \sigma_x(\varepsilon_x), \quad \varepsilon_x = \varepsilon_x(\sigma_x). \tag{2.60}$$

The functions A and B are then given by

$$A = \int_0^{\varepsilon_x} \sigma_x\, d\varepsilon_x, \quad B = \int_0^{\sigma_x} \varepsilon_x\, d\sigma_x. \tag{2.61}$$

These are illustrated in Fig. 2.7 by the shaded area OPS and unshaded area OSR, respectively. It is seen that A and B are complementary to each other in representing the area OPSR, namely $A + B = \sigma_x \epsilon_x$.

2.5.4 Compatible Displacement Function

The equilibrium relation between the stiffness matrix and, nodal force vector expressed in the form of Eq. (2.5) is based on the fundamental principles mentioned in the former section. Apparent, numerical method such as FEM may be considered as quite a different analytical method from the conventional ones used in the analyses of continuum mechanics, but it is not true. So long as the assumption on displacement of points in an element, that is, displacement functions

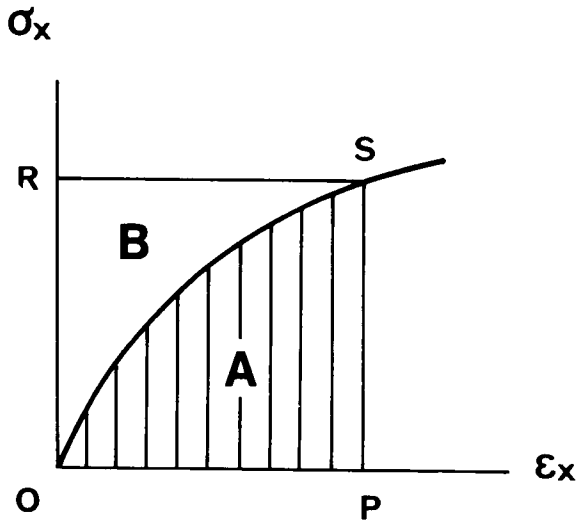

Fig. 2.7 Strain and Complementary Energies in a Uniaxial Tension [8]

are satisfied with compatibility, discretization to finite elements is verified to be considered as a system of continuum as a whole.

In FEM, there are several feasible shapes for the representation of element. For two-dimensional analysis, triangle and rectangle are representative, and tetrahedron, pentahedron, triangular prism, hexahedron, rectangular prism and so on are employed for three dimensional problem as shown Fig. 2.8 (a), (b).

Let us talk about how to obtain compatible displacement functions. For example, when displacement function is given in the forms of

$$\begin{Bmatrix} u \\ v \end{Bmatrix} = \begin{bmatrix} 1 & x & y & 0 & 0 & 0 \\ 0 & 0 & 0 & 1 & x & y \end{bmatrix} \begin{Bmatrix} \alpha_1 \\ \alpha_2 \\ \vdots \\ \alpha_6 \end{Bmatrix} \tag{2.62}$$

where u and v are the linear function with respect to x and y. Coefficients $\alpha_1, \alpha_2, \cdots, \alpha_6$ are determined by nodal displacement and nodal coordinates.

According to Eq. (2.62), displacement of an arbitrary point on a side of a triangular element is specified uniquely as the linear function by the displacements of nodes at both corner. This matter seems to be simple, but significant. Namely, when the displacement function such as

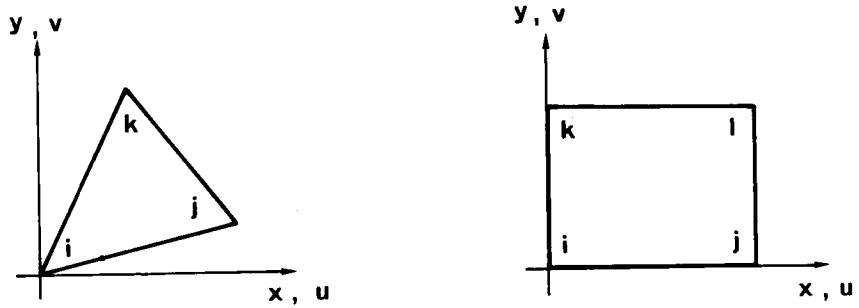

Fig. 2.8 (a) Two-dimensional Elements

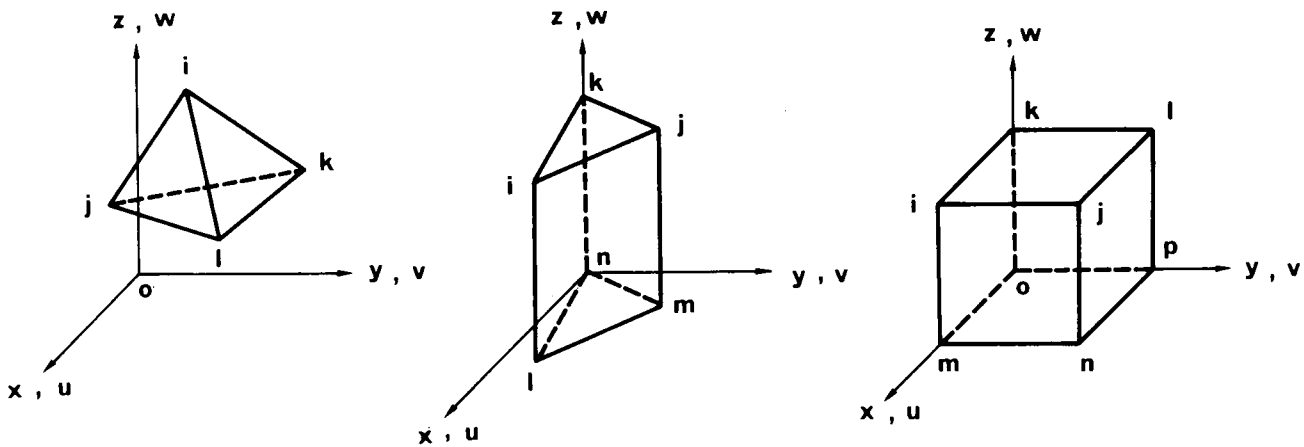

Fig. 2.8 (b) Three-dimensional Elements

Eq. (2.62) is assumed, it promises that there never happen " aperture " (as shown in Fig. 2.9 (a)) or " overlap " between elements. These " aperture " and " overlap " come from the application of unappropriate displacement function, and never guarantee the convergence to true solution even if finer elements are employed, so it means that displacement function should be assumed correctly.

(a) (b)

Fig. 2.9 Aperture and Overlap of Finite Elements

Here, let us discuss on how to confirm appropriateness of displacement functions for five cases, corresponding to five types of elements shown in Fig. 2.8, based on the conditions of compatibility as shown in Eq. (2.40).

a) For example, to pick up the function of Eq. (2.9) or Eq. (2.10), since all components of Matrix [R] can be obtained by differentiating strain to second order, it is clear [R] = 0, and Eq. (2.40) is satisfied.

b) For a rectangular element as shown in Fig. 2.8 (b), the number of displacement components regarding the element becomes eight. It means that the function $\{\alpha\}$ must be eight-dimensional vector.

When we assume the following displacement function,

$$\begin{Bmatrix} u \\ v \end{Bmatrix} = \begin{bmatrix} 1 & x & y & xy & 0 & 0 & 0 & 0 \\ 0 & 0 & 0 & 0 & 1 & x & y & xy \end{bmatrix} \begin{Bmatrix} \alpha_1 \\ \alpha_2 \\ \vdots \\ \alpha_8 \end{Bmatrix} \qquad (2.63)$$

strain is expressed in the form of

$$\begin{Bmatrix} \epsilon_x \\ \epsilon_y \\ \tau_{xy} \end{Bmatrix} = \begin{bmatrix} 0 & 1 & 0 & y & 0 & 0 & 0 & 0 \\ 0 & 0 & 0 & 0 & 0 & 0 & 1 & x \\ 0 & 0 & 1 & x & 0 & 1 & 0 & y \end{bmatrix} \begin{Bmatrix} \alpha_1 \\ \alpha_2 \\ \vdots \\ \alpha_8 \end{Bmatrix} \tag{2.64}$$

From Eq. (2.64), it is verified [R] = 0.

c) For a tetrahedron element, $\{\alpha\}$ should be twelve dimensional vector.

Assuming

$$\begin{Bmatrix} u \\ v \\ w \end{Bmatrix} = \begin{bmatrix} 1 & x & y & z & 0 & 0 & 0 & 0 & 0 & 0 & 0 & 0 \\ 0 & 0 & 0 & 0 & 1 & x & y & z & 0 & 0 & 0 & 0 \\ 0 & 0 & 0 & 0 & 0 & 0 & 0 & 0 & 1 & x & y & z \end{bmatrix} \begin{Bmatrix} \alpha_1 \\ \alpha_2 \\ \vdots \\ \alpha_{12} \end{Bmatrix} \tag{2.65}$$

we obtain

$$\begin{Bmatrix} \epsilon_x \\ \epsilon_y \\ \epsilon_z \\ \gamma_{yz} \\ \gamma_{zx} \\ \gamma_{xy} \end{Bmatrix} = \begin{Bmatrix} \frac{\partial u}{\partial x} \\ \frac{\partial v}{\partial y} \\ \frac{\partial w}{\partial z} \\ \frac{\partial w}{\partial y} + \frac{\partial v}{\partial z} \\ \frac{\partial u}{\partial z} + \frac{\partial w}{\partial x} \\ \frac{\partial v}{\partial x} + \frac{\partial u}{\partial y} \end{Bmatrix} \begin{bmatrix} 0 & 1 & 0 & 0 & 0 & 0 & 0 & 0 & 0 & 0 & 0 & 0 \\ 0 & 0 & 0 & 0 & 0 & 0 & 1 & 0 & 0 & 0 & 0 & 0 \\ 0 & 0 & 0 & 0 & 0 & 0 & 0 & 0 & 0 & 0 & 0 & 1 \\ 0 & 0 & 0 & 0 & 0 & 0 & 0 & 1 & 0 & 0 & 1 & 0 \\ 0 & 0 & 0 & 1 & 0 & 0 & 0 & 0 & 0 & 1 & 0 & 0 \\ 0 & 0 & 1 & 0 & 0 & 1 & 0 & 0 & 0 & 0 & 0 & 0 \end{bmatrix} \begin{Bmatrix} \alpha_1 \\ \alpha_2 \\ \vdots \\ \alpha_{12} \end{Bmatrix} \tag{2.66}$$

as [R] = 0 is clear from Eq. (2.66), Eq. (2.65) is compatible as displacement functions for a tetrahedron element.

d) For a rectangular prism element (in GEOFEM, this type of element is employed so conveniently specially in geomechanical problems because of the easy adaptability of the same system for display of computed results (i.e. graphic display, plotter or sometimes line printer) as application programme prepared for two-dimensional problems. For example, the design of bridge foundation on the multiple complex formations was carried out quite successfully. As known well among practical people, it is necessary condition for the daily application of three dimensional FEM programme to display OUTPUT in adequate way so as to make engineers understand better three dimensional state of stresses, strains and displacement on sheets of paper, which spread only in two-dimensional plane.

Assuming the displacement function in terms of

$$\begin{Bmatrix} u \\ v \\ w \end{Bmatrix} = \begin{bmatrix} 1 & x & y & z & xz & yz & 0 & 0 & 0 & 0 & 0 & 0 & 0 & 0 & 0 & 0 & 0 & 0 \\ 0 & 0 & 0 & 0 & 0 & 0 & 1 & x & y & z & xz & yz & 0 & 0 & 0 & 0 & 0 & 0 \\ 0 & 0 & 0 & 0 & 0 & 0 & 0 & 0 & 0 & 0 & 0 & 0 & 1 & x & y & z & xz & yz \end{bmatrix} \begin{Bmatrix} \alpha_1 \\ \alpha_2 \\ \vdots \\ \alpha_{18} \end{Bmatrix} \quad (2.67)$$

we obtain

$$\begin{Bmatrix} \epsilon_x \\ \epsilon_y \\ \epsilon_z \\ \gamma_{yz} \\ \gamma_{zx} \\ \gamma_{xy} \end{Bmatrix} = \begin{bmatrix} 0 & 1 & 0 & 0 & z & 0 & 0 & 0 & 0 & 0 & 0 & 0 & 0 & 0 & 0 & 0 & 0 & 0 \\ 0 & 0 & 0 & 0 & 0 & 0 & 0 & 0 & 1 & 0 & 0 & z & 0 & 0 & 0 & 0 & 0 & 0 \\ 0 & 0 & 0 & 0 & 0 & 0 & 0 & 0 & 0 & 0 & 0 & 0 & 0 & 0 & 0 & 1 & x & y \\ 0 & 0 & 0 & 0 & 0 & 0 & 0 & 0 & 0 & 1 & x & y & 0 & 0 & 1 & 0 & 0 & z \\ 0 & 0 & 0 & 1 & x & y & 0 & 0 & 0 & 0 & 0 & 0 & 0 & 1 & 0 & 0 & z & 0 \\ 0 & 0 & 1 & 0 & 0 & z & 0 & 1 & 0 & 0 & z & 0 & 0 & 0 & 0 & 0 & 0 & 0 \end{bmatrix} \begin{Bmatrix} \alpha_1 \\ \cdot \\ \cdot \\ \cdot \\ \cdot \\ \cdot \\ \cdot \\ \cdot \\ \cdot \\ \alpha_{18} \end{Bmatrix} \quad (2.68)$$

Hence, [R] = 0.

e) For a rectangular prism with the displacement function in the form of

$$\begin{Bmatrix} u \\ v \\ w \end{Bmatrix} = \begin{bmatrix} 1 & x & y & z & yz & zx & xy & xyz & 0 & 0 & 0 & 0 & 0 & 0 & 0 & 0 & 0 & 0 & 0 & 0 & 0 & 0 \\ 0 & 0 & 0 & 0 & 0 & 0 & 0 & 0 & 1 & x & y & z & yz & zx & xy & xyz & 0 & 0 & 0 & 0 & 0 & 0 & 0 & 0 \\ 0 & 0 & 0 & 0 & 0 & 0 & 0 & 0 & 0 & 0 & 0 & 0 & 0 & 0 & 0 & 0 & 1 & x & y & z & yz & zx & xy & xyz \end{bmatrix} \begin{Bmatrix} \alpha_1 \\ \alpha_2 \\ \cdot \\ \cdot \\ \alpha_{24} \end{Bmatrix}$$

(2.69)

$$\begin{Bmatrix} \epsilon_x \\ \epsilon_y \\ \epsilon_z \\ \gamma_{yz} \\ \gamma_{zx} \\ \gamma_{xy} \end{Bmatrix} = \begin{bmatrix} 0 & 1 & 0 & 0 & 0 & z & y & yz & 0 & 0 & 0 & 0 & 0 & 0 & 0 & 0 & 0 & 0 & 0 & 0 & 0 & 0 & 0 & 0 \\ 0 & 0 & 0 & 0 & 0 & 0 & 0 & 0 & 0 & 0 & 1 & 0 & z & 0 & x & xz & 0 & 0 & 0 & 0 & 0 & 0 & 0 & 0 \\ 0 & 0 & 0 & 0 & 0 & 0 & 0 & 0 & 0 & 0 & 0 & 0 & 0 & 0 & 0 & 0 & 0 & 0 & 0 & 1 & y & x & 0 & xy \\ 0 & 0 & 0 & 0 & 0 & 0 & 0 & 0 & 0 & 0 & 0 & 1 & y & x & 0 & xy & 0 & 0 & 1 & 0 & z & 0 & x & xz \\ 0 & 0 & 0 & 1 & y & x & 0 & xy & 0 & 0 & 0 & 0 & 0 & 0 & 0 & 0 & 1 & 0 & 0 & 0 & z & y & yz \\ 0 & 0 & 1 & 0 & z & 0 & x & xz & 0 & 1 & 0 & 0 & 0 & z & y & yz & 0 & 0 & 0 & 0 & 0 & 0 & 0 & 0 \end{bmatrix} \begin{Bmatrix} \alpha_1 \\ \alpha_2 \\ \vdots \\ \alpha_{24} \end{Bmatrix}$$

(2.70)

As the matrix [R] is expressed in terms of

$$[R] = \begin{bmatrix} Rx & Uz & Uy \\ Uz & Ry & Ux \\ Uy & Ux & Rz \end{bmatrix}$$

respective matrix elements can be represented as follows :

$$Rx = -\frac{\partial}{\partial y}([\ 0\ 0\ 0\ 0\ 0\ 0\ 0\ 0\ 0\ 0\ 0\ 0\ 0\ 0\ 0\ 0\ 0\ 0\ 0\ 0\ 0\ 1\ 0\ 0\ x\ ]\{\alpha\}) = 0$$

$$Ry = -\frac{\partial}{\partial z}([\ 0\ 0\ 0\ 0\ 0\ 1\ 0\ y\ 0\ 0\ 0\ 0\ 0\ 0\ 0\ 0\ 0\ 0\ 0\ 0\ 0\ 0\ 0\ 0\ ]\{\alpha\}) = 0$$

$$Rz = -\frac{\partial}{\partial x}([\ 0\ 0\ 0\ 0\ 0\ 0\ 0\ 0\ 0\ 0\ 0\ 0\ 0\ 0\ 1\ z\ 0\ 0\ 0\ 0\ 0\ 0\ 0\ 0\ ]\{\alpha\}) = 0$$

$$Ux = -\frac{\partial}{\partial y}([0\ 0\ 0\ 0\ 0\ 1\ 0\ y\ 0\ 0\ 0\ 0\ 0\ 0\ 0\ 0\ 0\ 0\ 0\ 0\ 0\ 0\ 0\ 0\ ]\{\alpha\})$$

$$+\frac{1}{2}\frac{\partial}{\partial x}(\{-[\ 0\ 0\ 0\ 0\ 0\ 0\ 0\ 0\ 0\ 0\ 0\ 0\ 0\ 0\ 1\ 0\ y\ 0\ 0\ 0\ 0\ 0\ 0\ 1\ z\ ]$$

$$+[\ 0\ 0\ 0\ 0\ 1\ 0\ 0\ x\ 0\ 0\ 0\ 0\ 0\ 0\ 0\ 0\ 0\ 0\ 0\ 0\ 0\ 0\ 0\ 1\ z\ ]$$

$$+[\ 0\ 0\ 0\ 0\ 1\ 0\ 0\ x\ 0\ 0\ 0\ 0\ 0\ 1\ 0\ y\ 0\ 0\ 0\ 0\ 0\ 0\ 0\ 0\ ]\{\alpha\})$$

$$= -[\ 0\ 0\ 0\ 0\ 0\ 0\ 0\ 1\ 0\ 0\ 0\ 0\ 0\ 0\ 0\ 0\ 0\ 0\ 0\ 0\ 0\ 0\ 0\ 0\ ]\{\alpha\}$$

$$+[\ 0\ 0\ 0\ 0\ 0\ 0\ 0\ 1\ 0\ 0\ 0\ 0\ 0\ 0\ 0\ 0\ 0\ 0\ 0\ 0\ 0\ 0\ 0\ 0\ ]\{\alpha\} = 0$$

In the same way, Uy = Uz = 0

Then, [R] = 0 verifies the compatibility of Eq. (2.69). Consequently, these five types of displacement functions, mentioned above, were verified to satisfy compatibility according to the variational principle in continuum mechanics, so in the programme of GEOFEM, coded by the author, four types of elements except tetrahedron are employed in daily uses.

2.6 Iterative Method for Solving Simultaneous Linear Equation

FEM is an epochmaking structural analysis for universal usage, and has developed simultaneously with the increasing use of high-speed electronic digital computers and with the growing emphasis on numerical methods for engineering analysis. As a matter of course, the most essential condition is for engineers, who wish to apply FEM reasonably, to develop their own programming for featured usages, and specially in the field of geomechanics, in which engineers have to be confronted to many uncertainties at the determination of INPUT data and are often required to carry out parametric analyses, it is suggested from the practical point of view not to make computer programme " Black Box " by giving INPUT automatically or without any check by engineers' hands. Regarding the routined works for practical engineers, Fig. 2.10 illustrates the flow of respective procedure in FEM analysis.

Due to the discretization of practical structure model, it is required to solve simultaneous linear equations with several hundreds or thousands unknown factors. This is the characteristic reason of FEM for the association with very capacious computers. It must be common that people, who have engaged in practical coding of FEM for themselves, have consumed so many hours to establish their own way to reduce necessary memory size, and understood that, even if it is required to employ a model consisting of only 100 nodal points subjected to simple elastic behavior, it is almost impossible practically to apply Cramer's or Gauss-Jordan elimination methods because of demanding for extraordinarily large capacity and too long time. As the practical methods for solving simultaneous linear equations, Wavefront method, Newton-Raphson method, Cholesky's square root method, Conjugated Gradient method, Bernoulli Iterative method, Bairstow Iterative method, Gauss-Seidel Iterative method and so on can be picked up. [13], [14], [15], [16]

The author made choice of Gauss-Seidel Iterative method with " Successive-Over-Relaxation " procedure (hereafter, abbreviated SOR) according to its simple applicability to large size of stiffness matrix [K], which contains many zero factors.

Now, let us talk about Gauss-Seidel Iterative method combined with SOR.

Denoting coefficient matrices of whole matrix, below-diagonal, diagonal, above-diagonal ; vector of unknown ; vector of constant and unit matrix, A, E, D, F ; B ; U and e_i, respectively ($A = E + D + F$ is recognized.), simultaneous linear equations can be expressed in the form of

$$AU = B \tag{2.71}$$

In the case of solving by means of Gauss-Seidel Iterative method (hereafter, abbreviated GSIM), Eq. (2.71) is rewritten in the form of

$$EU + DU + FU = B \tag{2.72}$$

Following iteration procedure step by step, Eq. (2.72) is specified by the following equation,

$$EU^{(k)} + DU^{(k)} + FU^{(k-1)} = B \tag{2.73}$$

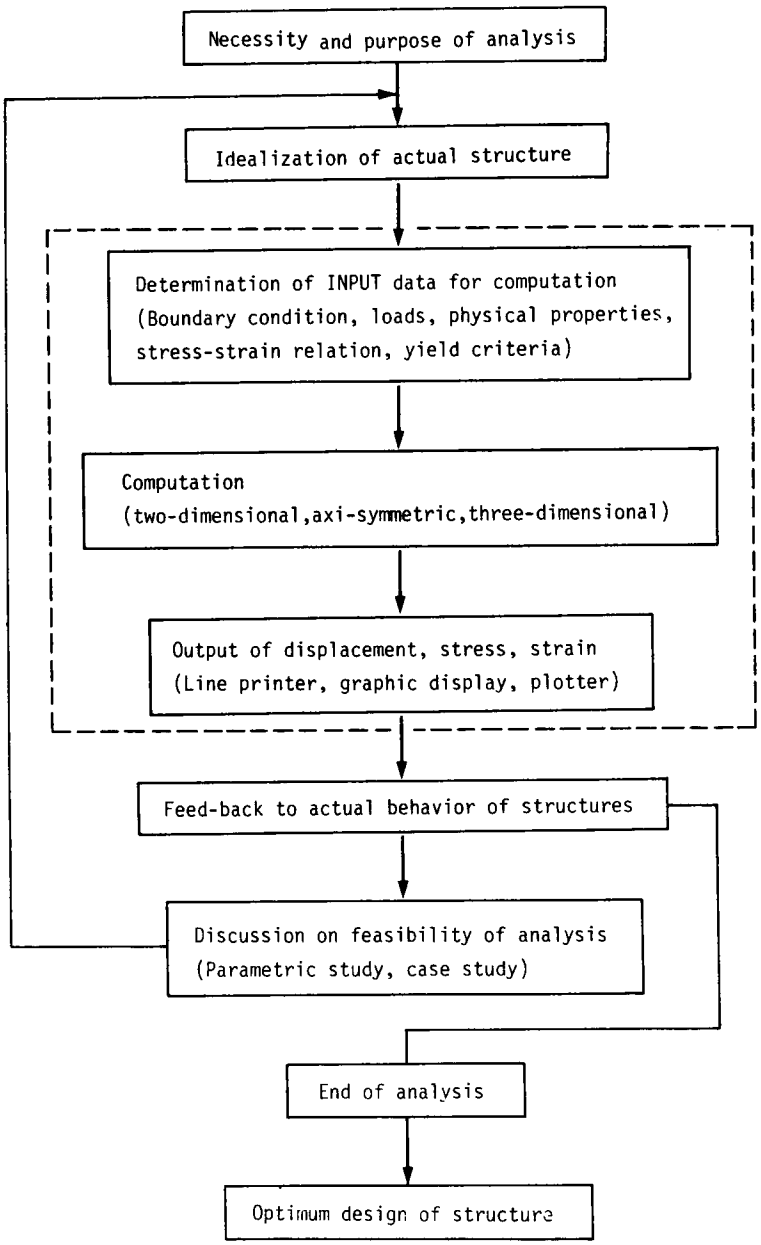

Fig. 2.10 Analytical Procedure of FEM

where $U^{(k)}$: solutions obtained in (k)-th cycle,
and $U^{(k-1)}$: solutions obtained in (k − 1)-th cycle.

In order to get higher approximation, coefficient α, which minimizes

$$E\left(U^{(k-1)} + \alpha e_i\right),$$

is introduced, and it means to calculate

$$U^{(k)} = U^{(k-1)} + \alpha e_i \tag{2.74}$$

by employing α.

For this relation, when SOR is applied, Over-Relaxation-Factor, ω, is employed, and it is introduced in the form of

$$U^{(k)} = U^{(k-1)} + \omega\alpha e_i \tag{2.75}$$

This ω accelerates the degree of approximation much higher than the case of Eq. (2.74). By using Eq. (2.74),

$$U^{(k)} = U^{(k-1)} + \omega\left(U^{(k-0.5)} - U^{(k-1)}\right)$$

that is,

$$U^{(k)} = \omega U^{(k-0.5)} + (1-\omega)U^{(k-1)} \tag{2.76}$$

To combine Eq. (2.73), we obtain

$$\left(E + \omega^{-1}D\right)U^{(k)} + \left[F + (1-\omega^{-1})D\right]U^{(k-1)} = B \tag{2.77}$$

The solution of this equation converges for $0 < \omega < 2.0$, but the range of $0 < \omega < 1$ is meanless in practice. The notation of $U^{(k-0.5)}$ corresponds with the amount of $U^{(k)}$ when ω is not employed.

Now, let us discuss the practical efficiency of ω through several examples in terms of which the author investigated the relation between values of ω and required cycles of iteration until reaching specified accuracy (the degree of approximation).

Judgement of convergency is determined by the amount of $C^{(k)}$, defined by

$$C^{(k)} = B - AU^{(k)} \tag{2.78}$$

is such a manner as to consider satisfactory convergence when the sum of absolute value of respective component becomes less than specified accuracy. In FEM, this amount of $C^{(k)}$ means unbalanced forces at nodal points.

Fig. 2.11 (a), (b) and (c) show examples of simple discretization, and with respect to various values of ω, the author investigated the relations between specified approximation (denoted ϵ)

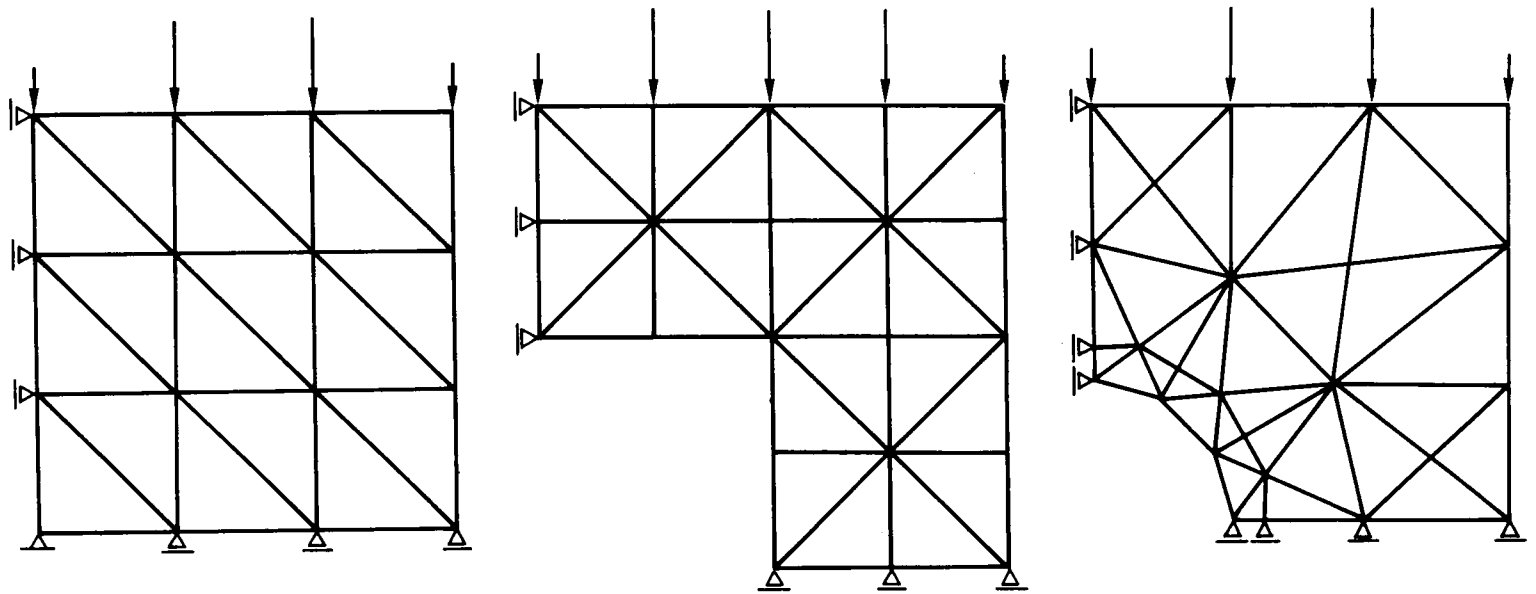

(a) Case – (1)

(b) Case – (2)

(c) Case – (3)

Fig. 2.11 Discretization

and required cycles of iteration under the condition of $\epsilon = 10^{-4}$. Corresponding with the discretizations as shown in Fig. 2.11 (a), (b) and (c), Curves (1), (2) and (3) in Fig. 2.12 show the results, respectively. ω which gives minimum value of n shows optimum value of ω, that is, ω_{opt}. of (1) - (3).

The values of ω_{opt} for respective case are

$\omega_{opt} = 1.4,\ 1.8$ and 1.8.

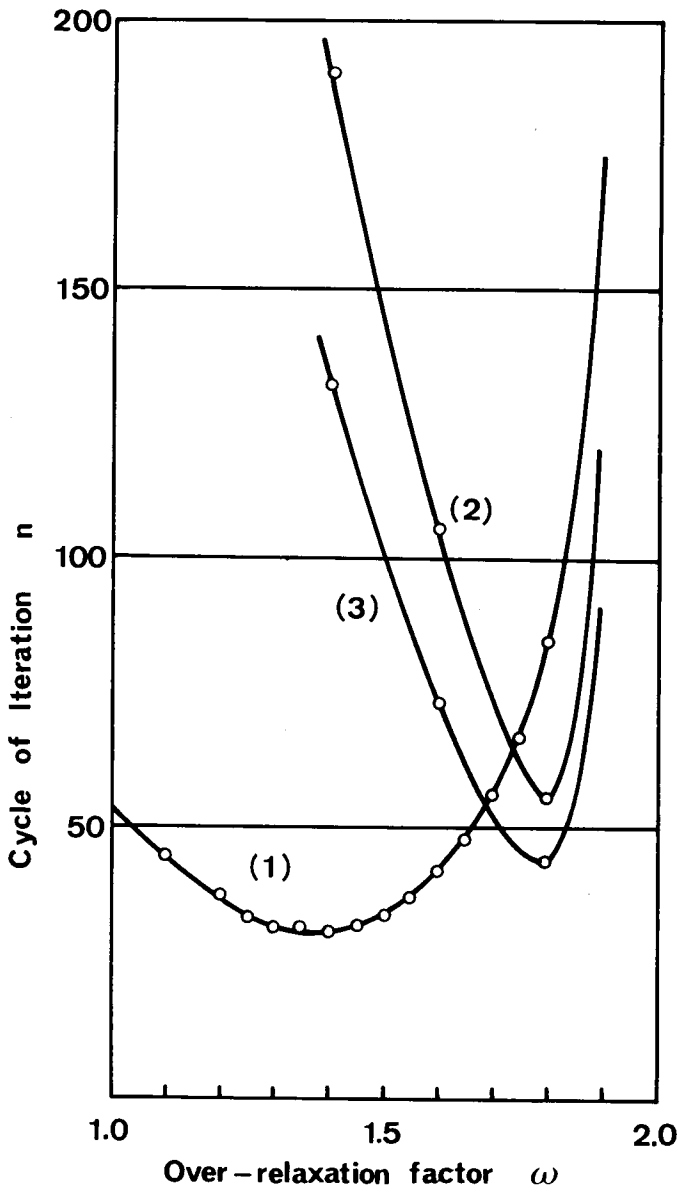

Fig. 2.12 n–ω Relation

Next, the investigation regarding the example, which is consisted of 162 elements and 104 nodes as shown in Fig. 2.13, conclude the relations between required time t (in second) and ω, and between n and ω under the condition of $\epsilon = 5 \times 10^{-4}$ as shown in Fig. 2.14. Judging from this results, it is known that cycles of iteration can be reduced so remarkably if optimum factor ω_{opt} is given. Thus, as a whole it is concluded that the higher accuracy is required, the more ω_{opt} plays an important role. (ω_{opt} is money saving factor in computation.)

Regarding case (4) (as shown in Fig. 2.13), the author tried to analyze furthermore about the relation between unbalanced forces and cycles of iteration. Fig. 2.15 shows unbalanced forces at respective nodes A and B in Fig. 2.13 with thin solid lines and norms of convergence δ and δ' for $\omega = 1.85$ and 1.76. Norm of convergence (ϵ) can be expressed by the ratio (δ) of, the total sum of absolute values of unbalanced forces in a certain cycle versus the one in first cycle of iteration. Lines (1) - (5) and (6) - (10) were obtained for $\omega = 1.85$ and 1.76. Thick lines of (5) and (10) are with respect to δ, and others show the reduction of norm related to displacement as a component in x- or y- direction at respective nodal point. From this figure, we recognize that the decreases (or norms) regarding displacement and regarding unbalanced force show common tendency with equal constant gradient, γ.

Therefore, the accuracy of solution (regarding displacement) can be specified by the ratio of the total unbalance force to the one in the first cycle.

Next, let us consider how to determine optimum value of ω_{opt} mathematically.

The convergency of solution in Eq. (2.77) is governed by the maximum absolute eigen value, μ_1, among eigen values μ_i in Matrix $H(\omega)$ which is defined by following equation :

$$H(\omega) = -(\omega^{-1}D + E)^{-1}\,[F + (1 - \omega^{-1})D] \tag{2.79}$$

μ_i is obtained as the root of

$$\det.\,[(\omega^{-1} + E)\mu + (1 - \omega^{-1})D + F] = 0 \tag{2.80}$$

On the other hand, let us make λ_i the root of

$$\det.\,(E + D\lambda + F) = 0 \tag{2.81}$$

According to the theory of D. Young [17], above mentioned ratio γ corresponds with μ_i, and it is given in the form of

$$\sqrt{\mu_i} = \frac{1}{2}\left\{\omega\lambda_i + \sqrt{\omega^2\lambda_i^2 - 4(\omega-1)}\right\} \tag{2.82}$$

Also, it is known that ω_{opt} is determined by the value of ω which minimizes $|\mu_i|$. From Eq. (2.82),

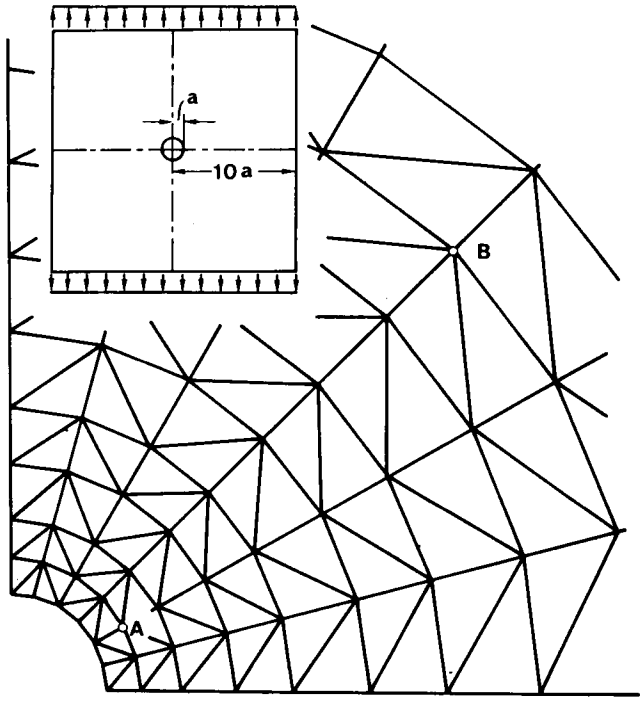

Fig. 2.13 Discretization with Rather Fine Mesh (Case–(4))

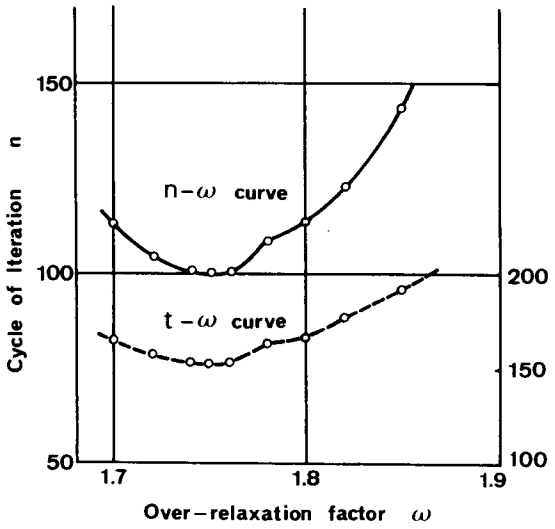

Fig. 2.14 n–ω Relation for Case – (4)

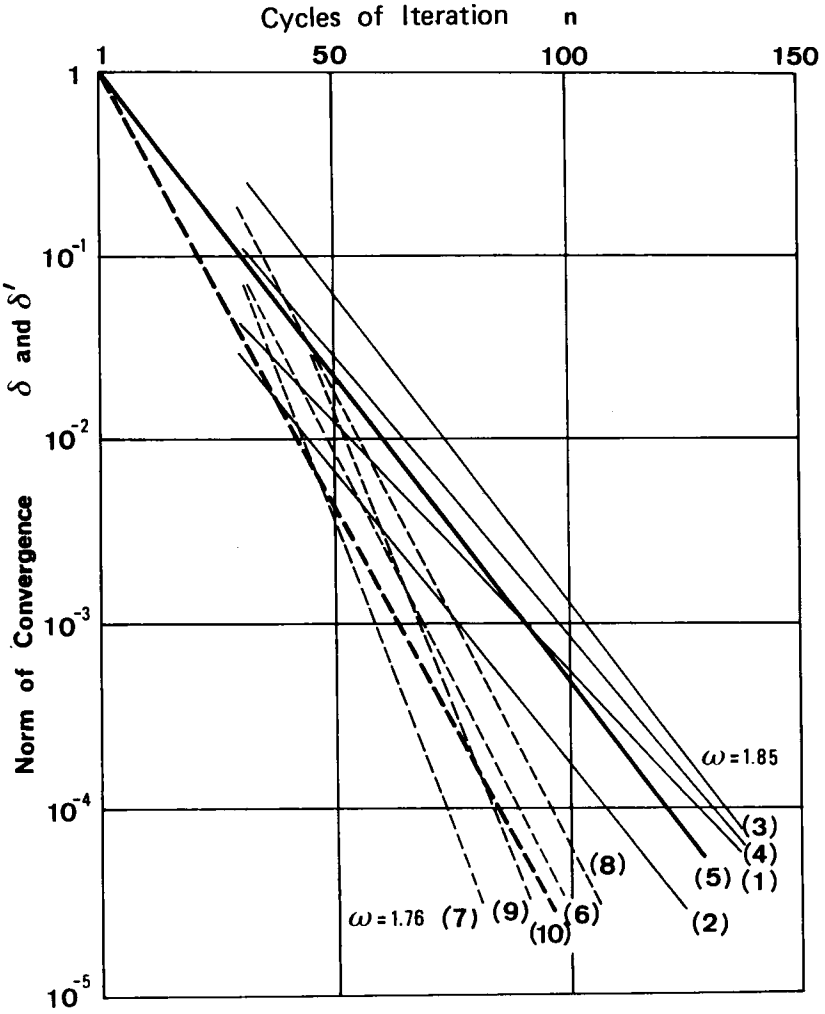

Fig. 2.15 Relation between Convergence Norm and Cycles of Iteration

$$\frac{d\sqrt{\mu_i}}{d\omega} = -\frac{1}{2}\frac{1-\lambda_i\sqrt{\mu_i}}{\sqrt{\mu_i}-\omega\lambda_i/2} \tag{2.83}$$

Eq. (2.83) gives the condition of minimization as follows :

$$\omega_{opt} = \frac{2}{1+\sqrt{1-\lambda_1{}^2}} \tag{2.84}$$

where $\lambda_1{}^2$ represents maximum of $\lambda_i{}^2$.

Consequently, the presumption of optimum ω_{opt} is attributed to eigen value problem, and no practical proposal has not yet been found in publication. As R. Clough recommended to use empirical value in practice [18], it seems to be the best way to presume ω_{opt} for new calculation judging from similar cases experienced in the past. In the case of the author's, $\omega = 1.75 - 1.80$ is given to the discretization model, having several hundreds nodal points.

REFERENCES for Chapter 2

[1] Zienkiewicz, O.C., Cheung, Y.K. : Application of the finite element method to problems of rock mechanics, Proceedings of 1st Congress of ISRM, 1966.

[2] Grishin, M.M., Schimelmitz : The effect of heterogeneous character of rock foundation on the stresses on concrete dams investigated experimentally, Proceedings of 1st Congress of ISRM, 1966.

[3] Anderson, H.W., Dodd, J.S. : Finite element method applied to rock mechanics, Proceedings of 1st Congress of ISRM, 1966.

[4] Reyes, S.F., Deere, D.U. : Elastic-plastic analysis of underground openings by finite element method, Proceedings of 1st Congress of ISRM, 1966.

[5] Goodman, R.E. : On the distribution of stresses around circular tunnels in non-homogeneous rocks, Proceedings of 1st Congress of ISRM, 1966.

[6] Desai, C.S., Abel, J.F. : Introduction to the finite element method for engineering analysis, Van Nostrand Reinhold Co., 1972.

[7] Timoshenko, S., Goodier, J.N. : Theory of Elasticity, McGraw-Hill, 2nd Edition, 1951.

[8] Washizu, K. : Variational principle in continuum mechanics, University of Washington, Dept. of Aeronautical Engg. Report 62–2, 1962.

[9] Love, A.E.H. : A Treatise on the Mathematical Theory of Elasticity, Cambridge University Press, 4th edition, 1927.

[10] Moriguchi, S. : Fundamental Theory of Dislocation of Elastic Bodies (in Japanese), Oyo-Sugaku-Rikigaku, Vol. 1, No. 2, pp.87–90, 1947.

[11] Pearson, C. : Theoretical Elasticity, Harvard University Press, 1959.
[12] Novozhilov, V.V. : Theory of Elasticity, Translated by J.K. Lusher, Pergamon Press, 1961.
[13] Weaver, W. : Computer Programs for Structural Analysis, D. Van Nostrand Co., N.Y., 1967.
[14] Yamaguchi, Moriguchi, Hitotsumatsu : Numerical method for computer, Vol. I, II, Baihukan, 1964. (in Japanese)
[15] Varga, R. : Matrix Iterative Analysis, Prentice-Hall/Maruzen, 1962.
[16] Moriguchi, S. : Introduction to ALGOL, Nihonkagakugijutsu-Renmei, 1962. (in Japanese)
[17] Young, D. : Trans. Amer. Math. Soc. 76, pp.184–187, 1954.
[18] Zienkiewicz, Holister : Stress analysis, John Wiley, 1965.

Chapter 3

EXPERIMENTAL STUDY ON THE DYNAMIC TENSILE STRENGTH OF ROCKS*

3.1 Introduction

The determination of the dynamic tensile strength of the rock substance is one of the most important studies in the blasting research project conducted at the present time, because the phenomena of the crater or the broken ground due to the explosion should be principally based on the stress distribution induced in the rock ground and its dynamic tensile strength.

In the Canadian Mining Research Laboratories, where the author had studied in 1966 ~ 67, an experimental study on the dynamic tensile strength of rocks has been conducted by using a modified Hopkinson Bar apparatus [1].

In this experimental study, the cylindrical rock specimen was used, and a No. 8 electric cap fired at one end of the specimen as impacting load.

The compressive stress wave induced at the end of the specimen is propagated along its axis and reflected at the other end as a tensile stress wave. Consequently, if the peak stress of the propagated wave at the free end is higher than the dynamic tensile strength of rock, the spalling phenomenon must be observed in the vicinity of the free end of the specimen.

The stress wave shape can be obtained by measuring the displacement versus time relationship at the free end, and the dynamic tensile strength of rock can be determined from the observed stress wave shape.

In order to measure the displacement of the free end of the specimen, the capacitance gauge system was used.

In this study, the propagation velocity of the induced stress wave, the stress wave shape, the stress attenuation of the stress wave with its propagation, and the dynamic strengths of rock are obtained, using quartzite, magnetite and limestone as rock specimens.

Especially, the dynamic tensile strength of rock is determined under the considerations of the decay of the stress wave with its propagation and the influence of the dynamic loading time to its strength.

Incidentally, the dynamic compressive strength of rocks used is also obtained and compared with the static strength.

---

* Experimental Study on the Dynamic Tensile Strength of Rocks, Divisional Report FMP 67/43–MRL, Fuels and Mining Practice Division, Mines Branch, Department of Energy, Mines and Resources, Canada, 1967. (Coauthor : Makoto Terada)

3.2 Principles of the Experiment

When the plane compressive stress wave, induced at an end of the cylindrical specimen which has relatively large length in comparison with its diameter, is propagated along its axis, it is well known that the stress level in the propagating wave can be expressed by the following equation :

$$\sigma = \rho C v \tag{3.1}$$

where σ is the stress level, ρ is the density of the specimen, C is the propagation velocity of the longitudinal wave, and v is the particle velocity corresponding to the stress level.

If the density, the propagation velocity and the particle velocity in the stress wave can be measured, the stress level in the wave can be calculated by using the equation (3.1).

If this stress wave is projected on the free surface, perpendicular to the propagating direction of the wave, the incident compressive stress wave is reflected perfectly as a tensile stress wave, and the reflected wave returns on the same route to the incident wave. Consequently, the free surface is displaced towards the propagating direction of the incident wave. According to the acoustic theory, the relation between the displacement of the free surface and the particle velocity in the incident stress wave at the free surface can be expressed by the following simple differential equation:

$$v = \frac{1}{2}\frac{dU}{dt} \tag{3.2}$$

where v is the particle velocity, U is the displacement of the free surface, and t is the time.

In this experiment, the particle velocity versus time relation of the stress wave induced in each shot was obtained by differentiating graphically the half displacement measured at the free end of the specimen with time.

On the other hand, the mean propagation velocity can be calculated by measuring the length of the specimen and the propagating time of the stress wave for its length as follows :

$$\overline{C}_i = \frac{l_i}{t_i} \tag{3.3}$$

where $\overline{C}_i$ is the mean propagation velocity obtained from the specimen with length l_i, and t_i is the propagating time.

Repeating the experiment by using specimens of various lengths under the same condition, the local propagation velocity with increasing distance from the shot point can be calculated. Using several of the specimens with different lengths, l_i and l_{i-1} the local mean propagation velocity, C_i, between the points at the distance l_i and l_{i-1} from the shot point can be calculated by the following equation :

$$C_i = \frac{l_i - l_{i-1}}{t_i - t_{i-1}} \tag{3.4}$$

where $l_i > l_{i-1}$, and t_i and t_{i-1}, respectively, are the propagating times obtained by using the specimens of lengths l_i and l_{i-1}. If the difference between l_i and l_{i-1}, is as short as possible, C_i must represent the local propagation velocity at the distance l_i from the shot point.

In this experimental study, the following assumptions are made. First, the stress wave generated in and propagated through the cylindrical rock specimen is plane, and next, the incident compressive stress wave at the free end of the specimen is perfectly reflected as a tensile stress wave with the same stress wave shape to the incident wave.

Now, let us assume that the stress distribution of the propagated wave in the rock specimen is a triangle, as shown in Fig. 3.1, and that, for easy consideration, it does not decay with its propagation. Fig. 3.1 (a) indicates the location of the stress wave when the front of the compressive wave propagated from the shot point arrives at the free end of the specimen ; (b) indicates the location when a part of the reflected tensile wave returns from the free end of the specimen and spalling just occurs. The thick solid line indicates the compounded stress distribution near the free end of the specimen, and the downward direction in the ordinate shows the tension. When the tensile peak of this compounded stress level exceeds the dynamic tensile strength of the rock, tensile fracture, that is, spalling occurs at the point where its stress level is induced. The spall runs from the main body of the specimen towards the direction of the free end by the energy of the stress wave transferred into itself. Consequently, the stress wave transferred in the spall repeats the reflection between the new spalling surface and the existing free end ; (c) indicates a location of the stress wave following the creation of the spall.

It can easily be understood that the wave shape measured at the free end of the specimen shows the compressive wave propagating from the shot point until the spalling occurs, but, after the spalling occured, it shows the wave shape due to the repeated reflection of the wave in the spall. Therefore, if the spalling phenomenon is recognized in this experiment, it is clear that the difference between the first peak stress and the first col stress in the wave shape measured at the free end of the specimen is equal to the dynamic tensile strength of the rock specimen, and it is also clear that the time interval between the first peak stress and the first col stress is the time for the stress wave to propagate through twice the length of the spall.

However, the actual stress distribution of the wave induced in the rock specimen is not so triangular in shape and also it always decays with its propagation. In determining the dynamic tensile strength of rock in this experimental study, the calibration for the shape of the induced stress wave is omitted because the accuracy of the measured wave shape is no match for its difficult calibration, but the calibration for the decay of the stress wave with its propagation is carried out by using the attenuation function of the stress wave obtained, as described in detail later. This attenuation function is obtained from the first peak stresses of waves measured by using several lengths of rock specimen.

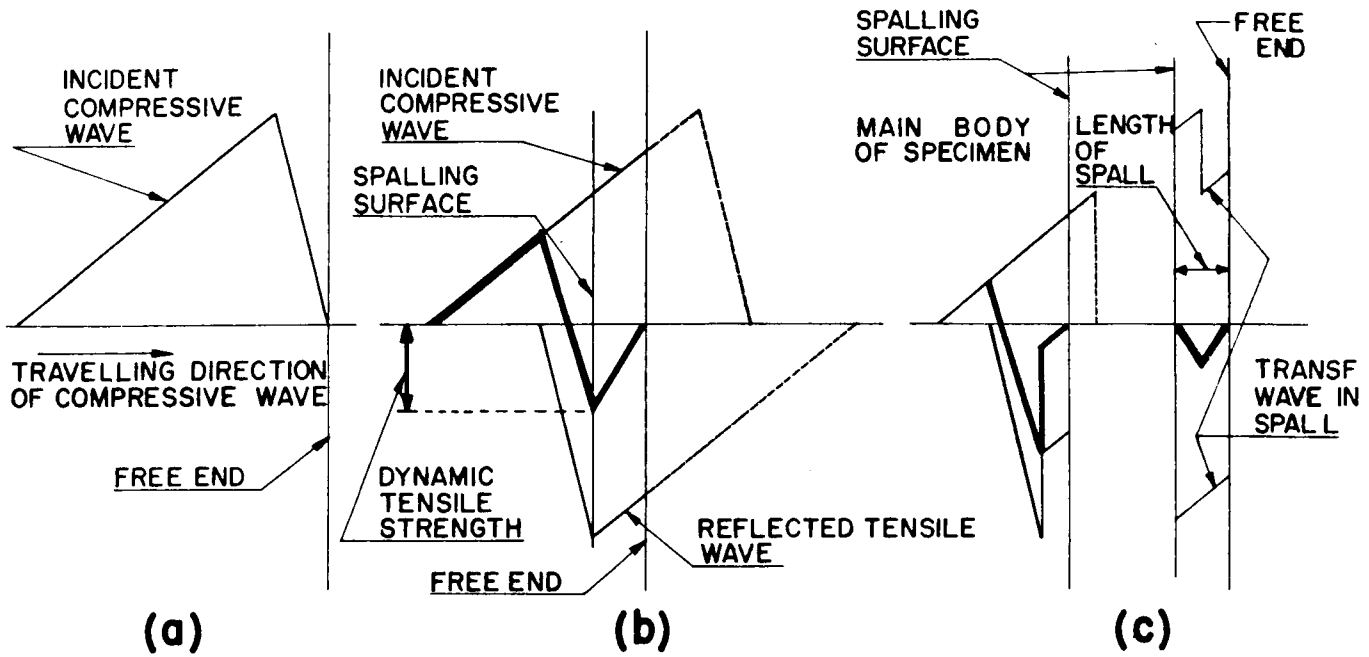

Fig. 3.1 Conception of Stress Condition for Spalling

3.3 Experimental Arrangement

The capacitance gauge system was used to measure the displacement of the free end of the specimen. [2], [3]. The general experimental arrangement is shown in Fig. 3.2.

The rock specimen was prepared by coring from the original rock mass, cutting the obtained core into proper length, and grinding both ends into flat and smooth planes, perpendicular to the axis of the core. The diameter of the core used was 1 inch. Aluminum foil was glued with Glyptal Cement onto the whole plane of each end of the specimen, taking care to ensure that the surface be as even as possible. The aluminum foil glued to the free end was used as a capacitance plate, and another foil was used as an electric switch for the trigger pulse generator of a single sweep of the oscilloscope.

A No. 8 detonator was inserted in the steel ring (1 in. outer diameter), the bottom of which was covered with cardboard (50/1000 in. thick), and then aluminum foil was glued on the bottom surface as well as the ends of the rock specimen. This ring was tightly affixed to the impacted end of the specimen with masking tape, keeping the electric insulation between aluminum foils on both ends of the specimen and the steel ring bottom by using thin wax paper (3/1000 in. thick).

As a special arrangement, a steel bar of 1 in. diameter and 12 in. length was inserted between the steel ring and the rock specimen, as shown at the bottom of Fig. 3.2. In this case, a longer time duration of the stress pulse of wave could be obtained and the disturbance through the noise, due to the ionization during detonation of the No. 8 cap in the oscilloscope trace, was relatively small.

This setup including the specimen was placed horizontally on the wooden block and tightly affixed with masking tape. As another capacitance plate, a brass disc of 7/8 in. diameter was used. The gap between the capacitance plates was adjusted to be exactly 5 mm, by using a micrometer and an ohmmeter. After the brass disc was locked into place by using a set screw, the micrometer was removed from the apparatus to prevent damage to it during the test.

The electrical block diagram of the recording system for measurement of the displacement is shown in Fig. 3.3. The output signal from the capacitance gauge is fed to a preamplifier (Keithley 102B) and then to a dual beam oscilloscope (Tektronix 545A).

3.4 Rocks Used for Specimen

Three kinds of rock were used for specimens in this experiment, viz., quartzite, magnetite and limestone. Quartzite was from Nordic Mine, Elliot Lake, Ontario, magnetite was from Carol Lake, Labrador, and limestone was sampled from the hill at Carlington Park, Ottawa.

The dimensions of the prepared rock specimens were designed to be of four sizes ; 2 in., 4 in., 6 in. and 8 in. in length and a constant diameter (1 in.) for each rock specimen. But, in limestone, a specimen of 8 in. length was not available, due to its brittle property. Therefore, the lengths of limestone specimens were 2 in., 4 in., 6 in. and 7 in.

The length, diameter and mass of the prepared specimens were precisely measured and then

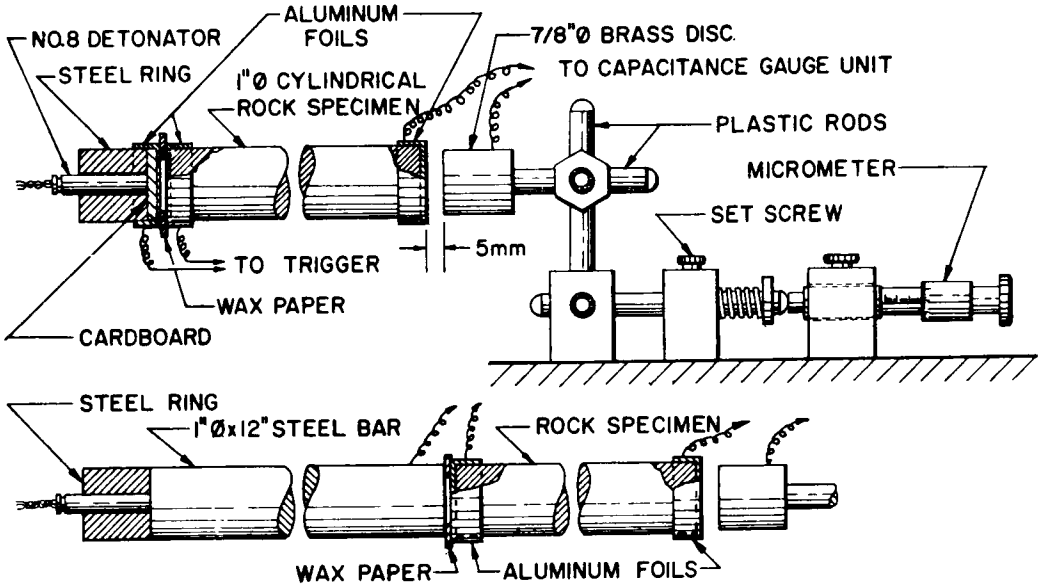

Fig. 3.2 Experimental Arrangement

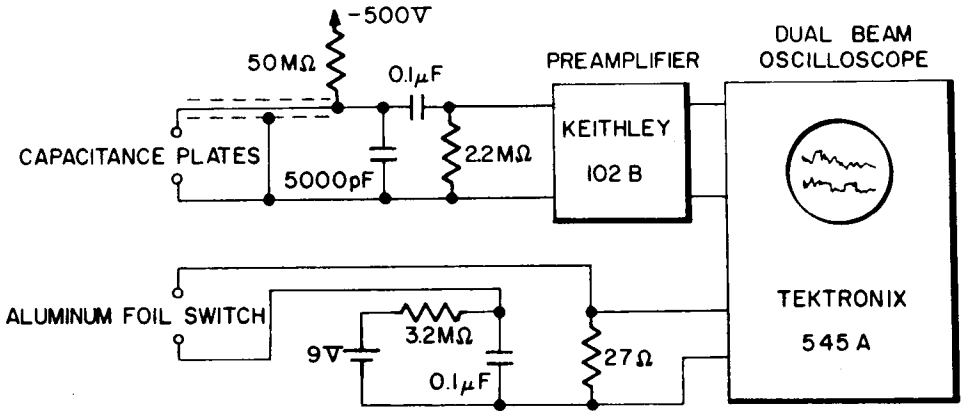

Fig. 3.3 Block Diagram of the Recording System

the density in each specimen was calculated. The mean calculated density of each kind of rock is shown in Table 3.1.

3.5 Experimental Results and Considerations

(1) Displacement Record

An example of the record for the displacement is shown in Fig. 3.4. The left end point A on the upper beam trace represents the starting point of single sweep, that is, the instant at which the stress wave was induced at the impacted end of the specimen by the action of a No. 8 cap. Point B on each trace represents the instant at which the stress wave front arrived at the free end of the specimen. The time duration between A and B in the upper beam trace is the propagating time of longitudinal stress wave from the impacted end to the free end. Therefore, the mean propagation velocity of the longitudinal stress wave in each specimen can be calculated from the time duration and the length of the specimen.

The lower beam trace represents a part of the upper beam trace enlarged electrically by using the delay circuit provided in the sweep unit of the oscilloscope.

The particle velocity versus time relationship in the stress wave at the free end can be obtained by using the trace beyond B, the calibration curve of the capacitance gauge and the relation of Equation (3.2).

(2) Propagation Velocity

The propagating time observed in each record, the length of the specimen and the propagation velocities are listed in Tables 3.2, 3.3 and 3.4.

Hereupon, the author defines the terms " plastic, shock and elastic wave zones " in terms of the propagation velocity of the longitudinal stress wave. " The plastic wave zone " is produced in rock close to the impacted end of the specimen, and the propagation velocity is relatively lower than sonic speed. " The shock wave zone " is subsequent to the plastic wave zone with increasing distance from the shot point, and the propagation velocity is relatively higher than sonic speed. Finally, " the elastic wave zone " is the region which does not belong to either the plastic or shock wave zone, and the propagation velocity is nearly equal to sonic speed.

In the three kinds of rock used for this experiment, it is considered that the following changes of property of the stress wave exist in the rock specimen. A plastic wave, involving relatively low speeds, is initially generated in the rock at the impacted end of the specimen, and as it progresses away from this end through the specimen, the velocity increases. At some distance, the plastic wave changes to the shock wave associated with its propagation. After the velocity of the shock wave has reached a maximum, it gradually decreases and approaches sonic speed.

The length of the plastic wave zone is approximately the same in all three rocks used, but the shock wave zone is longest in quartzite, next in magnetite and shortest in limestone. However, the maximum propagation velocity of the shock wave occurs in magnetite, next in quartzite, and is

Table 3.1 Mean Density of Used Rock

Quartzite	2.63 g/cm^3
Magnetite	3.48 g/cm^3
Limestone	2.69 g/cm^3

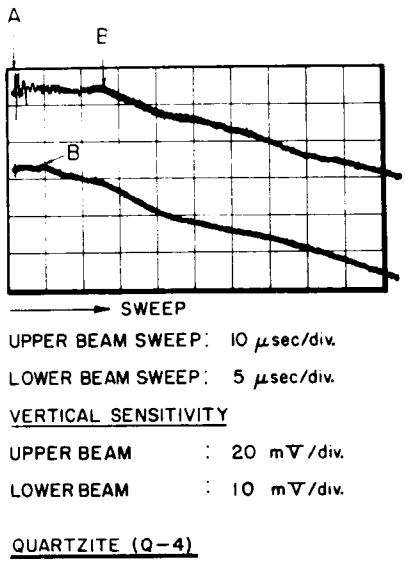

Fig. 3.4 Example of the Oscilloscope Trace

Table 3.2 Propagation Velocity of Quartzite

No. of specimen	Length of specimen (cm)	Propagating time (μsec.)	Mean propagation velocity (m/sec.)	Local propagation velocity (m/sec.)
Q- 1	5.080	12.7	4000	
Q- 2	5.080	11.8	4310	
Q- 3	5.103	11.5	4440	4760
Q- 4	5.080	12.9	3940	
Q- 5	5.098	10.7	4760	
Q- 7	10.173	21.8	4670	
Q- 8	10.135	19.7	5140	
Q- 9	10.160	20.4	4980	8500
Q-10	10.160	19.8	5130	
Q-11	10.180	21.4	4760	
Q-13	15.243	24.7	6170	
Q-14	15.222	23.6	6450	11970
Q-15	15.237	26.4	5770	
Q-17	20.320	29.6	6860	
Q-18	20.345	29.8	6830	9930
Q-19	20.328	29.9	6800	
Q- 6[x]	5.080	13.8	3680	
Q-22[x]	5.080	16.0	3180	
Q-12[x]	10.165	20.5	4960	
Q-23[x]	10.226	24.7	4140	6400
Q-16[x]	15.245	29.8	5120	
Q-24[x]	15.227	33.7	4520	
Q-21[x]	20.307	35.4	5740	

[x] A steel bar of 12 in. length and 1 in. diameter was inserted between the steel ring and the rock specimen.

Table 3.3 Propagation Velocity of Magnetite

No. of specimen	Length of specimen (cm)	Propagating time (μsec.)	Mean propagation velocity (m/sec.)	Local propagation velocity (m/sec.)
M- 1	5.131	10.7	4790	
M- 2	5.126	10.7	4790	5040
M- 3	5.113	11.2	4570	
M- 5	10.175	20.8	4890	
M- 6	10.147	17.4	5830	8130
M- 7	10.178	20.2	5040	
M-10	15.232	22.5	6770	
M-11	15.210	25.8	5900	16050
M-12	15.304	22.5	6800	
M-15	20.290	29.2	6950	
M-16	20.325	32.6	6230	7760
M-17	20.320	23.6	8610	
M- 4[x]	5.080	12.1	4200	
M- 8[x]	10.107	35.0	2890	
M- 9[x]	10.178	27.0	3770	
M-14[x]	15.311	52.8	2900	2600
M-18[x]	20.348	73.0	2790	
M-19[x]	20.343	59.5	3420	

[x] as in Table 3.2

Table 3.4 Propagation Velocity of Limestone

No. of specimen	Length of specimen (cm)	Propagating time (μsec.)	Mean propagation velocity (m/sec.)	Local propagation velocity (m/sec.)
L- 1	5.080	10.0	5080	
L- 2	5.085	10.0	5090	
L- 3	5.070	8.7	5830	5950
L- 4	5.077	9.6	5290	
L- 5	10.163	16.9	6010	
L- 6	10.155	15.7	6470	
L- 7	10.145	16.9	6000	7160
L- 8	10.155	16.9	6010	
L- 9	10.058	16.9	5950	
L-10	10.048	16.3	6160	
L-11	10.000	16.9	5920	
L-12	15.208	24.2	6280	
L-13	15.197	24.7	6150	6680
L-14	15.258	25.3	6030	
L-15	17.745	26.4	6720	
L-16	17.831	25.8	6910	
L-17	17.765	27.5	6460	
L-18	17.823	28.6	6230	6500
L-19	17.795	29.2	6090	
L-20	17.722	30.4	5830	
L-21[x]	17.775	31.4	5660	5660

[x] as in Table 3.2

lowest in limestone.

In the case in which a steel bar was inserted between the steel ring and the rock specimen, it is not recognized that the plastic or shock wave was induced in the specimens of the three kinds of rock, i.e., it is considered that the stress wave decays enough to become the elastic wave zone for the rock specimen, according to the travel through the long steel bar.

In the calculation of the stress level of the wave, the local propagation velocity was adopted.

(3) **Stress Wave Shape**

Using the displacement records and equations (3.1) and (3.2), described in Principles of the Experiment, examples of the obtained stress wave shape in each rock are shown in Fig. 3.5. Most of the obtained wave shapes do not show a simple pulse shape as found from this figure. The stress wave shape arrived directly from the shot point must be a simple pulse shape as indicated by the dotted line. But the stress wave shape, measured actually at the free end, must be influenced by spalling due to the tensile stress wave reflected at the free end. In detail, the first peak in the obtained wave shape is due to the pulse propagated directly from the shot point, and the other peaks following the first peak are produced by overlapping the reflected waves from new spalling surface

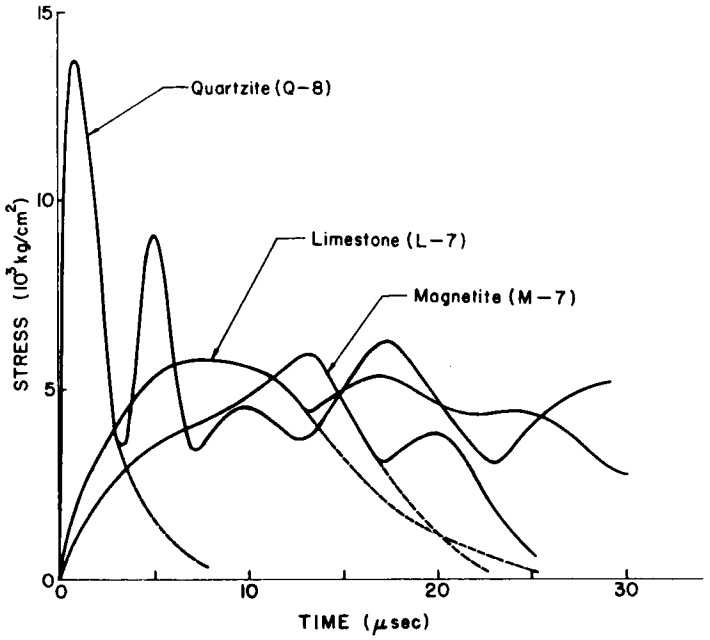

Fig. 3.5 Example of Measured Stress Wave Shape

on the tail of the direct wave from the shot point. But the new spalling surface is seldom as plane as the free end, due to the heterogeneity of the rock substance, so that the obtained wave shape beyond the first col is usually very irregular and complex.

(4) **Attenuation of the Stress Wave**

In order to obtain the attenuation function of the stress level decay of the wave propagating through the rock, the relation between the first peak stress of the measured wave in each shot and the distance from the shot point was obtained, as shown in Fig. 3.6. However, the data obtained by using the steel bar are excepted in this consideration, because the impacting load against the rock specimen is considerably decayed compared to the direct attack by a detonator. It is well known that this relation can be expressed by the following form of equation :

$$\sigma_{max} = \alpha e^{-\beta \ell} \tag{3.5}$$

where σ_{max} is the peak stress in kgf/cm^2, ℓ is the distance from the shot point in cm, α and β are constants, and e is the base of natural logarithms. Applying the method of least squares to fit equation (3.5) into this relation the constants α and β were obtained as listed in Table 3.5 :

In Table 3.5, the value of constant α should be approximately the detonation pressure of a No. 8 cap. But it varies a little in the three kinds of rock. It is considered that this variation is due to the amount of the transmitted energy in the coupling phenomenon between the detonator and the rock. If a considerable range of error is permissible, it is concluded that the detonation pressure of a No. 8 cap used in this experiment was 10 kb. It is also concluded that the decay of the stress wave with increasing distance from the shot point is strongest in magnetite, next in limestone, and weakest in quartzite.

Table 3.5 Constants for Equation (3.5)

Kind of Rock	α (kg/cm^2)	β
Quartzite	15.67×10^3	0.03288
Magnetite	13.46×10^3	0.05961
Limestone	8.22×10^3	0.04879

(5) **Dynamic Tensile Strength of Rock**

In the case in which the spalling phenomenon was observed in the broken rock specimen after the shot test, the dynamic tensile strength of the rock used was determined by the principle as described previously.

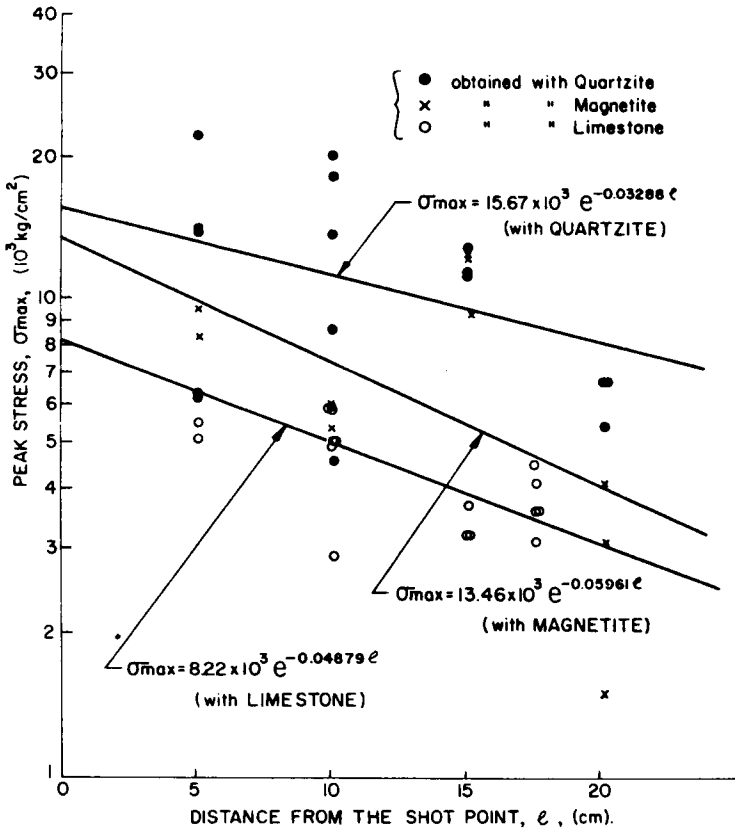

Fig. 3.6 Attenuation of the Stress Wave

First, the length of the first spall was measured by inspecting the broken rock specimen. The peak stresses corresponding to the length of the specimen, and the length of the specimen added and subtracted by the length of the spall were calculated by using the attenuation function of the stress wave in rock obtained previously, viz. :

$$\sigma_{\ell+s}=\alpha e^{-\beta(\ell+\ell s)} \quad , \qquad \sigma_{\ell}=\alpha e^{-\beta\ell} \quad , \qquad \sigma_{\ell-s}=\alpha e^{-\beta(\ell-\ell s)} \tag{3.6}$$

where $\sigma_{\ell+s}$, σ_{ℓ} and $\sigma_{\ell-s}$ were the peak stresses at the distances from the shot point, $\ell+\ell_s$, ℓ and $\ell-\ell_s$, respectively, and ℓ and ℓ_s were the lengths of the specimen and the spall, respectively.

Next, the first peak stress, σ'_p, and the first col stress, σ'_c, of the measured wave shape were found. The peak stress of the reflected tensile wave, σ_p, and the stress of the incident wave, σ_c, at the spalling surface when it occurred, were obtained by the following equations :

$$\sigma_p=\sigma'_p\cdot\frac{\sigma_{\ell+s}}{\sigma_{\ell}} \quad , \qquad \sigma_c=\sigma'_c\cdot\frac{\sigma_{\ell-s}}{\sigma_{\ell}} \tag{3.7}$$

When using the steel bar in the experimental arrangement, the attenuation coefficient of the stress wave β was assumed to be equal to the normal case without the steel bar.

Finally, the dynamic tensile strength of rock, St, was determined by subtracting σ_c from σ_p as follows :

$$S_t=\sigma_p-\sigma_c \tag{3.8}$$

If the decay of the stress wave with its propagation can be ignored, it is clear that both ratios $\sigma_{\ell+s}/\sigma_{\ell}$ and $\sigma_{\ell-s}/\sigma_{\ell}$ are equal to 1, and the dynamic tensile strength of rock is equal to the difference between the first peak stress and the first col stress of the measured wave shape.

The results obtained on the dynamic tensile strength in this experiment are listed in Tables 3.6, 3.7 and 3.8. From these tables, it is found that the dynamic tensile strength obtained in each rock is scattered over a wide range. This scattering is considered to be not only due to the heterogeneity of the rock but also due to the characteristic of the dynamic load, and especially the dynamic loading time.

In this experiment, the stress wave shape propagated near the free end of a specimen seems to be different in particular specimens, although the impact source with the same conditions (a No. 8 detonator) is used in each shot. Therefore, a simple stress pulse shape without the influence of spalling was deduced based on the first peak of measured wave shape in each shot, and the time duration from the peak to one-tenth of the peak in the simple pulse shape was measured, and it was recognized as the wave length of the pulse. Thus, the relation between the dynamic tensile strength obtained and the time duration of the stress pulse was checked and shown in Fig. 3.7.

From this figure, the following facts are roughly concluded. The wave length of the stress pulse induced by the attack of a No. 8 cap is shortest in quartzite, next in magnetite and longest in limestone in this experiment. The shorter the wave length of the induced pulse, the stronger

Table 3.6 Results for Quartzite

No. of specimen	Length of specimen l(cm)	Length of spall ls(cm)	from measured wave shape (10^3kg/cm^2) σ'_p	σ'_c	by equations (3.6) and (3.7) (10^3kg/cm^2) σ_p	σ_c	Dynamic tensile strength St (10^3kg/cm^2)	Time duration of pulse (μsec)	Number of spalls
Q- 1	5.080	0.683	14.0	5.1	13.9	5.3	8.6	4	1
Q- 2	5.080	0.668	13.9	2.5	13.8	2.6	11.2	3	1
Q- 3	5.103	0.589	6.2	1.8	6.1	1.8	4.3	4	1
Q- 4	5.080	0.729	6.3	1.6	6.2	1.7	4.5	4	1
Q- 5	5.098	0.780	22.2	1.6	21.7	1.7	20.0	2	1
Q- 7	10.173	1.593	4.6	3.5	4.4	3.7	0.7	10	1
Q- 8	10.135	1.224	13.7	3.5	13.3	3.6	9.7	5	1
Q- 9	10.160	1.473	18.1	3.4	17.4	3.6	13.8	5	1
Q-10	10.160	1.506	20.0	4.6	19.2	4.8	14.4	6	1
Q-11	10.180	1.534	8.6	1.1	8.3	1.2	7.1	5	1
Q-13	15.243	2.301	11.3	4.1	10.5	4.4	6.1	9	2
Q-14	15.222	2.281	12.8	3.2	11.9	3.4	8.5	7	2
Q-15	15.237	2.408	11.2	3.3	10.4	3.6	6.8	6	3
Q-17	20.320	2.441	6.7	0.7	6.2	0.8	5.4	8	3
Q-18	20.345	2.078	6.7	0.4	6.3	0.4	5.9	11	3
Q-19	20.328	1.590	5.4	1.3	5.1	1.4	3.7	7	3
Q-22*	5.080	1.565	2.6	0.4	2.5	0.4	1.9	11	1
Q-12*	10.165	3.254	8.6	0.9	7.7	1.0	6.7	7	1
Q-23*	10.226	2.172	2.9	1.2	2.7	1.3	1.4	13	1
Q-16	15.245	7.689	1.8	0.4	1.4	0.5	0.9	19	1
Q-24*	15.227	2.408	6.1	0.3	5.7	0.3	5.4	9	1
Q-21*	20.307	5.730	2.3	0.2	1.9	0.2	1.7	11	2

* A steel bar of 12 in. length and 1 in. diameter was inserted between the steel ring and the rock specimen.

Table 3.7 Results for Magnetite

No. of specimen	Length of specimen l(cm)	Length of spall ls(cm)	from measured wave shape (10^3kg/cm^2) σ'_p	σ'_c	by equations (3.6) and (3.7) (10^3kg/cm^2) σ_p	σ_c	Dynamic tensile strength St (10^3kg/cm^2)	Time duration of pulse (μsec)	Number of spalls
M- 1	5.131	1.359	9.5	2.0	8.8	2.2	5.6	13	1
M- 2	5.126	1.875	8.3	3.7	7.5	4.2	3.3	50	1
M- 6	10.147	3.985	5.4	3.8	4.3	4.8	-0.5	18	1
M- 7	10.178	2.314	6.0	3.1	5.3	3.6	1.7	22	1
M-10	15.222	5.273	12.3	0.0	9.0	0.0	9.0	21	1
M-11	15.210	2.954	12.0	0.0	10.1	0.0	10.1	29	2
M-12	15.304	2.459	9.2	4.0	7.8	4.6	3.2	18	2
M-15	20.290	3.835	3.1	0.7	2.4	0.9	1.5	16	3
M-16	20.325	5.116	1.5	0.0	1.1	0.0	1.1	18	2
M-17	20.320	6.434	4.1	0.7	2.8	1.0	1.8	25	1
M- 4*	5.080	2.121	2.30	0.46	2.02	0.52	1.5	11	1
M- 8*	10.107	6.137	1.09	0.27	0.76	0.40	0.36	30	1
M- 9*	10.178	4.204	0.62	0.21	0.48	0.27	0.21	35	1
M-14*	15.311	5.006	0.44	0.11	0.33	0.15	0.18	80	1
M-18	20.348	6.287	0.64	0.23	0.44	0.34	0.10	20	1

* as in Table 3.6

Table 3.8 Results for Limestone

No. of specimen	Length of specimen l(cm)	Length of spall ls(cm)	from measured wave shape (10^3kg/cm^2) σ'_p	σ'_c	by equations (3.6) and (3.7) (10^3kg/cm^2) σ_p	σ_c	Dynamic tensile strength St (10^3kg/cm^2)	Time duration of pulse (μsec)	Number of spalls
L- 3	5.070	0.292	5.5	0.2	5.4	0.2	5.2	3	1
L- 4	5.077	0.312	5.1	2.0	5.0	2.0	3.0	4	1
L- 5	10.163	1.387	5.9	1.9	5.5	2.0	3.5	20	1
L- 6	10.155	1.120	2.9	1.4	2.8	1.5	1.3	15	1
L- 7	10.145	1.283	5.8	4.4	5.5	4.7	0.8	21	1
L- 8	10.155	1.130	5.0	3.0	4.8	3.2	1.6	25	3
L- 9	10.058	1.290	4.9	2.5	4.6	2.7	1.9	23	3
L-10	10.048	1.636	5.0	3.5	4.6	3.8	0.8	26	3
L-11	10.000	1.349	5.9	1.4	5.5	1.5	4.0	33	2
L-12	15.208	1.643	3.2	1.4	2.9	1.5	1.4	24	4
L-13	15.197	1.681	3.7	2.3	3.4	2.5	0.9	27	4
L-14	15.258	1.600	3.2	2.3	2.9	2.5	0.4	34	5
L-15	17.745	1.717	3.6	1.4	3.3	1.5	1.8	24	4
L-16	17.831	1.641	3.6	1.3	3.3	1.4	1.9	28	5
L-17	17.765	1.590	3.1	1.8	2.9	2.0	0.9	32	3
L-18	17.823	1.494	4.1	2.3	3.8	2.5	1.3	41	4
L-19	17.795	1.654	3.6	1.0	3.3	1.1	2.2	28	4
L-20	17.722	1.427	4.5	2.2	4.2	2.4	1.8	32	3
L-21*	17.775	2.499	1.6	0.4	1.4	0.5	0.9	24	4

* as in Table 3.6

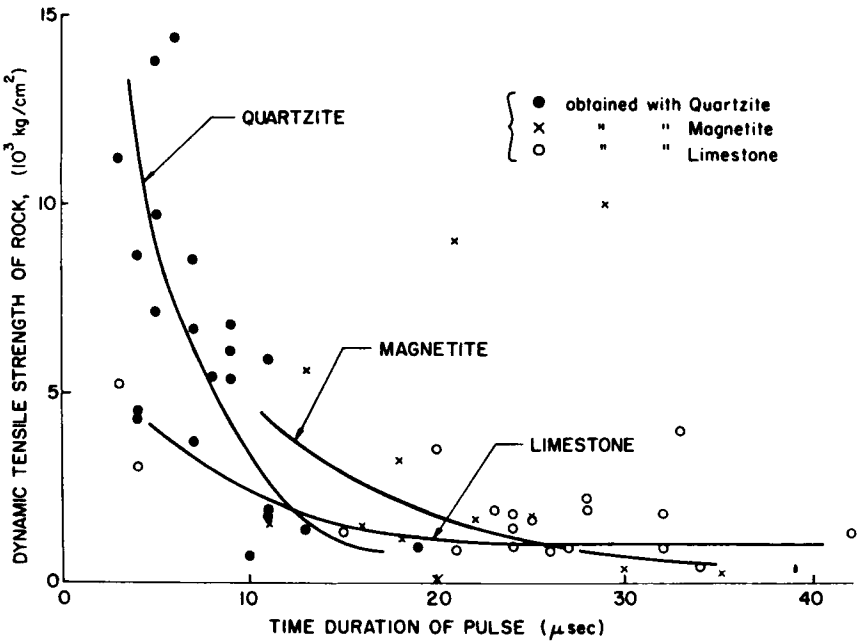

Fig. 3.7 Relations between the Dynamic Tensile Strength of Rock and the Time Duration of the Stress Pulse

the tensile strength of the rock. This fact can be proved from the number of spalls produced in this experiment, as listed in the right end column of Tables 3.6, 3.7 and 3.8. The number of spalls obtained with a short specimen was 1, but with long specimens, the number was 3, 4 or 5. It follows that, because the wave length of the stress pulse induced in a short specimen is short, the corresponding tensile strength is large. As the wave length of the stress pulse remaining in the specimen, following the first spalling, is short too, its peak stress seems to be lower than the corresponding tensile strength, rendering a second spalling impossible. But, as the wave length of the stress pulse induced in a long specimen is relatively long, due to the decay with its propagation, the corresponding tensile strength is relatively not so strong. The wave length of the stress pulse remaining in the specimen from the first spalling is also relatively long, but its peak stress seems to be still higher than the corresponding tensile strength, and a second spalling may thus occur. This behaviour is repeated until the peak stress of the pulse remaining in the specimen from the spallings, becomes lower than the corresponding tensile strength. Thus, the formation of many spalls is possible in long specimens.

The dynamic tensile strength of the three rocks used in this experiment seems to be strongest in quartzite, and approximately the same in magnetite and limestone. Howeyer the dynamic tensile strength of rock seems to change in accordance with the characteristics of the dynamic load, especially the dynamic loading time. As the extreme case, in which the loading time is infinite, corresponds to the static load, it is concluded that each curve in Fig. 3.7 approaches gradually the static tensile strength of each rock with increasing time duration of the dynamic load.

For reference, the dynamic tensile strengths obtained in this experiment and the static strengths of the same rock obtained by the conventional tests are listed together in Table 3.9. From this Table, it is an interesting fact that the order of strength for dynamic tension in the three kinds of rock is different from that for static tension.

From Fig. 3.7 and Table 3.9, it is found that the dynamic tensile strength of magnetite used as a rock specimen shows relatively more scattering than the other rocks used. Examples of the state of the rock specimens after the shot test are shown in Fig. 3.8. Magnetite specimens used in this experiment were carefully selected from as homogeneous core as possible, but the heterogeneous part is found in places of the magnetite specimen in Fig. 3.8, where the spalling surface was produced at the weak part parallel to the bedding. Therefore, the minimum dynamic strength of magnetite might be a little stronger than that obtained.

The impacting load obtained by attack of a No. 8 cap in this experiment was of very short time duration, such as 3–30 micro-seconds, and it also was of simple pulse shape. But, in the actual blasting of rock, it was reported from the result of the field experiment that the dynamic loading time was longer, namely 1–2 milli-seconds [5].

The dynamic tensile strength of rock used in order to predict the craters or the boundaries of broken ground in actual blasting should be the middle strength between the dynamic tensile strength obtained in this experiment and the static strength. It is therefore concluded that the

Table 3.9 Strength of Rock

Kind of rock	Dynamic strength (kg/cm^2)		Static strength (kg/cm^2)	
	tensile	compressive	tensile[x]	compressive
quartzite	800 - 14000	15300	89.7[xx] (19.6%)	2465[xx] (15.4%)
magnetite	200 - 5600	12500	96.2[xx] (19.7%)	2340[xx] (24.5%)
limestone	800 - 5200	7300	65.2 (6.4%)	1054 (22.2%)

[x] Tension test was substituted by Brazilian test.
[xx] These data were obtained by Muhammad Aslam (4).
() The figure in the parentheses shows the per cent standard variation of the value above.

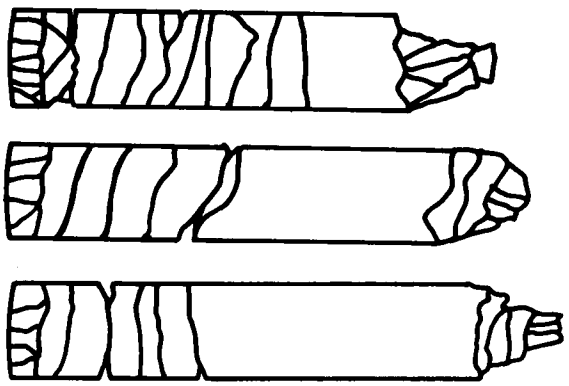

Fig. 3.8 State of Rock Specimen after Shot Test

tensile strength of 1–5 times the static strength of rock should be used in the problems for actual blasting.

In the case of direct attack against the rock specimen by a No. 8 cap, the crushing zone is found near the impacted end of the specimen, as shown in Fig. 3.8. This zone was crushed and driven away from the remaining specimen by the intense compressive pulse, due to the detonation of a No. 8 cap. The peak pressure of the compressive pulse can be deduced wave with the distance from the shot point. It can be considered that the peak pressure of the stress pulse at the interface between the crushing zone and the remaining rock specimen is equal to the dynamic compressive strength of rock.

The dynamic compressive strength of rocks used in this experiment was obtained by measuring the length of the crushing zone from the rock specimen remaining after the shot and listed in Table 3.9 together. These strengths are nearly equal to 5–7 times the strength obtained by the static conventional compression test.

3.6 Conclusion

In this experiment, three kinds of rock, Elliot Lake quartzite, Carol Lake magnetite ore and City of Ottawa limestone, were used for specimens.

Considering the observed changes in the propagation velocity when only a No. 8 cap was detonated at one end of the cylindrical rock specimen, the existence of three regions with different properties for the induced stress wave, plastic, shock and elastic wave zones, was recognized.

According to the obtained attenuation of the stress wave induced in and propagated through the rock specimen, it was concluded that the detonation pressure of a No. 8 cap was about 10 kb and that the attenuation of the stress wave in the rock specimen with increasing distance from the shot point could be expressed by a decreasing exponential function and that its attenuation coefficient was a little different in the three kinds of rock used.

From the observed stress wave shape and the length of the spall created near the free end of the specimen, the dynamic tensile strength of the rock was determined and it was found that the shorter the wave length of the stress pulse induced, the stronger the dynamic tensile strength of the rock, and that the order of the strength in the three rocks used was different from that for static tension.

In order to solve the problems in the actual rock blasting, it seems to be reasonable that 1–5 times the strength obtained by the conventional tension test is used for the dynamic tensile strength of the rock.

Also, the dynamic compressive strength of rock which was nearly equal to 5–7 times the strength obtained by the static conventional compression test, was observed in this experiment.

REFERENCES for Chapter 3

[1] Larocque, G.E. " Determination of the Dynamic Tensile Strength of a Magnetite Specimens from Carol Lake, Labrador ", Divisional Report FMP 65/9–MRL ;

[2] Terada, M. " Attenuation of the Spherical Stress Wave Induced in Elliot Lake Quartzite by an Explosion ", Divisional Report FMP 66/108–MRL ;

[3] Terada, M. " Attenuation of the Spherical Stress Wave Induced in Magnetite Ore of Carol Lake, Labrador, by an Explosion ", Divisional Report FMP 66. 151–MRL ;

[4] Aslan, M. " Coupling Relations in Blasting ", Divisional Report FMP 66/123–MRL ;

[5] Coates, D.F. " Progress Report 1965 Blasting Research ", Divisional Report FMP 65/131 –MRL , Dept. of Energy, Mines and Resources, Ottawa, Canada.

Chapter 4

THEORETICAL CONSIDERATION ON THE ATTENUATION OF THE STRESS WAVE INDUCED IN ROCK BY AN EXPLOSION*

4.1 Introduction

When an explosion is produced in rock, the state of the strain or stress distribution induced has been studied theoretically and experimentally by many researchers.

J.A. Sharpe [1] and W.I. Duvall [2] derived the equation to solve the problem of the wave motion produced when a detonation pressure of arbitrary form was applied to the interior surface of a spherical cavity in an ideally elastic medium. But, this equation was valid for only the medium, the Poisson's ratio of which was 0.25.

I. Ito and K. Sassa derived the equation similar to Sharpe's equation, which was valid in the elastic medium with arbitrary Poisson's ratio, and they investigated the effect of the Poisson's ratio on the values of stress induced in rock by an explosion [3].

Terada experimentally determined the attenuation of the stress wave induced in a rock by an explosion [4].

In this study, using the equations derived by Ito and Sassa, the attenuation of the spherical stress wave is obtained theoretically and it is compared with the actual attenuation determined by an experiment.

4.2 Equation used for the Computation of Stress

In general, when a spherical explosive charge is detonated in the infinite medium which is regarded as an elastic, isotropic and homogeneous material, the elastic equation of motion in the medium can be expressed by the following equation:

$$\rho \frac{\partial^2 S}{\partial t^2} = \mu \nabla_s^2 + (\lambda + \mu) \operatorname{grad} \Delta \tag{4.1}$$

where S is the displacement, t is the time, ρ is the density and λ and μ are the Lame's elastic constants. It is well known that a solution of the equation (4.1) is

$$S = \nabla \Phi \tag{4.2}$$

provided the potential Φ satisfies the wave equation:

$$\frac{\partial^2 \Phi}{\partial t^2} = C^2 \nabla \Phi \tag{4.3}$$

---

* Theoretical Consideration on the Attenuation of the Stress Wave induced in Rock by an Explosion, Divisional Report DR–MR 67/7, Fuels and Mining Practice Division, Mines Branch, Department of Energy, Mines and Resources, Canada, 1967. (Coauthor: Makoto Terada)

where C is the propagation velocity and it is expressed by the following equation:

$$C=\sqrt{(\lambda+\mu)/\rho} \tag{4.4}$$

Now, the spherical coordinates which have the origin at the centre of the spherical cavity for the explosive charge are adopted and it is used as the boundary condtion that the radial stress applying on the interior surface of the cavity in the medium is equal to the detonation pressure, Pt, which is an arbitrary function of the time. Thus, the wave equation (4.3) can be solved and the stress or strain distribution in the medium can be analyzed.

In the special case in which Poisson's ratio of the medium is 0.25, J.A. Sharpe and W.I. Duvall derived the solution. In general case in which Poisson's ratio is variable in the range of $0-0.5$, I. Ito and K. Sassa derived the solution.

Hereupon, the author introduces the derivation of the solution by I. Ito and K. Sassa [3].

According to the theory of elasticity, the Lame's elastic constants can be respectively represented by the Young's modulus E and the Poisson's ratio ν as follows:

$$\lambda=\frac{E\nu}{(1+\nu)(1-2\nu)} \tag{4.5}$$

$$\mu=\frac{E}{2(1+\nu)} \tag{4.6}$$

If the ratio of λ to μ is represented by k, the following equation is satisfied from the equations (4.5) and (4.6):

$$k=\frac{\lambda}{\mu}=\frac{2\nu}{1-2\nu} \tag{4.7}$$

In this derivation of the solution, k is used instead of the Poisson's ratio for convenience.

If the detonation pressure, Pt, is expressed by the following form of a function of the time:

$$\begin{aligned} &Pt=P_0(e^{-\alpha t}-e^{-\beta t}), && t\geqq 0\\ &Pt=0 && t<0 \end{aligned} \tag{4.8}$$

where t is the time from the initiation of the explosion, P_0 is a constant to control the peak value of the detonation pressure, α and β are constants to control the shape of the detonation pressure with the time, and e is the base of the natural logarithm, the potential Φ at the arbitrary distance from the centre of the explosive charge, r, can be derived as follows:

$$\begin{aligned} \Phi=&\frac{aP_0}{\rho r}\cdot\frac{1}{\left(\frac{\omega}{\sqrt{k+1}}-\alpha\right)^2+\omega^2}\left[-e^{-\alpha\tau}+e^{-\frac{\omega\tau}{\sqrt{k+1}}}\right.\\ &\left.\times\left\{\left(\frac{1}{\sqrt{k+1}}-\frac{\alpha}{\omega}\right)\sin\omega\tau+\cos\omega\tau\right\}\right]\\ &+\frac{aP_0}{\rho r}\cdot\frac{1}{\left(\frac{\omega}{\sqrt{k+1}}-\beta\right)^2+\omega^2}\left[e^{-\beta\tau}-e^{-\frac{\omega\tau}{\sqrt{k+1}}}\right.\\ &\left.\times\left\{\left(\frac{1}{\sqrt{k+1}}-\frac{\beta}{\omega}\right)\sin\omega\tau+\cos\omega\tau\right\}\right], \quad \tau\geqq 0\\ \Phi=&0, \quad \tau<0 \end{aligned} \tag{4.9}$$

where a is the radius of the spherical cavity for the explosive charge, and ω and τ are respectively the angular frequency and the time and these are also defined by the following equations:

$$\omega = \frac{2\sqrt{k+1}}{k+2} \cdot \frac{C}{a} \tag{4.10}$$

$$\tau = t - \frac{r-a}{C} \tag{4.11}$$

where C is the propagation velocity of the longitudinal wave as defined by the equation (4.4).

If n and m and the angles of phase θ_1, θ_2 and θ_3, are respectively defined by the following equations:

$$\alpha = \frac{n\omega}{\sqrt{k+1}} \tag{4.12}$$

$$\beta = \frac{n\omega}{\sqrt{k+1}} \tag{4.13}$$

$$\theta_1 = \tan^{-1}\left(\frac{\sqrt{k+1}}{1-n}\right), \tag{4.14}$$

$$\theta_2 = \tan^{-1}\left(\frac{\sqrt{k+1}}{1-m}\right), \tag{4.15}$$

$$\theta_3 = \tan^{-1}\sqrt{k+1} \tag{4.16}$$

the radial stress, σ_r, and the tangential stresses, σ_θ and σ_ϕ, in the medium can be respectively derived as follows:

$$\begin{aligned}
\sigma_r = {} & \frac{(k+2)^2 P_0}{4\rho c^2} \cdot k\mu \cdot \left(\frac{a}{r}\right)\left[-\frac{4n^2}{(k+2)^2} \cdot \frac{e^{-\frac{n\omega\tau}{\sqrt{k+1}}}}{k+2-2n+n^2} + \frac{4m^2}{(k+2)^2} \cdot \frac{e^{-\frac{m\omega\tau}{\sqrt{k+1}}}}{k+2-2m+m^2}\right. \\
& + \frac{4}{k+2} \cdot \frac{e^{-\frac{\omega\tau}{\sqrt{k+1}}}}{\sqrt{k+1}\sqrt{k+2-2n+n^2}} \sin(\omega\tau + \theta_1 - 2\theta_3) \\
& \left. - \frac{4}{k+2} \cdot \frac{e^{-\frac{\omega\tau}{\sqrt{k+1}}}}{\sqrt{k+1}\sqrt{k+2-2m+m^2}} \sin(\omega\tau + \theta_2 - 2\theta_3)\right] \\
& + \frac{(k+2)^2 P_0}{4\rho c^2} \cdot 2\mu \cdot \left(\frac{a}{r}\right)\left[-\left\{2\left(\frac{a}{r}\right)^2 - \frac{4n}{k+2}\left(\frac{a}{r}\right) + \frac{4n^2}{(k+2)^2}\right\} \cdot \frac{e^{-\frac{n\omega\tau}{\sqrt{k+1}}}}{k+2-2n+n^2}\right. \\
& \left. + \left\{2\left(\frac{a}{r}\right)^2 - \frac{4m}{k+2}\left(\frac{a}{r}\right) + \frac{4m^2}{(k+2)^2}\right\} \cdot \frac{e^{-\frac{m\omega\tau}{\sqrt{k+1}}}}{k+2-2m+m^2}\right. \\
& + \frac{e^{-\frac{\omega\tau}{\sqrt{k+1}}}}{\sqrt{k+1}\sqrt{k+2-2n+n^2}}\left\{2\left(\frac{a}{r}\right)^2 \sin(\omega\tau + \theta_1) - \frac{4\sqrt{k+2}}{k+2}\left(\frac{a}{r}\right)\sin(\omega\tau + \theta_1 - \theta_3)\right. \\
& \left. + \frac{4}{k+2}\sin(\omega\tau + \theta_1 - 2\theta_3)\right\} - \frac{e^{-\frac{\omega\tau}{\sqrt{k+1}}}}{\sqrt{k+1}\sqrt{k+2-2m+m^2}}\left\{2\left(\frac{a}{r}\right)^2 \sin(\omega\tau + \theta_2)\right. \\
& \left.\left. - \frac{4\sqrt{k+2}}{k+2}\left(\frac{a}{r}\right)\sin(\omega\tau + \theta_2 - \theta_3) + \frac{4}{k+2}\sin(\omega\tau + \theta_2 - 2\theta_3)\right\}\right], \quad \tau \geqq 0
\end{aligned} \tag{4.17}$$

$$
\begin{aligned}
\sigma_\theta = \sigma_\phi = {} & \frac{(k+2)^2 P_0}{4\rho c^2} \cdot k\mu \cdot \left(\frac{a}{r}\right)\left[-\frac{4n^2}{(k+2)^2} \cdot \frac{e^{-\frac{n\omega\tau}{\sqrt{k+1}}}}{k+2-2n+n^2} + \frac{4m^2}{(k+2)^2} \cdot \frac{e^{-\frac{m\omega\tau}{\sqrt{k+1}}}}{k+2-2m+m^2}\right. \\
& + \frac{4}{k+2} \cdot \frac{e^{-\frac{\omega\tau}{\sqrt{k+1}}}}{\sqrt{k+1}\sqrt{k+2-2n+n^2}} \sin(\omega\tau + \theta_1 - 2\theta_3) \\
& \left. - \frac{4}{k+2} \cdot \frac{e^{-\frac{\omega\tau}{\sqrt{k+1}}}}{\sqrt{k+1}\sqrt{k+2-2m+m^2}} \sin(\omega\tau + \theta_2 - 2\theta_3)\right] \\
& + \frac{(k+2)^2 P_0}{4\rho c^2} \cdot 2\mu \cdot \left(\frac{a}{r}\right)^2\left[\left(\frac{a}{r} - \frac{2n}{k+2}\right)\frac{e^{-\frac{n\omega\tau}{\sqrt{k+1}}}}{k+2-2n+n^2} - \left(\frac{a}{r} - \frac{2m}{k+2}\right)\frac{e^{-\frac{m\omega\tau}{\sqrt{k+1}}}}{k+2-2m+m^2}\right. \\
& - \frac{e^{-\frac{\omega\tau}{\sqrt{k+1}}}}{\sqrt{2+1}\sqrt{k+2-2n+n^2}}\left\{\left(\frac{a}{r}\right)\sin(\omega\tau + \theta_1) - \frac{2\sqrt{k+2}}{k+2}\sin(\omega\tau + \theta_1 - \theta_3)\right\} \\
& \left. + \frac{e^{-\frac{\omega\tau}{\sqrt{k+1}}}}{\sqrt{k+1}\sqrt{k+2-2m+m^2}}\left\{\left(\frac{a}{r}\right)\sin(\omega\tau + \theta_2) - \frac{2\sqrt{k+2}}{k+2}\sin(\omega\tau + \theta_2 - \theta_3)\right\}\right], \quad \tau \geqq 0
\end{aligned}
\tag{4.18}
$$

4.3 Detonation Pressure and Radial Stress Distribution

The laboratory experiment to determine the attenuation of the spherical stress wave induced in magnetite ore by an explosion was carried out by using 100 grams of Pentolite or 200 grams of Belite A. From the results, the detonation pressures produced by the two kinds of explosive were deduced and applied into the equation (4.8).

The density, the Poisson's ratio and the propagation velocity of magnetite ore and the value of k calculated by the equation (4.7) are listed in Table 4.1.

The radius of the explosive charge, a, in the equation (4.10) or (4.11) was calculated by regarding the explosive as a spherical charge. Also, when the parameters of α and β or n and m are determined, the shape of the detonation pressure of the explosive is necessary, but it could not be directly measured in the laboratory experiment. Therefore, its peak pressure was deduced by the extrapolation from the attenuation curve of the peak stress measured in the experiment and the time duration corresponding to the pressure pulse length and its rising time duration (time duration from its front to the peak) were deduced from the stress wave shape measured in the experiment in which the thinnest rock specimen was used. The data used for the detonation pressure are listed in Table 4.2.

The necessary parameters in the calculation of the stress by the equations (4.17) and (4.18), P_0, ω, n, m, θ_1, θ_2 and θ_3 can be easily calculated by the equations (4.8) and (4.10) – (4.16). These parameters calculated for the two kinds of the explosive are listed in Table 4.3.

Using the parameters shown in Table 4.3, the radial stresses at the points of several distances from the centre of the spherical charge were theoretically calculated by the equation (4.17). For the convenience of the calculation, multiples of radius of the spherical charge were used as distance r, namely the distances under the consideration were a, 1.5a, 2a, 3a, 4a, 6a and 10a.

Table 4.1 Physical Properties of the Used Magnetite Ore

Density, (g/cm^3)	Poisson's ratio, ν	Propagation Velocity, C (m/sec)	Ratio of Lame's constants $k = (\lambda/\mu)$
3.7	0.3	5500	1.5

Table 4.2 Data Used for the Detonation Pressure

Explosive	Radius of charge a (cm)	Peak Pressure (kg/cm^2)	Time duration for pulse length (μsec)	Rising time duration (μsec)
Pentolite	2.4	649×10^3	2.0	0.23
Belite A	3.5	76.3×10^3	5.0	0.50

Table 4.3 Parameters

Explosive	P_o	w	n	m	θ_1	θ_2	θ_3
	($10^6 kg/cm^2$)(10^5radian)				(degree)		
Pentolite	5.8105	2.0702	28	38	-3.35	-2.45	57.69
Belite A	0.1654	1.4196	10.53	40.53	-9.42	-2.29	57.69

The calculated stress wave shapes are shown in Figs. 4.1 and 4.2. In these figures, the ordinate represents the value of σ_r/P_0, the abscissa represents the time, τ, in micro-seconds. The peak stress of the wave shape decreases with increasing distance of r, but the time duration corresponding to the stress wave length and the rising time duration are both constant at each distance of r. The behaviors on these time durations are very different from the stress wave shape obtained experimentally.

In order to obtain the theoretical stress attenuation, the relationship between the peak stress of wave shape calculated by the equation (4.17), σ_{rpt}, and the scaled distance r/a, is checked and shown in Fig. 4.3, where the scaled distance is defined as the ratio of the distance from the shot point to the charge radius. For comparison with the stress attenuation obtained experimentally, the results of the experiment is plotted from the report [4] in this figure.

It is found that the theoretical attenuation curve illustrated in the logarithmic graph is not a straight line and its decrement gradually increases with increasing distance from the shot point. However, it is also found that the theoretical attenuation curve is always overlying upper than the experimental curve.

Fig. 4.4 shows the relation between the ratio of the peak stress obtained experimentally to the theoretical peak stress, $\sigma_{rpe}/\sigma_{rpt}$, and the scaled distance r/a. It is found that the stress ratio suddenly decreases in the vicinity of the explosive charge and then the decrement of the stress ratio gradually decreases. At the distance of 10a, the stress ratio shows about 0.1 -- 0.2.

It can be considered that the peak stress obtained experimentally shows the actual stress amplitude of the wave induced in the rock. Therefore, the amplitude lost in the theoretical amplitude of the stress wave can be calculated as the difference between σ_{rpt} and σ_{rpe}. Fig. 4.5 shows the percentage of the lost stress amplitude to the theoretical stress amplitude, $100\ (\sigma_{rpt} - \sigma_{rpe})/\sigma_{rpt}$, with the scaled distance, r/a.

It is found that the lost stress amplitude at the vicinity of the explosive charge increases suddenly with increasing distance and the degree of its increase gradually decreases associated with the propagation of the stress wave. For the reason of the lost stress amplitude, the energy loss with the propagation of the stress wave through the rock cannot be only considered, but the increase of the stress wave length with its propagation can be also considered.

4.4 Conclusion

Using the equations derived by I. Ito and K. Sassa, on the basis of the elastic theory, when a spherical explosive charge was detonated in the magnetite ore rock, the spherical stress wave shape induced in and propagated through the magnetite ore rock by the explosion was theoretically calculated. And then, the theoretical attenuation of the spherical stress wave with the distance from the shot point was determined and it was compared with the actual attenuation determined in the experimental study.

As the results, the peak stress of the induced wave shape decreased with increasing distance

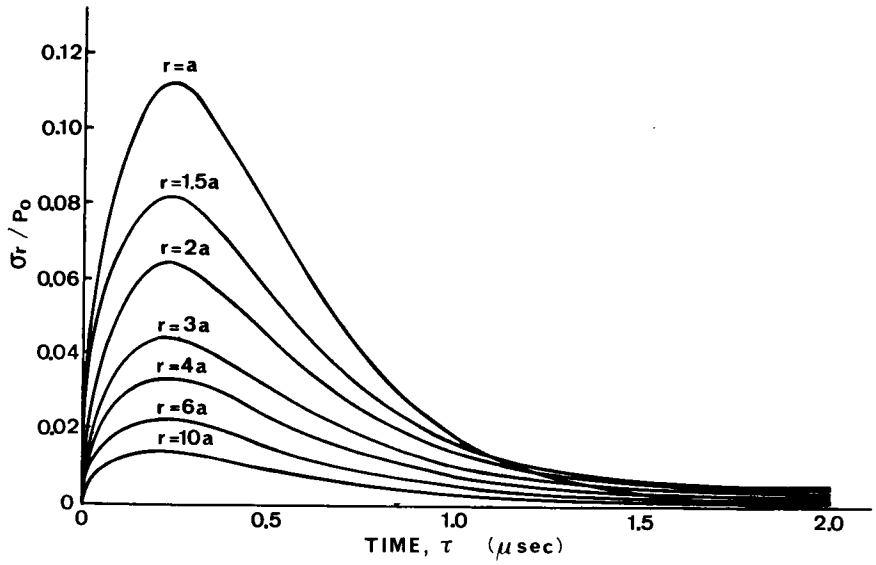

Fig. 4.1 The Theoretical Stress Wave Shape Calculated with Pentolite

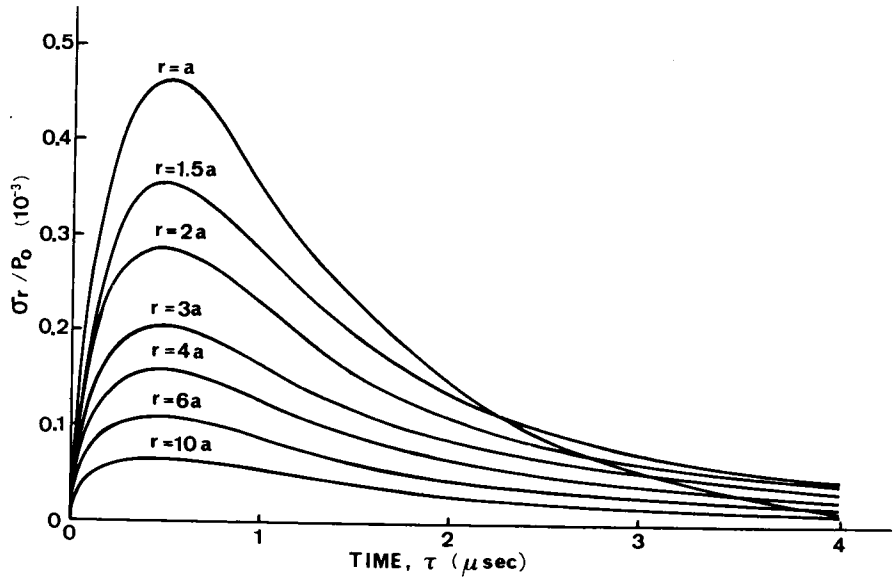

Fig. 4.2 The Theoretical Stress Wave Shape Calculated with Belite A.

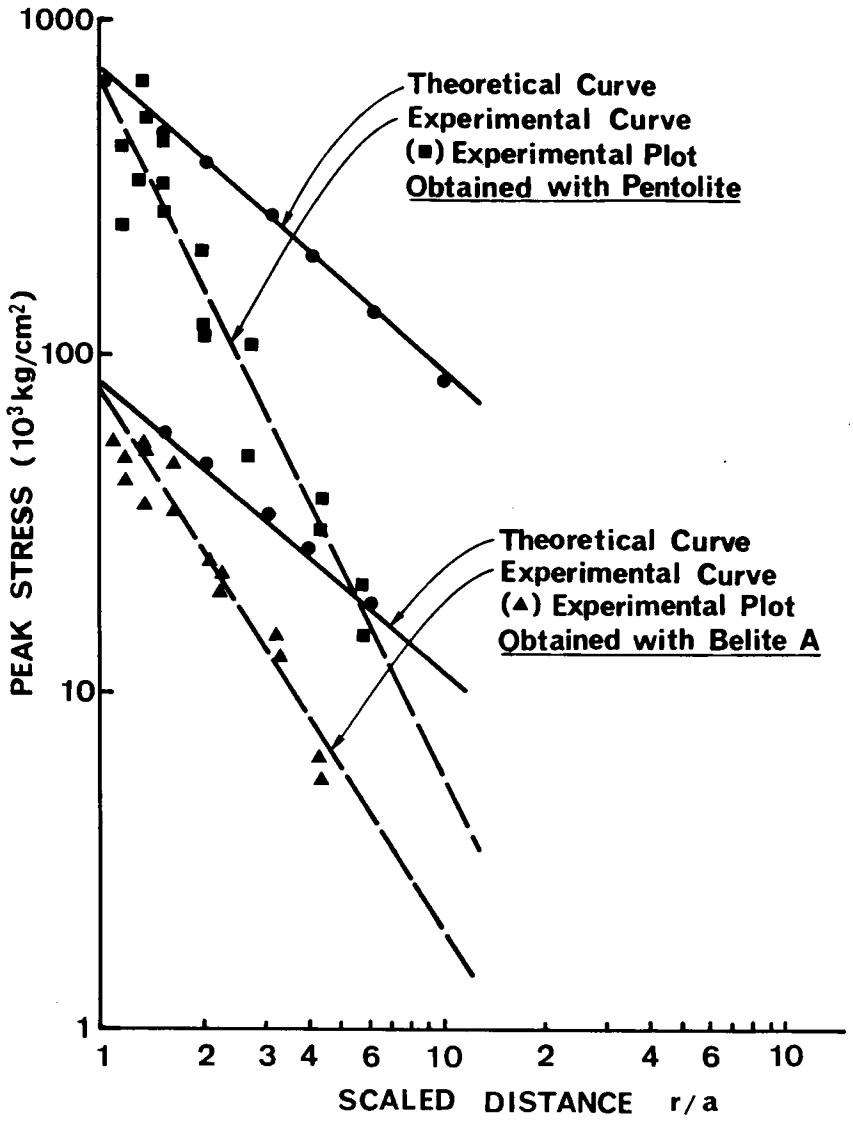

Fig. 4.3 Stress Attenuation Curves Obtained Theoretically and Experimentally.

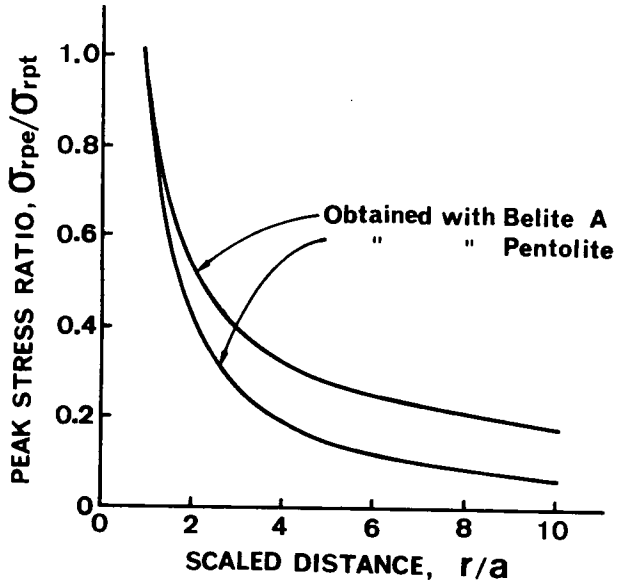

Fig. 4.4 The Comparison of the Peak Stress Obtained Experimentally with the Theoretical Peak Stress.

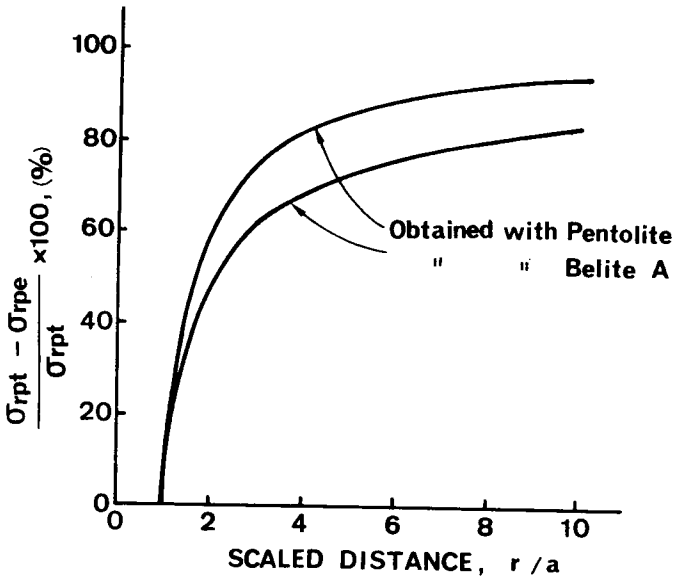

Fig. 4.5 The Lost Stress Amplitude with the Scaled Distance.

from shot point, but the attenuation coefficient of the stress wave obtained experimentally was larger than the attenuation coefficient of the stress wave calculated theoretically. In the stress wave shape obtained experimentally, the behavior of increasing wave length with the distance from the shot point was recognized, but the theoretical equations used for the stress wave shape was not considered on the increase of the stress wave length. In the comparison of the actual stress wave, it is considered that the lost stress amplitude of the wave induced in rock was not only due to the energy loss with its propagation, but also due to the increase of the stress wave length. Consequently, in the calculation of the stress induced in the rock, the theory of the elasticity should not be used only, but the theories of the viscosity and the plasticity should be also used, and the exactly theoretical analysis appears to be an interesting problem remaining in future.

REFERENCES for Chapter 4

[1] Sharpe, J.A.: The Production of Elastic Waves by Explosion Pressures. I. Theory and Empirical Field Observations, Geophysics, Vol. 7, No. 2, 1942, p. 144–154.

[2] Duvall, W.I.: Strain-Wave Shapes in Rock near Explosions, Geophysics, Vol. 18, No. 2, 1953, p. 310–323.

[3] Ito, I. and Sassa, K.: Effects of the Poisson's Ratio on the Values of Stresses Induced in Rock by an Explosion, Suiyoqwai-Shi (Transactions of Mining and Metallurgical Alumini Association, Dept. of Mining and Metallurgy, Kyoto University, Japan) Vol. 16, No. 2, 1966, p. 75–78.

[4] Terada, M.: Attenuation of the Spherical Stress Wave Induced in Magnetite Ore of Carol Lake, Labrador, by an Explosion, Divisional Report FMP 66/ 151–MRL, 1966.

Chapter 5

GROUND VIBRATIONS GENERATED BY BLASTING

5.1. Introduction

In tunnel driving through hard or soft rocks, the usage of blasting has been conventional and typical excavation method, and still more efficient and economical. With the demands of tunnels and the development of rock blasting technique the problem of ground vibrations has become increasingly important, and it has become more or less routine to excavate rocks close to or below houses and buildings.

Blasting is carried out for the purpose to fragment and to demolish rocks for removal by utilizing vast energy which the explosion of explosives generates. Near the explosive charge, the high-amplitude stress wave and borehole gases produced by the detonation process create a crushed zone in the rock whose thickness is about equal to the borehole radius. Beyond the crushed zone, additional structural damage to the rock ranges from the microstructual level up to visible fractures that may extend several meters. This type of rock damage, resulting primarily from the explosive charges near the final excavation lines, weakens the rock and increases the possibility of failure of the tunnels from subsequent vibrations or stresses. Beyond the zone of crushing and fracturing, where the amplitude of the stress wave does not exceed the strength of the rock, the wave is propagated elastically. The elastic stress waves spread out in all directions and cause the surface of the underground opening to oscillate as a free surface. If the amplitudes of the wall vibrations, and particularly of the roof vibrations, are sufficiently high, loose blocks of rock may be dislodged or fractures in the rock may be extended, further weakening the tunnel (opening). The propagating vibrations may also influence support systems and other facilities, or even houses with sensitive inhabitants and structures on the surface. If vibration levels can be predicted by using empirical propagation equations and if vibration differences can also be correlated with factors, such as delay type, shot location, explosive type and so on, vibration amplitudes may be reduced without materially altering the efficiency of the blast. With a vast increase of underground excavation anticipated for the future, a better understanding of vibrations from underground blasting is necessary.

The fundamental behavior of stress waves generated blasting was discussed in Chapter 4, and the dynamic strengths of seveal rocks were described in Chapter 3. In this chapter, vibration levels from blasting in tunnelling, correlated factors, such as explosive type, delay type and shot location, damage to nearby structures and how to reduce vibration amplitudes are discussed.

5.2 Differences among Types of Explosive Charge

As an explosion of blasting agents generates ground vibration, a type of explosive charge is considered as one of the major correlated factors which determine amplitudes of vibration.

An amplitude of vibration generated by blasting is influenced so much by time-dependent characteristic of detonating gas pressure even if an equal maximum gas pressure might be given. Namely, raise time of gas pressure, defined by a time reaching to its peak from the initiation of detonation, can be an important factor.

Let us discuss on the behavior of vibration generated around a spherical cavity with the radius a is subjected to inner pressure given by the following equation.

$$P(t) = P_0 (1-e^{-qt}) \tag{5.1}$$

where $P(t)$, P_0 and q are detonating gas pressure, peak of detonating gas pressure and a constant to specify raise time of gas pressure, respectively.

Fig. 5.1 shows changes of $P(t)$ with respect to time under various values of q such as ∞, $10C_L/a$, C_L/a and $C_L/10a$, and based on Senozawa's solution [1], Fig. 5.2 shows displacements of the cavity wall (u) subjected to the inner pressures as shown in Fig. 5.1. C_L denotes propagating velocity of longitudinal wave in an elastic medium.

By comparing Fig. 5.1 with Fig. 5.2, it is well understood that values of constant q, that is, raise time of detonating gas pressure, correlate much with amplitudes of vibration and that amplitude of vibration rapidly decreases when raise time becomes long in some degree. On the other hand, raise time of gas pressure acting onto the wall of a charged borehole is related to the detonation velocity of explosive, and it is better to take longer raise time in such a way as detonation velocity becomes lower. Additionally, it should not be slipped that the magnitude of detonating gas pressure itself has great influence to the amplitude of vibration.

There are very few examples in which the relation between the amplitude of vibration and types of explosive was confirmed practically under the equal situation. Here, several results obtained by U.S. Bureau of Mines and the author can be picked up.

U.S. Bureau of Mines had carried out their series of researches and investigations on blasting in 1960s. In them, J. Olson et al obtained interesting results with respect to the difference on vibration between AN–FO (Ammonium Nitrate Fuel Oil Blasting Agents) and dynamite from the investigations at the sandstone roof of the White Pine Copper Mine, Mchinga. [2] Fig. 5.3 shows their results under the conditions that investigations were carried out on the same face, with the same drilling pattern for V-cut centering and with the same quantity of charge (20 kg). As shown in Fig. 5.3, vibration amplitude by AN–FO might be reduced to 1/3 of dynamite. For the guidance, it should be pointed out that detonation velocities and detonating gas pressures of AN–FO and 60%–ammonium dynamite are 2700 m/s, 15000~20000 kgf/cm^2 (1.5~2.0x10^6 kN/m^2) and 3600 m/s, 40000 kgf/cm^2(4.0x10^6 kN/m^2), respectively and that production efficiency did not differ in both of cases.

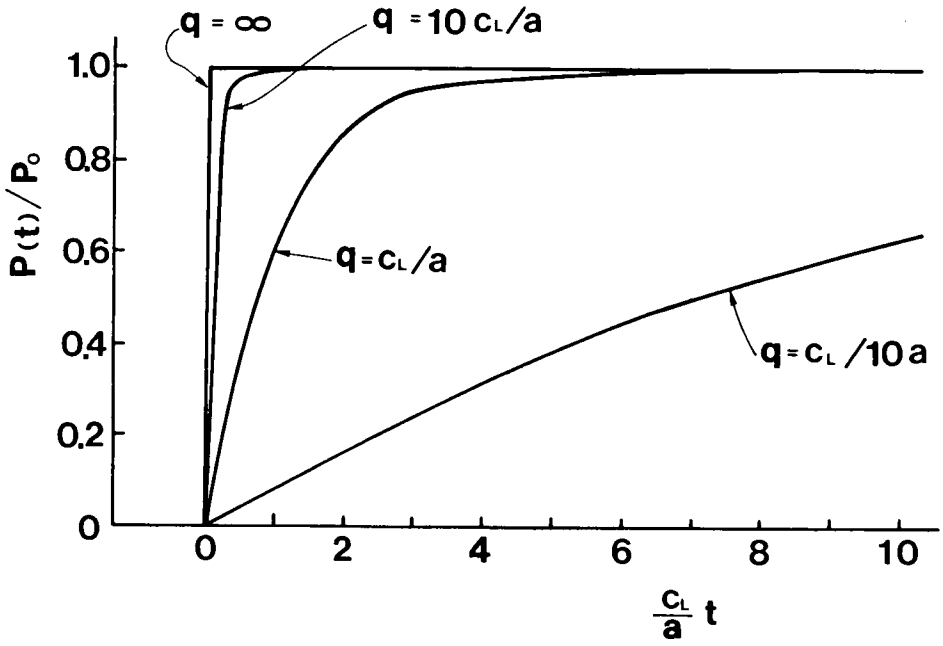

Fig. 5.1 Relation between Raise Time of Gas Pressure at Detonation and Value of q.

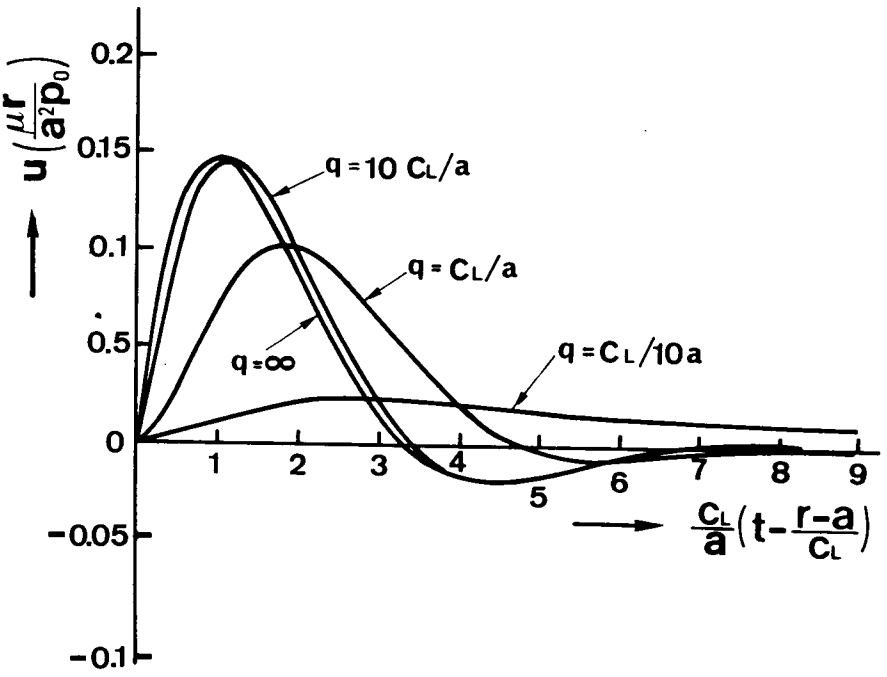

Fig. 5.2 Relation between Displacement and Dynamic Pressure for the Spherical Cavity

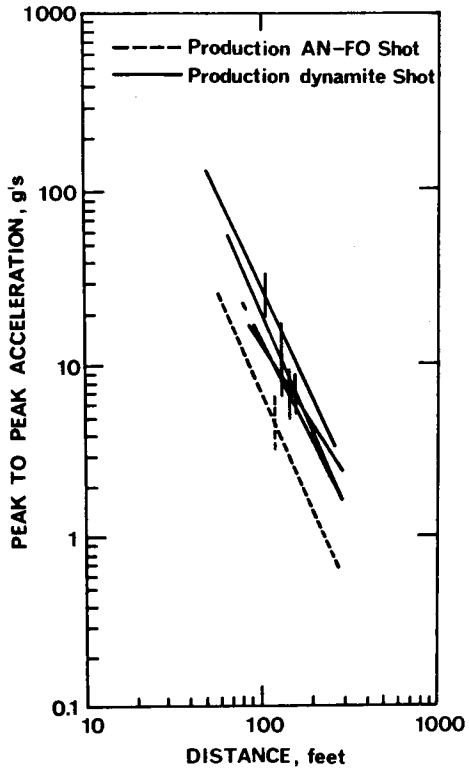

Fig. 5.3

Comparison on Peak-to-peak Accelerations at White Pine Copper Mine between AN–FO and Dynamite (after J.J. Olson [2])

Since 1970, the author has been carrying out the researches aiming at the reduction of vibration generated by underground blasting operations. [3]–[8] Based on the results obtained by the above mentioned researches, the author confirmed a following empirical propagation equation.

$$V = K \cdot L^{2/3} \cdot D^{-2} \tag{5.2}$$

where V: maximum amplitude of particle velocity [cm/sec], L: quantity of charge per delay [kg], D: distance from the center of the charge [m] and K: constant determined by four kinds of conditions such as geological situation, namely characteristics of rock and state of overburden, type of charged explosive, method of initiation (instantaneous shot, MS-or DS-delayed shot, centering or easer cut) and paths of propagating wave. The adaptability of Eq. (5.2) will be discussed in the following section, and here in this section let us consider on the differences among types of explosive which were used under the same conditions.

For the discussion on the differences derived from types of explosive, Table 5.1 shows the properties of explosives commonly used in Japan.

The author had discussed the differences through several field measurements in tunnelling sites and surfaces which were carried out in and on granite, shale and Izumi Formations, i.e. the alternative layers consisting of sandstone and shale widely spreading over south-west part of Japan. Table 5.2 shows the result obtained in the construction of Kompira water supply tunnel driven

Table 5.1 Properties of Explosives Manufactured in Japan

Explosive	Detonation velocity (m/s)	Specific volume (l/kg)	Force of explosive ($l \cdot kg/cm^2$)	Purpose
Shinkiri dynamite	6500 - 7000	870 - 880	9600 - 11100	tunnel, open cut
2-Enoki dynamite	5800 - 6300	870	9000	tunnel
SB-dynamite	3500	-	9300	controlled blasting
AN-FO	2500	950	9600	open cut
Urbanite	1500 - 2000	-	9600	demolition in urban area
Black powder	300	280	-	quarry
Concrete cracker(CCR)	150	50	-	demolition in urban area
Detonating fuze	7000	-	-	initiation

Table 5.2 Coefficient K Observed in Granite (Kompira Tunnel)

Explosive	Detonation velocity (m/s)	Point P on rock			Point O on overlaying soil		
		Vert.	Hor.EW	Hor.NS	Vert.	Hor.EW	Hor.NS
2-Enoki dynamita	6000	7.2	2.9	2.1	4.7	5.3	8.1
Smokeless poeder	2500	2.8	0.84	1.0	3.0	4.6	7.7
Concrete cracker	300	0.54	0.45	0.6	0.66	-	-

Notation Vert.: in vertical direction,
Hor.EW: in horizontal,east-west direction,
Hor.NS: in horizontal,north-south direction

through granite. Three types of explosives, 2–Enoki dynamite with a high detonation velocity, smokeless powder with a medium velocity and concrete cracker CCR with a low velocity, were discussed. [3], [4] The explosives were charged on the wall of the tunnel with 50 m thick overburden, and two groups of vibration sensors were located on the surface in such a manner that one group is directly on the foundation rock (Point–P) and another is on the overlaying earth (Point–Q) as shown in Fig. 5.4. The applied sensors were moving coil typed ones manufactured by Geo–Space Co. (Type GS–11D) and one group, for measuring one point, was consisted of three sensors which were set in the directions of vertical, horizontal in east-west and horizontal in north-south, respectively.

The drilling pattern for charged explosives is as shown in Fig. 5.5, which corresponds to the most popular centering cut in rock tunnelling in Japan, and the total quantity of 400 g of explosive with 100 g for each borehole were fire instantaneously by Zero-delayed electric blasting caps.

From Table 5.2 it can be considered that the amplitude of ground vibration by CCR is approximately 1/10 of 2–Enoki Dynamite and also the one by smokeless powder is 1/2 to 1/3 of Dynamite.

In analyzing characteristics of blasting vibrations by different types of explosives, spectrum analyses were also executed, and it was realized that each type of explosive shows the unique distribution of prominent peaks of spectrum, corresponding to its detonation velocity. Fig. 5.6 shows the result of spectrum analyses for 2–Enoki dynamite and CCR. In the case of dynamite with 600 m/s detonation velocity the spectrum shows that the highest peak is found in the vicinity of 200 Hz and other prominent peaks are distributed in the range of 200 – 800 Hz. On the other hand, in the cases of smokeless powder and CCR, it was found in the same manner as the case of dynamite to show their highest peaks round 200 Hz, but no prominent peak was found in the range over 300 Hz and most of prominent peaks existed in the range below 200 Hz. From these results it is concluded that an explosive with higher detonation velocity is apt to generate higher frequency. When we discuss on damages of structures and assessment to inhabitants influenced by blasting vibrations, it is important to consider on not only the amplitude of vibration, but also the prominent frequency to be generated, with the consideration of natural frequencies of surface soil on rock and structures on it.

In the project of Kinki Regional Highway south of Osaka, the differences among Shinkiri-dynamite, AN–FO and Urbanite, which had been newly developed in the reduction of vibration with the consideration of decoupling effect of charged explosive. Rock at the experimental sites, at the faces of vertical shafts, was mainly Izumi–Formation. The same measurement system as Kompira Tunnel was applied. The result obtained in this investigation is as shown in Table 5.3. It concludes that the amplitudes of vibrations by Urbanite and AN–FO are 50% and 35% of dynamite, respectively. (It should be noted that the effect of decoupling charge was lost much due to the inflow water at the face, therefore Urbanite with 1500 – 2000 m/sec

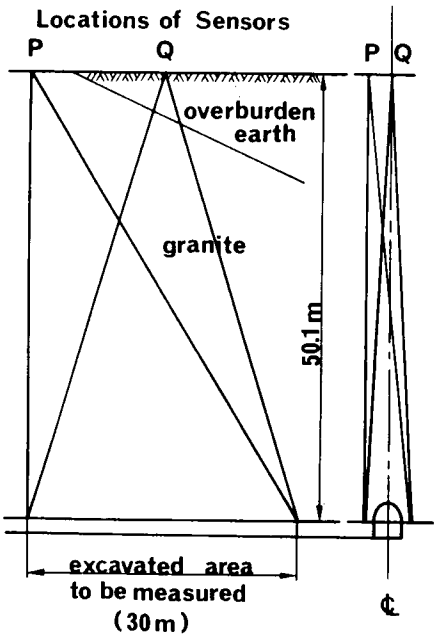

Fig. 5.4 Locations of Blasting Points and Sensors in Kompira Tunnel

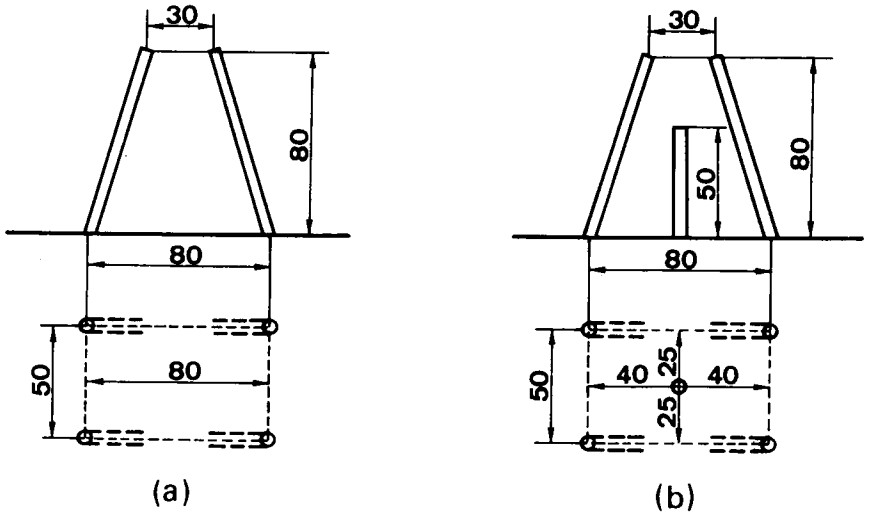

Fig. 5.5 Drilling Pattern for Tests in Kompira Tunnel

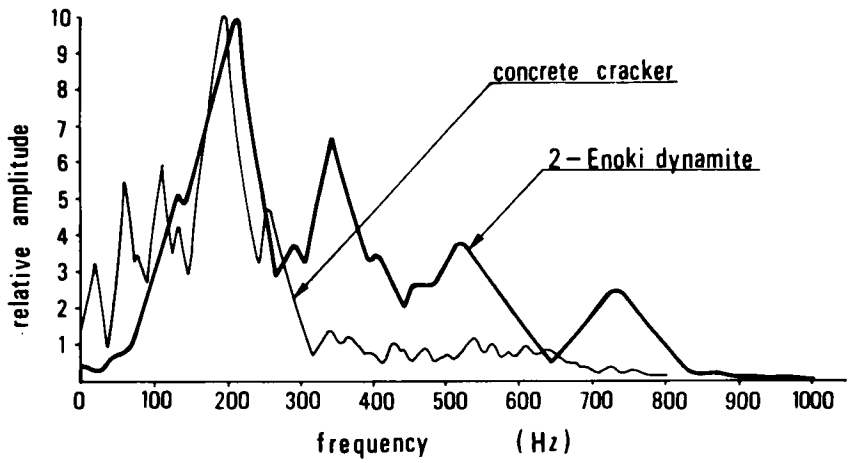

Fig. 5.6 Spectrum of Blasting Vibration

Table 5.3 Coefficient K Observed in Izumi Formation (Vertical Shafts for Yamanaka Bridge)

Explosive	Charge per delay (kg)	Distance (m)	Particle velocity (cm/s)	Coefficient K	Mean	Relative ratio
Shinkiri dynamite	0.4	16.7	0.47	2.41	0.81	1.0
	0.9	15.6	0.02	0.05		
	1.5	13.8	0.56	0.82		
	1.5	15.9	0.16	0.30		
	1.2	12.5	0.35	0.49		
Urbanite	0.8	13.6	0.06	0.12	0.65	0.80
	0.6	15.3	0.38	1.24		
	0.2	16.0	0.08	0.58		
AN-FO	1.05	14.9	0.01	0.03	0.39	0.48
	0.7	14.2	0.01	0.03		
	0.9	16.7	0.38	1.12		

detonation velocity showed higher amplitude than AN–FO with 2500 – 3000 m/sec.)

5.3 Empirical Propagation Equation

The amplitude and behavior of ground vibration generated by blasting are determined by many factors such as distance from the blasted point, types of explosives, quantity of charge, tamping condition, drilling pattern, method of initiation, path of propagating waves, characteristics of ground, state of formation and so on. Therefore, it is extremely difficult from the practical point of view to establish some general equation for blasting vibration which can be applied uniquely in any cases.

Therefore, several empirical propagation equations for blasting vibration have been proposed as the second best approach in such a manner that only two factors of distance (D) and quantity of charge (L) are picked up as variables under the fixed blasting conditions in specified rocks and correlations among the amplitude of vibration (V), distance (D) and quantity of charge (L) are obtained empirically. These equations can be applied only in the reliable range depending on frequency of measurement, number of measured point, certainty of geomechanical condition and measurement system. Corresponding to the requirement for an empirical equation in each case, it is necessary to obtain informations about geological condition and blasting methods under well prepared planning as more as possible.

The referential empirical propagation equations which had been proposed in the past are as follows. U, V, A, L, D and K denote the amplitudes of displacement in μ, particle velocity in cm/sec, acceleration in cm/sec^2, quantity of charge in kg distance in meter and constant.

1) Empirical equation for maximum amplitude of displacement (peak displacement)

Hatanaka's equations [9], [10] are

$$\begin{aligned} U &= 4 \times 10^4 \cdot K \cdot L^{2/3} \cdot D^{-2.0} \quad \text{for } 15\text{m} < D < 250\text{m} \\ U &= 5.2 \times 10^2 \cdot K \cdot L^{2/3} \cdot D^{-1.2} \quad \text{for } 250\text{m} < D < 1500\text{m} \end{aligned} \tag{5.3}$$

where K is determined by the thickness of overlaying soil formation (h).
When λ denotes wave length,

$$K = 7.0 \text{ for } h > \lambda$$
$$K = 2.5 \text{ for } h < \lambda$$
$$K = 1.0 \text{ for } h = 0$$

and $K > 10.0$ for water bearing alluvial layers.

Through the investigations carried out in 1930s, U.S. Bureau of Mines [11] gives

$$U = 30.1 \cdot K \cdot (e^{-0.00469D} + 0.014) \cdot L^{2/3} \tag{5.4}$$

for $152\text{m} < D < 1829\text{m}$ and $454\text{ kg} < L < 4536\text{ kg}$, and K is 1.0 for overlaying soil and 3.0 for water saturated layers of sand, gravel or loam.

2) Empirical equation for maximum amplitude of acceleration (peak acceleration)

Olson et al, the group of U.S. Bureau of Mines, obtained the equations

$$AL^{1/2} = 29000\,(D/L^{1/2})^{-2.07} \tag{5.5}$$

for the limestone-dolomite of the Shullsburg zinc-lead mine, Wis. [12].

3) Empirical equation for maximum amplitude of particle velocity (peak particle velocity)

Based on many field investigations associated with the author, Asahi Chemical Industry has suggested the equation [13]

$$V = K \cdot L^{2/3} \cdot d^{-n} \tag{5.6}$$

for $30m < D < 1500m$, $10\ kg < L < 3000\ kg$.

K is 500 – 1000 for center-cut in tunnelling, 200 – 500 for bench-cut, and n is 2.5 – 3.0 for clayey layer and 2.0 for rock.

And also the author has proposed the following empirical propagation equation obtained in the investigations [3] – [8].

$$V = K \cdot L^{2/3} \cdot D^{-2} \tag{5.7}$$

where K = 800 – 1000 for center cut by gelatine dynamite

K = 400 – 600 for center cut by AN–FO,

K = 50 – 100 for center cut by CCR,

and each value of K should be reduced to 60% – 70% for easer cut in tunnelling through medium hard rock. Table 5.4 shows the results obtained in 21 tunnelling sites and employed equations in past fifteen years, and Table 5.5 shows the summary of the empirical propagation equations to be employed rather widely in Japan.

Now, it can be concluded by comparing the above mentioned equations that a general empirical equation for blasting vibration takes the form of

$$A,\ U,\ V = K \cdot L^{m} \cdot D^{-n} \tag{5.8}$$

and the indices of m and n take the values of $1/3 \sim 3/4$ and 2.0 as the mean.

By plotting the results obtained by U.S. Bureau of Mines [11], Reid [14], Itoh [15], [16] and Hatanake [17] onto the monograph expressed with maximum displacement (A in mm) in the ordinate and scaled distance $D/L^{1/3}$ in the abscissa, Fig. 5.7 is obtained, and it verifies that appropriate indices, m and n, for the general empirical equation are 2/3 and 2, respectively.

Also the author carried out the investigation aiming at the behavior of attenuating vibration generated by blasting in Izumi Formation under the constant condition. [18] Fig. 5.8 shows the result giving n = 2.012 as a mean value.

Table 5.4 The List of Investigation Carried out in Japan

No.	Site	Object	Purpose	Cs[m²] xAPR[m]	Geology <Vp>[km]	Explosives	Charge[kg] per delay	Charge[kg] total	Qc[kg/m³]	Nh	Nh per m²	Observed equation	f[Hz]	D(m)	Va (cm/s)	
1	K-Paper Mill Tunnel	Houses	channel	3x1.5	liparite	2-Enoki	Cc 1.2	26.2	5.82	41	13.6	$V=500L^{3/4}D^{-2}$	90 ~100	50 ~110	0.3	Cc; Is
							Ec 0.6					$V=170L^{2/3}D^{-2}$				
				3x1.0	4 5	Urbanite	Cc 0.8	17.4	5.80	41	13.6	$V=300L^{2/3}D^{-2}$				Ec; DS2 8
							Ec 3.5					$V=100L^{2/3}D^{-2}$				
2	Koi T. (East Sector)	Houses	railway	14.7x1.0	Weathered Granite <1.3-2.6>	Modified Sugi-Dynamite	Cc 0.16	59	0.59	58	40.1	$V=500L^{3/4}D^{-2}$	120 ~180	16 ~20	0.2	Cc; DS1 4
							Ec 1.2					$V=300L^{3/4}D^{-2}$				Ec; DS5 15
	-do-	-do-	-do-	14.7x 0.9 1.0	-do-	-do-	Cc 0.2		0.6 ~1.0	58	3.95	$V=405L^{3/4}D^{-2}$	65 ~100	30 ~80	0.2	Cc; DS1 4
							Ec 1.2					$V=260L^{3/4}D^{-2}$				Ec; DS5~1
	-do-	-do-	-do-	35.1x 0.9 1.0	-do-	-do-	Cc 0.4 ~0.5		0.55 ~0.86	127	3.62	$V=350L^{3/4}D^{-2}$	65 ~100	30 ~80	0.3	Cc; DS1~4
							Ec 5.9					$V=150L^{3/4}D^{-2}$				Ec; DS5~15
3	Koi T. (East Sector)	Existing tunnel	railway	14.7x1.5	Hard rock <4>	2-Enoki	Cc 3.2	48.8	2.11	68	4.60	$V=500L^{3/4}D^{-2}$		40 ~70	2.0	Cc; DS1~4
							Ec 7.0					$V=380L^{3/4}D^{-2}$				Ec; DS5~15
	-do-	-do-	-do-	14.7x1.5 35.1x0.9	-do-	-do-	Cc 0.2 Ec 2.2	30.0	1.36	70	4.76	$V=320L^{3/4}D^{-2}$		~30	2.0	
							Cc 0.2 Ec 2.2	27.7	0.88	127	3.62	$V=208L^{3/4}D^{-2}$				
4	A-Tunnel	Houses		7.0x1.1	Hard rock (Slate) <3.0 3.5>	2-Enoki	Cc 0.8		1.08	38	5.43	$V=60L^{3/4}D^{-1.5}$		50	0.35	Cc; Is
							Ec 2.0					$V=40L^{3/4}D^{-1.5}$				Ec; DS2 7
5	B-Tunnel	Houses		7.8x1.0	Andesite	2-Enoki	Cc 1.2 Ec 4.9		1.52	39	5.00	$V=30.5\pm13L^{3/4}D^{-1.5}$ $V=9\ 5.5L^{3/4}D^{-1.5}$		63 ~200	0.1	Cc; Is
				7.8x1.5			Cc 1.6 Ec 4.9		1.41	4	5.77	$V=30.5\pm13L^{3/4}D^{-1.5}$ $V=9\pm5.5L^{3/4}D^{-1.5}$				Ec; DS2 7
6	C-Tunnel	Houses	railway	(9.5,12.4) x1.0	weathered granite	2-Enoki	Cc 0.2		0.25	23/31	2.42	$V=106L^{3/4}D^{-1.5}$		40	0.45	Cc; Is
							Ec 0.5					$V=82L^{3/4}D^{-1.5}$				Ec; DS2 8
7	D-Tunnel	Houses		25.2x1.0	weathered granite	2-Enoki	Cc 0.8		0.75	62	2.16	$V=44.2L^{3/4}D^{-1.5}$		154 ~267	0.2	Cc; Is
							Ec 3.6					$V=15.7L^{3/4}D^{-1.5}$				Ec; DS2 10
8	E-Tunnel	Houses		32x1.0	Hard rock	2-Enoki	Cc 1.2		0.72	87	2.72			67 ~120	0.1	
							Ec 4.0									
9	Kompira T.	Houses			granite	2-Enoki	Ec 0.4			4		$V=10L^{2/3}D^{-2}$				

10	Sasago T.	Existing tunnel	Highway	7.9x1.2 6.0x0.9	Soft rock Shale <3.5-4>	2-Enoki	Cc 2.4 Ec 3.9 Cc 0.3 Ec 7.1		1.42 0.70	35 116	4.43 1.93	$V=1540L^{2/3}$ $V=580L^{2/3}$ $V=200L^{2/3}$ $V=170L^{2/3}$	300 ~400 300 ~400	140 ~150 20-30	6.53	Cc; Is Ec; DS2~10 Cc; MS1~5 Ec; DS2~10
11	Suma water Supply T.	Existing tunnel	Channel	8.9x1.2	Soft rock weathered granite	2-Enoki	Cc 1.6 Ec 3.2		1.41	39	4.38	$V=503L^{2/3}$ $V=190L^{2/3}$		30-40		Cc; Is Ec; DS2~7
12	Anya water power sta.	Existing tunnel		13.8x1.3	Hard rock conglomerate		Cc 0.6 ~ 2.4		1.48 ~2.54	65 ~77	4.71 ~5.58	$V=1514L^{0.87}D^{1.33}$			3.0	
13	Uryuno T.	Existing tunnel	Railway		Hard rock granite		Cc 0.5 Ec 1.0			47		$V=300L^{3/4}D^{1.92}$		50	2.5	
14	2nd Yokoo T.	Existing tunnel	Railway		Hard rock granite	2-Enoki	Cc 0.4 Ec 1.2	8.2		35		$V=470L^{3/4}D^{2}$		2-27	1.0	
15	Kitakyushu T.	Houses	Railway	15.3x1.5	porphyry	2-Enoki	Cc 1.6 Ec 5.0	28.4	1.23	54 ~58	3.66	$V=3880L^{1/2}D^{1.6}$	20-30	50 ~200		
16	Hiroshima T.	Houses	Railway	15x1.5 15x0.9	Hard rock granite <4-5>	2-Enoki	Cc 4.8 Ec 7.0 Cc 0.8 Ec 2.5	35.8 21.8	1.51 1.61	67 64	4.47 4.27	$V=10L^{2/3}D^{-2}$ $V=5L^{2/3}D^{-2}$ $V=10L^{2/3}D^{-2}$ $V=5L^{2/3}D^{-2}$		20-50		Cc; Is Ec; DS2~13
17	Bingo T.	Houses	Railway	16x1.5 38x1.5	Hard rock granite	2-Enoki	Cc 2.4 Ec 2.0	15.8 19.7	0.66 0.35			$V=1000L^{2/3}D^{-2}$ $V=890L^{2/3}D^{-2}$		170 ~350		Cc; Is Ec; DS2~10
18	Kameura T.				Soft rock Sand Stone <1.3>	3-kiri ANFO Concrete cracker						$V=700L^{2/3}D^{-2}$ $V=700L^{2/3}D^{-2}$ $V=70L^{2/3}D^{-2}$				
19	Vertical Shaft				Soft rock Shale-Sand Stone <0.8-3.7>	Shinkiri Shinkiri Urbanite Urbanite	3.8 ~ 5.4			37		$V=1800L^{2/3}D^{-2}$ $V=1000L^{2/3}D^{-2}$ $V=1200L^{2/3}D^{-2}$ $V=600L^{2/3}D^{-2}$		30		
20	F-Tunnel	Houses		38x1.2	Hard rock granite			47.5	1.04	125	3.29			127		
21	G-Tunnel				Hard rock basalt <3>	2-Enoki		31.9						40 ~122		

Notation:

Cs: Cross section [m^2]
APR: Advance per round [m]
Vp: P-wave velocity [km/s]
Qc: Charge per m^3 [kg/m^3]

Nh: Number of drill holes
f: frequency of wave [Hz]
D: Distance from shot point [m
AL: Allowable limit

Va: particle velocity [cm/s]
Cc: Center cut
Ec: Easer cut
Is: Instantaneous shot

Table 5.5 Summary of Empirical Propagation Equations

	Proposer	Equation	Conditions	Remarks	
Maximum particle velocity (V)	Itoh, Sassa and Tanimoto	$V=K\cdot L^{2/3}\cdot D^{-2}$	$8<D<300$	K=250~1000 K= 15~21	gelatine dynamite black powder
	Asahi Chemical	$V=K\cdot L^{2/3}\cdot D^{-n}$	$30<D<1500$ $10<W<3000$	K=500~1000 K=300~500 K=200~500 n=2.0 n=2.5~3.0	for center-cut shot for easer shot for bench cut for rock for clay
	Nihon Chemical	$V=K\cdot L^{3/4}\cdot D^{-2}$	$5<D<3000$ $0.2<W<4000$	K=450~900 k=200~500 K=300~700 K=100~300 K=300~2000	for tunnelling for easer, roof shot in tunnelling for lifter shot in tunnelling for bench cut using large bore holes for lifter, loosening shot
	Nihonyushi	$V=K\cdot(\frac{D}{\sqrt{L}})^{-1.5}$		K=80±40 K=60±20 K=20±10 K=50±30 K=45±25 K=15±10	for tunnelling, dynamite (2-Enoki, 3-Kiri) for tunnelling, control blasting for tunnelling, concrete cracker for open blasting, dynamite (2-Enoki, 3-Kiri) for open blasting, control blasting for open blasting, concrete cracker
Maximum amplitude(A)	Hatanaka	$A=400\cdot K\cdot L^{2/3}\cdot D^{-2}$ $A=5.2\cdot K\cdot L^{2/3}\cdot D^{-1.2}$	$15<D<250$ $250<D<1500$	K=700 K=250 K=100	for the case of $H_b>L_w$ for the case of $H_b<L_w$ for the case of no surface soil
	Yoshikawa etal.	$A=K\cdot L^{3/4}\cdot D^{-2}$		K=100~700	
	U.S.Bureau of Mines	$A=30.1\cdot K\cdot(e^{-0.00469D}+0.0143)$ $+0.0143)\cdot L^{2/3}$	$152<D<1829$ $454<L<4536$	K=0.1 K=1 K=3	for the case of no surface soil $H_b<(1/2\text{-}1/4)L_w$ $H_b>1/2L_w$

V: Velocity of vibration [cm/sec],
A: Maximum amplitude [μ],
K: Constant,
L: Charge per delay [kg]
D: Distance from blasting site [m]
H_b: Thickness of surface soil [m]
L_w: Wave length [m]

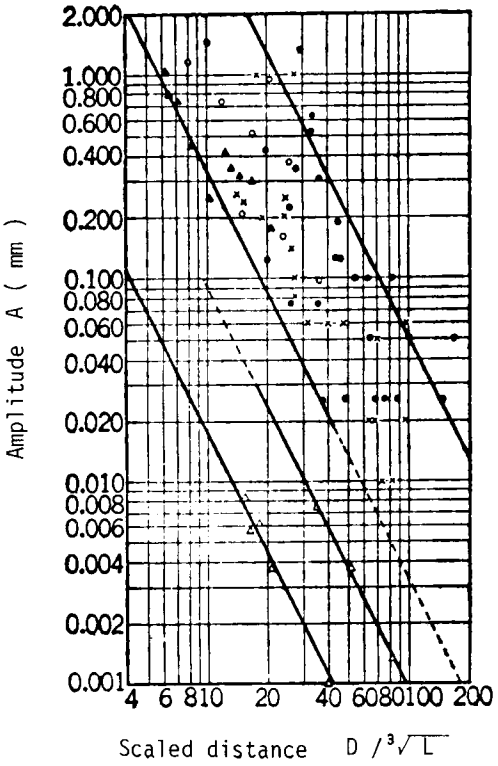

Fig. 5.7 Particle Velocity and Scaled Distance

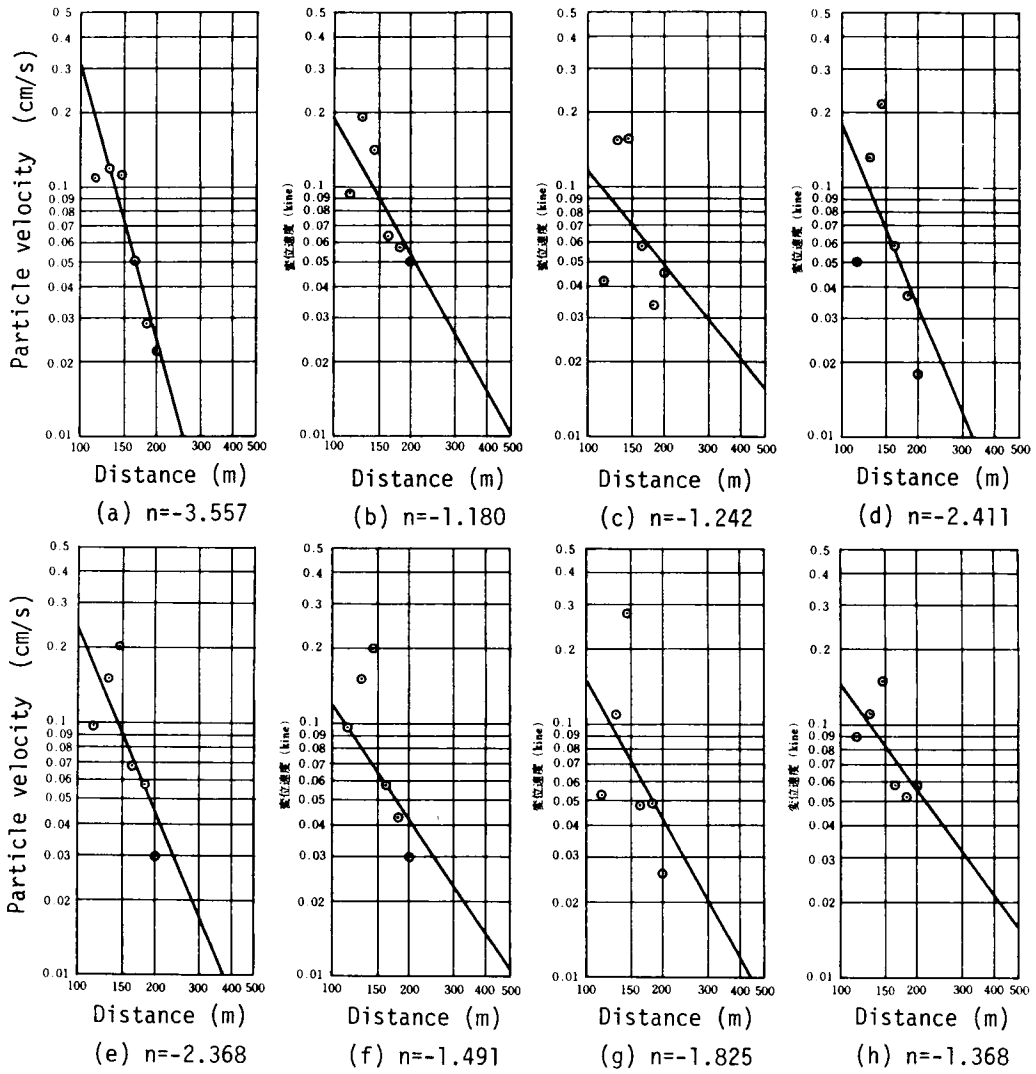

Fig. 5.8 Attenuation of Blasting Vibration in Izumi Formation

5.4 Influence to Amplitude of Vibration by Ground Condition

In general, amplitude observed on the roof or the wall of a tunnel is smaller than one observed on the surface of the ground, for it is considered that the rock near the surface is affected much by weathering and overlaid by earthen material. In Fig. 5.7, the measured values of displacement related to the ground surface show wide scattering in the range of 10 times to the same scaled distance, and this suggests the magnitude of the influence by ground condition.

Aptikaev [19] analyzed the relation between peak amplitude of displacement and specific impedance (defined by the product of density of the ground and propagation velocity of longitudinal wave), and obtained the result as shown in Table 5.6. It agrees with the above mentioned observation that the amplitude of displacement of ground vibration varies inversely as the specific impedance of the ground.

Water content is also another factor correlated to the amplitude of vibration. It is pointed out that the wave propagating through water bearing ground shows higher amplitude than the ground in dry state. For example, Kirillov [20] reported that vibration in wet state became 2 – 2.5 times of one in dry state, and vibration by blasting in the river propagated five times farther than in the field. And also Gaskell [21] reported that vibration caused by blasting in water saturated clayey ground reached 3 – 4 times farther than in dry sandy ground, and underwater blasting generated vibration of four times more than the case of clayey ground.

5.5 Damage Caused by Blasting Vibration

5.5.1 Vibration to human body

In the field of earthquake engineering, many researches and investigations have been carried out aiming at finding the relation between the vibration generated by earthquake and damages to be caused, and the seismic intensity scale established by the Japanese Meteorological Agency shows the practical relation between amplitude of acceleration and observed phenomena classified to the eight categories. [22] (Table 5.7) According to this seismic intensity scale the perceptible limit of human being to vibration is specified with the amplitude of acceleration and it is 0.8 gal (= 0.8 cm/s^2). Also the safety limit without any damage against houses in Japan is considered 80 gal.

As many studies and investigations dealing with acceleration have been proceeded so widely, it may be considered to be convenient to employ the factor of acceleration in the discussion on the vibration-damage relation.

Commonly in both cases of earthquake and blasting, longitudinal waves, lateral waves and various surface waves were observed in the same manners. (For example, [23], [24], [25]) Though there is substantially no difference on the vibration between earthquake and blasting, we should consider in the detailed discussion on the behaviors of vibration generated by them that there may exist some tight correlations among the magnitudes of vibration energy sources, the mechanism of occurrence, relative positions of vibration source and observed point, path of

Table 5.6 The Relation between Amplitude and Specific Impedance of Ground (after Aptikaev [19])

No.	Specific impedance ρc ($g/cm^3 \cdot km/s$)	$(\rho c)_1/(\rho c)_i$	Amplitude A (μ)	A_1/A_i
1	14 5	1	120	1
2	4.4	3.3	400	3.3
3	1.25	11.6	1500	12.5
4	0.75	19.5	2200	18.3

Table 5.7 JMA Intensity Scale (by the Japan Meteorological Agency)

Intensity	Description	Acceleration in gal
0	No sensation:registered by seismographs but no perception by the human body.	below 0.8
I	Slight: felt by persons at rest or persons especially sensitive to earthquake.	0.8 - 2.5
II	Weak: felt by most persons; slight rattling of doors and japanese latticed paper sliding doors(shoji).	2.5 - 8.0
III	Rather strong: shaking of houses and buildings; heavy rattling of doors and shoji; swinging of chandeliers and other hanging objects; movement of liquids in vessels.	8.0 - 25.0
IV	Very strong: strong shaking of houses and buildings; overturning of unstable objects; spilling of liquids out of vessels four-fifths full.	25.0 - 80.0
V	Very strong: cracking of plaster walls; overturning of tombstones and stone lanterns; damage to masonry chimneys and mudplastered warehouses.	80.0 - 250.0
VI	Disastrous: demolition of up to 30% of Japanese wooden houses; numerous landslides and embankment failures; fissures on flat ground.	250.0 - 400.0
VII	Ruinous: demolition of more than 30% of Japanese wooden houses.	over 400.0

propagation and so on. Comparing the vibration by blasting with the one by earthquake in general, we should pointed out two distinctive differences between them. One of them is the difference on the range of frequency. In most cases of earthquake vibrations with relatively low frequencies such as 0 – 10 Hz have been observed, and in blasting, higher frequencies such as 30 – 300 Hz, sometimes over 1000 Hz, have been realized. Another distinctive difference is on duration. In earthquake records the duration of the vibration is ordinarily observed in the range from several seconds to several minutes, and vibration by blasting diminished within several hundreds milliseconds at longest.

Reiher and Meister [26] reported the relations among human sensitivity to vibration, amplitude of displacement and frequency of vibration as shown in Fig. 5.9, which has been quoted very frequently. Onto Fig. 5.9, in which thick curves were shown by Reiher–Meister, the author added two relations to be referred in the following consideration by giving the relation between the displacement amplitude and frequency under constant acceleration of 0.8 gal with the broken line and also the relation between the displacement amplitude and frequency under constant particle velocity 0.038 cm/s with the dotted line. From Fig. 5.9, the perceptible limit to human body can be specified with the acceleration, 0.8 gal, in cases with frequencies below 2 Hz as well as most cases of earthquake, but in cases with frequencies higher than 5 Hz it becomes unappropriate to specify the sensible limit in terms of acceleration amplitude. Then, it is concluded that an appropriate expression as a major correlated factor in the discussion on the sensible limit to human body should not be specified by the acceleration amplitude, but by the peak particle velocity in cases generating vibrations with the frequency of 5 – 60 Hz.

Thus, in the cases of blasting vibration accompanied by higher frequency comparing with earthquake, the influence by blasting vibration, that is, the sensitivity to human body, has the tight relationship with the peak particle velocity, and the sensible limit in the particle velocity can be specified 0.038 cm/s.

On the other hand, Goldman [27] gave a little higher value of 0.051 cm/s to the perceptible limit in the cases of 6 – 60 Hz, based on the results about the relations among particle velocity, frequency and human sensibility which were obtained by applying the vibration in the form of sine wave. And, related to the vibration with 6 – 30 Hz, the Japanese Society of Archtectures has specified the value of 0.06 cm/s as the allowable limit in designing structures and buildings with inhabitants against the mechanical vibration, which are caused by the equipped machineries. [28] I.S.O. announced the specification on the vibration with respect to the allowable limit of exposure to human body in the range of 1 – 80 Hz. [29] The objects in this specification are aircraft pilots and vehicle drivers who are exposed to constant vibration lasting for a long time. In the consideration on the influences caused by blasting vibration, the differences of frequency and of exposure time should be discussed well.

5.5.2. Damages to structures, building and houses

The magnitude of vibration, which causes some damage to structures, buildings and houses,

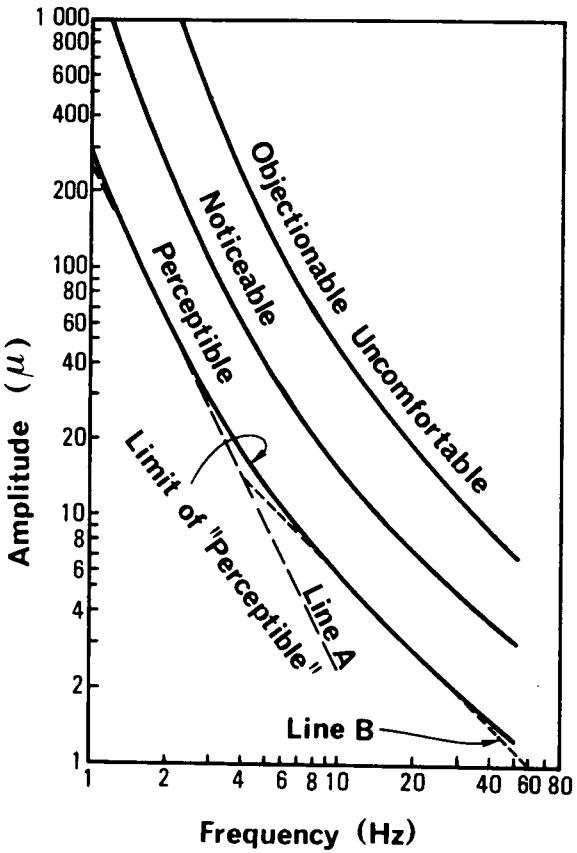

Fig. 5.9 Relation among Human Sensitivity, Amplitude and Frequency (after Reiher–Meister)

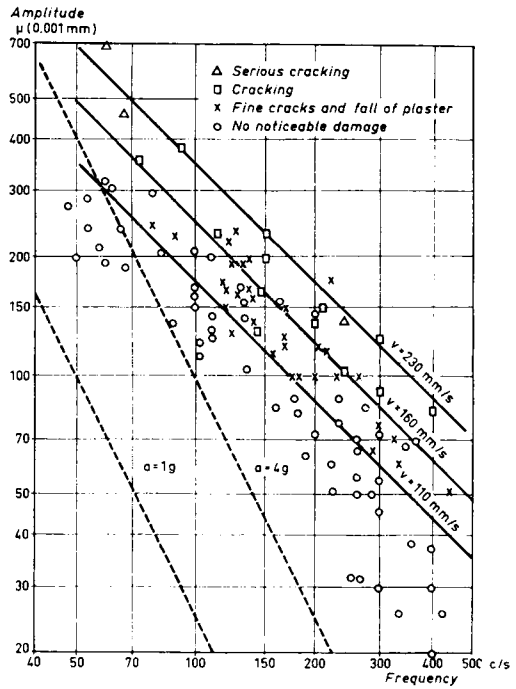

Fig. 5.10 Relation among Amplitude, Frequency and Damage (after Langefors)

depends on frequency as well as the sensitivity of human body mentioned in the former section. Langefors et al [30] gave the summarized relations among displacement amplitude, frequency and damage as shown in Fig. 5.10. It shows in the range of 50 – 500 Hz that, even if the amplitudes of displacement and acceleration do not vary, the magnitude of damage may differ by far, and also that the amplitude of particle velocity has the proportional relationship with damages of structures. (Numerical expression for the magnitude of damages is difficult, but conceptionally, the above mentioned proportional relation can be accepted.) To speak of the possibility of occurrence of damage to structures and buildings, it can be concluded from Fig. 5.10 that the safety limit may exist round 10 cm/s with respect to particle velocity. Fig. 5.11 is the summary, based on the data reported by Thoenen–Windes [11], Reiher–Meister [26], Banik [31], and Crandel [32]. By adding the allowable limit of vibration investigated by Wiss [33], Fig. 5.12 can be obtained. Langefors [30], Edwards [33] and Bumines [33] pointed out the indication by particle velocity as the most predominant factor correlated with damages to structures and buildings, and also it should be remarked that they gave the almost same value, that is 5 cm/s, as the safety limit. According to Banik [31], the safety limit of 0.5 cm/s is rather lower than 5 cm/s. This disagreement comes from the differences on the condition related to ground, for the investigations by Langefors and others were carried out on the ground consisting of the rocks with the longitudinal wave propagation velocity of 2000 – 3000 m/s and Banik's conclusion was obtained from the investigation related to buildings on the alluvial layers, which were considered to response excessively against vibration.

U.S. Bureau of Mines had carried out their large scaled experiments aiming at the relation between vibration and damages of buildings. [33] In this project the measurement of blasting vibration was done 171 times totally. The method of initiation was mainly the MS-delayed blasting, the charge weight per delay was 11 – 8900 kg and the objective rocks were limestone, dolomite, granite, diabase, schist, sandstone and so on. Fig. 5.13 shows the results obtained by U.S. Bureau of Mines, whose conclusion suggested that particle velocity should be dealt with as the main parameter in the discussion on the safety of buildings for vibration, and that the allowable limit might be 5 cm/s.

Concerning the designation for the allowable limit of vibration, Crandell [32] proposed the application of Energy Ratio (ER). Denoting acceleration and frequency, A (in ft/s^2) and f (in Hz), respectively, Energy Ratio is defined by A^2/f^2. According to ER, no damage is prospected for $ER<3$, to be cautious and fine cracks for $3<ER<6$, and damages to houses and brick-structures for $ER>6$. Energy Ratio, ER, can be expressed in metric unit in terms of

$$ER = 0.01674\, f^2 U^2 \tag{5.9}$$

where U is amplitude. Fig. 5.14 shows the safety limit by ER. In the same manner as Crandell, Thoenen [11] introduced another expression defined by $f^2 \cdot U$ (in metric unit), which indicates the occurrence of damages for $f^2 \cdot U>10$ and to be safe for $f^2 \cdot U<1$. In Fig. 5.14, the results by

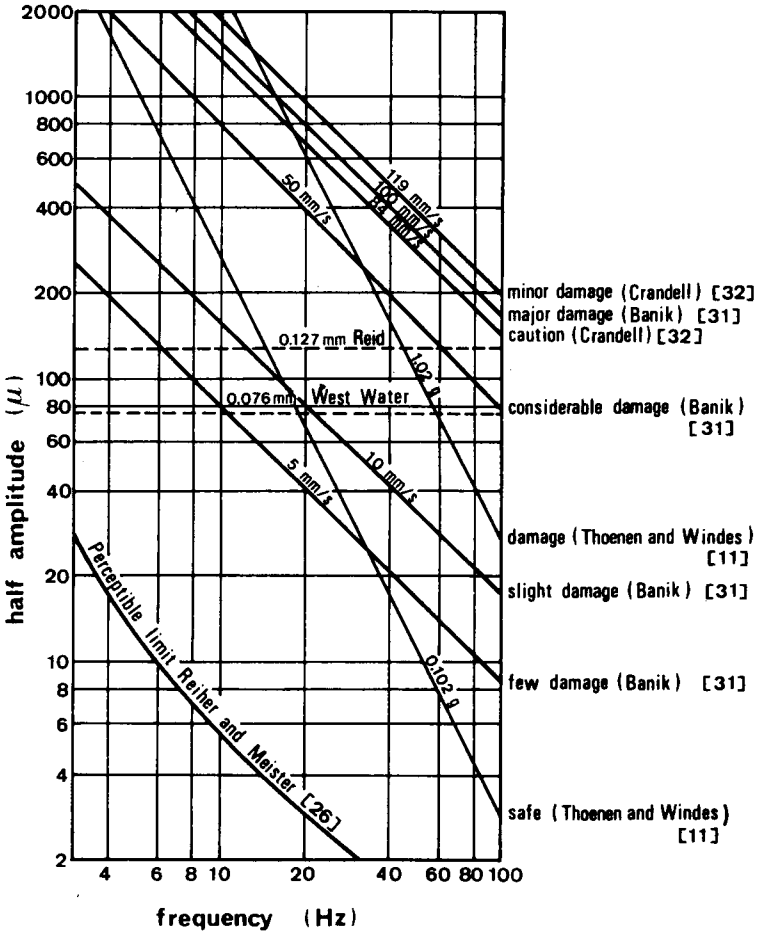

Fig. 5.11 Relations among Amplitude, Frequency and Damage

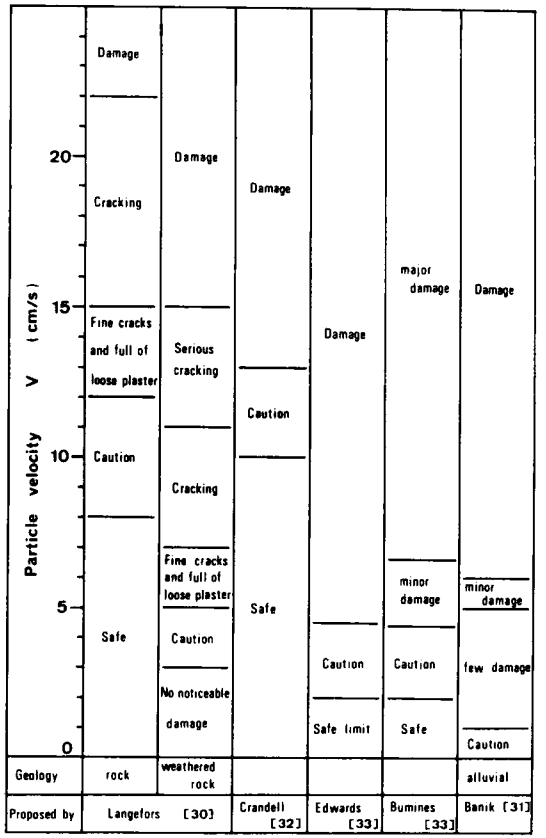

Fig. 5.12 Relations between Particle Velocity and Damage

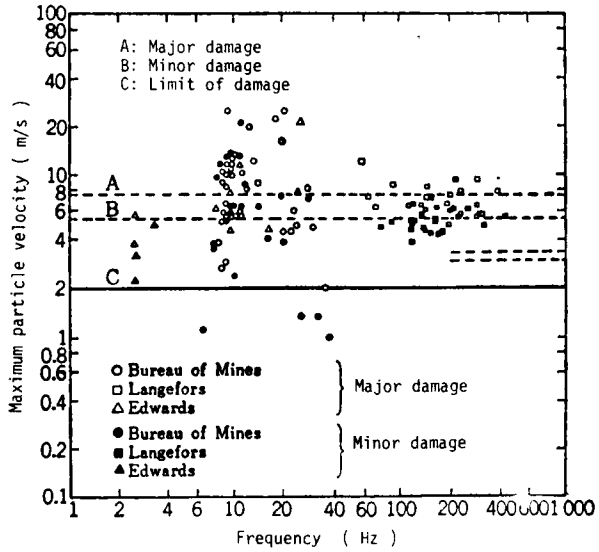

Fig. 5.13 Relation between Particle Velocity and Damage Observed by U.S. Bureau of Mines.

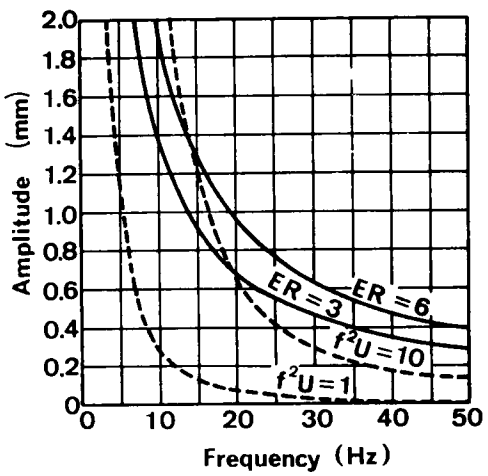

Fig. 5.14 Allowable Limit Specified by Energy Ratio

Thoenen are shown by broken curves. In the range of low frequency the both results of Crandell's and Thoenen's agree well, but the disagreement is recognized for high frequency.

Here, the author introduced several reports published in foreign countries, together with the author's opinions. The research on the relation between vibrations and damages to buildings is quite practical, but with the exception of Hatanaka [17] there are very few investigation which aims at the systematic study on the detailed relation between the blasting vibration and the damages to buildings. Adding to the behavior of propagating blasting vibration mentioned above, further research on related damages should be advanced widely.

5.6 Reduction of Blasting Vibration

So long as the breakage mechanism of rock by blasting depends on dynamic action generated by explosion more or less, it is impossible to carry out blasting without any vibration propagating beyond crushed zone in the vicinity of charged boreholes. Therefore, it should be realized that blasting operation is always accompanied by vibration and noise whatever their magnitudes may be. From the point of environment assessment during the constructions of rock works including tunnelling, it is required to discuss the reduction of vibration generated by blasting. Ahead of the detailed consideration on the reduction of blasting vibration, it should be emphasized to execute blasting in such an adequate way as considering feasible design aiming at utilizing energy most efficiently.

The author picks up following items as the practical methods for the reduction of blasting vibration.

(1) To employ explosives with low detonation velocity:

The fundamental breakage mechanism of rock blasting consists of two actions, namely dynamic one by the propagation of highly stressed waves and static one by quasistatic gas pressure. It is pointed out by Murata [34], Langefors [35], Fogelson et al [36] that for a high explosive, for example, dynamite with high detonation velocity, the shock wave energy most probably amounts only to 5 – 15% of the total energy of the explosive at a theoretical estimate, and at least 2/3 of its energy will disappear without affecting the breakage, as the shock wave is distributed all around a charge, and it is concluded that the shock wave is not responsible for the actual breakage of the rock, but only for providing the basic conditions for this process. The efficiency of explosives is determined by several factor such as detonation velocity, specific volume (properties of representative explosives available in Japan are shown in Table 5.1) and geological conditions of rock. As mentioned in Section 5.2, it is concluded that the explosives with lower detonation velocities generate lower magnitude of vibration. In the comparison between dynamite and AN–FO, whose specific volumes are almost the same, there was not any noticeable difference on the efficiency of blasting operation, but there may exist rather remarkable differences on blasting effect in rock excavation among other various explosives with quite different values of specific volume like the case of dynamite to CCR or AN–FO to black powder. Anyhow, the ef-

ficiency and the necessary quantity per unit volume for several types of explosive should be confirmed first of all by test blasting, and then it is recommended to choose a suitable type of explosive according to the indication obtained in the discussion of Section 5.2.

By making the magnitude of vibration caused by the explosion of gelatine dynamite in the case of one free face blasting applied to medium hard rock (center cut in tunnelling) 1.0 as a basis for comparison, relative values for some types of explosive and proposed values of constant K in the empirical propagation equation, Eq. (5.2), are shown in Table 5.8.

(2) To initiate with delayed EB-caps:

Once the type of explosive and the distance from blasting site are fixed under the limited condition, the only way to reduce the magnitude of vibration by blasting is to reduce weight of charge per delay as shown in Eq. (5.2). Also, it is well known among practical engineers that vibration amplitudes gained by employing delayed shot (DS–or MS–delayed) are 1/2 – 1/3 of the ones by simultaneous shot. This means the same fact that center cut generates much higher vibration amplitudes than ones observed in easer cut. The author tried to confirm this fact under the constant conditions. Table 5.9 and 5.10 show the results obtained in the investigations at Kompira Tunnel [3] and vertical shafts with 4 m dia. for Yamanaka Bridge [6]. These tests were carried in such a manner as executed center cut (one free face blasting) by initiating with instantaneous EB–caps (zero-delayed), DS–2 and MS–5 EB–caps at the faces under the constant condition (equal type of explosive, equal weight of charge per hole, equal number of boreholes, equal geological situation etc.). From those results it is concluded that vibration amplitudes in easer cut by DS–2 caps and MS–5 caps are 30% and 60% of amplitude in center cut by zero-delayed caps.

Let us discuss furthermore about considerable treatments for the reduction of vibration. In ordinary blasting, explosive is not loaded to a sole borehole as concentrated charge, but by loading to many drilled holes it is initiated with many detonating caps as distributed charge. Therefore, if the total amount of charge might be initiated just instantaneously (in the strict sence) for the case that the amount of W [kg] per hole is loaded to several boreholes with the number of N, the generated vibration amplitude should be subjected to the value of L=NW [kg] in Eq. (5.2). On the other hand, if every explosive in each hole might be initiated at a certain time interval and generated vibration from each hole might be separated completely, vibration amplitude should be determined by L=W [kg], and it would be reduced to $1/N^{2/3}$ of the case for L=NW [kg]. This difference is considerable.

In order to get better understanding about the time-dependent change of particle velocity generated by the wave from the explosion of the sole charge, let us consider the results obtained from the both of theoretical calculation and practical observation. Under the dynamic pressure acting onto the inside of spherical cavity in an elastic body as shown in Fig. 5.15, the change of particle velocity of radial component is as shown in Fig. 5.16. [37] Comparing with this theoretical result, it can be seen that many waves recorded in the investigations ([3] – [8]) show

Table 5.8 Comparison on Relative Magnitude of Vibration among Different Types of Explosive

Explosive	in center cut	in easer cut
Gelatine dynamite	1.0 (800-1200)	0.4 (320-480)
AN-FO	0.35 (280-420)	0.15 (120-180)
Smokeless powder	0.3 (240-360)	0.12 (100-150)
Urbanite	0.5 (400-600)	0.2 (160-240)
Concrete cracker	0.1 (80-120)	0.04 (30-50)

Table 5.9 The Values of Coefficient K given by Different Types of Initiation (for Granite)

Shot point	EB-cap	Observed at Point P			Observed at Point Q		
		Vert.	Hor.EW	Hor.NS	Vert.	Hor.EW	Hor.NS
A	Zero	10.4	3.8	3.7	6.7	9.1	11.1
	DS-2	5.2	2.1	1.8	2.9	2.6	5.7
	DS-2	3.6	1.4	1.1	2.4	3.9	4.7
B	Zero	8.5	3.5	2.1	5.8	6.9	7.5
	DS-2	1.7	0.9	0.7	1.6	2.8	4.4
	DS-2	2.7	1.1	0.87	1.7	1.9	3.2

Notation Zero: instantaneous cap, Vert.: vertical direction,
Hor.EW: horizontal,east-west direction,
Hor.NS: horizontal,north-south direction

Table 5.10 The Values of Coefficient K given by Different Types of Initiation (Sandstone–Shale)

EB-cap	Point D	Point E	Point F
Zero	6.19 (1.0)	12.44 (1.0)	8.25 (1.0)
MS-5	4.83 (0.78)	7.42 (0.60)	4.91 (0.60)
DS-2	2.02 (0.33)	3.18 (0.26)	2.13 (0.26)

quite similar shape to the one as shown in Fig. 5.16 when the simultaneous shot is applied with zero-delayed caps. Thus, we realize that the vibration from instantaneous shot, corresponding to ordinary center cut in rock tunnelling, behaves almost in the same manner as solely charged explosion. When delayed shot is applied, vibration records show that $2-3$ serial groups of waves, having similar shape to zero-delayed shot, are apt to be observed in each delay. (For example, as shown in Fig. 5.17) This means the separation of wave motion with respect to each explosion per hole due to the scattering of initiation, for the accuracy of initiation of zero-delayed EB cap is below 1.0 ms and DS–delayed cap has the scattering of ± 10 to 100 ms. The one of MS–delayed cap is considered approximately 1/10 of the DS–delayed.

To speak of the separation of vibration with respect to various delays, being based on the observations, the duration of the main parts of wave motion showing high peaks is considered as approximately 100 ms. [6], [37] When the EB–caps such as Zero–, MS–2 to MS–4 delay are used for initiation, superposition of wave motion is prospected more or less, but noticeable superposition cannot happen at the usage of DS–delay caps and MS–delay caps with higher number than MS–4.

Consequently, the amplitude of vibration can be specified by the quantity of explosive per delay in the case of DS– and MS–delayed blasting, and specially in the case of DS–delayed shot it is presumed that the amount per hole might be a more significant parameter in actual blasting.

Beside the above mentioned method to reduce blasting vibration, the application of pre-splitting blasting method, one of the controlled blasting, can be proposed, and the author carried out the investigation aiming at searching the effect of the fractured zone produced by pre-splitting around the charged area for center cut as shown in Fig. 5.18. [3], [4], [37] The alignment of presplit holes as shown in Fig. 5.18 was not enough to give noticeable effect.

The result of this investigation concludes that it is necessary to establish considerably wide and thick presplit zone which can cover the whole vicinity of mining face in order to get satisfactory effect for the reduction of vibration. From the theoretical point of view, the existence of aperture produced by pre-splitting can be useful for the reduction of propagating vibration. Assuming the aperture distributed in the fractured zone to be one uniform layer consisting of air gap as a whole, the vibration, namely propagating stress wave, which enters into the aperture perpendicularly with the particle velocity w(t), removes the nearer free face along the aperture with the initial velocity of 2w(t).

Referring to the discussion in Chapter 3, the propagation equation of plane stress wave is expressed in terms of

$$w(t) = \sigma(t) \cdot (1/\rho \cdot C_L) \tag{5.10}$$

where $w(t)$: particle velocity in propagating direction, $\sigma(t)$: dynamic stress in propagating direction, ρ: density of propagated medium, and C_L: velocity of longitudinal wave. By con-

Fig. 5.15 Dynamic Gas Pressure Acting onto the Inside of a Spherical Cavity in an Elastic Body

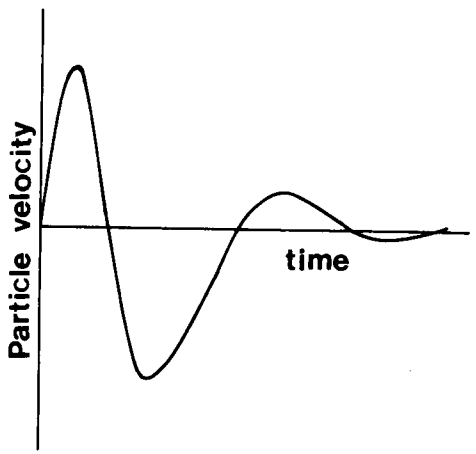

Fig. 5.16 Resultant Particle Velocity Subjected Dynamic Pressure

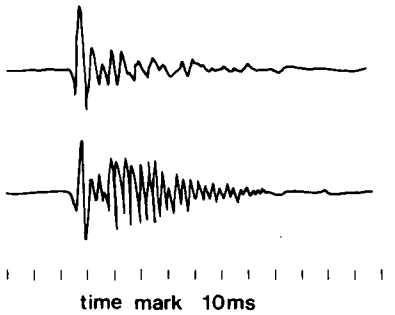

(a) Initiated with instantaneous EB-caps

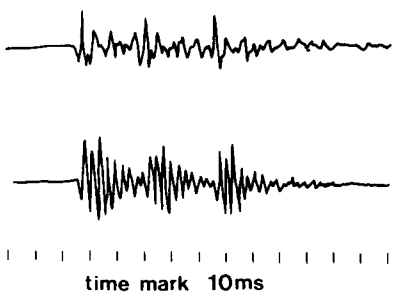

(b) Initiated with MS-delayed EB-caps

Fig. 5.17 Oscillogram of Blasting Vibration

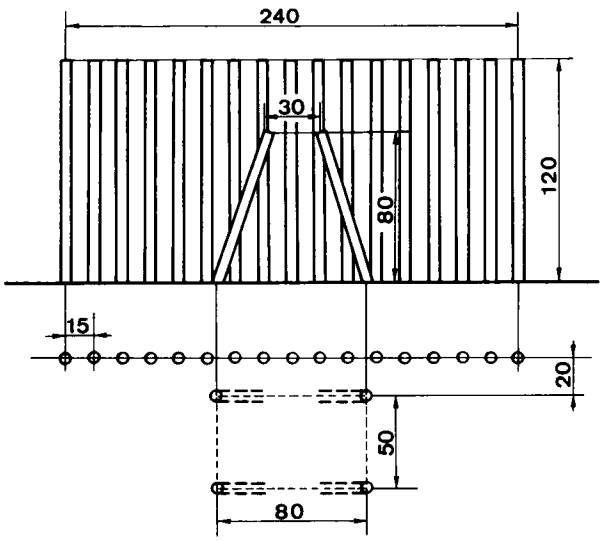

Fig. 5.18 Alignment of Boreholes for Pre-splitting

sidering stress wave as a part of sine wave, maximum particle velocity ($W_{max.}$) is expressed in the form of

$$W(t) = W_{max.} \sin(2\pi f \cdot t) \tag{5.11}$$

where f: frequency

and assuming the amplitude of displacement to be zero at $t=0$, maximum value of displacement, $U_{max.}$, is

$$U_{max.} = W_{max.}/(\pi \cdot f)$$

Therefore, the necessary width of aperture, Dc, for the effective reduction should be

$$Dc > W_{max.}/(\pi \cdot f) \tag{5.12}$$

In order to confirm this condition and the noticeable effect of pre-splitting, furthermore field studies are required from the practical point of view.

5.7 Conclusions

In Chapter 5, being based on many results obtained from the field measurements, which were carried out in medium hard rocks, the actual behaviors of propagating vibration generated by blasting operation were discussed, and the simple empirical propagation equation was proposed

from the practical point of view by the author. The reduction of blasting vibration has become the important subject in the field of environmental assessment accompanied by civil works due to the rapid and strong demands for tunnels with nearby structures and inhabitants. Main results derived from the study in this chapter are as follows.

(1) The behavior of ground vibration generated by blasting is governed by the following factors: a) distance from the blasted point; b) type of explosive; c) quantity of charge; d) method of initiation; e) drilling pattern; f) tamping condition; g) path of propagation; h) characteristics of ground; and i) state of ground formation.

(2) Differing from earthquake with frequency lower than 10 Hz, blasting generates vibration with the frequency of 30 – 800 Hz. The frequency should be the predominant factor correlated with the magnitude of damages.

(3) In the discussion on the damage of structures and the sensitivity of human body caused by blasting vibration the particle velocity should be dealt with as the main parameter because the intensity of damage and human sensitivity has the proportional relation with the particle velocity in the case of being subjected to the vibration with frequency over 30 Hz.

(4) For the prediction of blasting vibration, the following propagation equation can be applicable.

$$V = K \cdot L^{2/3} \cdot D^{-2}$$

where V: maximum particle velocity [cm/s],

L: charge weight per delay [kg],

D: distance from blasted point [m],

and K: constant determined by the type of explosive, method of initiation, and geological condition. For example, K=1000 for the case of center cut by initiating gelatine dynamite with instantaneous EB caps.

(4) The raise time of gas pressure induced by explosion correlates much with amplitude of vibration, and this means that explosive with lower detonation velocity generates less vibration. The relative ratios of gelatine dynamite (De), AN–FO (Ao), smokeless powder (Sp) and concrete cracker CCR (Cr) are

$$De : Ao : Sp : Cr = 1.0 : 0.35 : 0.3 : 0.1 \quad .$$

(5) The usage of explosive with higher detonation velocity generates vibration with higher frequency. According to spectrum analyses, the vibration generated by dynamite shows the prominent peaks in the range of 200 – 800 Hz, and others show their prominent peaks on wave records in the range below 300 Hz.

(6) The sensible limit of blasting vibration to human body is considered 0.038 – 0.05 cm/s in particle velocity.

(7) The allowable limit of vibration to buildings can be specified by the particle velocity in the

range of 3 – 5 cm/s.

(8) To initiate with the delayed EB–caps reduces the vibration. In general, center cut generates higher vibration than easer cut, and the vibration amplitude in easer cut is 50% – 60% of the amplitude in center cut with Zero-delayed caps. By utilizing the slight scattering of initiation time of delayed EB–caps such as DS–delay caps or MS–delay caps with higher number than MS–4, it is possible to reduce more.

(9) As the duration of the main parts of wave motion showing high peaks is considered as 100 ms approximately, no noticeable superposition of wave motion can happen at the usage of DS–delay caps and MS–delay caps with higher number than MS–4. Consequently, it is verified that the amplitude of vibration can be specified by the quantity of explosive per delay.

(10) Pre-splitting blasting is considered as one of the solution for reducing vibration to nearby structures and it is necessary to produce considerably wide and thick presplit zone which can cover the whole vicinity of mining face in order to obtain fruitful effect.

REFERENCES for Chapter 5

[1] Senozawa, K., Kanai, K.: Memoirs of Earthquake Research Institute, Tokyo Imperial University, 14–1, pp. 10, 1939. (in Japanese)

[2] Olson, J.J., Dick, R.A., Condon, J.L., Hendrickson, A.D., Fogelson, D.E.: Mine roof vibrations from underground blasts, Report of investigations 7330, U.S. Dept. of the Interior, Bureau of Mines, 1970.

[3] Fujii, T., Tanimoto, C.: Experimental approach to the reduction of vibration in blasting, J. of Dobokukensetsu (Constructions in civil works), pp. 33–40, Vol. 19, No. 12, 1970. (in Japanese)

[4] Ito, I., Sassa, K., Tanimoto, C.: The reduction of ground vibration by underground blasting, Proc. of 26th JSCE Annual Sympo., III–38, pp. 117–120, 1971. (in Japanese)

[5] Tanimoto, C.: Feasibility study on the blasting operation to nearby structures and inhabitants in highway construction, Technical Report–Nishimatsu Co., April, 1971. (in Japanese)

[6] Tanimoto, C.: Experimental study on the ground vibrations by the excavation of vertical shafts in Izumi Formations, Technical Report–Nishimatsu Co., Feb., 1972. (in Japanese)

[7] Kimura, T., Tanimoto, C.: The prevention of public nuisances caused by blasting –Vibration, noise and throw, Proc. of 12th Conference of Japan Road Association, Specialty Session 215, pp. 60–62, 1975. (in Japanese)

[8] Imanaka, Y., Kawai, K., Maruyama, T., Tanimoto, C.: Ground vibrations and explosion noise by blasting in Izumi Formation, Proc. of 10th Sympo. on Rock mechanics, JSCE, pp. 36–40, 1976. (in Japanese)

[9] Hatanaka, M.: Technical report of Construction Engineering Institute, Kobe University, No. 3, pp. 31, 1962. (in Japanese)

[10] Makiyama et al.: Rock mechanics and its application, The society of Material Science–Japan, pp. 385–386, 1966. (in Japanese)

[11] Thoenen, J.R., Windes, S.L.: U.S. Bureau of Mines, Bull. 442, 1942.

[12] Olson, J.J., Dick, R.A., Fogelson, D.E., Fletcher, L.R.: Mine roof vibrations from production blasts, Shullsburg Mine, Shullsburg, Wis., Report of Investigations 7462, U.S. Dept. of the Interior, Bureau of Mines, 1970.

[13] Hashimoto, J.: Proc. of Autumn Meeting, Japanese Society of Mining and Metallurgy, Q–12 1972, (in Japanese)

[14] Reid, A.G.: Australian Institute of Mining and Metallurgy, 186, 1951.

[15] Ito, I., Fujinaka, Y.: J. of Suiyokwaishi, 15–4, pp. 171, 1964. (in Japanese)

[16] Ito, I., Murata, T., Shimizu, T.: J. of the Society of Mining and Metallurgy–Japan, pp. 285, 1953. (in Japanese)

[17] Hatanaka, M., Otsuki, T.: Technical Report of Construction Engineering Institute, Kobe University, No. 3, pp. 21, 1962. (in Japanese)

[18] Tanimoto, C., Maruyama, T.: Technical Report on the Naruto experimental construction for cutting long slope in the project of Honshu–Shikoku Bridge, Japan General Contractors Association, pp. 145–190, 1975. (in Japanese)

[19] Aptikaev, F.F.: Seismic vibrations due to Earthquakes and Explosions, English Translations, Univ. of California, Laurence Radiation Lab., pp. 19, 1971.

[20] Kirillov, F.A.: Trudy Seismolog, in–ta AN SSSR, No. 121, 1947.

[21] Gaskell, T.F.: Geophysical Prospect, 4–2, 1959.

[22] Okamoto, S.: Earthquake Engineering, p. 29, English Edition, University of Tokyo Press, 1973.

[23] Leed, L.D.: Vibrations from blasting rock, Harvard University Press, pp. 67–94, 1960.

[24] Iida, K., Hattori, S.: Geophysical Prospecting, 22–1, pp. 1, 1969. (in Japanese)

[25] Iida, K., Hattori, S., Matsueda, F.: Geophysical Prospecting, 23–2, pp. 76, 1970. (in Japanese)

[26] Reiher, H. and Meister, F.J.: Forschung auf dem Gebiet des Ingenieurwesens, 2–11, pp. 381, 1931.

[27] Goldman, D.F.: Naval Medical Research Inst. Report, No. 1, Project NM 004001, March, 1948.

[28] Committee on Structure Standardization, Session of Vibration, J. of Archtecture, 74–870, pp. 59, 1959. (in Japanese)

[29] I.S.O.: Draft International Standard ISO/DIS 2631, 1972.

[30] Langefors, V., Kihlström, B.: The modern technique of rock blasting, John Wiley and Sons, Inc., pp. 269, 1963.

[31] Banik, E.: Sprengparxis, 4, 1958.

[32] Crandell, F.J.: J. of Boston Society of Civil Engineers, No. 36, p. 222, 1949.

[33] Wiss, J.F.: Civil Engineering, 38–7, pp. 48, 1968.
(Nicholls, H.R., Johnson, C.F., Duvall, W.I.: U.S. Bureau of Mines, Bull. 656, 1971.)

[34] Murata, T., Tanaka, I.: J. of Industrial Explosives, 15–4, pp. 294, 1954, and 16–1, pp. 32, 1955. (in Japanese)

[35] Langefors, V., Kihlstrom, B.: The modern technique of rock blasting, John Wiley and Sons, pp. 18, 1963.

[36] Fogelson, D.E., Duvall, W.I., Atchison, T.C.: U.S. Bureau of Mines, R.I. 5514, pp. 15, 1959.

[37] Ito, I., Sassa, K., Tanimoto, C. et al: Report on the experimental study on blasting vibration at Kompira Tunnel, submitted to Water Resources Authority, 1970. (in Japanese)

Chapter 6

ROCK BREAKAGE BY SMOOTH BLASTING*

6.1 Introduction

Smooth blasting is a technique to make the final contour created by blasting appear almost as if it was cut out of rock with a knife and to leave the remaining rock practically undamaged without overbreaking. Through the observation of the face created by this technique, it can be recognized practically that a line of major crack is created from hole to hole which has been drilled in parallel in the projected plane of breakage and the cracks in the other directions are few. The crack pattern shown above is obvious in practice, but it seems that the reason why the major crack from hole to hole is created without cracks in the other directions has not been clarified completely. Therefore, a smooth blasting research project has been conducted to clarify the mechanism of rock breakage by smooth blasting and to find out a better technique which can be used more satisfactory to the purpose.

6.2 State of Dynamic Stress and Breakage Around a Bore Hole Caused by Stress Wave

In smooth blasting operation, the charges are fired usually with instantaneous blasting caps, but even if the charges are fired with instantaneous caps, all the charges may not be initiated simultaneously in the strict sence, because of a very few difference in the ignition time. Therefore, the effect of empty circular holes near an explosion on the distribution of dynamic stress caused by a stress wave must be discussed at first.

In this study, dynamic stresses produced in a polymethyl methacrylate plate of 18 mm in thickness by a detonation of 0.3 g DDNP loaded in a 7.2 mm diameter hole was computed by using the equation derived from the theory of elasticity [1] and the cylindrical coordinate of which origin is the centre of the explosion. As an example of the results, the effect of the existence of an empty hole on the maximum value of the dynamic tangential stress $\sigma_{\theta max}$ is shown in Fig. 6.1 which is obtained for the case where an empty hole of 4 mm in diameter is placed at 3 cm apart from the centre. It is clear from the result shown in Fig. 6.1 that in case of the plate having an empty hole adjacent from the explosion, a remarkable increase in the tangential tensile stress is produced near the two points on the empty hole which are closest to and farthest from the explosion.

As has generally been recognized, such a tangential tensile stress caused by a stress wave may create the radial cracks in the material, next, let us discuss how the radial cracks grow with time.

---

* Rock Breakage by Smooth Blasting, Proceedings of the 2nd Congress on Rock Mechanics, International Society of Rock Mechanics, Vol. III, pp. 53 ~ 57, September, 1970. (Coauthors: I. Ito, K. Sassa and K. Katsuyama)

Fig. 6.2 shows the change in the tangential tensile stress with time after the detonation along the direction from the centre to the empty hole, which is obtained in the same experiment treated in the former discussion. The numbers attached on the curves indicate the time after the detonation. In the following discussion, the dynamic tensile strength of the polymethyl methacrylate is assumed as 700 kgf/cm^2 (7×10^4 kN/m^2) (about $1.0 \sim 1.5$ times of the static tensile strength). It is clear from the curve at 30 μs after the detonation that radial cracks are considered to be created in the arbitrary direction until the effect of the existence of the empty hole comes out on the state of stress, and some of the tips of the cracks may reach the points of r = 15 mm at this instant, where r is the distance from the centre. These radial cracks grow with time, and at the instant of 35 μs after the detonation some of the tips reach the points of r = 22 mm, but they do not yet reach the surface of the empty hole. While at this instant, the values of the tensile stresses at the two points in question on the empty hole already exceed the dynamic tensile strength of the material. This means that new cracks of which origins are the points of intersection between the surface of the empty hole and the direction from the centre to the empty hole are created along this direction before the radial cracks from the explosion reach the empty hole. And also, by referring to the results shown in Figs. 6.1 and 6.2, it can be understood that the length of the crack along the direction from the centre to the empty hole is much longer than that in the other direction.

In order to make sure the results of this stress analysis, small scale blasting tests are conducted under the same condition as that for the stress analysis, and it is concluded that the pattern of the cracks created actually in the small scale blasting coincides very well with that predicted from the results of the stress analysis.

6.3 State of Stress and Breakage Caused by Quasi-Static Pressure in a Bore Hole

In smooth blasting operation, normally a decoupled charge has been used in each bore hole. When such a decoupled charge is detonated, it seems that a fairly high quasi-static pressure may act on the inner surface of the charge hole after the stress wave caused by the detonation of the charge has been projected. Therefore, besides the breakage due to the stress wave mentioned above, the breakage caused by this quasi-static pressure may have a fairly important role on the formation of the smooth cut created by a smooth blasting. Consequently, as the next theme, the stress distribution caused by the static pressure has been analyzed by using the finite element method.

The basic configuration of the holes and the free face used to analyze the stress distribution in the material is shown in Fig. 6.3. In this study, the stress distribution is analyzed for the following three cases to simulate the conditions which may be considered to appear in turn in the phenomena caused by a smooth blasting: namely, (1) a pressure is applied only in the hole B and no pressure is applied in the holes A and C; (2) two cracks of a definite length along the x-axis exist at the points of intersection between the surface of each hole and the x-axis and a pressure is applied in each hole; and (3) many radial cracks of the same length exist around the surface of the hole and

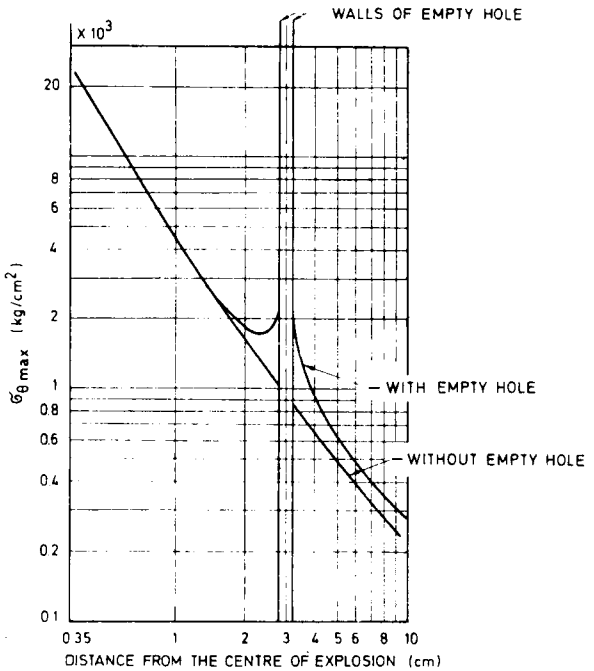

Fig. 6.1 Change in $\sigma_{\theta max}$ with time along the direction from the centre of explosion to the empty hole.

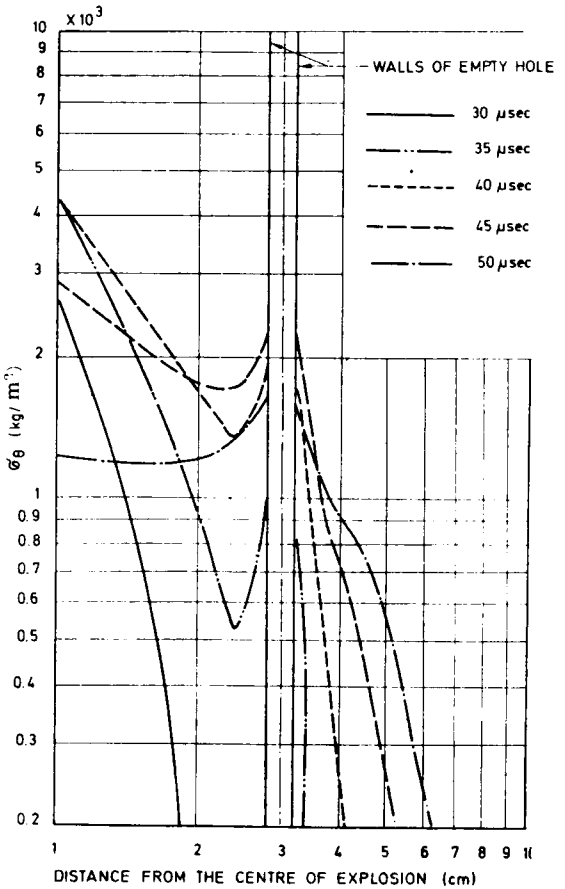

Fig. 6.2 State of stress σ_θ at a definite time after the detonation.

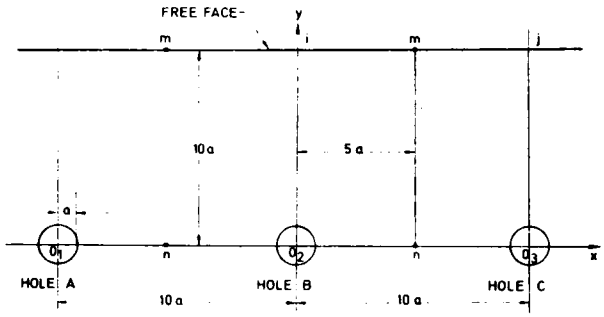

Fig. 6.3 Basic configuration of the holes and the free face.

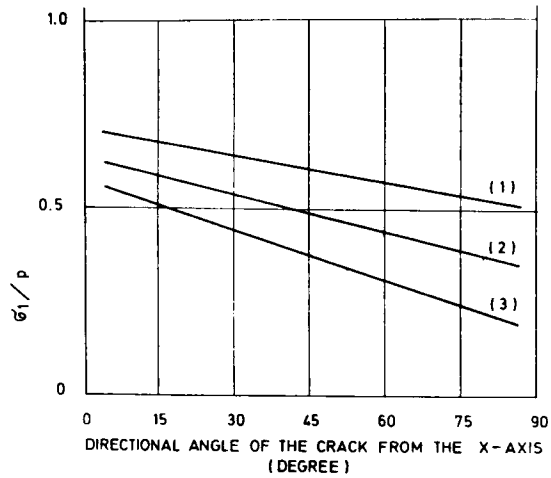

Fig. 6.4 Relation between the degree of stress concentration at the tip of the crack and the directional angle of the crack from x-axis for the cases, (1) C = 0.5 a, (2) C = a, and (3) C = 1.75 a, where C is the length of the crack and a is the radius of the hole.

a pressure is applied on the inner surface of each hole.

From the results obtained in the stress analysis for these three cases, the conclusion can be summarized as follows.

(1) The existence of the empty holes of which configuration is shown in Fig. 6.3 has almost no effect on the stress distribution near the hole with the pressure, but a remarkable increase of the principal tensile stress comes out at the point of intersection between the inner surface of the empty hole and the x-axis. From this fact, it is understood that the crack along the x-axis are created from the inner surface of the holes A and C ahead of the cracks towards the other directions.

(2) Once the cracks along the x-axis have been created at the inner surface of the hole, the principal tensile stresses near the tips of the cracks increase quite a bit, but those at the points far from the cracks decrease with the existence of the crack. This means that the crack along the x-axis may grow further more and more, but new other radial cracks may not be initiated near the x-axis because the values of the tensile stress at the points on the inner surface of the hole are less than that at the tip of the crack.

(3) As an example of the results obtained in the stress analysis for a case where 24 radial cracks of the same length in directions separated by 15° with each other exist around the surface of the hole and a pressure is applied on the inner surface of the hole, Fig. 6.4 shows the relation between the value of σ_1/P at the tip of each crack and the directional angle of each crack from the x-axis, where σ_1 is the maximum principal tensile stress and P is the pressure applied on the inner surface of the hole. It is understood from the result shown in Fig. 6.4 that even in the case where many cracks exist around the surface of the hole, the maximum value of σ_1/P appears at the tip of the crack on the x-axis and the value of σ_1/P decreases linearly with the increase of the directional angle of the crack until finally attains its minimum on the y-axis. Moreover, the difference between the maximum and minimum values of σ_1/P is magnified with the increase of the length of the crack. Therefore, the crack on the x-axis is always apt to be lengthened more and more compared with the cracks towards the other directions.

6.4 Effect of Guide Hole on the Breakage

In smooth blasting, in order to leave the remaining rock as undamaged as possible, a special technique must be necessary to repress the growth of the crack towards unfavourable directions. It can be supposed that this request may be solved to a certain extent with an application of a guide hole, that is, an empty hole which is drilled close to the loaded one[2].

In order to confirm the above supposition, some model experiments shown below have been conducted. As shown in Fig. 6.5(a), a charge hole and a guide hole, of which diameters are 7.2 mm and 2.7 mm respectively, are drilled in a polymethyl methacrylate plate of 18 mm in thickness and three wire strain gauges are cemented on the plate to measure how the hoop stress in the material

is relaxed by a rarefaction wave from the crack. Three-tenth gram of DDNP is used as a charge and a photo-transistor is used to detect the instant when a crack through the guide hole reaches the point A from which a rarefaction wave is projected into the material. The trace A in Fig. 6.5(b) is an oscillogram of the out-put signal of the photo-transistor and in this case the negative deflection of the beam means the decrease in the intensity of the light to the photo-transistor, therefore, the point a indicated on the trace is considered to correspond with the instant when the tip of the crack reaches the point A. The trace B in Fig. 6.5(b) is a strain oscillogram of gauge 3 and in this case the positive deflection corresponds to the tensile strain. It is understood from the oscillograms shown in Fig. 6.5(b) that the hoop stress in the material is relaxed rapidly by the rarefaction wave from the crack and in this case the time required to relax the hoop stress is about $10\,\mu$s.

Next, let us discuss the mechanism to repress the growth of cracks towards unfavourable directions by utilizing the guide hole. In Fig. 6.6(b), the curves A and B are assumed to represent the change in the tangential tensile stress with time at the points A and B shown in Fig. 6.6(a), in which the reason why the curve A attains the larger value of the tangential tensile stress is the existence of the guide hole. If we suppose that a material is broken when the tensile stress in the material has reached its dynamic tensile strength S_t, then at the instant of $\tau = t_1$ in Fig. 6.6(b), a crack will be created at the point A and the tangential tensile stress at this point is relaxed, which in turn would result in the projection of the rarefaction wave in the material. As the rarefaction wave travels with the velocity of C_L, the front of the rarefaction wave may reach the point B at $\tau = t_\theta = t_1 + \ell/C_L$, where ℓ is the length of the arc between the points A and B. As soon as the rarefaction wave arrives at the point B, the hoop stress at that point is relaxed rapidly. Therefore, it may be concluded that there is no possibility to produce a crack within the range where the point B satisfies the condition of $\ell < (t_2 - t_1)\,C_L$, and if the point B exists within the range satisfying the condition of $\ell > (t_2 - t_1)\,C_L$, there is a possibility to produce another radial crack near the point B.

6.5 Mechanism of Rock Breakage by Smooth Blasting

Now, let us consider the mechanism of rock breakage by smooth blasting by synthesizing the results of the above discussion. In smooth blasting, a decoupled charge is normally used. In this case, the so-called pressure spike which generally appears in the case of the fully coupled charge is considered to disappear by the action of the air gap in the charge hole and the extent of the radial crack caused by an explosion is decreased with the increase of the degree of decoupling [3]. Moreover, in smooth blasting the hole space is not so large and the charges loaded in each hole are not initiated quite instantaneously because of the existence of the difference in ignition time between each detonation cap. Therefore, in many cases, the tangential tensile stresses on the line towards the adjacent hole become larger than those in the other directions because the adjacent holes act as an empty hole to the charge hole. Consequently, the crack along the projected plane of breakage

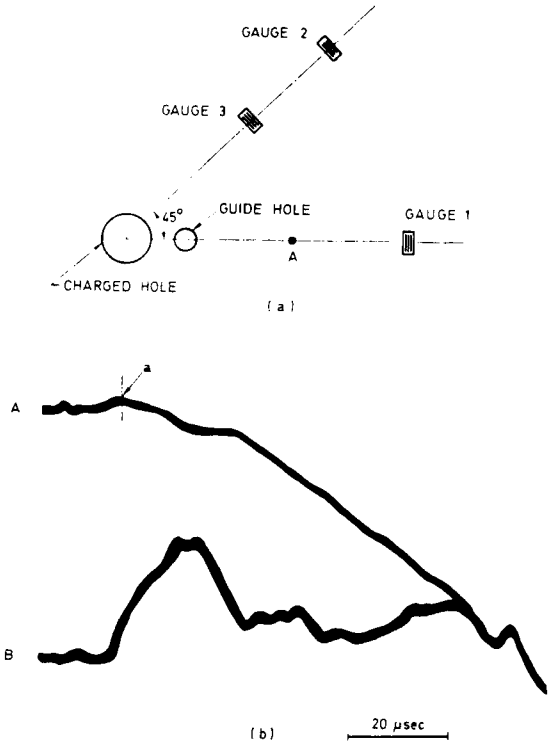

Fig. 6.5 Configuration of the holes and gauges, and examples of the oscillograms.

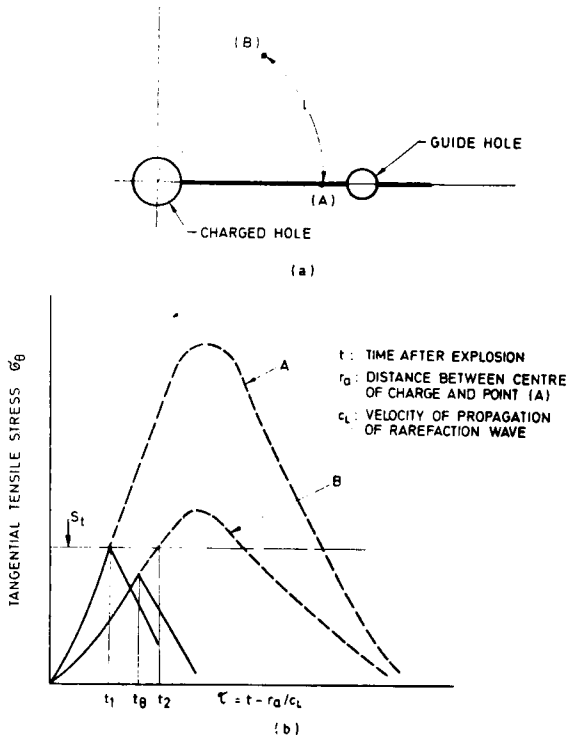

Fig. 6.6 Relaxation of the hoop stress

may develop much longer than the cracks towards the other directions, and in the case where the hole space is close enough, this crack may reach the adjacent hole. On the other hand, even in the case where this crack can not reach the adjacent hole, there is a possibility of producing other new cracks from the adjacent hole because of the stress concentration at the two points on this hole which are closest to and the farthest from the explosion. Furthermore, as the quasi-static pressure due to the explosion gases in the adjacent hole may act on the hole for a pretty long period of time, the hole must be kept under considerable prestressed condition. Thus, in smooth blasting, the cracks along the projected plane of breakage can develop extremely and the quasi-static pressure in the hole acts to force the growth of these cracks and make them as open ones. While the growth of cracks towards the other directions is repressed to a considerable extent by the action of the rarefaction wave from the main crack mentioned above and can not grow as open ones. In this way, a smooth wall along the projected plane of breakage can be produced finally.

REFERENCES for Chapter 6

[1] I. ITO, K. SASSA and K. SHIGEMATSU, - Jour. Min. and Met. Inst. of Japan, 83, 952. 1967, p.983-990.

[2] U. LANGEFORS and B. KIHLSTROM, - Rock Blasting, John Wiley and Sons, Inc., 1963, p.297-301.

[3] I. ITO and K. SASSA, - Jour. of Min. and Met. Inst. of Japan, 84, 964, 1968, p.1059-1065.

Chapter 7

FIELD MEASUREMENT AND CONSIDERATION ON DEFORMABILITY OF THE IZUMI LAYERS

7.1. Introduction

In the design of underground openings and structures related to rock mass, it is important to determine the appropriate moduli of deformation of rock mass and evaluate its mechanical properties although it is known to be difficult. The apparent deformation behavior of rock mass can be considered as the sum of the deformation of the solid rock itself and the deformation due to the discontinuities, and it is well known that the latter is greater than the former.

Two basic procedures, static and dynamic methods, are used for determining the deformability of rock masses. In the static method, relatively large static loads are applied to the selected surface of rock mass, and the resulting deformations are measured. In the dynamic method, the velocity of propagation of vibrational disturbances is measured.

Plate loading test, hydraulic jack pressure test, borehole loading test, water loading test etc. are the examples of the static method, and seismic velocity measurement is used as the dynamic method. Judging from the experiences and the knowledges in practice, however, it seems that the results obtained by the static methods are strongly affected by the local geological conditions particularly of the region where the loads are applied, and also the dynamic method is generally impractical in determining the deformability of rock mass directly.

The author had some opportunity to discuss about deformability of rock mass called "Izumi-layers" in the design of the 120,000 m^3 volumed anchorage block of 1629 m long suspension bridge, Ohnaruto Bridge. This chapter deals with the methods and results of the displacement measurement on large scale undertaken at the various locations during the operation of the transportation tunnel (called Kameura Tunnel) of which excavation caused some change of stress distribution in the ground.

The author developed the aluminium-pipe-deformation-meter which showed good agreement with the result of the convergence measurement, and comparing this global measurement with the result obtained in the plate loading test and the borehole loading test, it was found that the former gave half deformation coefficient as the latter's.

Anisotropy of Izumi-layers was also discussed the results from the seismic survey and the convergence measurement, but there still exists disagreement between them.

The rock classification mentioned in this chapter is derived from the paper of Ochi et al. [1].

7.2. Geological Condition of the Test Site

The foundation rock of the testing site is the Cretaceous system (Izumi-layers) consisting

of 10 - 50 cm thick and remarkably fissured alternative layers of sandstone, shale, mudstone and their composed zones. The strike is in the direction of NE-SW, and the dip angle is 45 degree.

The tunnelling was initiated from the landside portal (on the left hand side in Figs. 7.1 and 7.2) by the upper-half-heading method, and its cross section was semi-circular shape of 5 m in radius. Geological plane and profile are shown in Figs. 7.1 and 7.2 respectively.

In those figures, notations of "ss", "sh" and "alt" indicate sandstone, shale and their alternative layers respectively.

The results of the laboratory test on cores are as follows.

Specific gravity:

2.59 for sandstone

2.56 for shale

Ultrasonic velocity:

4.7 km for medium sandstone

4.0 km for medium shale

Static Young's modulus:

5.3×10^5 kgf/cm^2 (5.3×10^7 kN/m^2) for medium sandstone

3.3×10^5 kgf/cm^2 (3.3×10^7 kN/m^2) for medium shale

Static Poisson's ratio:

0.2 for medium sandstone

0.3 for medium shale

Uniaxial compressive strength:

1280 kgf/cm^2 (1.28×10^5 kN/m^2) for medium sandstone

620kgf/cm^2 (6.2×10^4 kN/m^2) for medium shale

7.3. Field Measurements and Results

7.3.1 Plate Loading Test.

The plate loading test conducted according to the standard proposed by Japanese Society of Civil Engineers [3] by using the steel plate of 60 cm in dia. was undertaken at 16 different points in the test gallery of 80 m long located 150 m away from (and parallel to) the tunnel [2]. At least two kinds of rocks were observed even in the narrow region covered by the loading plate of 60 cm in dia. because of the complication of Izumi-layers, which is the well known characteristic of them.

The results of the plate loading tests are shown in Table 7.1, and also few examples of load-displacement curves are shown in Fig. 7.3.

7.3.2 Borehole Loading Test

At 20 different points in the horizontal borehole of 50 m long which was drilled at the center of the tunnel cross section, the borehole loading test was undertaken. The pressure was applied on the full surface just like a pressuremeter in soil investigation, and its maximum was 50 kgf/cm^2

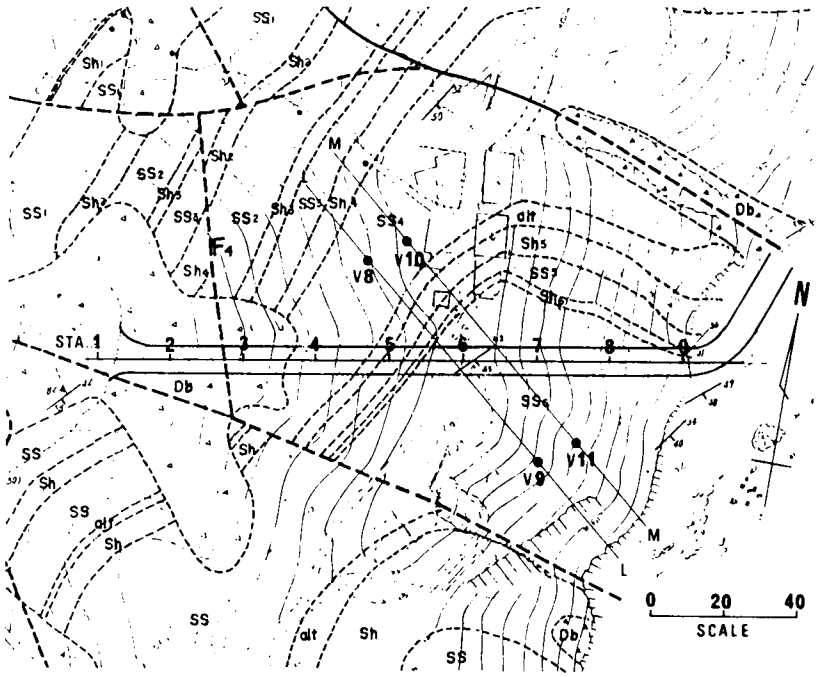

Fig. 7.1 Geological plan of the tunnel site

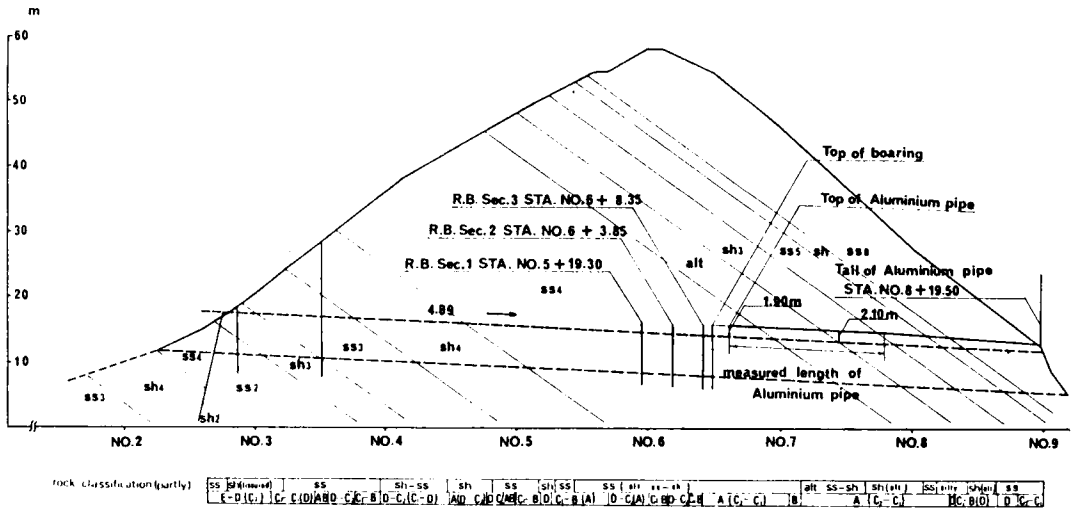

Fig. 7.2 Profile of the tunnel and rock classification

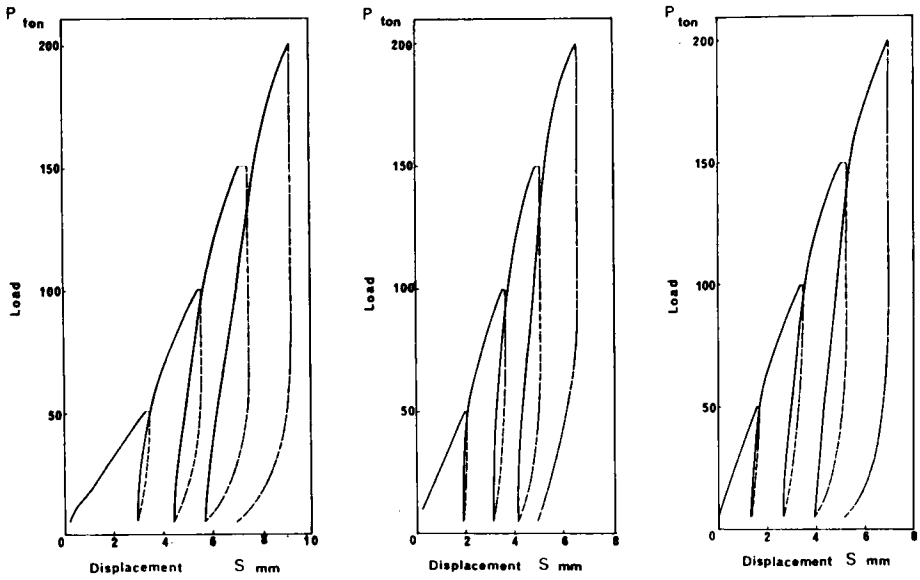

Fig. 7.3 Load-displacement curves, obtained by plate loading tests

Table 7.1 Results of Plate Loading Test

Site No.	Classification	1st Cycle (5—50 t)			1st and 2nd Cycle (5—100 t)		
		D (kg/cm²)	E_t (kg/cm²)	E_s (kg/cm²)	D (kg/cm²)	E_t (kg/cm²)	E_s (kg/cm²)
1	$A_{ss}+C_{sh}$	4 500	3 950	3 030	4 630	5 100	8 520
2	$A_{ss}+C_{sh}$	2 800	2 190	2 080	3 150	3 150	7 810
3	A_{ss}	4 710	5 250	6 060	4 630	5 020	7 810
4	$A_{ss}+B_{ss}+C_{sh}$	3 840	3 750	4 160	3 900	4 060	5 620
5	C_{alt}	4 140	3 700	3 510	4 630	4 930	7 400
6	C_{alt}	4 140	4 290	4 440	4 630	4 170	9 370
7	$D_{sh}+C_{ss}$	2 070	1 870	1 750	3 080	2 000	3 520
8	$D'-E_{sh}$	1 520	1 610	3 120	2 060	1 740	2 930
9	A_{sh}	4 140	3 750	3 950	6 170	4 490	8 270
10	$B'-C_{sh}$	3 570	3 400	3 290	5 690	4 770	8 790
11	$A'-C_{sh}$	10 360	4 490	4 550	5 290	5 290	8 790
12	$C'-D_{sh}$	1 210	1 060	900	1 370	1 290	2 270
13	$C-D_{sh}$	5 180	4 770	5 550	5 290	5 100	8 270
14	$A'+B+C+E_{sh}$	1 150	1 420	1 280	1 160	1 420	2 010
15	$A-A_{sh}'$	2 960	2 210	2 150	3 520	3 480	5 620
16	$A'-B_{sh}$	20 720	10 030	12 110	14 800	19 730	23 430

Note: 1) e. g. $A_{ss}+C_{sh}$ means alternative layers of A-class sandstone and C-class shale.
2) E_t: tangential elastic modulus, E_s: secant elastic modulus.

$(5 \times 10^3\ kN/m^2)$[4].

No definite difference in values of Esp, deformation coefficient obtained by the borehole loading test, was observed from the view point of kind of rock. This was because the deformability of Izumi-layers was strongly influenced by the presence of the discontinuities. Therefore, all were classified into three groups depending on the status of discontinuities as follows.

a–group: Esp = 6,500 – 8,000 kgf/cm^2 ($6.5 - 8.0 \times 10^5\ kN/m^2$)

b–group: Esp = 3,000 – 4,500 kgf/cm^2 ($3.0 - 4.5 \times 10^5\ kN/m^2$)

c–group: Esp = 1,000 – 2,500 kgf/cm^2 ($1.0 - 2.5 \times 10^5\ kN/m^2$)

7.3.3 Deformation Measurement of Rock Mass

Because of the reasons pointed out in the previous section, field measurement was undertaken in and around the transportation tunnel in order to get better understanding of the behaviour of rock mass.

Following the excavation of the tunnel which was initiated from the landside portal, the aluminium pipe, 6 cm in dia. and 50 m long, which has 48 strain gauges attached on its inner surface in axial direction, was inserted into the horizontal borehole of 9 cm in dia. drilled at 2 m above the tunnel crown as shown in Figs. 7.4, 7.5 and 7.6. Then the borehole was grouted such that the pipe deformed together with the surrounding rock mass. Deformation of rock was calculated from the change of the longitudinal curvature of the aluminium pipe.

The results are shown in Fig. 7.7, and the change of displacement in the vicinity of the mining face could be known so clearly. The overall displacement of the point 2 m above the crown was 14.5 mm downward at the final stage.

Hereafter the notations "a", "d" and "r" indicate the radius of the tunnel, the distance from the face in direction of tunnel axis and the distance from the center of the tunnel in cross section respectively.

7.3.4 Convergence Measurement

In three cross sections shown in Figs. 7.2 and 7.5, where special rockbolts were installed for the measurements of supporting effect and loosened area, convergence of the tunnel was measured with the (steel tape) convergence-meter by forming triangles interconnecting 3 points among 10 points at any convergence measurement, and the deviations of the points 1 and 10 from their original positions were checked by conventional tunnel survey from the portal too.

The curves consisting of solid dots and rectangles shown in Fig. 7.8 were obtained for B-class (in rock classification) rock mass and C-class rock mass respectively.

7.4 Analysis and Discussion

7.4.1. Evaluation of Deformability of Rock Mass

On the assumption that the rock mass behaved as an elastic body, several cases were analyzed mainly being based on the results obtained by the measurements of the aluminium-pipe-deformation-

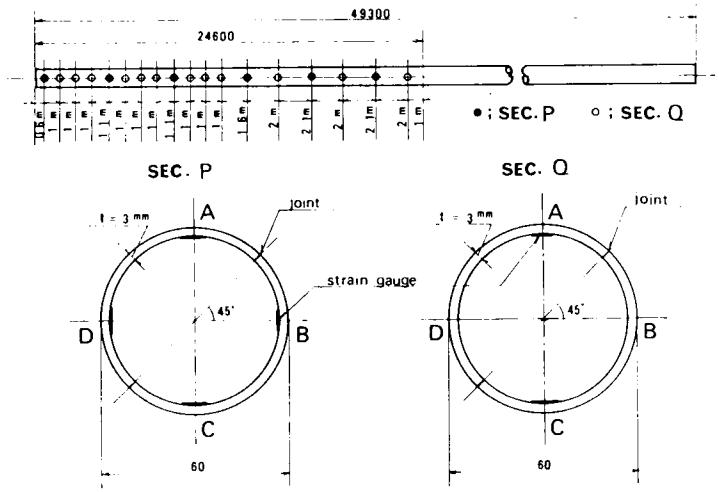

Fig. 7.4 Deformation meter, using aluminium pipe of 6 cm dia.

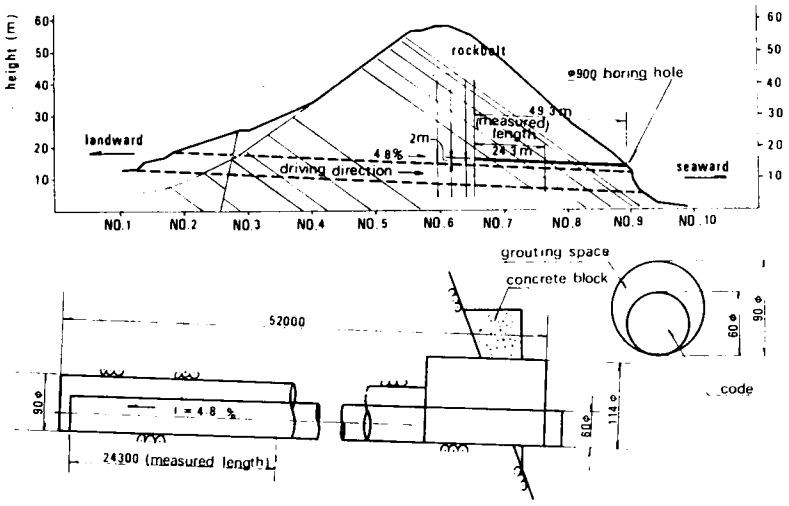

Fig. 7.5 Instrumentation in a profile

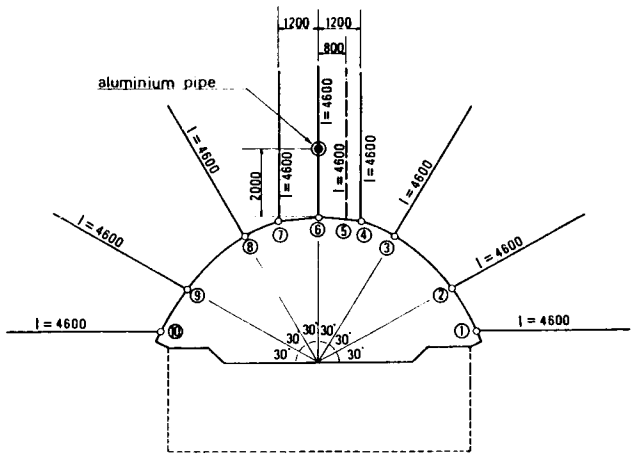

Fig. 7.6 Location of the deformation meter, rockbolts and convergence measurement

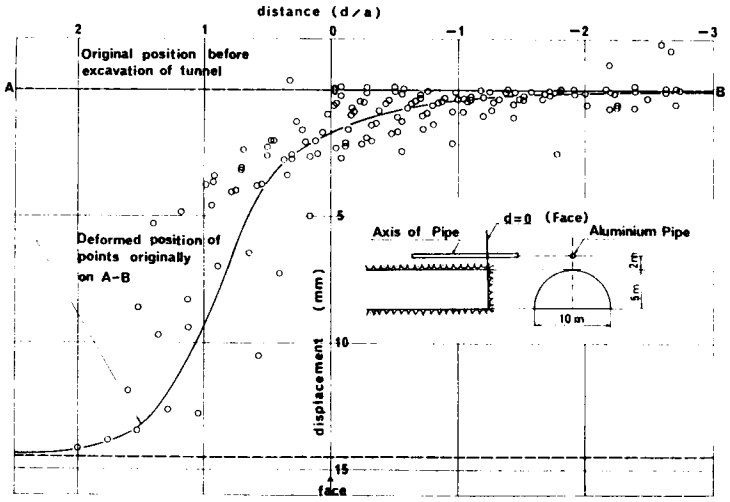

Fig. 7.7 Displacements measured by the deformation meter

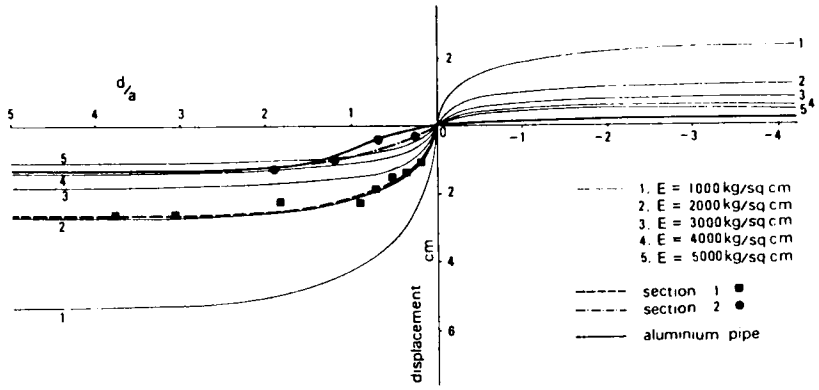

Fig. 7.8 Fitting measured displacements, obtained by the deformation meter and convergence survey to theoretical curves

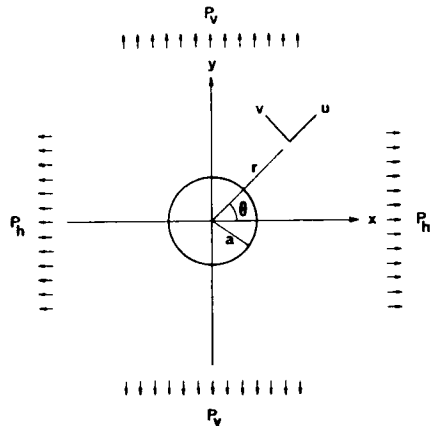

Fig. 7.9 Analytical condition for a circular opening in anisotropic stress field

meter and convergence. In the discussion of the theoretical estimation of displacements of the prototypes the following assumptions were used.

Young's modulus $E = 1000\ \text{kgf/cm}^2\ (10^5\ \text{kN/m}^2)$

Poisson's ratio $\nu = 1/3$

The ratio of the measured displacement to the prototype is going to give the actual deformability.

Prototype-1

The displacement around a circular opening in two dimensional stress field as shown in Fig. 7.9 was calculated. 'x', 'y', 'p_h', 'p_v', 'a', 'r', 'u', 'v' and 'θ' denote horizontal displacement, vertical displacement, external horizontal stress, external vertical stress, radius of a circular opening, distance from the center of the opening, radial displacement, tangential displacement and counter-clockwise angle from the horizontal axis respectivily.

In this case, horizontal and vertical displacements are:

$$\begin{aligned} x &= \frac{(1+\nu)\,a}{2E}\left[(p_v+p_h)\cos\theta-(3-4\nu)\,(p_v-p_h)\cos 3\theta\right] \\ y &= \frac{(1+\nu)\,a}{2E}\left[(p_v+p_h)\sin\theta-(3-4\nu)\,(p_v-p_h)\sin 3\theta\right] \end{aligned} \tag{7.1}$$

where E and ν indicate Young's modulus and Poisson's ratio respectively.

By assuming the values of $E = 10^3\ \text{kgf/cm}^2\ (10^5\ \text{kN/m}^2)$, $\nu = 1/3$, $p_v = 2p_h = 10\ \text{kgf/cm}^2$ $(10^3\ \text{kN/m}^2)$ and $a = 5$ m, we obtained 8.89 cm and 7.51 cm for the vertical displacements of the points at the crown (r = a) and the aluminium pipe (r = 1.4a) respectively.

The result that the measured displacement at r = 1.4a is 1.45 cm as shown in Fig. 7.7 reduces $5180\ \text{kgf/cm}^2\ (5.18 \times 10^5\ \text{kN/m}^2)$ as the deformation modulus for B-class rock.

Prototype-2

By using $E = 10^3\ \text{kgf/cm}^2\ (10^5\ \text{kN/m}^2)$, $\nu = 1/3$, $p_v = p_h = 10\ \text{kgf/cm}^2\ (10^3\ \text{kN/m}^2)$, a = 5m, the axisymmetric model for a circular opening was analysed with the finite element method, and the numerical result of the elastic displacement is shown in Fig. 7.10.

The displacements at r = a and r = 1.4a are 6.7 cm and 4.8 cm respectively. Comparing these values with the measured values of 1.77 cm at r = a and 1.45 cm at r = 1.4a, the value of 3550 kgf/cm^2 $(3.55 \times 10^5\ \text{kN/m}^2)$ is obtained as the deformation modulus for B-class rock.

Prototype-3

The displacement around the semi-circular opening was analyzed by the three dimensional finite element model having 924 nodal points and 660 elements. This can be considered as the most feasible model for the actual structure. This result is shown in Fig. 7.11. Comparing the calculated displacements of 7.8 cm at r = a and 6.0 cm at r = 1.4a with the measured ones of 1.69 cm at r = a and 1.45 cm at r = 1.4a, we obtain $4200\ \text{kgf/cm}^2\ (4.2 \times 10^5\ \text{kN/m}^2)$ as the deformation modulus for B-class rock, and also we obtain $2240\ \text{kgf/cm}^2\ (2.24 \times 10^5\ \text{kN/m}^2)$ as the deformation

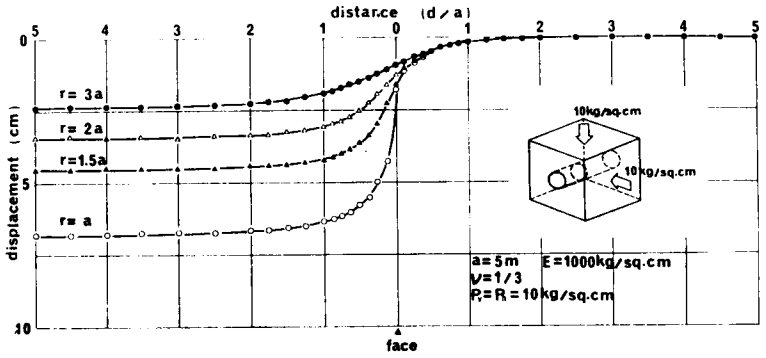

Fig. 7.10 Theoretical displacements of the elastic ground around a circular opening and its mining face (assuming a lateral pressure equal vertical pressure)

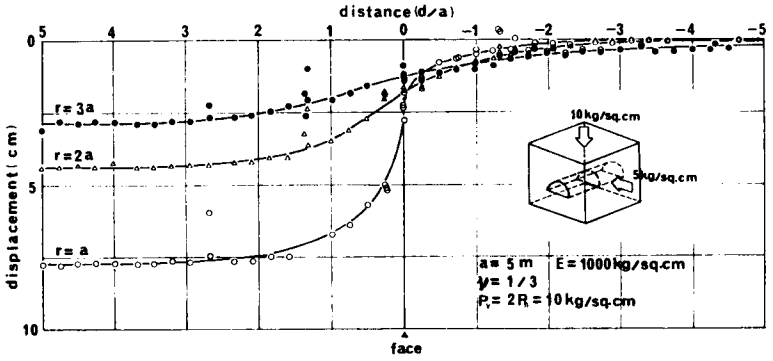

Fig. 7.11 Theoretical displacements of the elastic ground around a semi-circular opening and its mining face (assuming a lateral pressure of 1/2 vertical pressure)

modulus for C-class rock in the same manner.

As shown in Fig. 7.8, we can determine deformation modulus for two kinds of rock by fitting measured displacements obtained with the deformation meter and convergence survey onto theoretical displacement curves of various Young's moduli. Comparison of the dotted curve for Sec. 2 (corresponding to convergence survey) with the thick solid curve (corresponding to the aluminium-pipe-deformation-meter) shows very good agreement with respect to B-class rock.

Consequently, since two different measurements give almost same result, the value of 4200 kgf/cm^2 (4.2×10^5 kN/m^2) is considered to be a reasonable deformation modulus for B-class rock.

7.4.2 Correlation Among Plate Loading Test, Borehole Loading Test and Displacement Measurement

A plate loading test is most popular conventional method for determination of deformability of rock in situ and Japanese Society of Civil Engineers designated the plate loading test standard in 1975 [3].

But the test cannot be carried our on an underwater rock mass. Then, a borehole loading test becomes very practical method instead of the plate loading test in the investigation of foundations of the bridge like Ohnaruto Bridge where rapid current runs.

For the practical application of the borehole loading test, correlation between the plate loading test and the borehole loading test should be explored. For this purpose Takeuchi et al. investigated this relation, being based on the several results of the past tests. They reported that the direct correlationship between the ratio of D/E_{sp} and E_{sp} (D: deformation modulus by the plate loading test, E_{sp}: one by the borehole loading test) was recognized and it depended on stress level when tensile strength of rock was exceeded [5]. And, Mori et al. emphasize it depends on strain level [6].

It is very difficult to recognize the relation among rock classification (based on inspection and core recovery), the plate loading test and borehole loading test. In Table 7.2 we show the results of the plate loading test, borehole loading test and displacement measurement which were carried out at the same Izumi-layers.

Though the quantity of the data is relatively small, the result of displacement measurement may be considered reasonable [7]. We believe that further displacement measurement to fissured and weathered alternative layered rock mass like Izumi-layers should be carried out.

7.4.3 Anisotropy of Izumi-layers

Stratification, distribution of joints and their influence to the strength of rock mass should be discussed as well as engineering classification in case that the rock is presumed to show an anisotropic behavior. Comparing with investigations at dam construction site and at the laboratory, the number of field measurements about the anisotropic behavior at tunnels is very little. At the same site as mentioned in this chapter, the anisotropic behavior of Izumi-layers was investigated using the results of the convergence measurement and the seismic survey [8].

The displacement of a circular opening in an anisotropic body (in the state of plane strain)

Table 7.2 Comparison of Moduli of Deformability and Elasticity (in kg/cm²)

Rank	E_{sp}	E'	D	E_s	E_m
A	7970	5580	5400	8040	
A'	6530	5060	3524	5620	4200
B	7450	5400	—	—	4200
B'	3470	3820	—	—	2240
C	2400	3120	4560	8040	2240
C'	1840	2760	3250	4680	2240
D	1950	2730	1610	2470	

E_{sp}: Elastic constant by borehole loading test.
E': Converted moduli of deformability from E_{sp}.
D: Moduli of deformability by plate loading test.
E_s: Tangential moduli of elasticity by plate loading test.
E_m: Moduli of deformability by deformation meter and convergence measurement.

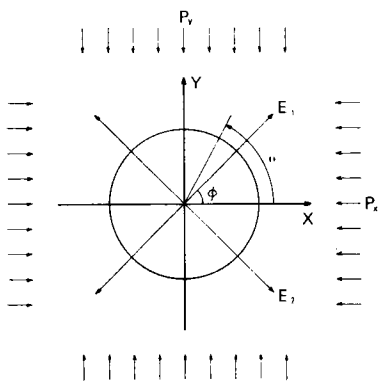

Fig. 7.12 Analytical condition for a circular opening in an anisotropic body under anisotropic stress field

being subjected to the stress field shown in Fig. 7.12 is given by following equations.

$$\begin{aligned} U_r &= U_r^* - U_r^0 \\ U_\theta &= U_\theta^* - U_\theta^0 \end{aligned} \tag{7.2}$$

$$\begin{aligned} U_r^* = &-\frac{p_x}{2} a\,[(\alpha_1' + \beta_1') - (\alpha_1' - \beta_1')\cos 2\theta - (\alpha_2' + \beta_2')\sin 2\theta] \\ &-\frac{p_y}{2} a\,[(\alpha_1 + \beta_1) + (\alpha_1 - \beta_1)\cos 2\theta + (\alpha_2 + \beta_2)\sin 2\theta] \end{aligned}$$

$$\begin{aligned} U_\theta^* = &\frac{p_x}{2} a\,[(\alpha_2' - \beta_2') - (\alpha_1' - \beta_1')\sin 2\theta - (\alpha_2' + \beta_2')\cos 2\theta] \\ &+\frac{p_y}{2} a\,[(\alpha_2 - \beta_2) + (\alpha_1 - \beta_1)\sin 2\theta - (\alpha_2 + \beta_2)\cos 2\theta] \end{aligned}$$

$$\begin{aligned} U_r^0 = &\frac{p_x}{2} a\,[(a_{11}^* + a_{12}^*) + (a_{11}^* - a_{12}^*)\cos 2\theta] \\ &+\frac{p_y}{2} a\,[(a_{12}^* + a_{22}^*) + (a_{12}^* - a_{22}^*)\cos 2\theta] \end{aligned}$$

$$U_\theta^0 = \frac{1}{2} a\,[(a_{22}^* - a_{12}^*)p_y + (a_{12}^* - a_{11}^*)p_x]\sin 2\theta$$

$$a_{11}^* = a_{11}\cos^4\phi + (2a_{12} + a_{66})\sin^2\phi\cos^2\phi + a_{22}\sin^4\phi,$$

$$a_{12}^* = a_{12} + (a_{11} + a_{22} - 2a_{12} - a_{66})\sin^2\phi\cos^2\phi,$$

$$a_{22}^* = a_{11}\sin^4\phi + (2a_{12} + a_{66})\sin^2\phi\cos^2\phi + a_{22}\sin^4\phi,$$

$$a_{66}^* = a_{66} + 4(a_{11} + a_{22} - 2a_{12} - a_{66})\sin^2\phi\cos^2\phi$$

$$\alpha_1 = a_{11}\,[(1+n)\cos^2\phi - m\sin^2\phi]$$

$$\alpha_1' = a_{11}'\,[(1+n')\cos^2\phi - m'\sin^2\phi]$$

$$\alpha_2 = \left[a_{11}(m+n) + a_{12} + \frac{1}{2}a_{66}\right]\sin\phi\cos\phi$$

$$\alpha_2' = \left[a_{11}(m'+n') + a_{12}' + \frac{1}{2}a_{66}'\right]\sin\phi\cos\phi$$

$$\beta_1 = a_{22}\left[\left(1 + \frac{n}{m}\right)\sin^2\phi - \frac{1}{m}\cos^2\phi\right]$$

$$\beta_1' = a_{22}'\left[\left(1 + \frac{n'}{m'}\right)\sin^2\phi - \frac{1}{m'}\cos^2\phi\right]$$

$$\beta_2 = \left[a_{22}\left(\frac{1+n}{m}\right) + a_{12} + \frac{1}{2}a_{66}\right]\sin\phi\cos\phi$$

$$\beta_2' = \left[\alpha_{22}'\left(\frac{1+n'}{m'}\right) + a_{12}' + \frac{1}{2}a_{66}'\right]\sin\phi\cos\phi$$

$$m = \sqrt{\frac{a_{22}}{a_{11}}},\quad n = \sqrt{\frac{2a_{12} + a_{66}}{a_{11}}} + 2\sqrt{\frac{a_{22}}{a_{11}}}$$

$$m' = \sqrt{\frac{a_{22}'}{a_{11}'}},\quad n' = \sqrt{\frac{2a_{12}' + a_{66}'}{a_{11}'}} + 2\sqrt{\frac{a_{22}'}{a_{11}'}}$$

$$a_{11} = \frac{1}{E_1}(1-\nu_{12}\nu_{21}),\quad a_{22} = \frac{1}{E_2}(1-\nu_{23})^2$$

$$a_{11}' = \frac{1}{E_2}(1-\nu_{12}\nu_{21}),\quad a_{22}' = \frac{1}{E_1}(1-\nu_{23})^2$$

$$a_{12} = -\frac{1}{E_1}(\nu_{12}+\nu_{23}^2),\quad a_{66} = \frac{1}{E_1}+\frac{1}{E_2}+\frac{2\nu_{12}}{E_1}$$

$$a_{12}' = -\frac{1}{E_2}(\nu_{12}+\nu_{23}^2),\quad a_{66}' = \frac{1}{E_1}+\frac{1}{E_2}+\frac{2\nu_{12}}{E_2}$$

where E_1: Young's modulus in the direction perpendicular to the bedding plane, E_2: Young's modulus in the direction parallel to the bedding, $\nu_{12}(\nu_{21})$: Poisson's ratio in the direction of $E_1(E_2)$ subjected to strain in the direction of $E_2(E_1)$, ν_{23}: Poisson's ratio in the bedding plane.

From Eq. (7.2), we obtain displacements in horizontal (U) and vertical (V) directions under several stress conditions, for instance

$$p_x = p_y,\ 2p_x = p_y,\ 3p_x = p_y,\ 4p_x = p_y \text{ etc.}$$

as shown in Fig. 7.13 (θ = 90deg., at the crown) and Fig. 7.14 (θ = 30deg., at the side wall) where $n = E_1/E_2$, p_y = 10 kgf/cm^2 (10^3 kN/m^2), E_2 = 1000 kgf/cm^2 (10^5 kN/m^2) and ν_{12}, ν_{23} = 0.2 and 0.3.

Then, by plotting measured displacements (noted as small closed triangles) using the result of convergence measurement onto Figs. 7.13 and 7.14, the lines of Sec. 1 and 2 are obtained. The distance between the original point and the triangle shows 75% of displacement from the original point as we explained already in Fig. 7.11.

Graduating the line passing the origin and the triangle by using the unit of the length multiplied by 1.33 (inverce of 3/4) which indicates 1000 kgf/cm^2 (10^5 kN/m^2), we can evaluate the degree of anisotropy from the point where the line meets the curves showing assumed stress condition.

If we assume that $2p_x = p_y$ = 10 kgf/cm^2 (10^3 kN/m^2), the following results are obtained.

E_1 = 9800kgf/cm^2 (9.8×10^5 kN/m^2), E_2 = 4900kgf/cm^2 (4.9×10^5 kN/m^2), n = 2.0 for B-class rock

E_1 = 3000kgf/cm^2 (3.0×10^5 kN/m^2), E_2 = 2200kgf/cm^2 (2.2×10^5 kN/m^2), n = 1.36 for C-class rock

On the other hand a seismic survey gave the different result as shown in Table 7.3. P-waves propagating parallel and perpendicular to the bedding plane were detected at Point V_8/V_{10} and V_9/V_{11} respectively (see Fig. 7.1) by using blasting vibration caused at the mining face. This disagreement should be discussed further in future.

7.5. Conclusions

(1) In order to determine a deformability of compound rock mass remarkably fissured like Izumi-layers, field measurements aiming at deformation of the rock mass give much more practical result than a plate loading test. It was found to be 2240 kgf/cm^2 (2.24×10^5 kN/m^2) for

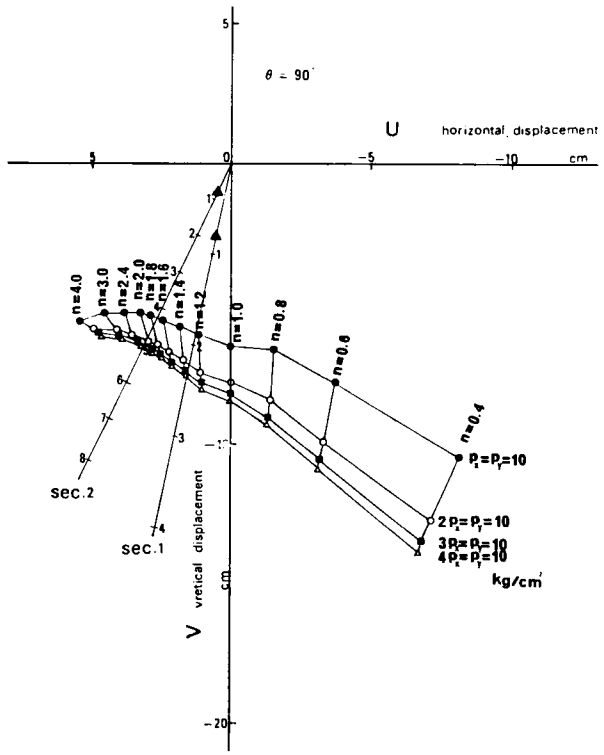

Fig. 7.13 Observed anisotropy at the crown

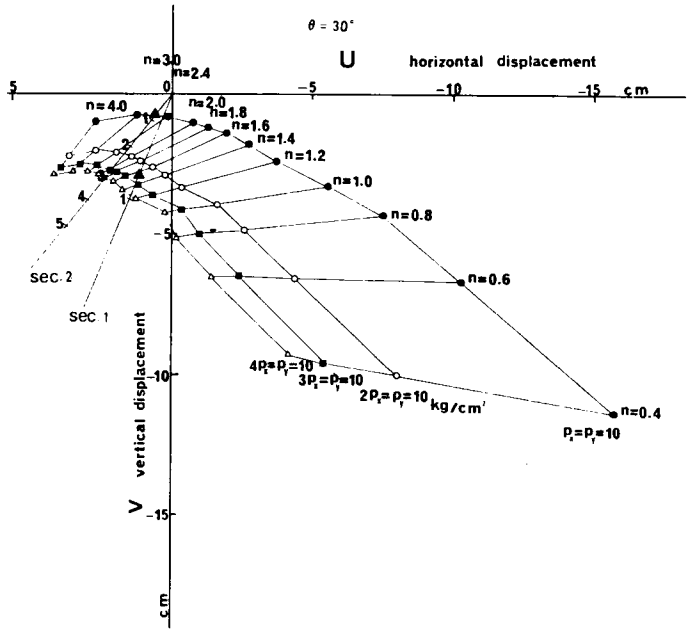

Fig. 7.14 Observed anisotropy on the side-wall

Table 7.3 Observed Velocities of P-Wave and Anisotropy of the Ground

1		2	
V_p (x) (km/s)	V_p (z) (km/s)	V_p (x) (km/s)	V_p (z) (km/s)
—	1.7	—	1.6
1.9	1.6	2.1	1.9
1.7	1.7	2.1	1.6
1.8	1.6	2.1	1.2
1.9	1.6	2.1	2.0
ave. 1.9	ave. 1.6	ave. 2.1	ave. 1.7

V_p (x): P-wave propagating along the stratification plane.
V_p (z): P-wave propagating perpendicularly to the stratification plane.

C-class rock mass whereas the deformation modulus by the plate loading test was 4560 kgf/cm^2 (4.56×10^5 kN/m^2).

(2) The aluminium pipe deformation meter place in the horizontal borehole gave good result in order to represent the deformation behavior of the rock mass near the tunnel.

(3) The values of displacement measured by two different ways, i.e. the aluminium-pipe-deformation-meter and convergence measurement, showed good agreement.

(4) Though the borehole loading test is considered as a practical approach for the investigation of the underwater rock mass, the correlation with the result of the plate loading test is not so clear at this moment and further research is required.

(5) A large scale experiment in order to know the anisotropy of rock mass is required, and the disagreement between the experimental result and the analytical result should be investigated in the further research.

REFERENCES for Chapter 7

[1] Ochi, H., Noto, T., Fukuzawa, H.: Proposed Method About the Evaluation of Rock Quality, 4th Sympo. of Rock Mechanics, Japanese National Committee of ISRM, 1973.

[2] Honshu-Shikoku Bridge Authority: Report on Rock Test in Naruto Region (No.4). 1972.

[3] Committee on Rock Mechanics of Japanese Society of Civil Engineers: Plate Loading Test

Standard for Rock-in-situ, 1976.

[4] Honshu-Shikoku Bridge Authority: Report on Geology of Kameura Tunnel 1975.

[5] Takeuchi, T., Suzuki, T., Tanaka, S.: A study of Results of the Rock Measurement by Bore-hole Load Tester. 5th Sympo. of Rock Mechanics, Japanese National Committee of ISRM, 1977.

[6] Mori, H., Takahashi, K., Noto, T.,: Field Measurement of Deformation Characteristics of Soft Rocks. International Sympo. on Field Measurement in Rock Mech. by ISETH, Zurich, 1977.

[7] Hata, S., Tanimoto, C., Kimura, K.: Deformation Measurement of the Tunnel in the Izumi-Layer. Proc. of 32nd Annual Sympo. of Japanese Society of Civil Engineers, Vol. 3, No. 284, 1977.

[8] Hata, S., Tanimoto, C., Kimura, K.: On the Anisotropy of Izumi-Layer. Proc. of 33rd Annual Sympo. of Japanese Society of Civil Engineers, Vol. 3, No. 244, 1978.

Chapter 8

FUNDAMENTAL CONCEPT OF DESIGNING TUNNEL SUPPORTS IN CONSIDERATION OF ELASTO-PLASTIC AND STRAIN SOFTENING BEHAVIOR OF ROCK

8.1 Introduction

In most cases of tunnel driving through rock, the fundamental requirement is how to advance the mining face so as to make the original state of the ground as undisturbed as possible. It can be pointed out (with the exception of seriously creeping ground) that the most predominant deformation occurs in the vicinity of the advancing face. It is subjected to a positional (geometrical) condition, judging from experience and the observations of convergence surveys which showed that the increase of convergence was almost negligible when (the advance of) the face stopped. The surveys also showed that the time dependency of deformation depended on the progressive failure of rock, caused by having allowed too much displacement near the opening. This means that the face plays an important role as a temporary support. The rock mass near the face is stabilized by the 'half-dome action' in the profile and the 'ring action' in the cross section. When advancing the face, it is required to place artificial supports to substitute for the half-dome action within a span length from the face, in the driving direction, so as to mobilize the bearing capacity of the rock mass as fully as possible.

The so-called New Austrian Tunnelling Method (NATM), where rock-bolting and shotcrete lining are applied, is the latest and most feasible tunnelling method for this purpose, especially from the practical point of view. Such supports as rockbolts, shotcrete lining and steel arch ribs are placed tightly near the face, and are subjected to a three dimensional stress field. The main subject discussed in the following sections is how to design a support system, considering the half-dome action given by the face itself, and the elastic / elasto-plastic behavior of the rock mass. From the point of view that the effects of systematic supports are 'mobilizing confining stress' and 'decreasing shear stress', a procedure to design supports can be proposed by replacing the effects of the supports by the inner pressure acting on the surface of the tunnel wall.

The competence factor (C_f) is defined as the ratio of unconfined compressive strength (q_u) to overburden pressure (i.e. $\rho \cdot h$, the product of density ρ and depth h), $q_u/(\rho \cdot h)$ [1] Based on the observed behavior at more than 50 tunnelling sites in Japan, Nakano points out the relation between the rock pressure and the competence factor as follows [2] :

$C_f > 10$ for slight or no rock pressure,

$4 < C_f \leqq 10$ for loosening rock pressure,

$2 < C_f \leqq 4$ for light ~ large squeezing rock pressure,

$C_f \leqq 2$ for heavy ~ very heavy squeezing - swelling rock pressure

There has been no discussion in detail for the case of $C_f \leqq 2$. In this range, the following discussion will give more detailed analysis and information for a practical design of tunnels.

8.2 Basic Idea of Tunnelling

Consider a circular opening in an isotropic stress field p_o, as shown in Fig. 8.1. In this figure, the state of (A), on the left hand side is the most conventional model. However, when we discuss supports in tunnelling, it is important to consider the timing of the setting supports and the stress changes caused by the advance of the mining face. The state of (B), in the middle, shows the initial state, being subjected to primary stress (p_o). The state of (C), on the right hand side, shows the stress concentrations around a circular opening caused by the extraction force acting on the wall of the opening, without the primary stress. State (A) is obtained by superposing State (C) on State (B). In tunnelling, State (B) exists before excavation. When we pay attention to the change of the extraction force p_e, which is equal to p_o in case of no support and is sometimes called 'excavation force', we can explain the basic idea of tunnelling very easily.

Fig. 8.2 shows the stress state near the face. By the result of a simple FEM computation using an axi-symmetric model, we obtain the stress-changes of σ_r, σ_t, σ_z and τ_{rz}, as shown in Fig. 8.3. The notations ' a ', ' r ' and ' d ' are the radius of a circular opening, the distance from the center in the cross section, and the distance from the face in the profile, respectively. A negative value of ' d ' means a position ahead of the face.

To speak of the case at $r = 1.05\,a$ near the wall, the radial normal stress σ_r varies from p_o to $2p_o$, and the normal stress σ_z and the shear stress τ_{rz} vary only near the face. Among these stresses, σ_r especially corresponds to the change of the wall displacement, that is, the convergence curve.

The displacement curves in Fig. 8.4 show a theoretical curve of displacement for an elastic body. The displacement varies within the range of $d/a = -2$ or -3 and $d/a = 2$ or 3. Fig. 8.5 shows the displacement curves obtained by field measurements which were carried out in the Kameura and Seikan Tunnels. [3], [4] Fig. 8.6 shows the change of the extraction force mentioned already. Without support, p_e varies from zero to p_o. The increase of p_o has a one to one correspondence to the decrease of σ_r. Consequently, a convergence survey means monitoring the change of σ_r or the extraction force p_e as well as the displacement of the wall. When it is found that the bearing capacity of the ground is insufficient without any artificial supports in the final state, it is required to introduce an inner pressure p_i, mobilized by the reaction of the supports, and only pre-stressing rockbolts can give an active p_i.

By considering this " p_i " as a main parameter, we can calculate the width of the plastic zone, the displacement of the wall and the plastic strain near the wall, and can design the support system.

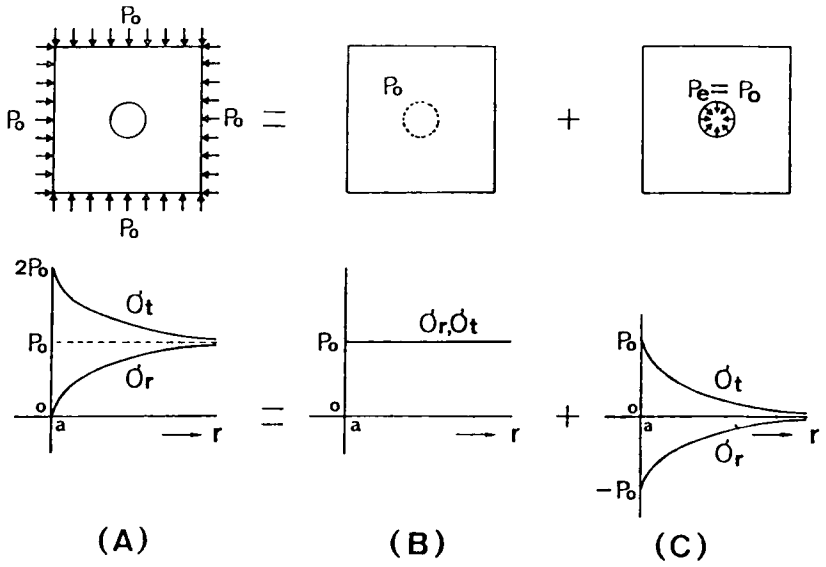

Fig. 8.1 Stresses around a Circular Opening

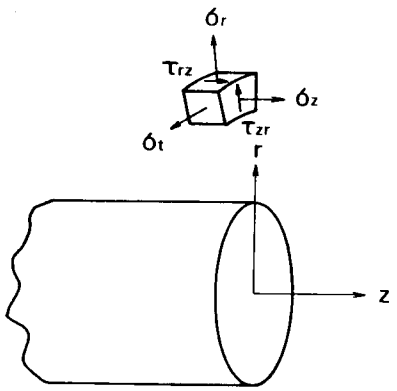

Fig. 8.2 State of Stresses near the Face

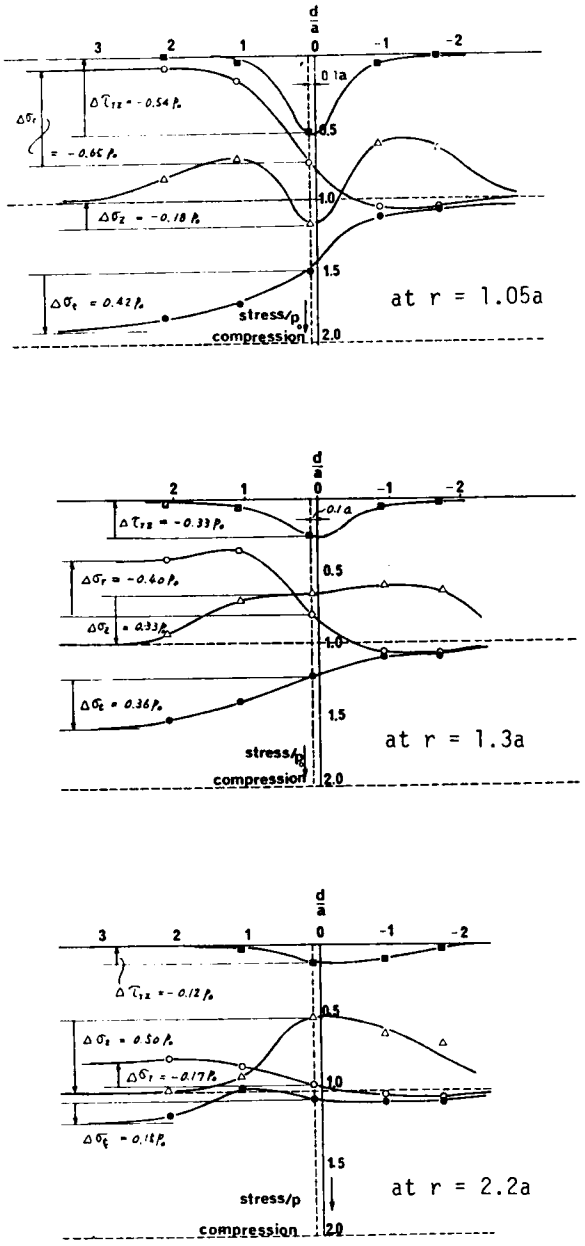

Fig. 8.3 Stress changes caused by the Advance of the Face

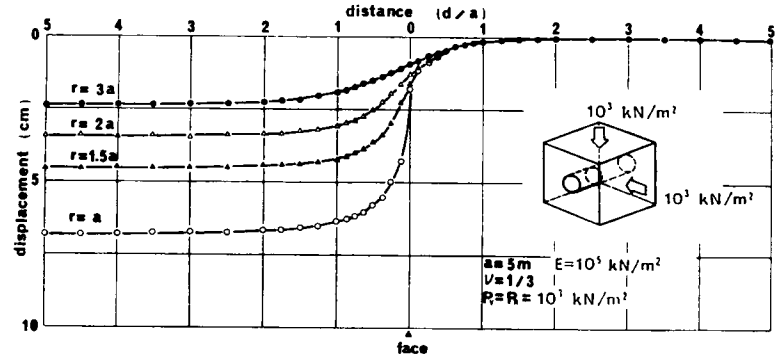

(a) A circular opening

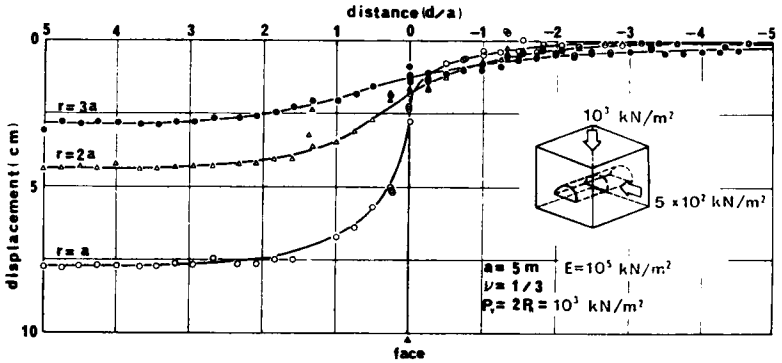

(b) A semi-circular opening

Fig. 8.4 Theoretical Displacement Curves for an Elastic Body

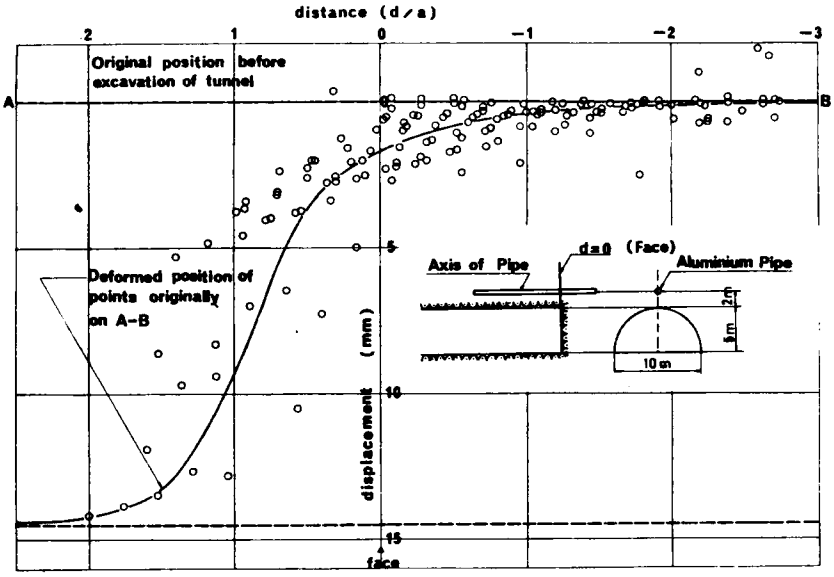

(a) Kameura Tunnel through Shale-Sandstone [3]

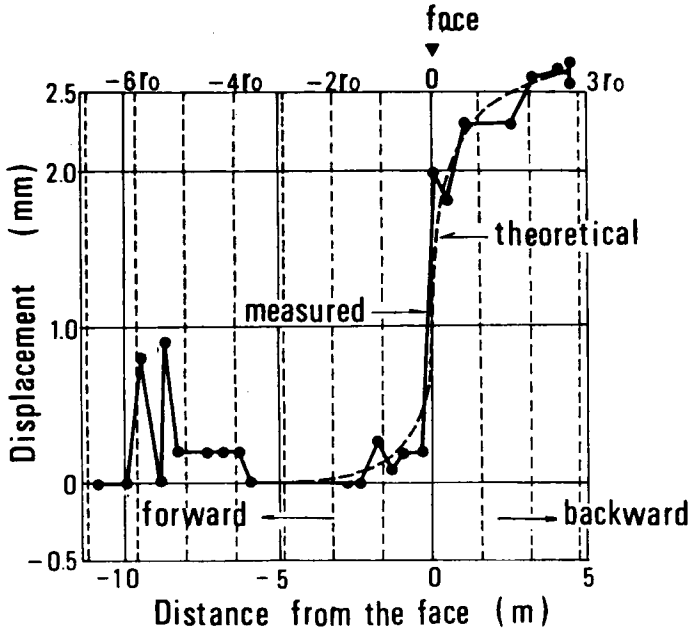

(b) Seikan Tunnel through Andesite-Tuff [4]

Fig. 8.5 Measured Displacement Curves during Construction

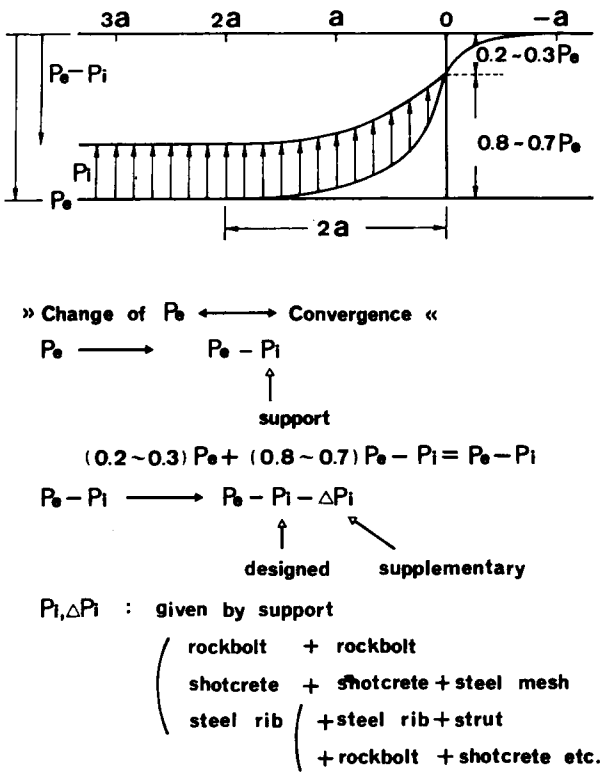

Fig. 8.6 Superposed Forces around an Opening Induced by Excavation

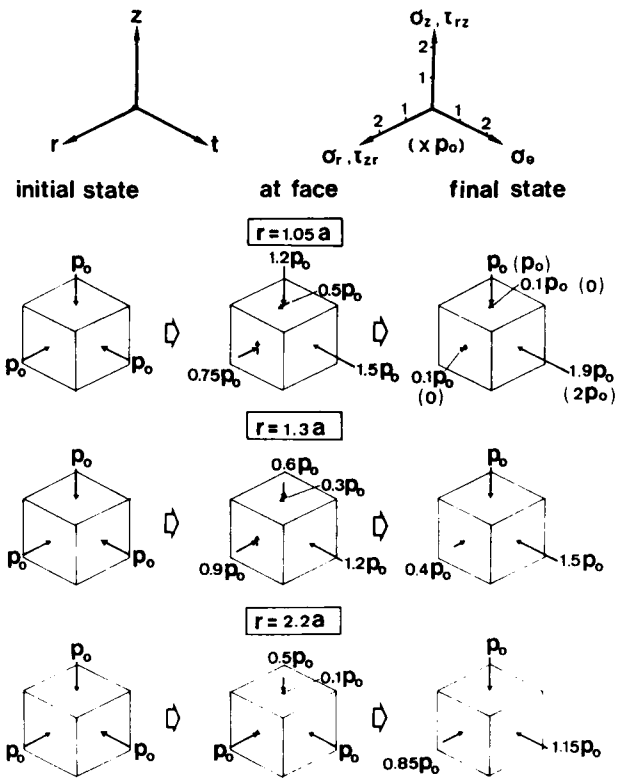

Fig. 8.7 Three Dimensional State of Stresses Associated with the Advance of the Face

8.3 Design of Pre-stressed Type Rockbolt Support

By assuming a circular tunnel driven through ground being subjected to an isotropic stress field p_o, it is possible to discuss the behavior of the ground near the opening. Fig. 8.7 shows the change of three dimensional stresses at r = 1.05 a (near wall), 1.3 a and 2.2 a, and we can image how Mohr's circle varies from the initial state to the final one. Also, Fig. 8.8 shows the state of principal stress directions and the displacement of free surface. When fully bonded systematic rockbolts are placed near the face (d = 0.1 a, 50 cm behind of the face in the case of a conventional two-lane motorway tunnel), and the ground behaves in the manner of an elastic body, each rockbolt may finally be subjected to the stress increments as shown in Fig. 8.9. The difference between systematic bolting placed only at a single cross section and placed serially at the interval of 1 m in the profile can be seen in Fig. 8.10.

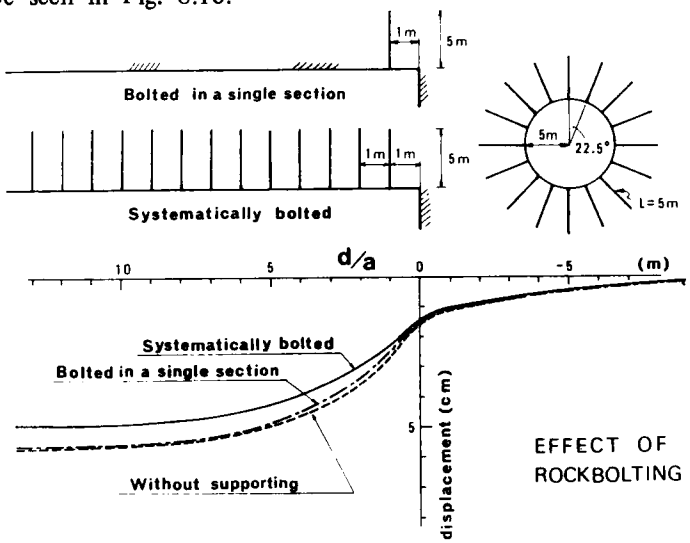

Fig. 8.10 Decrease of Displacement by Systematic Rockbolts in an Elastic Body
(Elastic Constant for the ground E = 10^5 kN/m^2)

Next, before discussing designing the rockbolt supports, let us touch on the distribution of the plastic zone around an opening. Fig. 8.11 shows the plastic zone obtained by a parametric analysis based on Drucker's plasticity criterion. The radius of an opening is 5 m and the notation C and ϕ mean the cohesion and the angle of internal friction, respectively. From Fig. 8.8 and Fig. 8.11 we can presume the effect of spiling rockbolts for the pre-reinforcement and bolting on the mining face. Under the condition of $p_o = 10^3$ kN/m^2, the relationships in the plastic zones, C and ϕ, are shown by Fig. 8.12.

If the ground deforms as a continuum in the elastic range, no support will be required. But, as a matter of course, it is confirmed that the plastic behavior of the ground should be considered in designing the support.

Then, let us proceed in our discussion on designing supports by using an elasto-plactic (strictly

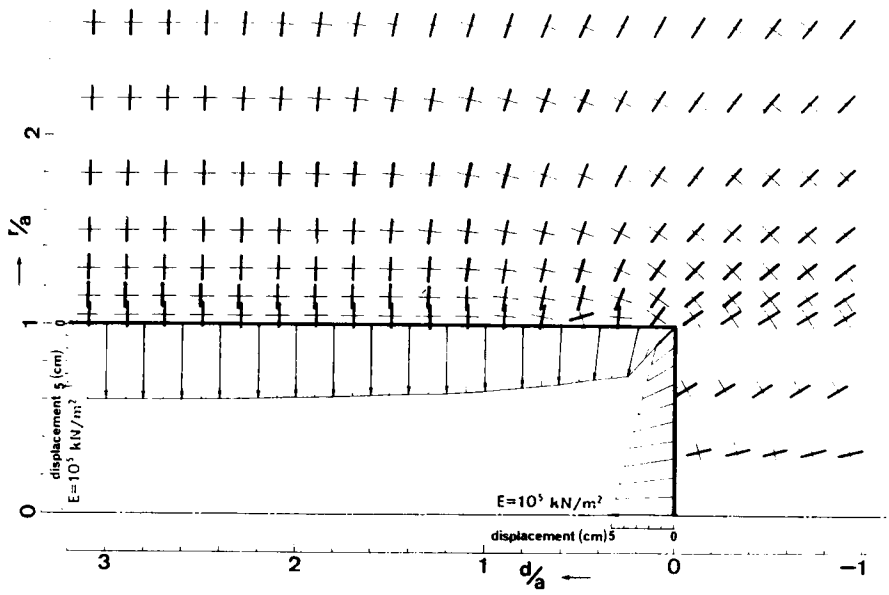

Fig. 8.8 Directions of Principal Stresses and Displacement of a Free Surface

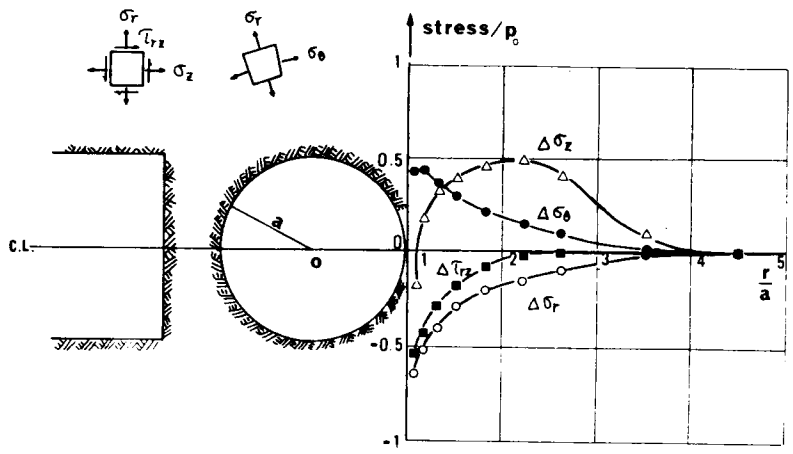

Fig. 8.9 Stress Increments Acting on a Fully Bonded Rockbolt

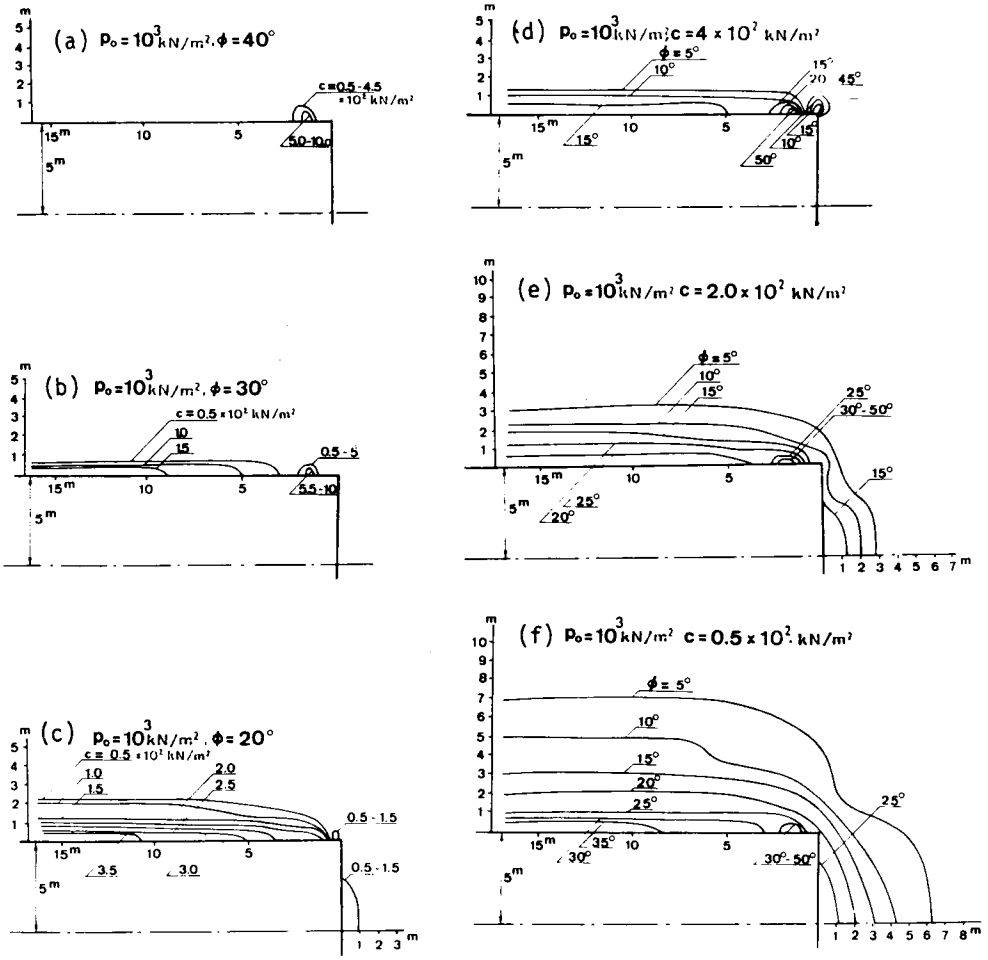

Fig. 8.11 Distribution of Plastic Zone

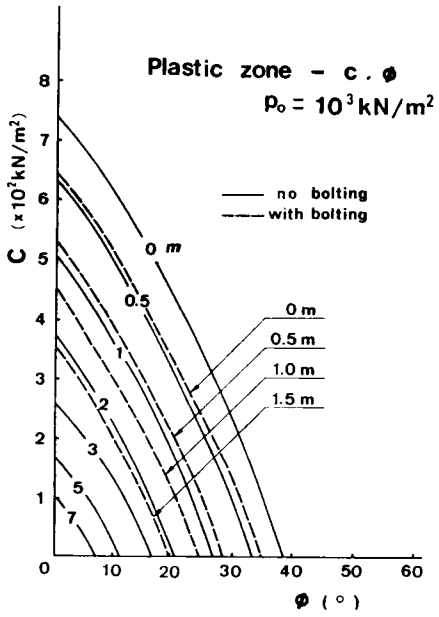

Fig. 8.12 C, ϕ and Plastic Zone

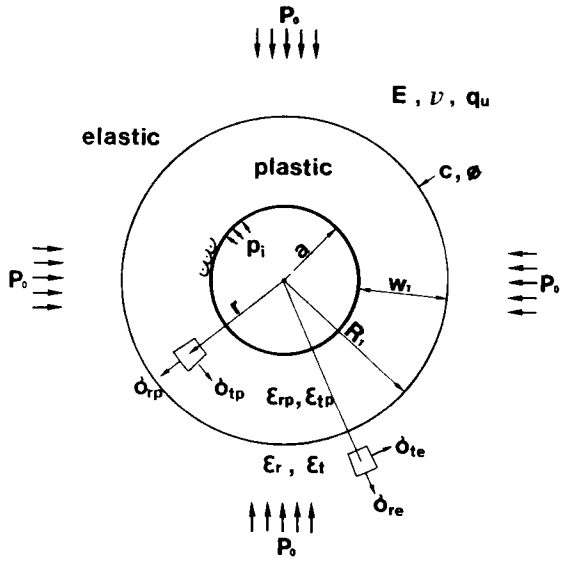

Fig. 8.13 Analytical Model for Elasto-Plastic Behavior

speaking, elastic-perfectly plastic) model, as shown in Fig. 8.13.

When Coulomb's yield criterion is employed, the width of the plastic zone W_1, the displacement of the wall U_w and the mean plastic strain ϵ_p, defined by $(\epsilon_{t,\,plastic}-\epsilon_{r,\,plastic})$, can be expressed in the forms of the following equations, by giving figures to the radius of a circular opening a, elastic constant E, Poisson's ratio ν, unconfined compressive strength q_u, angle of internal friction ϕ, hydrostatic initial stress field p_o and support-reaction (bearing capacity of supports) p_i.

$$W_1 = a\left[\frac{2\{p_0(\zeta-1)+q_u\}}{(1+\zeta)\{(\zeta-1)p_i+q_u\}}\right]^{\frac{1}{\zeta-1}} - a \tag{8.1}$$

$$U_w = \frac{1}{2\mu}\left\{p_0 - \frac{2p_0-q_u}{1+\zeta}\right\}\cdot\frac{R_1^2}{a} \tag{8.2}$$

$$\epsilon_p = \frac{p_0(\zeta-1)+q_u}{\mu(1+\zeta)}\cdot\left\{\frac{R_1}{a} - \frac{1}{\zeta}\cdot\frac{R_1^\zeta - a^\zeta}{R_1^{\zeta-1}(R_1-a)}\right\} \tag{8.3}$$

where

$$\zeta = \frac{1+\sin\varphi}{1-\sin\varphi} \quad , \qquad \mu = \frac{E}{2(1+\nu)}$$

Being based on the results of laboratory tests, let us assume the allowable plastic strain to be 2.5%. This is the first step in the design process.

Fig. 8.14 (a), (b) and (c) have the same parameter p_i with respect to abscissa under the same condition of $p_o = 3 \times 10^3$ kN/m^2, $E = 2 \times 10^5$ kN/m^2. When we pick the case of $\phi = 20°$ (curve 5), we can read the value of p_i corresponding to $\epsilon_p = 2.5\%$ in the figure on the right hand side, namely $p_i = 200$ kN/m^2. In the case of applying p_i of 200 kN/m^2, we can read the displacement of the wall, namely, $U_w = 0.20$ m. Therefore, $70 \sim 80\%$ means the quantities of displacement which occur from the position of the face (d/a = 0) as mentioned before. For the observational construction, the limit of allowable convergence should be 30 cm. When $p_i = 2.0 \times 10^2$ kN/m^2, the width of the plastic zone becomes 6.5 m. Fig. 8.15 shows the bearing capacity of fully bonded rockbolts 10 m long, which is determined from a value of 1.5 times W_p (width of plastic zone). Also from Fig. 8.15, it is concluded that 32 bolts of 25 mm dia. are required to be set (circumferentially) radially per 1 m shift, although the interaction between pre-stressed rockbolts and the ground has not yet been described clearly.

8.4 Strain Softening Behavior

Through field measurements and observations in the Nabetachiyama Tunnel [5], [6], [7], we found that the elasto-plastic model could not simulate the actual deformation of the ground

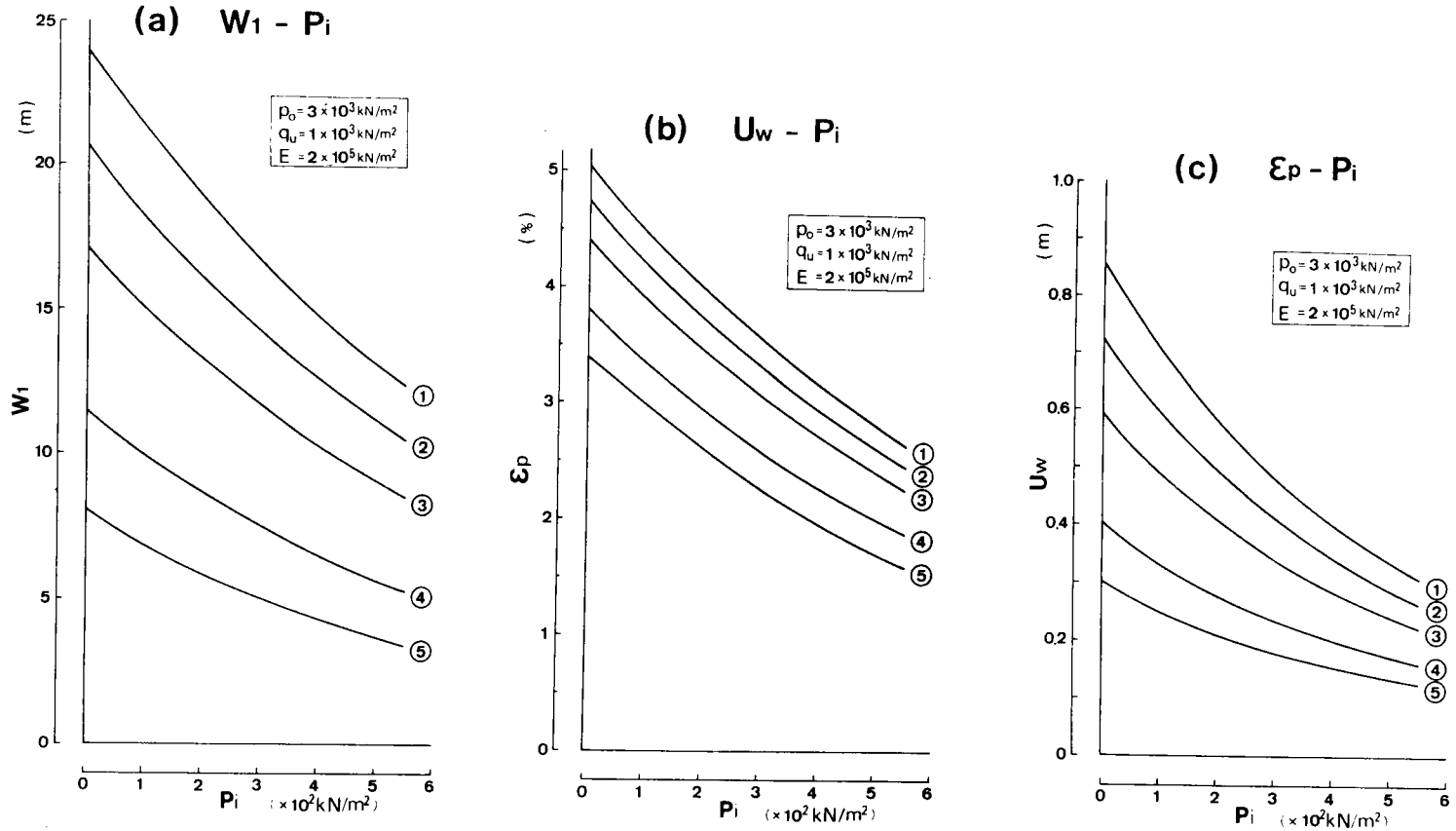

Fig. 8.14 Plastic Zone, Displacement of Wall and Plastic Strain around an Opening
(p_o = 3000 kN/m^2, q_u = 1000 kN/m^2, E = 2 x 10^5 kN/m^2)

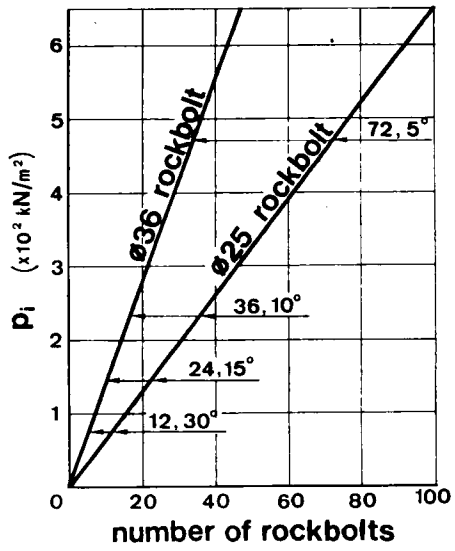

Fig. 8.15 Bearing Capacity of Systematic Rockbolt Supports

very well, and that a consideration of the strain softening behavior was required. From the results obtained by many triaxial tests, we tried to determine schematic stress-strain curves for the Neogene mudstone sampled from the sites of the Nabetachiyama Tunnel as shown in Fig. 8.16. As the Neogene formation contained numerous microscopic fissures due to repeated foldings, it was very difficult to get satisfactory specimens having the specified shape and dimension, even in the case of $q_u = 3 - 5 \times 10^3$ kN/m^2.

Regarding such ground showing typical strain softening behavior, we can assume the idealized model shown in Fig. 8.17. The width of the plastic zone (W_p) is the sum of the softening zone (W_1) and the flow zone (W_2). The fundamental equations, which express the strain softening behavior, can be derived from strain energy theorems. That is, assume the relationship between the axial stress and the axial strain as shown by the three segmented straight lines in Fig. 8.18. Then, the rock specimen behaves in the manner of an elastic body along the straight path through Point O, A and B. Then, it takes a softening path to a certain stress level, and thereafter it causes flow at a constant stress level. By simplifying the stress-strain relations in such a way, the following fact can be confirmed with respect to the product $\sigma \cdot \epsilon$ of stress σ and strain ϵ. Namely, in the region exhibiting the elastic behavior, '$\sigma \cdot \epsilon$' can be expressed in the form of a quadratic function of 'ϵ'. The increasing rate of $\sigma \cdot \epsilon$ to ϵ becomes maximum at Point C, and thenceforth follows the curve in a concave parabolic form. Finally, when flow is caused, $\sigma \cdot \epsilon$ increases at a constant gradient. [8]

If it is accepted that the strain continues to increase, the total strain energy (W) given to the specimen which shows softening can be expressed in the following form of expansion, in terms of the second degree regarding strain components ϵ_t and ϵ_r.

$$W = a + b \cdot \epsilon_t + c \cdot \epsilon_r + \frac{1}{2} d \cdot \epsilon_t^2 + e \cdot \epsilon_t \cdot \epsilon_r + \frac{1}{2} f \epsilon_r^2 \tag{8.4}$$

where a, b, c, d, e and f are constants.
This strain energy W should agree with the elastic strain energy.
According to the definition,

$$\left.\begin{aligned} \sigma_t &= b + d \cdot \epsilon_t + e \cdot \epsilon_r \\ \sigma_t &= c + e \cdot \epsilon_t + f \cdot \epsilon_r \end{aligned}\right\} \tag{8.5}$$

Eq. (8.5) can be rewritten in the following form.

$$\left.\begin{aligned} \sigma_t &= \left(b - \frac{ec}{f}\right) + \frac{e}{f}\sigma_r + \left(d - \frac{e^2}{f}\right)\epsilon_t \\ \sigma_t &= \left(b - \frac{dc}{e}\right) + \frac{d}{e}\sigma_r + \left(e - \frac{df}{e}\right)\epsilon_t \end{aligned}\right\} \tag{8.6}$$

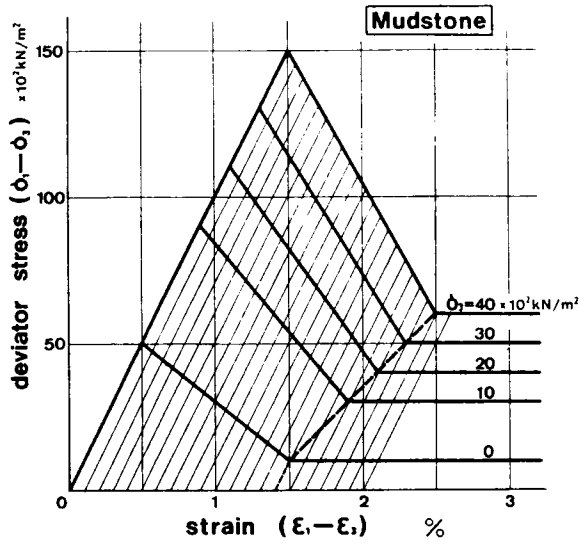

Fig. 8.16 Schematic Stress-Strain Curves of Nabetachiyama Mudstone

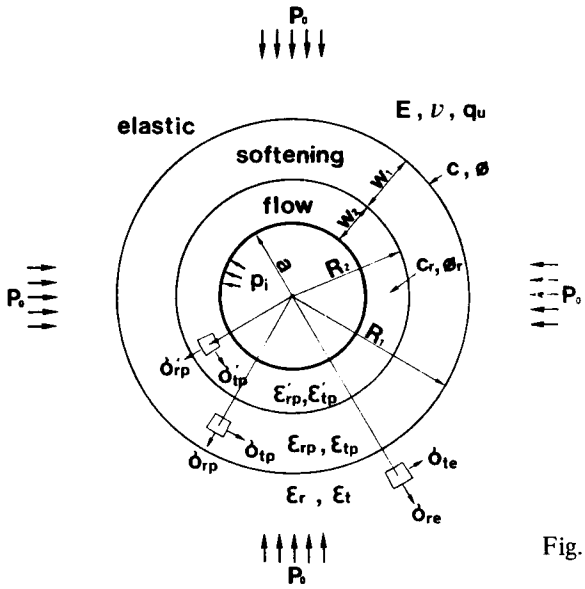

Fig. 8.17 An Idealized Strain Softening Model

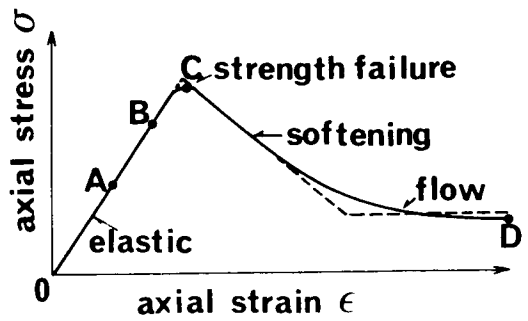

Fig. 8.18 Stress-Strain Relation for Strain Softening

In a simpler form,

$$\left.\begin{aligned}\sigma_t &= k_1 + k_2\sigma_r + k_3\varepsilon_t \\ \sigma_t &= k_4 + k_5\sigma_r + k_6\varepsilon_t\end{aligned}\right\} \tag{8.7}$$

where,

$$\left.\begin{aligned} k_1 &= b - \frac{ec}{f} \quad , \quad k_2 = \frac{e}{f} \quad , \quad k_3 = d - \frac{e^2}{f} \\ k_4 &= b - \frac{dc}{e} \quad , \quad k_5 = \frac{d}{e} \quad , \quad k_6 = e - \frac{df}{e}\end{aligned}\right\} \tag{8.8}$$

also, $$k_2 \cdot k_6 + k_3 = 0 \tag{8.9}$$

On the other hand, the elastic strain at the yield point is

$$\left.\begin{aligned} E\cdot\varepsilon_t &= (1-\nu^2)\sigma_t - \nu(1+\nu)\sigma_r \\ E\cdot\varepsilon_t &= -\nu(1+\nu)\sigma_t + (1-\nu^2)\sigma_r\end{aligned}\right\} \tag{8.10}$$

At the yield point, the stresses and strains given by Eq. (8.10) agree with those given by Eq. (8.7). Here, the Mohr-Coulomb yield criteria is given by the following equation.

$$\sigma_t = q_u + q\cdot\sigma_r \tag{8.11}$$

Where q_u is the unconfined compressive strength and q is given by

$$q = \tan^2\left(\frac{\pi}{4} + \frac{\varphi}{2}\right) \tag{8.12}$$

where ϕ : angle of internal friction

By substituting Eqs. (8.10) and (8.11) for Eq. (8.7), we obtain

$$k_1 - q_u + \frac{k_3}{E}(1-\nu^2)q_u + \left[k_2 - q + \frac{k_3}{E}\{(1-\nu)q - \nu\}(1+\nu)\right]\sigma_r = 0$$

$$k_4 - q_u + \frac{k_6}{E}\nu(1+\nu)q_u + \left[k_5 - q - \frac{k_6}{E}\{(\nu q - (1-\nu)\}(1+\nu)\right]\sigma_r = 0$$

As these equations should be valid for any σ_r, the following four equations are obtained for the coefficients k_1, k_2 $\cdots$ k_6.

$$
\left.
\begin{aligned}
&k_1 - q_u + \frac{k_3}{E}(1-\nu^2)q_u = 0 \\
&k_4 - q_u + \frac{k_6}{E}(1+\nu)\nu q_u = 0 \\
&k_2 - q_u + \frac{k_3}{E}\{(1-\nu)q - \nu\}(1+\nu) = 0 \\
&k_5 - q - \frac{k_3}{E}\{\nu q - (1-\nu)\}(1+\nu) = 0
\end{aligned}
\right\} \qquad (8.13)
$$

By the assumption that the relation between σ_t and ϵ_t is shown by the straight line with the negative gradient $(-\omega)$ under constant σ_r, k_3 becomes $-\omega$.

$$k_3 = -\omega \qquad (8.14)$$

ω has the same dimension as the elastic constant E.

By solving Eq. (8.9), Eq. (8.13) and Eq. (8.14) simultaneously, $k_1, k_2 \cdots k_6$ are obtained in the form of the following equations.

$$
\left.
\begin{aligned}
&k_1 = \left\{1 + \frac{\omega}{E}(1-\nu^2)\right\} q_u \qquad k_2 = q + \frac{\omega}{E}\{(1-\nu)q - \nu\}(1+\nu) = \frac{\omega}{k_6} \\
&k_3 = -\omega \qquad\qquad\qquad k_4 = \left\{1 + \frac{k_6}{E}(1+\nu)\nu\right\} q_u \\
&k_5 = q + \frac{k_6}{E}\{\nu q - (1-\nu)\}(1+\nu) \qquad k_6 = \frac{\omega}{k_2}
\end{aligned}
\right\} \qquad (8.15)
$$

Consequently, the stress-strain relation in the softening state can be expressed uniquely by the parameters of the elastic constants of E and ν, the yielding constants of q_u and ϕ, and the negative gradient ω. This relation can be applied until the flow begins to occur. The condition of the flow is given by

$$\sigma_t = q_u' + q' \cdot \sigma_r \qquad (8.16)$$

where $\sigma_t > \sigma_r$, $q' = \tan^2\left(\frac{\pi}{4} + \frac{\varphi}{2}\right)$ and
q_u' and ϕ' are the unconfined compressive strength and angle of the internal friction at the residual state respectively.

The rock in the softening state has the following relation:

$$q_u' + q' \cdot \sigma_r < \sigma_t \leqq q_u + q \cdot \sigma_r \qquad (8.17)$$

Being based on these assumptions, the fundamental equations, which express the elastic-softening behavior and the elastic-softening-flow behavior, can be obtained by the derivation men-

tioned in reference [8]. In this chapter, only the final equations modified for convenient usage are shown.

8.5 Analytical Solution for Strain Softening Behavior

Input data for calculation or computation are as follows:

- a : radius of a circular opening,
- E : Young's modulus,
- ν : Poisson's ratio,
- q_u : unconfined compressive strength,
- ϕ : angle of internal friction,
- ω : negative slope of deformation coefficient for softening zone,
- p_o : hydrostatic initial stress,
- p_i : inner pressure acting on the wall of an opening (= reaction of supports),
- q'_u : unconfined compressive strength at residual state,
- ϕ' : angle of internal friction at residual state

Output data are:

- R_1 : radius of ' elastic-softening ' boundary,
- R_2 : radius of ' softening-flow ' boundary,
- S_1 : ratio of R_1 to R_2 ($= R_1/R_2$),
- S_2 : ratio of R_2 to a ($= R_2/a$),
- S_3 : ratio of R_1 to a ($= R_1/a$),
- ϵ_t^*, ϵ_r^* : plastic strains on the wall in tangential and radial directions respectively,
- σ_t^*, σ_r^* : stresses on the wall in tangential and radial direction,
- U* : displacement of the wall in the radial direction

Computation procedure is as follows:

There are two cases: the case of induced softening and flow, and the case of induced softening only.

PROCEDURE

Case of induced 'softening and flow'

(1) INPUT DATA :

$a, E, \nu, q_u, \varphi, \omega, p_0, p_i, q'_u, \varphi'$

(2) Solve the following equation. (S_1 : unknown)

$$A_1 S_1^{-2} - A_2 S_1^{n_2 - 1} + A_3 S_1^{n_1 - 1} = 0 \rightarrow S_1 \qquad (8.18)$$

where

$$S_1 = R_1 / R_2$$

$$A_1 = (b - d\gamma - e\gamma - q'_u - q'c + q'e\gamma + qf\gamma)(e^2 - df)(n_1 - n_2)$$

$$A_2 = (d + en_1 - q'e - q'fn_1)[\{b - d\gamma - e\gamma - (2p_0 q + q_u)/(1+q)\}$$
$$(e + fn_2) - \{c - e\gamma - f\gamma - (2p_0 - q_u)/(1+q)\}(d + en_2)]$$

$$A_3 = (d + en_2 - q'e - q'fn_1)\{b - d\gamma - e\gamma - (2p_0 q + q_u)/(1+q)\}$$
$$(e + fn_1) - \{c - e\gamma - f\gamma - (2p_0 - q_u)/(1+q)\}(d + en_1)$$

$$n_1 = \sqrt{d/f}\ , \quad n_2 = -n_1$$

$$\gamma = (c - b)/(f - d)\ , \quad b = (k_2 k_4 - k_1 k_5)/(k_2 - k_5)$$

$$c = -(k_1 - k_4)/(k_2 - k_5)\ , \quad d = k_2 k_5 k_6/(k_2 - k_5)$$

$$e = k_2 k_6/(k_2 - k_5)\ , \quad f = k_6/(k_2 - k_5)$$

$$k_1 = \{1 + (\omega/E)\cdot(1 - \nu^2)\}\, q_u$$

$$k_2 = q + (\omega/E)\{(1-\nu)q - \nu\}(1+\nu)$$

$$k_3 = -\omega$$

$$k_4 = \{1 + (k_6/E)\cdot(1+\nu)\nu\}\, q_u$$

$$k_5 = q + (k_6/E)\{\nu q - (1-\nu)\}(1+\nu)$$

$$k_6 = \omega/[q + (\omega/E)\{(1-\nu)q - \nu\}(1+\nu)]$$

$$q = \tan^2\alpha \qquad \alpha = \pi/4 + \varphi/2$$

$$q' = \tan^2\alpha' \qquad \alpha' = \pi/4 + \varphi'/2$$

$$q_u = 2c\tan\alpha$$

Here, the unknown parameter is S_1, namely the ratio R_1/R_2.

R_2 is the radius of the elastic-softening boundary, and R_2 is the radius of the softening-flow boundary.

We can obtain the solution for S_1 by an iterative numerical method on a hand-held calculator having several memory devices.

(3) To obtain the value of S_2.

$$S_2 = [\{c + e(\alpha + \beta - \gamma) + f(\alpha_1 n_1 + \beta_1 n_2 - \gamma) - q'_u/(1-q')\}$$
$$/\{p_i - q_u/(1-q')\}]^{\frac{1}{q'-1}} \tag{8.19}$$

where

$$S_2 = R_2/a$$

$$\alpha_1 = (A_8 - A_9)/A_{10} S_1^{n_1-1}$$

$$A_8 = \{b - d\gamma - e\gamma - (2p_0 q + q_u)/(1+q)\}(e + fn_2)$$

$$A_9 = \{c - e\gamma - f\gamma - (2p_0 - q_u)/(1+q)\}(d + en_2)$$

$$A_{10} = (e^2 - df)(n_2 - n_1) \cdot S_1^{n_1 - 1}$$

$$\beta_1 = (A_{11} - A_{12})/A_{13} S_1^{n_2-1}$$

$$A_{11} = \{b - d\gamma - e\gamma - (2p_0 q + q_u)/(1+q)\}(e + fn_1)$$

$$A_{12} = \{c - e\gamma - f\gamma - (2p_0 q - q_u)/(1+q)\}(d + en_1)$$

$$A_{13} = (e^2 - df)(n_1 - n_2) \cdot S_1^{n_2 - 1}$$

By this equation we can obtain the value of S_2.

S_2 is the ratio of R_2/a.

Here we can see the softening-flow boundary.

(4) To obtain the strains, stresses and displacement of the wall.

$$\left.\begin{aligned}
&\varepsilon_t^* = (\alpha_1 + \beta_1 - \gamma) S_2/a \quad , \qquad \varepsilon_r^* = -\varepsilon_t^* \\
&\sigma_t^* = q_u'/(1-q') + q'\{p_i - q_u'/(1-q')\} \\
&\sigma_r^* = q_u'/(1-q') + \{p_i - q_u'/(1-q')\} \\
&\dot{u}^* = \{(\alpha_1 + \beta_1 - \gamma) - p_0/2(\lambda + \mu)\} S_2^2 \cdot a \\
&\varepsilon_p^* = \varepsilon^* - \varepsilon_e^* \\
&\varepsilon^* = \varepsilon_t^* - \varepsilon_r^* \qquad\qquad \varepsilon_e^* = (\sigma_t^* - \sigma_r^*)/2\mu
\end{aligned}\right\} \qquad (8.20)$$

Also through a similar procedure, we can obtain solutions for the case of the induced softening only.

Case of induced 'softening' only

(1) Solve the following equation. (S_3 : unknown)

$$B_1 S_3^{n_1-1} + B_2 S_3^{n_1-n_2} + B_3 = 0 \rightarrow S_3 \qquad (8.21)$$

where

$$S_3 = R_1/a$$

$$B_1 = \{c - (e+f)\gamma - p_i\}\{fd - e^2\}(n_1 - n_2)$$

$$B_2 = [(d + en_1)\{c - e\gamma - f\gamma - (2p_0 - q_u)/(1+q)\} - (e + fn_1)\{b - d\gamma - e\gamma - (2p_0 q + q_u)/(1+q)\}](e + fn_2)$$

$$B_3 = [(e + fn_2)\{b - d\gamma - e\gamma - (2p_0 q + q_u)/(1+q)\} - (d + en_2)\{c - e\gamma - f\gamma - (2p_0 - q_u)/(1+q)\}](e + fn_1)$$

(2) Obtain the strains, stresses and displacement of the wall.

$$\varepsilon_t^* = \alpha_2 + \beta_2 - \gamma \quad , \quad \varepsilon_r^* = \alpha_2 \cdot n_1 + \beta_2 \cdot n_2 - \gamma \tag{8.22}$$

where

$$\alpha_2 = \{(1-S_3^{n_2-1})(c-e\gamma-f\gamma) - (2p_0-q_u)/(1+q) + p_i S_3^{n_2-1}\} / \{(e+fn_1)(S_3^{n_2-1}-S_3^{n_1-1})\}$$

$$\beta_2 = \{(1-S_3^{n_1-1})(c-e\gamma-f\gamma) - (2p_0-q_u)/(1+q) + p_i S_3^{n_1-1}\} / \{(e+fn_2)(S_3^{n_1-1}-S_3^{n_2-1})\}$$

$$\left.\begin{aligned} &\sigma_t^* = b + d\varepsilon_t^* + e\varepsilon_r^* \qquad \sigma_r^* = c + e\varepsilon_t^* + f\varepsilon_r^* \\ &u^* = (\alpha_2 + \beta_2 - \gamma)\, a - p_0 a/2(\lambda+\mu) \\ &\varepsilon_p^* = \varepsilon^* - \varepsilon_e^* \\ &\varepsilon^* = \varepsilon_t^* - \varepsilon_r^* \qquad \varepsilon_e^* = (\sigma_t^* - \sigma_r^*)/2\mu \end{aligned}\right\} \tag{8.23}$$

8.6 Relation among Plastic Zone, Inner Pressure and Competence Factor

Here, let us go back to the discussion about the strain softening behavior. Fig. 8.19 ((a), (b) and (c)) shows the results of a parametric study with respect to W_p, C_f and p_i under the same condition of $p_o = 2 \times 10^3$ kN/m^2. It can be seen that a small change of p_i has a large influence on W_p. Also, a higher p_i makes W_p much less even in the case of $C_f = 0.5$, equal to the average value for the Middle Sector. Namely, when such a poor support system as $p_i = 200$ kN/m^2 was placed, the plasticized zone (W_p) exceeded 15 m for the case of $C_f = 0.5$, and a fairly poor support system, only giving $p_i = 400$ kN/m^2, resulted in a 7 m wide plastic zone. In Fig. 8.19, the results obtained by the elasto-plastic model with no consideration of the reduction of the peak strength are also plotted. When the support system gives $p_i = 600$ kN/m^2, no flow zone is induced for the case of $C_f = 0.5$, and the result obtained by the softening model agrees with that of the elasto-plastic model, as shown in Fig. 8.19 (c).

The comparison of the obtained results between the softening model and the elasto-plastic model is interesting, since many people use an elasto-plastic model because of its easy application. In order to get some results by an elasto-plastic model, it is required to establish some bi-linear stress-strain relations, which are expressed by the positive solid line and the dotted lines as shown in Fig. 8.20. By assuming $q_u = 2$, 4, 6, 8 and 10×10^2 kN/m^2 for $p_o = 2 \times 10^3$ kN/m^2, $E = 2 \times 10^5$ kN/m^2; $\nu = 0.3$, $\phi = 20°$, $\phi = 10°$, Eqs. (8.1), (8.2) and (8.3) give W_p, U_w and ϵ_p res-

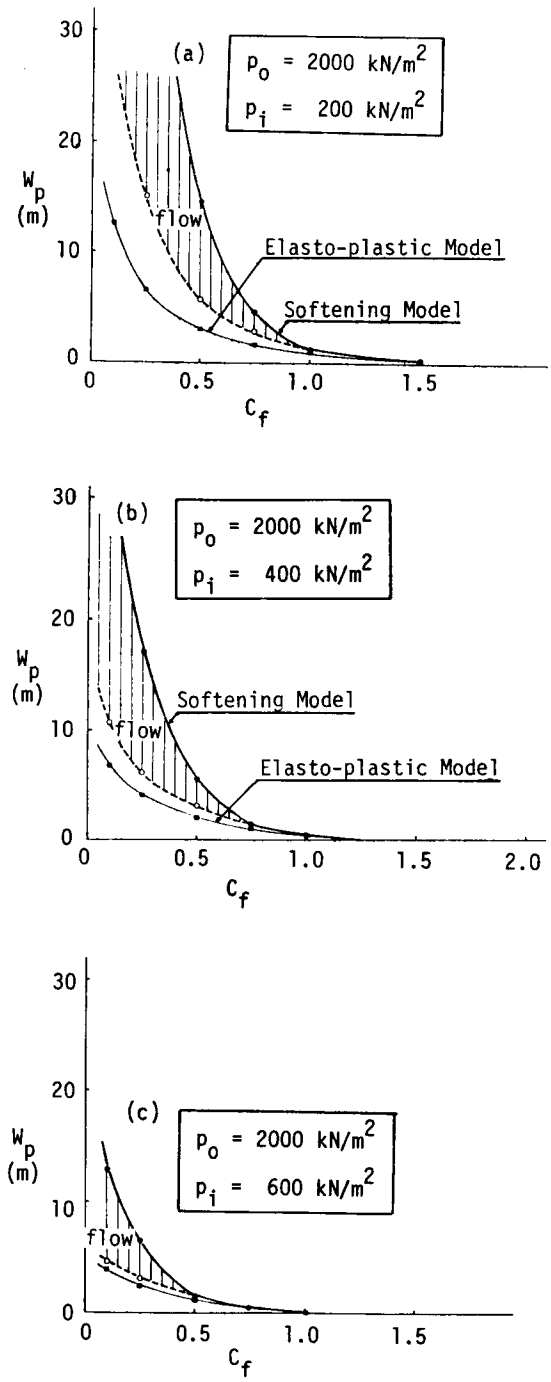

Fig. 8.19 Relations among W_p, C_f and p_i

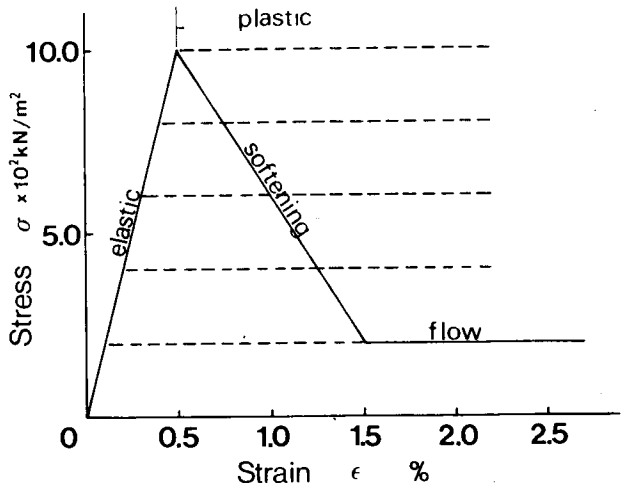

Fig. 8.20 Stress-Strain Relation
for an Elasto-Plastic Model

pectively. The results with respect to W_p are plotted by the thin curves shown in Fig. 8.21, in which (a) and (b) correspond to the cases of $\phi = 10°$ and $20°$ respectively. Also, the results of the strain-softening model are plotted by the thick curves in (a) and (b), where the curves are the same because of considering $\phi = 20°$ at peak and $\phi' = 10°$ at the residual at the same time. As shown in these figures, there exists a big difference between these two types of models, and thus it is quite difficult to consider a strain softening phenomenon by a bi-linear elasto-plastic model.

Being based on further parametric studies under the condition of $p_o = 2 \times 10^3$ kN/m^2, $E = 2 \times 10^5$ kN/m^2, $\omega = 0.4$ E, $\phi = 20°$, $\phi' = \frac{1}{2}\phi$ and $q_u' = \frac{1}{5} q_u$, Fig. 8.22 concludes the condition for the appearence of a flow zone. This relates the stability of an opening for the most part, with the introduction of a competence factor (C_f) and a support intensity factor (p_i / p_o). For example, no flow zone appears in the region of $p_i = 0.2\ p_o$ for the case of $C_f = 1.0$, and $p_i = 0.6\ p_o$ is required for the case of $C_f = 0.5$. This shows that the opening becomes unstable considering the decrease of the half-dome action if the supports had not been placed very close to the face after mining. When this condition is included in the shaded area, the result obtained by the elasto-plastic model, which maintains its peak strength after yielding will not show so serious a difference from the result by a strain softening model.

In order to get a better understanding of the strain softening model proposed by us, let us discuss the relation between the axial stress (σ_1) and the axial strain (ϵ_1) in the case of a triaxial test. Also to be discussed will be the change of the shear stress in the simulation of the cir-

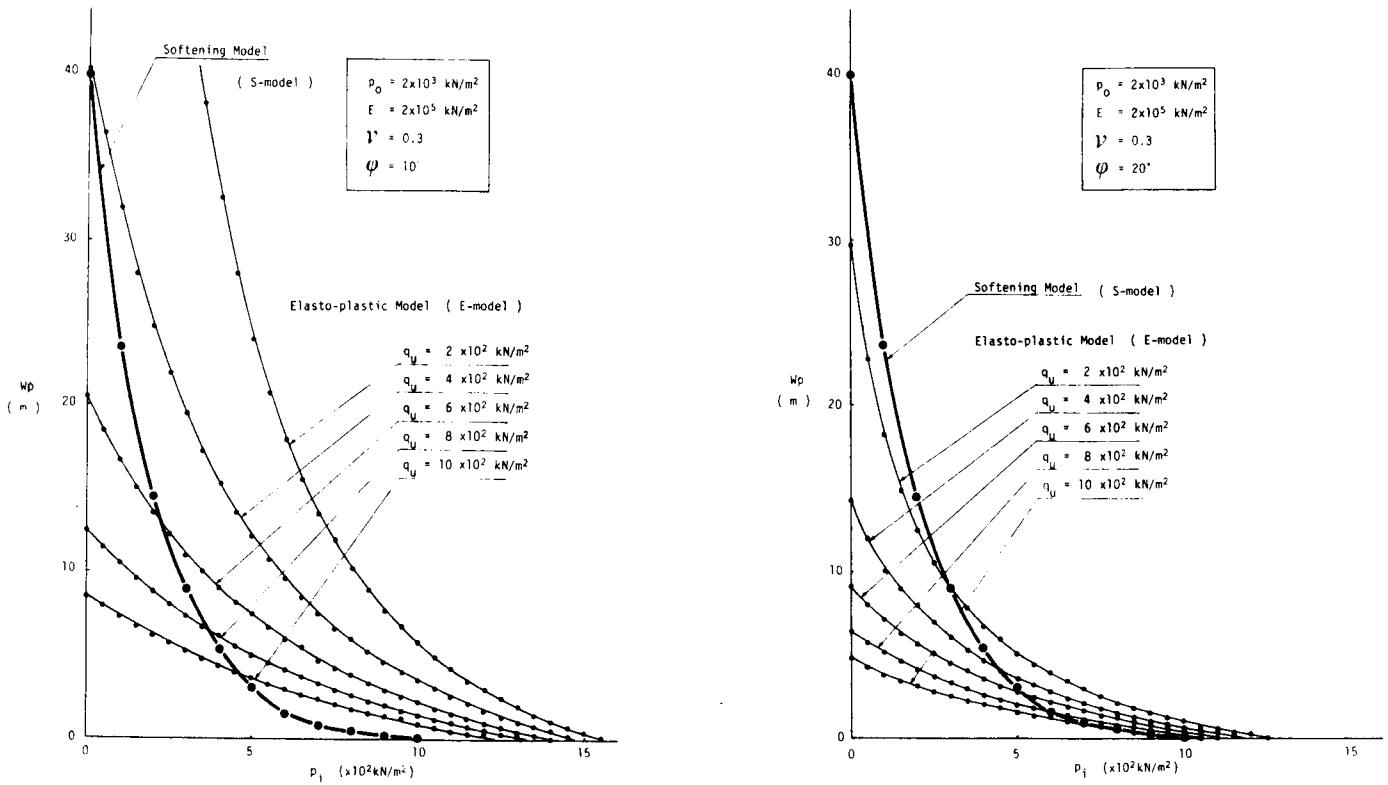

(a) $\phi = 10°$ (b) $\phi = 20°$

Fig. 8.21 Difference of W_p Between an Elasto-Plastic and a Strain Softening

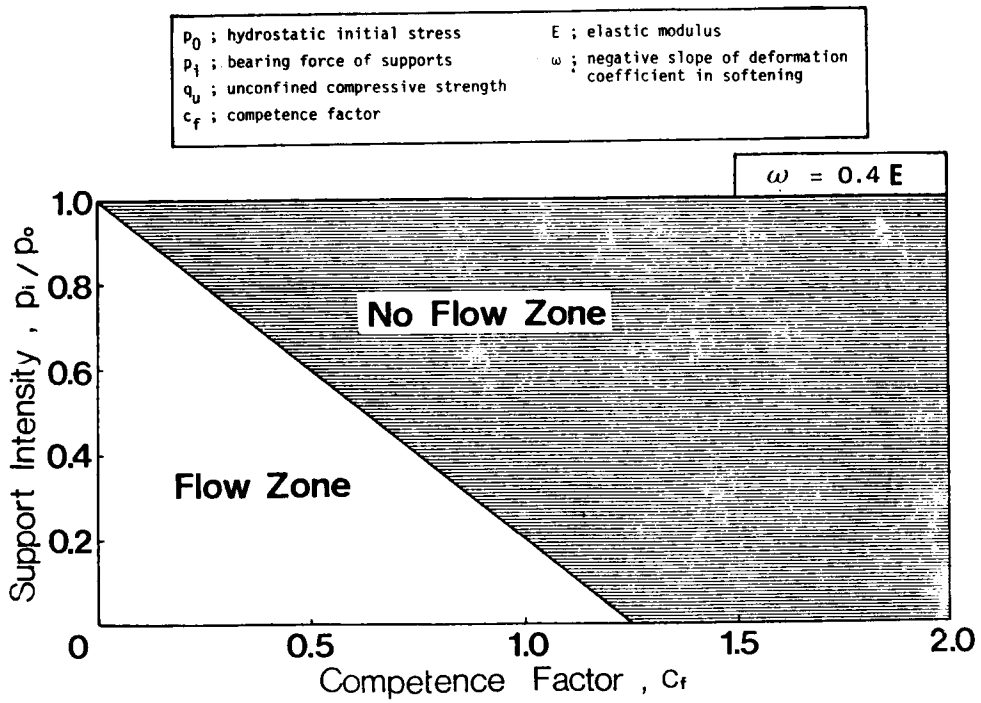

Fig. 8.22 Condition for the Appearence of Flow Zone

cular tunnel under the same condition of $C_f = 0.5$ ($p_o = 200\ kN/m^2$, $q_u = 1000\ kN/m^2$, $E = 2 \times 10^5\ kN/m^2$, $\upsilon = 0.3$, $\phi = 20°$, $\phi' = 10°$, $q_u' = 200\ kN/m^2$, $\omega = 0.4\ E$). Fig. 8.23 shows a schematic stress-strain relation based on our assumption corresponding to a tri-axial test. In the state of strain softening, there exists the relation that the negative gradient of the deformation coefficient $-\omega\ (= -0.4\ E)$ is always unchanged. From the Mohr-Coulomb yield criteria, $\tau = C + \sigma\tan\phi$, the following equation is derived corresponding to each peak stress (σ_1) under a constant confining pressure (σ_3).

$$\sigma_1 = q_u + 2.04\sigma_3 \tag{8.24}$$

Also, the equation, $\tau = C' + \sigma\tan\phi'$ for the state of ' flow ' gives another form as follows:

$$\sigma_1 = q_u' + 1.42\sigma_3 \tag{8.25}$$

Both Eqs. (8.24) and (8.25) show a rather high increase of allowable stresses of σ_1 at the peak and at the residual state, which are given by the increase of the confining pressure σ_3 at low levels, such as 1 to 500 kN/m^2. This fact might be important in explaining the effect of the supports acting on the tunnel wall as a sort of passive inner pressure, with the exception of the active pressure such as pre-stressed rockbolts, compressed air etc. In Fig. 8.23 the dotted line, corresponding to the boundary of the states between the softening and flow, expresses the increase of allowable axial strain associated with the confining pressure, which is a major proposition in our concept of designing supports.

In the case of a tunnel model, a Mohr circle expressing the initial state before excavation is a point at $\sigma = 2000\ kN/m^2$ (equal to p_o) and the shear stress τ becomes high, attendant upon the advance of the mining face until the circle touches the yielding line, $\tau = C + \sigma\tan\phi$ ($\tau = 350 + \sigma\tan 20°$ in kN/m^2). Fig. 8.24 shows the path of shear stress caused by the advance of the face. From Point A, as the shear strength of the ground decreases gradually attendant upon strain softening, the shear stress follows the segment $\overline{AB}$, and ' flow ' appears at Point B with $\epsilon_t = 2.81\ \%$. After passing Point B, the increasing rate of the tangential normal strain ϵ_t (corresponding to ϵ_1 in the tri-axial test) becomes very high, and the magnitude of ϵ_t reaches 96.4 % in the case of no support (equal to $p_i = 0$). It can be estimated easily from this history of shear stress that the supports would be subjected to a large deformation and heavy load if the high normal strain ϵ_t was allowed beyond the state of Point B. Consequently, the maximum allowable strain should be designated by the magnitude not reaching the state of flow.

The stress state around the circular opening under the hydro-static initial stress field in the case of $p_o = 2 \times 10^3\ kN/m^2$, $q_u = 10^3\ kN/m^2$, $C_f = 0.5$ is illustrated by Fig. 8.25. The small increment of an inner pressure (p_i) such as 200 kN/m^2, which is equal to 10 % of the initial stress (p_o) or of the final excavation force (p_e), changes the stress distribution in quite a different manner. Fig. 8.25 (a) shows the state in which the flow progresses, (b) shows the beginning of ' flow ', (c)

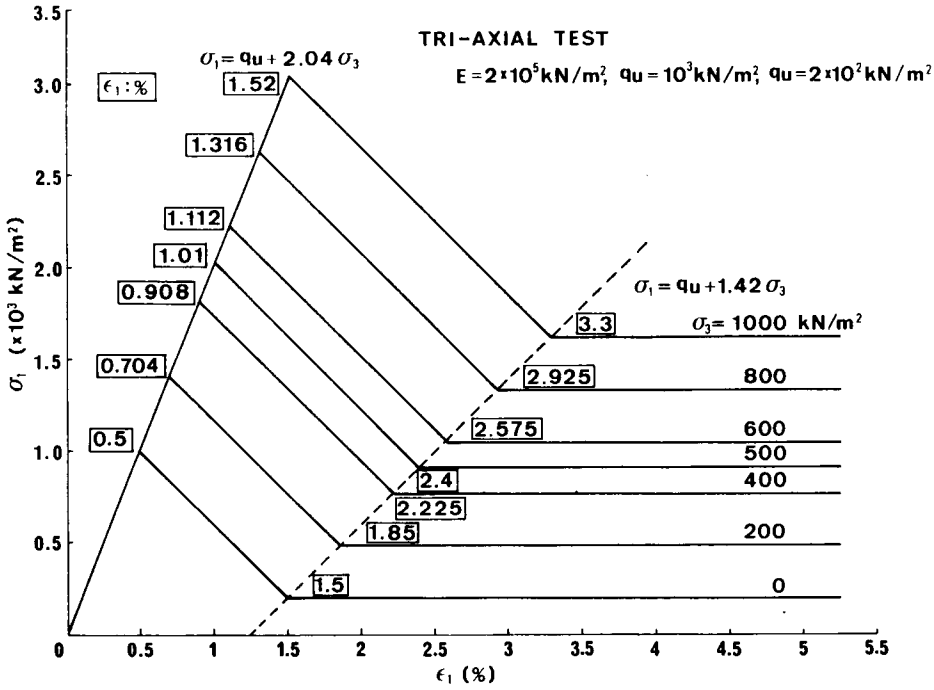

Fig. 8.23 Schematic Stress-Strain Relation for Tri-Axial Test

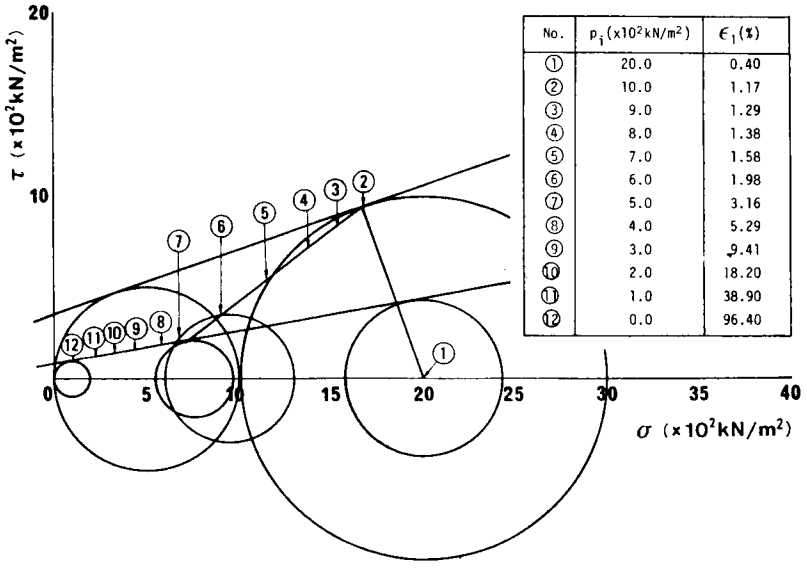

Fig. 8.24 The Path of Shear Stresses Associated with the Advance of the Face

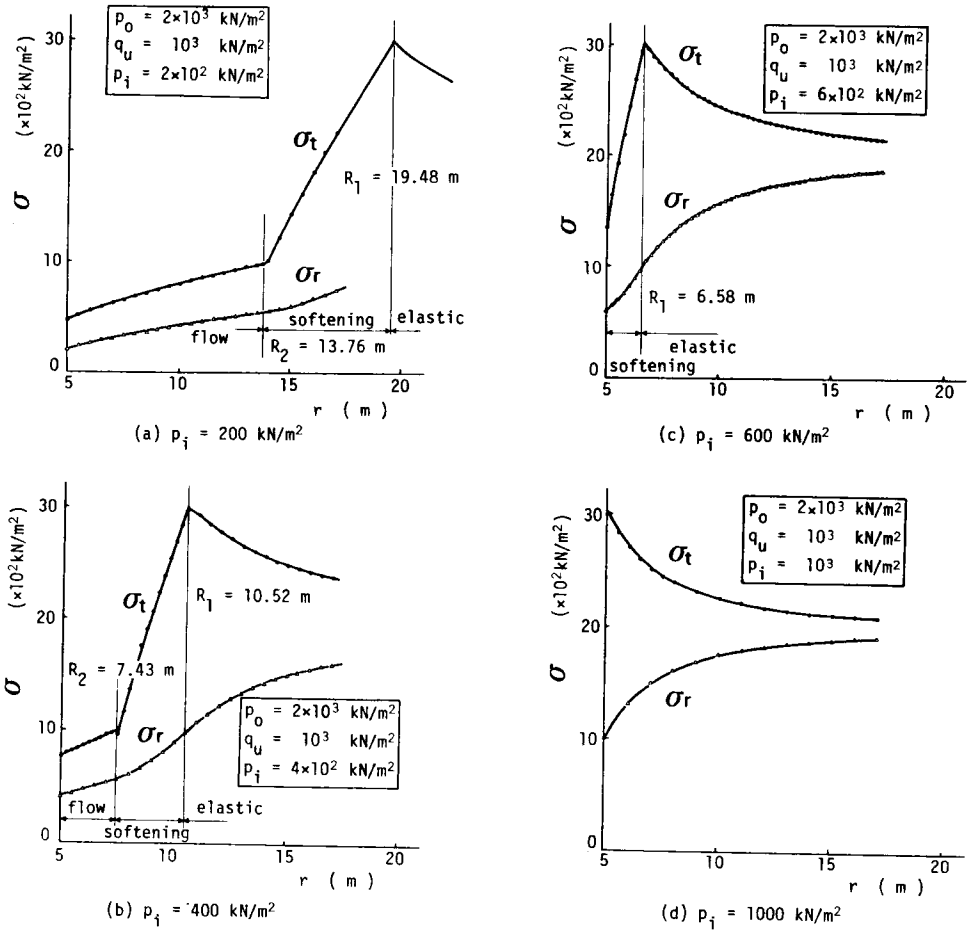

Fig. 8.25 Stress Distribution around a Circular Opening in Elastic, Strain and Flow State

is the state in which no flow is induced and the stress reduction near the wall is intensive, and (d) is still in the elastic state under the load of $p_i = 10^3$ kN/m^2, 50 % of p_o.

8.7 A Procedure of Designing Supports

To briefly explain the procedure for designing the support system, the significant steps are

(1) Determine the maximum allowable strain to be caused around an opening at the final state, being based on laboratory tests such as tri-axial test, stiff loading test, direct shear test etc. and, if possible, some preliminary field measurements. Empirical data and engineering judgement should be considered.

(2) Analyze the softening behavior of the rock mass in case of $C_f \leqq 4$.
The width of plastic zone, maximum strain, plastic strain, stresses and displacement of the wall corresponding to the various magnitudes of the inner pressure to be given by the support system as a whole can be obtained by Eq. (8.18) ~ Eq. (8.23). Before calculation, 10 pieces of input data should be prepared. These are : radius of an opening (a), Young's modulus (E), Poisson's ratio (υ), unconfined compressive strength (q_u), angle of internal friction at peak strength (ϕ), negative gradient of deformation coefficient (ω), primary stress field (p_o), unconfined compressive strength at residual state (q_u'), angle of internal friction at residual strength (ϕ') and inner pressure (p_i).

(3) Set up the magnitude of the inner pressure to be given by supports other than rockbolt support, being based on the results obtained by the softening analysis mentioned in Item (2). Also, depending on the stiffness of the supports and physical properties of the rock, the limit of the allowable displacement of the wall should be determined. Further, magnitude of the inner pressure given by the shotcrete lining ($(p_i)_{sc}$) and that given by the steel ribs ($(p_i)_{sr}$) would be set respectively with regard to the same magnitude of displacement. It is common and a fundamental concept of designing that, so long as it is possible to replace the supporting effect by the equivalent inner pressure, every kind of support should be estimated with the consideration of a rapidly decreasing half-dome action from the face position.

(4) Evaluate the magnitude of the inner pressure to be given by fully bonded rockbolt support, $(p_i)_{rb}$ at the confining stress level which can be set up in Item (3).

(5) Monitor convergence, displacement of rock and stress increment in lining as major measurements for checking the stability of an opening and compatibility of the original design. The magnitude of the displacement of the wall (U_w) is most convenient and reliable as the monitored parameter. Being different from the preliminary field measurement executed before the construction, the monitoring system during construction should be as simple as possible from the point of view of time and handling.

(6) Estimate the magnitude of the supplementary supports ($\triangle p_i$) to be added, being based on the result obtained in the daily monitoring. Judging from the necessary magnitude of $\triangle p_i$

and the convenience of the application of the basic construction procedure, some combinations among the following methods will be adapted : setting rockbolts at increased density; spiling rockbolts for pre-reinforcement; face stabilization by rockbolts made of steel, fiberglass or high polymer resin which is placed perpendicularly to the face; secondary shotcrete lining with reinforcement mesh, fiber mixture, Bernold sheet etc.; placing supplementary steel ribs; grouting; compressed air; segmented lining with or without shield driving and so on. From now, let us discuss the supports-ground interaction on the assumption that the competence factor is 0.5 (as a mean value) in the case of a circular tunnel with 10 m diameter. The inner pressure of 4 or 5×10^2 kN/m^2 is given by shotcrete lining and steel ribs ($(p_i)_1 = (p_i)_{sc} + (p_i)_{sr}$), and a fully bonded rockbolt system gives some additional inner pressure, $(p_i)_{rb}$, being associated with the stress increment, $\triangle p_e$, caused by the advance of the face. Consequently, the wall is subjected to a total inner pressure, $(p_i)_1 = (p_i)_{sc} + (p_i)_{rb}$, at the final state in which the tunnel should be stabilized as a ring structure.

Fig. 8.26 shows (a) W_p, (b) U_w, (c) ϵ_1^* and (d) the change of p_i given by the face as well as the excavation force p_e, having the relation [$p_i + p_e = p_o = 2 \times 10^3$ kN/m^2], on the same abscissa expressing the magnitude of p_i. In order to distinguish p_i, given by the half-dome action from other artificial supports, let us denote $(p_i)_f$ as

$$(p_i)_f + p_e = p_o = 2 \times 10^3 \text{ kN/m}^2 \tag{8.26}$$

$(p_i)_f$ which is equal to $p_o = 2000$ kN/m^2 initially, begins to decrease at $d = -15$ m ahead of the face. It becomes approximately 1.5×10^3 kN/m^2 at the face position and diminishes at the section about $d = 25$ m behind the face. Within 1 m behind the face, $(p_i)_f$ decreases from 1.5×10^3 kN/m^2 to 600 kN/m^2 (corresponding to ' from d = 0 to d = 1 m '). This means that the face loses 45 % of it soriginal bearing capacity as a temporary support only 1 m behind the face. This is considered one of the main reasons why such concrete operations as placing rockbolts and shotcrete lining to the face position as early and close as possible are required in the application of the New Austrian Tunnelling Method (NATM). When the face advances one more meter, namely from d = 1 m to 2 m, $(p_i)_f$ varies from 6 to 4×10^2 kN/m^2. Being associated with this 1 m advance, the width of the plastic zone (W_p) develops from 1.6 m to 5.5 m according to Fig. 8.26 (a). At the position of d = 0 m, no plastic zone occurs and the width of the plastic ring (W_p), softening ring (W_1) and flow ring (W_2) at each position behind the face are as follows.

at d = 0 m	: $W_p = 0$ m	$W_1 = 0$ m,	
at d = 1 m	: $W_p = 1.58$ m,	$W_1 = 1.58$ m,	$W_2 = 0$ m
at d = 1.25 m	: $W_p = 3.13$ m,	$W_1 = 2.39$ m,	$W_2 = 0.74$ m
at d = 2 m	: $W_p = 5.52$ m,	$W_1 = 1.09$ m,	$W_2 = 2.42$ m
at d = 5 m	: $W_p = 18.39$ m,	$W_1 = 6.89$ m,	$W_2 = 11.52$ m
at d = 10 m	: $W_p = 30.40$ m,	$W_1 = 10.40$ m,	$W_2 = 20.00$ m

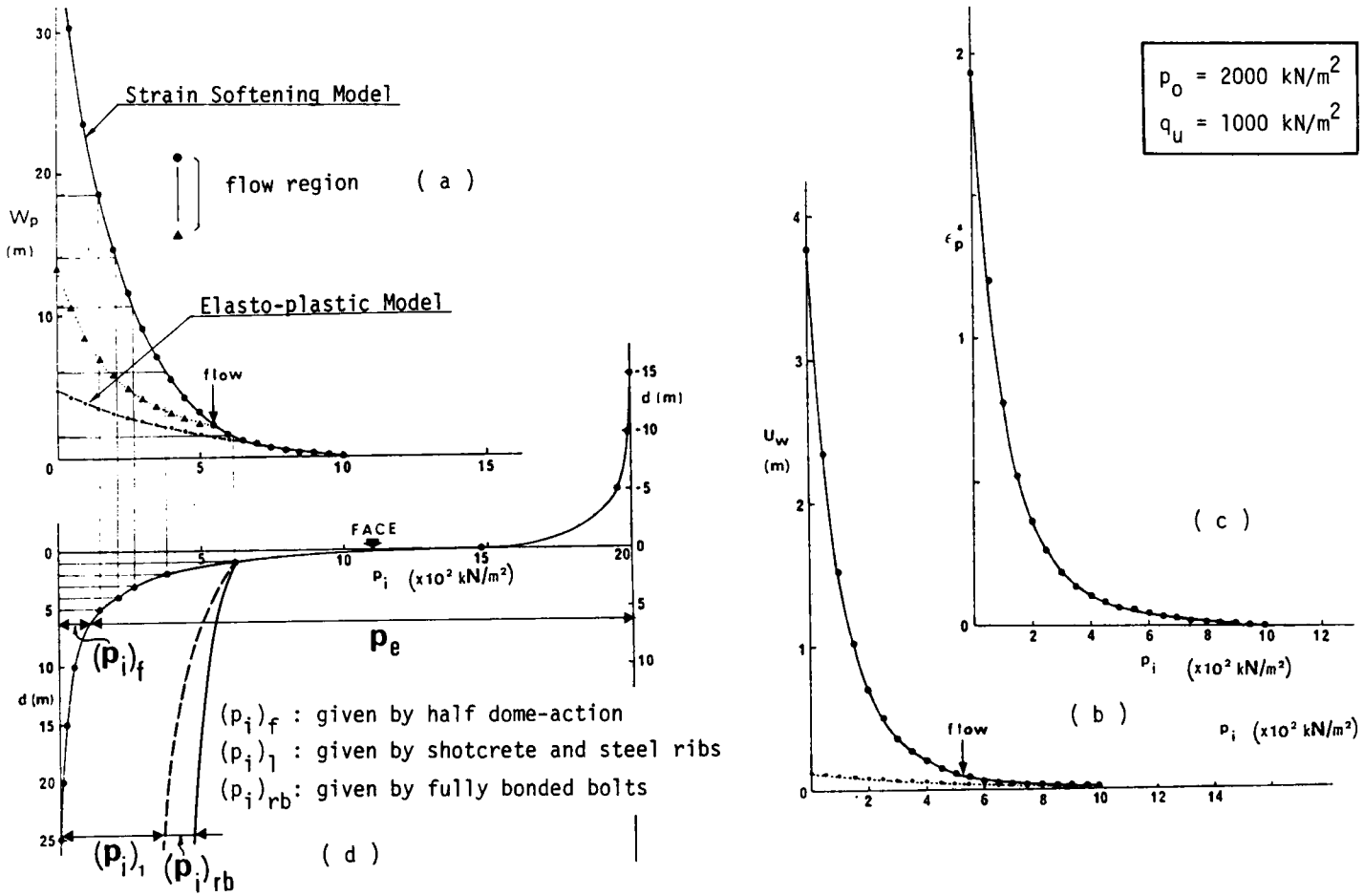

Fig. 8.26 Decrease of Half-Dome Action and Relations among W_p, U_w, ϵ_p^* and p_i in Case of $C_f = 0.5$

at d = 25 m : $W_p = 39.90$ m, $W_1 = 13.19$ m, $W_2 = 26.72$ m

where, notations are subject to Fig. 8.17 and the relation, $W_p = W_1 + W_2$, is realized.

8.8 Conclusion

Concerning tunnel driving and rockbolting in rock which shows strain softening behavior, the following may be concluded.

1) The mining face plays an important role as a temporary support, due to half-dome action, and when advancing the face, it is necessary to place artificial supports, as a substitute for the half-dome action, within a span length from the face, so as to mobilize the bearing capacity of the rock mass as fully as possible.

2) As the effects of the systematic supports are the mobilizing of confining stress and the decreasing of shear stress, a procedure to design supports can be proposed, based on the idea of replacing the effects of supports by an inner pressure acting on the surface of the tunnel wall. By employing this inner pressure as the main parameter, it is possible to calculate the width of the plastic zone, the displacement of the wall and the plastic strain near the wall.

3) The half-dome action of the face is formed within a range of double the length of the span or the height, in the vicinity of the face.

4) Convergence survey means monitoring the change of the radial normal stress or extraction force, as well as the displacement of the wall.

5) Concerning a tunnel in rock whose competence factor is less than 1.0, it is difficult to evaluate the plastic zone without consideration of the strain softening behavior. The equations presented in this chapter give solutions for stresses, strains and displacements in the case of a circular opening.

REFERENCES for Chapter 8

[1] Muirwood, A. : Tunnels for roads and motorways, the quarterly J. of Engineering Geology, Vol. 5, No. 1 & 2, pp.119–120, 1972.

[2] R. Nakano : Geotechnical properties of mudstone of Neogene tertiary in Japan, Proc. Int'l Sympo. on Soil Mechanics, Oaxaca, Mexico, Vol. 1, pp.75–92, 1979.

[3] S. Hata, C. Tanimoto, K. Kimura : Field measurement and consideration of deformability of the Izumi Layers, Rock Mechanics, Suppl. 8, pp.349–367, 1979.

[4] Report on the investigation of the earth/rock pressure in Seikan Tunnel, JSCE, pp.352, 1977. (in Japanese)

[5] S. Hata, C. Tanimoto : Deformation of Nabetachiyama Tunnel and expansive behavior of mudstone, Technical report for Japan Railway Construction Authority, March 1979. (in Japanese)

[6] S. Hata, C. Tanimoto, K. Kimura : Evaluation of rockbolt effect in tunnelling, 12th Sympo.

on Rock Mechanics, pp.61–65, JSCE, 1979. (in Japanese)

[7] T. Inoue, T. Kawahara, S. Miyabayashi : Challenge to tunnelling through expansive mudstone - Nabetachiyama Tunnel, Tunnels and Underground, Vol. 9, No. 4, pp.7–14, April 1978. (in Japanese)

[8] K. Sugawara, C. Tanimoto : Strain softening behavior around a circular opening - Analytical solution, Int. J. of Rock Mechanics and Mining Science (under submitting)

Chapter 9

INTERACTION BETWEEN FULLY BONDED BOLTS AND ROCK

9.1 Introduction

In the discussion on the designing concept of the support system, the replacement of the supporting effect given by the face as a temporary support with an equivalent inner pressure was proposed in Chapter 8. Shotcrete lining, concrete lining, steel arch ribs etc. are considered as direct methods to give inner pressure to the tunnel wall, but rockbolts support cannot be the same method as mentioned above, from the theoretical point of view, for the interaction between rockbolts and ground is not caused only on the wall, but is distributed in the region outside the wall face. Therefore, the stress distribution around an opening would be rather complicated, and it becomes more or less difficult to estimate the inner pressure given by rockbolt support. Also, it should be pointed out that there exists a fundamental difference between a fully bonded rockbolt and a prestressed rockbolt.

Ahead of the detailed discussion, let us review the history of investigations for rockbolting. It is considered to be the early time of this century when rockbolts were applied for underground use in the first place, and there remains the record that Alfred Bush had employed rockbolts in Frieden Coal Mine, Aberschlerin, in 1912. However, it is since the Second World War that rockbolts have been widely developed. For example, in United States rockbolts were employed at only 50 mines in 1949, but it increased more than 500 mines in 1951. Influenced by the development and results in United States, Sweden, Germany, France and so on started researches to confirm the effect of rockbolting. It should be noted that the application of rockbolts has been helping to decrease the occurrence of accidents less than 50%, and also that further development has been related with the remarkable progress in tunnelling method, specially with mechanization aiming at rapid excavation in full section.

As the rockbolting has been developed mainly in mines from the point of view on safety, planning or designing of rockbolts in most cases is determined very empirically, not so statically. Nevertheless, many researchers have been making their efforts to clarify the concrete effect of bolting qualitatively and quantitatively as well as to improve anchoring mechanism.

Rabcewicz [1] introduced his research with respect to the mechanical effect, cost study and adaptability of various types of rockbolts corresponding to geological conditions in 1955, and Panek ([2] – [8]) published his papers on the theory and design of rockbolting continuously in 1956 – 1964. Most papers, which were published those days, were related with wedge-type or expansion-type bolts, and the effect of bolting was represented in intuitive form such as suspending effect or beam effect.

Lang [9], [10] developed his experimental research by using photoelastic stress measure-

ment and applied the results to Snowy Mountain Project successfully. The results obtained by Panek show interesting and significant facts, which require to be analyzed theoretically furthermore. Pearse [11] and Cardon et al [12] discussed the reinforcement of rock by bolting, and they emphasized that cohesion of rock is increased by bolting. Stefanco [13] pointed out the necessity of re-stressing by showing examples of stress relaxation along bolts in practical use. At the middle of 1960s, Gaddy [14] and Thiel [15] reported on the status of development of bolting, and Tincelin [16] and Pralle et al [17] suggested the advantages of resin anchored bolts by the reason that bearing capacity of resin-anchored bolts can be improved approximately 30% higher than mechanically anchored (like wedge-type or expansion-type) or cement-anchored ones, and resin-anchored bolts showed much higher stability against dynamic load such as shock wave generated by blasting. Not only in tunnelling, but also in dam construction, it was introduced the example in which rockbolting was applied to keeping down seepage flow in the foundation of the dam according to Bedringer's report at 1st Congress of ISRM in 1966.

Ortlepp et al [18] considered the mechanical behavior of bolted rock with stress-strain relation based on the increase of stiffness of rock by fully bonded bolts, and McNiven et al [19] developed the theory of elasticity to designing rockbolting. Also, Kmetz [20] analyzed jointed rock with bolts, considering as truss structure.

In Japan, Fujimoto et al [21], [22] investigated bolting effect including resin bonded anchorage, and Japanese Society for Civil Engineers designated the practical guide for rockbolting in tunnels from the results of applications in 1960s. [23] Misawa et al [24], [25] reported the comparison for bearing capacity between expansion-type and top-bonded-resin bolts by pull out tests and field measurement. The tunnelling research group for Japan Highway Research Association discussed anchoring mechanism, bearing capacity, relation to geological condition collectively, based on the past studies and the experiment in Enasan Tunnel, and published the well edited guide for rockbolting in tunnels. [26]

Recently, in accordance with the development of numerical analysis (such as FEM) and field measurement in tunnels, Freeman [27], Farmer [28], Bouvard [29] etc. discussed the relation between shear force and axial force along a fully bonded bolt. However, they did not indicate the practical interpretation how to connect the conclusions obtained by the researches to the application at tunnelling sites and rockbolt design.

In this chapter, the author wishes to analyze the interaction between fully bonded rockbolts and rock with the consideration of non-elastic behavior of rock around an opening, and to interpret the stress distribution along a bolt. Moreover, his own designing method of bolting is proposed specially in the execution of NATM.

9.2 Anchoring Mechanism

To classify systems of rockbolt with respect to anchoring mechanism, we have two categories, namely, 'prestressed' and 'fully-bonded'.

The bolt of the prestressed system consists of a bolt body, anchoring device at its top, a bearing plate and a nut at another end, and by tensioning a bolt with torque or direct pulling, a bolt is subjected to tensile stress. Anchoring is carried out mechanically or by aid of chemical bondage. There are several types of prestressed-system bolts such as wedge-type, expansion-type, top-bonded-type and combined-type.

Anchoring of wedge-type bolt is done in following manner. A wedge is pushed into a pre-splitted slit at the top, and it gives lateral force anchoring a bolt to rock (Fig. 9.1) This type has the longest history due to its easy handling, but it is required to drill exactly at specified length, which influences greatly to anchoring capacity. If the top of a bolt is not enlarged sufficiently, resultant lateral force cannot resist applied tension, and occasionally it is pulled out by small force. Recently, it has become very rare to employ this type of bolt because of the uncertainty of bearing capacity and the limited flexibility of drill hole length.

The anchoring mechanism of expansion-type bolt is done in such a way that the tapered top of a bolt is pulled or screwed into the shell, and through the shell, lateral force to resist bolt tension is introduced. (Fig. 9.2) This is applicable to various types of rock, soft to hard rock, by easy handling and the bearing capacity of bolt is much steadier than a wedge-type one. It is the point to be considered that its bearing capacity is influenced by the misfit of sizes between the diameter of a hole and the dimension of a shell, and occassionally bearing capacity depends on rock properties.

Regarding a top-bonded-type bolt, anchoring is fulfilled by bonding the top of a bolt in a hole with cementing agent such as cement mortar, cement milk, epoxy resin, polyester resin etc. Fig. 9.3 shows one example. Its bearing capacity is very steady, comparing with other types, and can correspond to different rocks in the wide range from soft to hard ones. The problems in this type are the requirement of time for hardening and high cost. In case of requiring some long time, it may happen to miss an appropriate time for prestressing or may make setting procedure troublesome.

To speak of bolts to be classified to fully bonded system, this type of bolt is bonded with cement mortar or some kinds of resin along full length of a bolt by intruding a bolt quickly into a drill hole, where cementing material is already packed in. (Fig. 9.4) No prestressing is introduced, therefore this bolt acts as a certain kind of anchor bar or reinforcing bar and its very easy to be dealt with. Comparing with the hardening time of cement mortar, resin's one is very short, and ordinarily within several minutes. As a disadvantageous point, it is picked up that the adhesion between rock and resin is lost more the existence of inflow or seeping water.

Recently, fully-bonded-type of bolt by using cement mortar with accelerator has been available in accordance with the development of mortar feeding apparatus and well controlled accelerator.

Combined-type of rockbolt as shown in Fig. 9.5 has both functions of prestressed-type and fully-bonded-type. After setting in rock as a prestressed-type one, annular space along a bolt is filled by grouting with cement mortar or milk, whose adhesion to be yielded between a bolt and

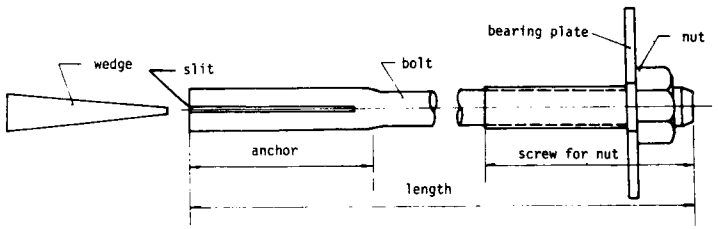

Fig. 9.1 Wedge-Type Rockbolt

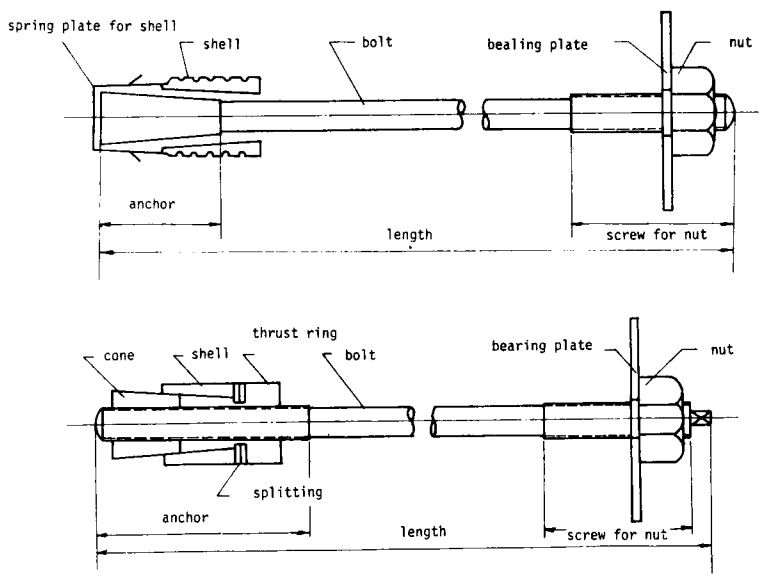

Fig. 9.2 Expansion-Type Rockbolt

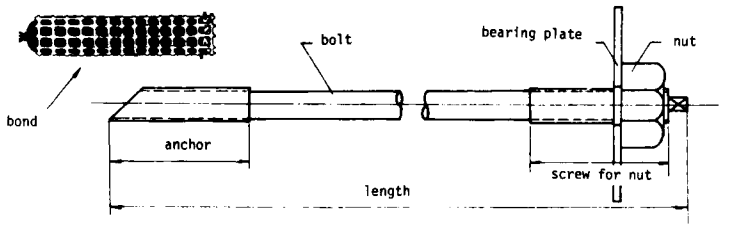

Fig. 9.3 Top-Bonded-Type Rockbolt

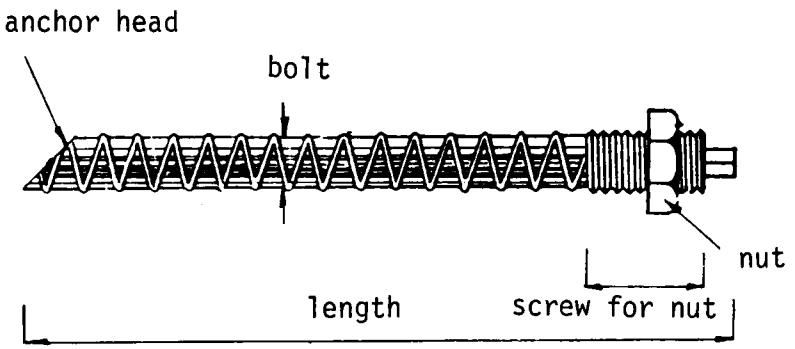

Fig. 9.4 Fully-Bonded-Type Rockbolt

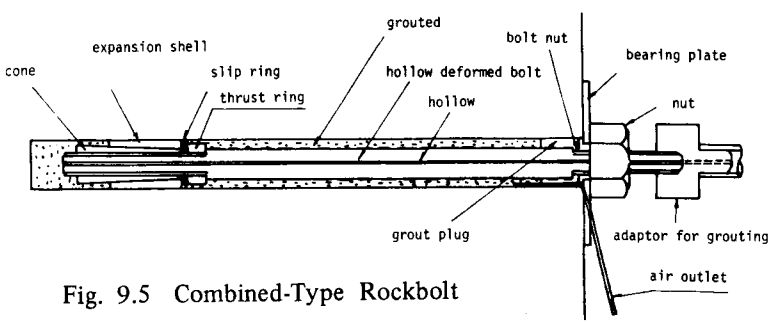

Fig. 9.5 Combined-Type Rockbolt

surface of a hole gives shearing resistance as a fully-bonded bolt. This type of bolt has remarkable advantages, namely, to prevent relaxation of applied prestress and corrosion of a bolt. Newly developed SN–anchor is quite reasonable and employed at many tunnelling sites, for it becomes unnecessary to grout by means of placing special stick-like package of accelerator at the top, ahead of feeding mortar, and then intruding a bolt body strongly in such a manner as to break open the package, make accelerator mixed with mortar and to harden mortar only in the vicinity of the top. After one or several hours, prestressing is introduced within very short time by a hydraulic jack.

9.3 Stress Increment in Rock and Stress Distribution along a Bolt

Henceforth, let us discuss the fully bonded rockbolt – ground interaction on the assumption that the competence factor is 0.5 (as a mean value) in the case of the circular tunnel with 10 m in dia., the inner pressure of 4 or 5×10^2 kN/m^2 is given by shotcrete lining and steel ribs, that is, $(p_i)_l = (p_i)_{sc} + (p_i)_{sr}$, and fully bonded rockbolt system gives some additional inner pressure, (pi)rb, being associated with stress increment, Δp_e, caused by the advance of the face, so consequently the wall is subjected to total inner pressure, $p_i = (p_i)_l + (p_i)_{rb}$, at the final state in which the tunnel should be stabilized as a ring structure.

When a strain softening model shown in Fig. 9.6 is employed, Fig. 9.7 shows (a) W_P, (b) U_W, (c) ϵ_l* and (d) the change of p_i given by the face as well as the excavation force p_e, having the relation $[p_i + p_e = p_0 = 2 \times 10^3$ kN/m$^2]$, on the same abscissa expressing the magnitude of p_i. In

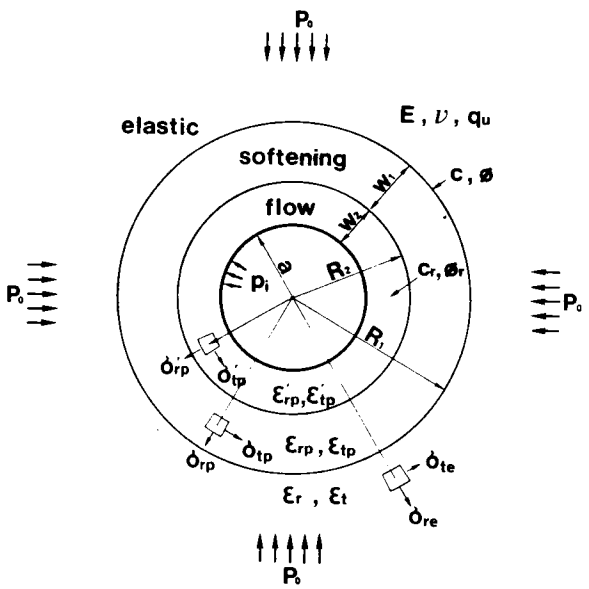

Fig. 9.6 An Idealized Strain Softening Model

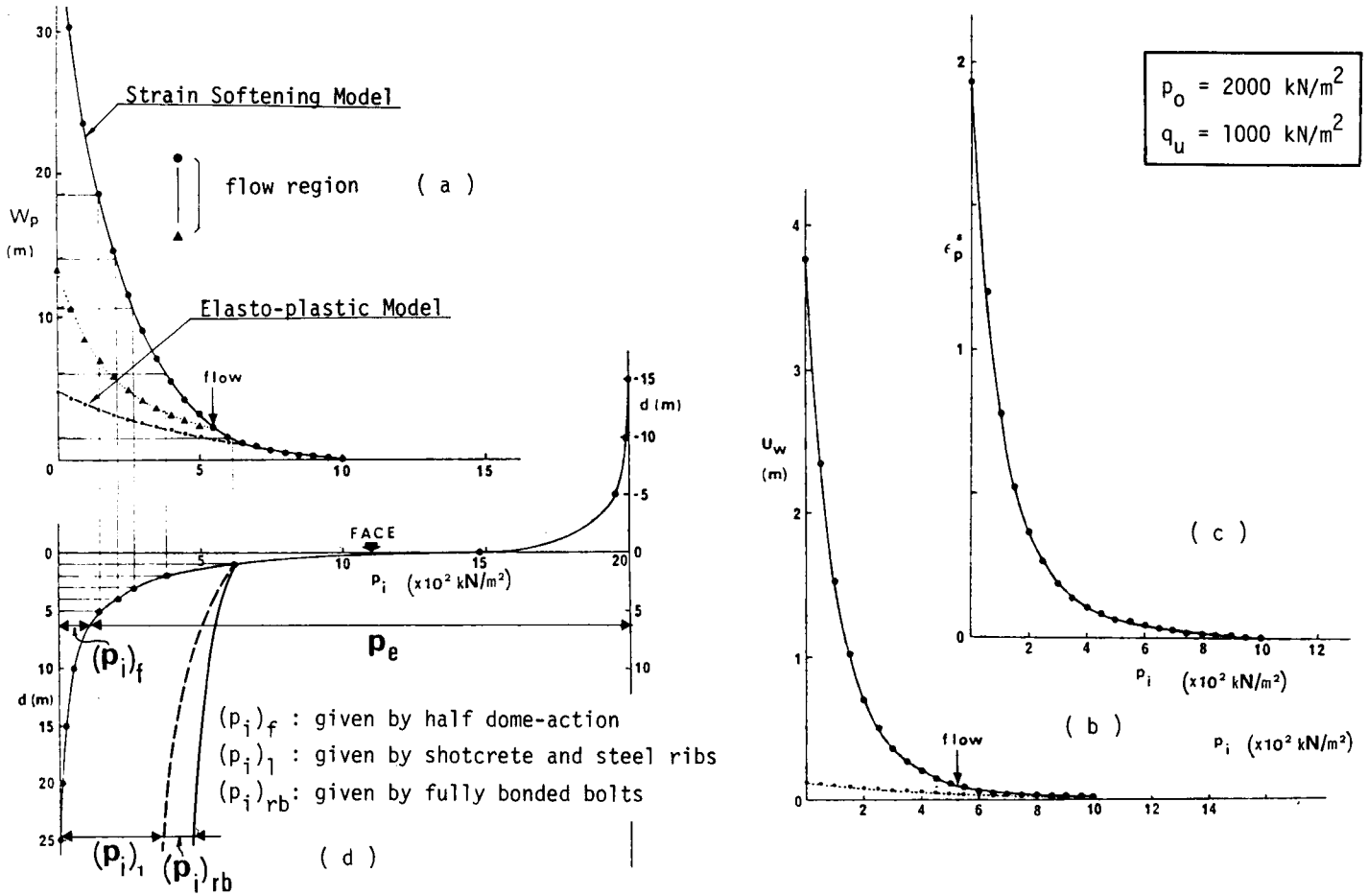

Fig. 9.7 Decrease of Half-Dome Action and Relations among W_p, U_w, ϵ_p* and p_i in Case of $C_f = 0.5$

order to distinguish p_i given by half-dome action from other artificial supports, let us denote $(p_i)_f$.

$$(p_i)_f + p_e = p_o = 2 \times 10^3 \text{ kN/m}^2 \tag{9.1}$$

$(p_i)_f$, which is equal to $p_o = 2000$ kN/m^2 initially, begins to decrease at d = −15 m ahead of the face, become approximately 1.5×10^3 kN/m^2 at the face position and diminishes at the section about d = 25 m behind the face. Within 1 m behind the face, $(p_i)_f$ decreases from 1.5×10^3 kN/m^2 to 600 kN/m^2 (corresponding to 'from d = 0 to d = 1 m'). This means that the face loses 45% of its original bearing capacity as a temporary support only 1 m behind the face, and this is considered one of the main reasons why such concrete operations as placing rockbolts and shotcrete lining to the face position as early and close as possible are required in the application of the New Austrian Tunnelling Method (NATM). When the face advances one more meter, namely from d = 1 m to 2 m, $(p_i)_f$ varies from 6 to 4×10^2 kN/m^2. Being associated with this 1 m advance, the width of plastic zone (W_p) develops from 1.6 m to 5.5 m according to Fig. 9.7 (a). At the position of d = 0 m, no plastic zone occurs and width of the plastic ring (W_p), softening ring (W_1) and flow ring (W_2) at each position behind the face are as follows.

at d = 0m	:	W_p=0m	W_1=0m,	
at d = 1m	:	W_p=1.58m,	W_1=1.58m,	W_2=0m
at d = 1.25m	:	W_p=3.13m,	W_1=2.39m,	W_2=0.74m
at d = 2m	:	W_p=5.52m,	W_1=3.09m,	W_2=2.42m
at d = 5m	:	W_p=18.39m,	W_1=6.89m,	W_2=11.52m
at d = 10m	:	W_p=30.40m,	W_1=10.40m,	W_2=20.00m
at d = 25m	:	W_p=39.90m,	W_1=13.19m,	W_2=26.72m

where, notations are subject to Fig. 9.6 and the relation, $W_p = W_1 + W_2$, is realized.

The four cases as mentioned below were analyzed by increasing stress to axisymmetric finite element models including rockbolt members with various lengths (1−8 m long). The finite element models applied to this analysis are as shown in Fig. 9.8, and the stress increments were obtained from the difference with respect to σ_r and σ_t between the stress distributions given by the softening model shown in Fig. 9.6. Deformation coefficients for softening state, which were applied to the respective elements, are modified in such a way that, for example, in Fig. 9.9 the deformation coefficient of Point F, whose path is Point $0 \rightarrow A_4 \rightarrow F$, is replaced with a straight line passing through Point 0 and F. This modification is justified only for small increments of strain in the softening state by the reason that the increment of strain given by the rockbolt confinement is correspondingly nearly equal to the absolute value of the stress increment.

CASE (1) : Rockbolts are placed at d = 1 m with the density of 1 bolt/m^2, and the stress increment from the state of p_i = 600 kN/m^2 to p_i = 500 kN/m^2 obtained by the softening model is given to FEM model.

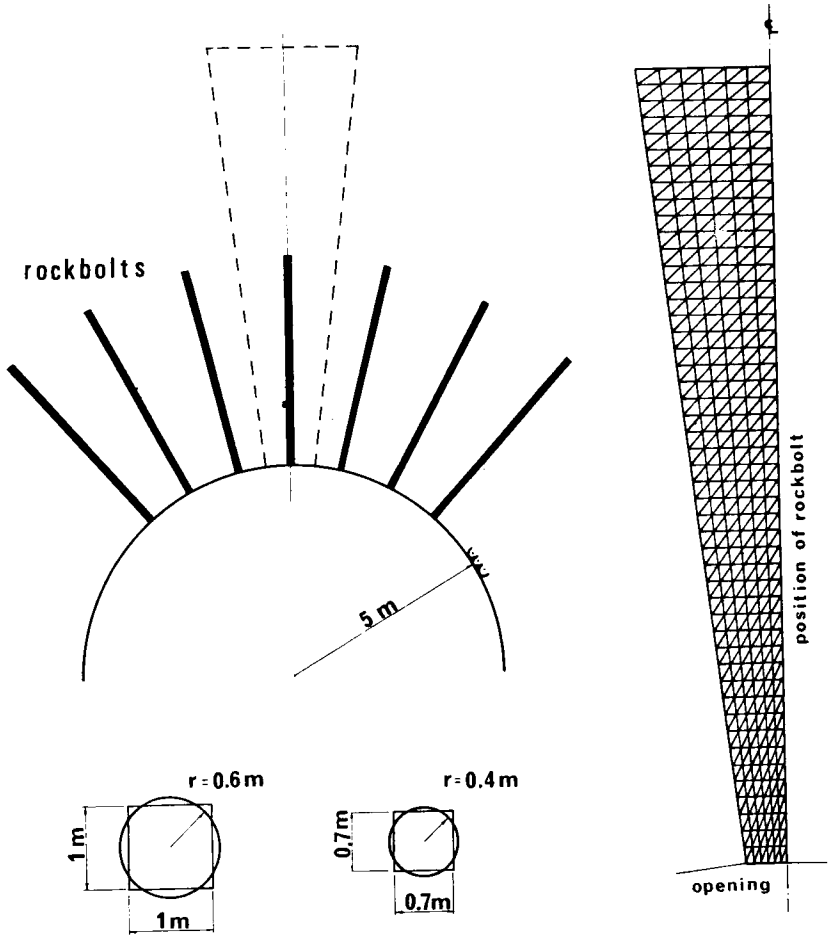

Fig. 9.8 Finite Element Method for Analysis

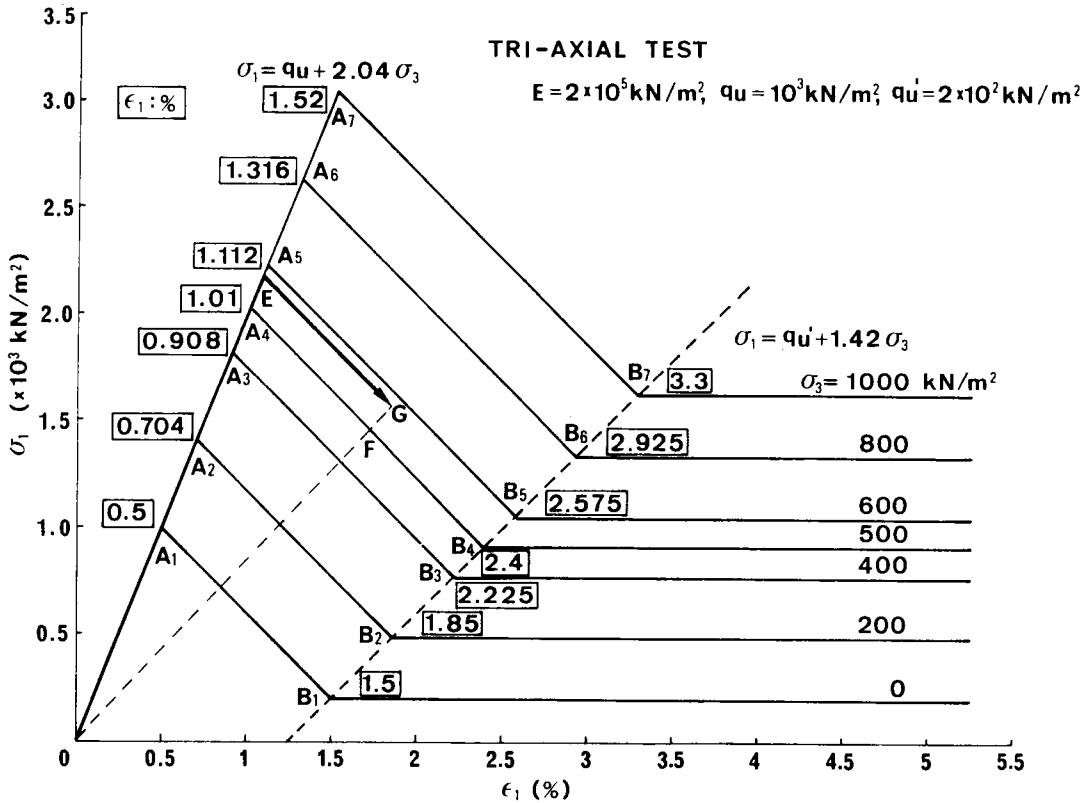

Fig. 9.9 Schematic Stress-Strain Relation for Tri-Axial Test
(Tertiary Neogene Mudstone Sampled in Hokuriku Region)

CASE (2) : The density of rockbolting is 2 bolts/m^2, and other conditions are the same as CASE (1).

CASE (3) : Rockbolts are placed at d = 1.25 m with the density of 1 bolt/m^2, and stress increment from the state of p_i = 500 kN/m^2 to p_i = 400 kN/m^2 obtained by the softening model is given to the FEM model.

CASE (4) : The density of rockbolting is 2 bolt/m^2, and other conditions are the same as CASE (3).

In CASE (1) and (2), only softening is induced, and in CASE (3) and (4), both softening and flow are caused near the opening. Therefore we can discuss the distributions of axial force and shear force along a rockbolt and the stress distribution in the rock mass influenced by rockbolts which are placed through different types of plastic zones. Also, it is assumed that an annular space between a rockbolt and rock mass is tightly filled with the bond whose physical properties are the same as that of the rock mass and that no slip occurs.

Let us consider the fundamental interaction between the rock and a fully bonded rockbolt. As the face is driven forward, the rock moves towards the opening. The rock near the opening moves more than the rock farther back, and thus differential movement occurs. The rock movements along a line parallel to the bolt and the movement of the bolt itself are shown in Fig. 9.10, after Freeman [27]. The bolt has been carried bodily towards the opening by the rock and at one point along the bolt there is no relative movement between the rock and the bolt (the neutral point).

Relative movement between the rock and the bolt induces longitudinal shear stresses on the bolt. The shear stresses, at points farther back than the neutral point, are anchoring the bolt to the rock and the shear stresses closer to the opening are picking up load from the rock and dragging the bolt into the opening. In this way, the rock bolt is split into two parts, namely, an "anchor length" and a "pick-up length." [27] The bolt is subjected to two kinds of shear stresses, one positive and another negative, being demarcated by the neutral point.

The shear stress acting on the bolt is given in terms of the differential form of axial stress. [28]

$$\tau_x = -\frac{b}{2} \cdot \frac{d\sigma_x}{dx} \tag{9.2}$$

where, b: radius of a bolt, and x : direction parallel to the bolt axis.

Therefore, a position, showing the peak of the axial stress distribution, agrees with the neutral point. To monitor the interaction between the rock and the bolt in field measurements, there are two methods: measure 1) the strain distribution in the bolt (from which the shear stresses acting on the bolt can be calculated), 2) the displacements in the rock. The results of numerical analysis for CASE (1) – (4) are shown in Fig. 9.11 (a) – (d) respectively. Fig. 9.11 (a) and (b) conclude that the bolt placed only in a softening zone shows its peak at a middle point and the pick-up length is nearly equal to the anchor length, and that the peak value of the axial force in the bolt is proportional to the bolt length. Also, it can be concluded that the distribution of axial force in the bolt placed into an elastic through softening zone shows a constant peak value at the same position

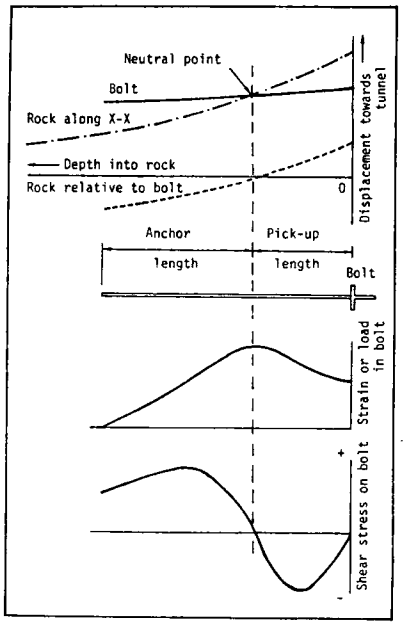

Fig. 9.10 The Movement of a Bolt Fully Bonded in Rock
(after T. Freeman [27])

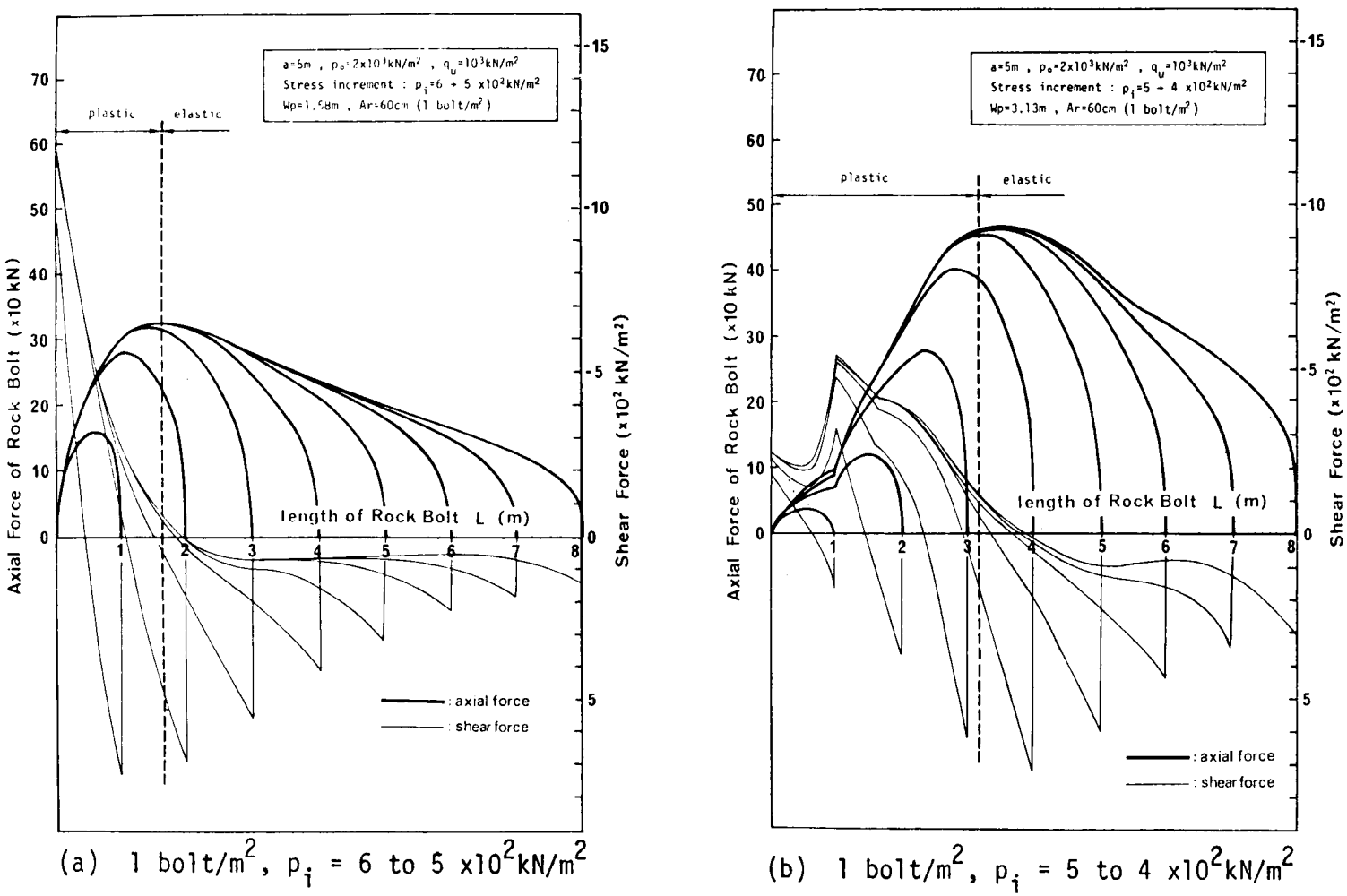

Fig. 9.11 Distribution of Axial Force and Shear Stress

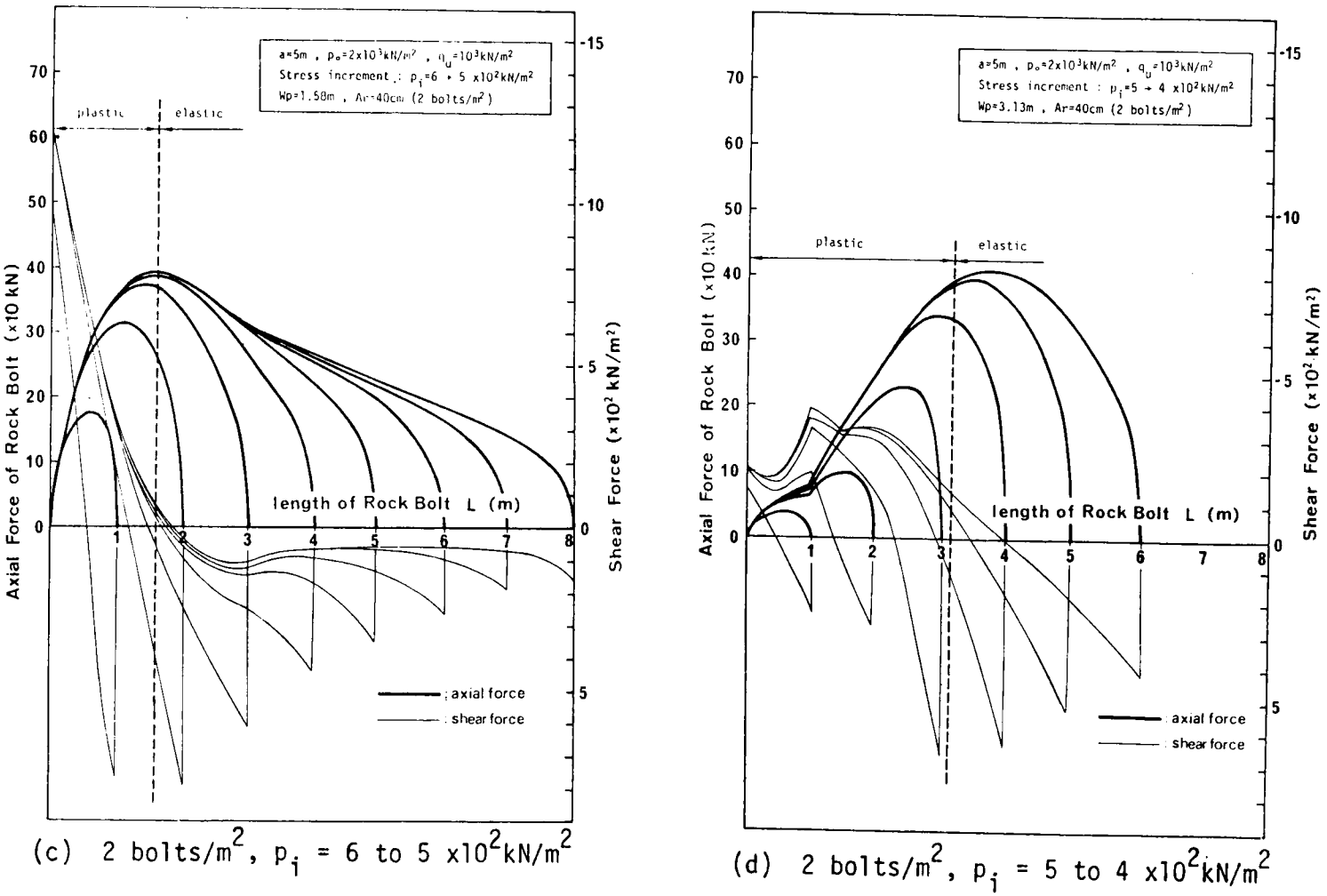

Fig. 9.11 (Continued) Distribution of Axial Force and Shear Stress

in the case that the bolt is longer than twice the width of the plastic zone (W_p), and the position of its peak (the neutral point) agrees with the boundary between the elastic and nonelastic zones in the rock. Further, as the maximum absolute value of the shear stress always appears on the wall, slip along the bolt would occur near the wall initially, if it is caused by a shortage of adhesive capacity. In such a case, the bolt would act partially in the same manner as a prestressed bolt.

Consequently, typical modes of axial force distribution in the bolt for these cases show simple convex shapes and are classified in two types: Mode(A) which has its peak at the middle point of the bolt, and Mode(B) in which the anchor length becomes longer than the pick-up length. Otherwise, Fig. 9.11 (c) and (d), corresponding to the cases in which the rock contains three phases such as elastic, softening and flow, conclude that a bolt with shorter length than the width of the flow zone shows its peak of axial force at the middle point and the value of this peak is less than 1/10 of that shown by the bolt placed in the elastic zone. Also the following may be concluded. The distribution of axial force in the bolt placed into a softening zone, through a flow zone, shows a point of inflexion at the boundary between flow and softening, and the position of this peak is located farther back and the anchor length becomes shorter than pick-up length. Anchor length becomes longer than pick-up length only when the length of the bolt is longer than double the width of the plastic zone, and in that case the position of the peak is fixed and agrees with the boundary between the softening and elastic zone. When the absolute value of shear stress shows its maximum about at the middle, it may be possible that slip is caused in the plastic zone near the elastic-plastic boundary, if shear stress overcomes adhesive capacity of the bond material.

Typical modes of axial force distribution are classified into three, for these cases: Mode (C) shows its peak at the middle point, corresponding to the case in which the bolt is placed only in the flow zone; Mode (D) has a point of inflexion and its anchor length is much shorter than the pick-up length, corresponding to the case in which most of the bolt body is placed in a non-elastic zone; and Mode (E) shows longer anchor length than pick-up length, corresponding to the case in which the bolt is placed sufficiently into the elastic zone.

These five modes as mentioned above are shown in Fig. 9.12. By referring to these modes, we can evaluate the effect of bolting, and it is possible to determine a width of plastic zone with some measuring rockbolts having a length longer than double the width of the presumed plastic zone. Sometimes, some practical people in Japan, who are engaged in field measurements with bolts, attached strain gauges on their surfaces, and/or with mechanical anchor devices, are apt to consider that the peak of the axial force shows the elastic-plastic boundary, even if the length of the measuring bolt is not long enough, and bolts with a length of 3 – 5 m are applied in most cases, with no consideration whether the competence factor has a low value or not. This practice should be corrected.

9.4 Rearrangement of Stresses in Rock due to Bolting

Next, let us consider the stress distribution in rock along a bolt due to stress increments, as

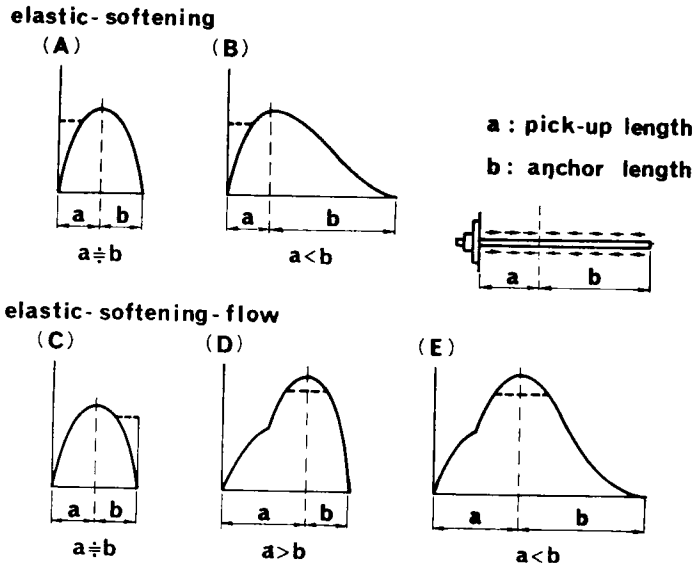

Fig. 9.12 Modes of Axial Force Distribution in a Bolt

mentioned in CASE (1) – (4). Fig. 9.13 and 9.14 show the magnitude of stresses, $\Delta\sigma_r$ and $\Delta\sigma_t$ within 10 cm of the bolt, induced by a bolt under the conditions of CASE (1) and (4), respectively. With regard to $\Delta\sigma_r$, induced stress in the radial direction, it is concluded that a bolt shorter than the width of plastic zone shows lower stresses than those of a bolt reaching into the elastic zone, as the distribution of axial force indicates. On the contrary, the distribution of $\Delta\sigma_t$, induced stress in the tangential direction, shows that a shorter bolt gives higher stress in the case of softening only, and that the magnitude of peak stress is almost constant and has a rather low value compared with $\Delta\sigma_r$, but is reduced near the boundary between softening and flow in the case of flow occurring.

Fig. 9.15 shows the stress distribution of σ_t and σ_r within p_i = 600, 500 and 400 kN/m^2. Curve ① – ③ and ④ – ⑥ are corresponding to σ_t and σ_r. For example, the longitudinal difference between Curve ① and ② shows the stress increment at the time when p_i varies from 600 to 500 kN/m^2 or when the face moves only 0.25 m from the position of d = 1 m. This can be easily understood by plotting stress increments, which are normalized with respect to the cross section governed by one bolt, onto these curves. Fig. 9.16 and 9.17 show the stress change for CASE(1) and (2) respectively by placing bolts with various lengths. The increment of σ_t is almost negligible and the shear stress, which can be expressed in terms of half of the magnitude of $(\sigma_t - \sigma_r)$, is reduced corresponding to each bolt length. The occurrence of flow reduces the stress induced by a bolt quite a bit. Consequently, from the point of view of the decrease of shear stress due to the increase of confining pressure, rockbolting acts most effectively when the rock is in a state of strain-softening.

Generally it is very difficult to measure the change of stress in rock, but displacement is easy to measure and is a direct method which gives fairly accurate results. Thus, convergence surveys during construction is a fundamental measurement in tunnelling by NATM. Even if the analysis of stress distribution around an opening could be done very reliably, the observational construction of tunnel driving might become almost impossible or meaningless without any consideration of the relation between stress and displacement.

Corresponding to the stress distributions shown in Fig. 9.16 and 9.17, Fig. 9.18 (a) and (b) show the state of displacement caused by bolts with various lengths. It is clear that rockbolts reduced the displacement near the wall according to their lengths and increased the displacement in the vicinity of the anchoring end. Even bolts placed only in the plastic zone cause a decrease of 20 – 30% of the displacement of the wall which occurs without any bolts. Bolts of longer than $2W_p$ do not show any significant effect on the displacement of the wall.

In order to take into account the effect of fully bonded rockbolts in design, we have to replace the rockbolt by an equivalent inner pressure. The following can be used to define an equivalent inner pressure:

1) From the stress increment,

$$\triangle p_i = (\Delta T / T_o) \times p_e \qquad (9.3)$$

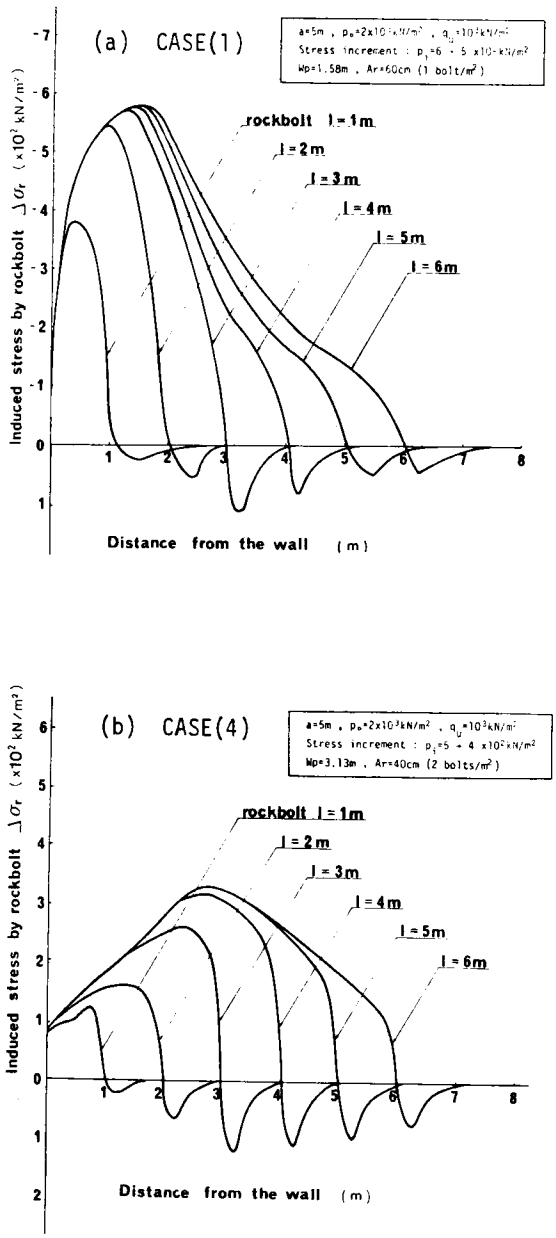

Fig. 9.13 Induced Stress $\Delta\sigma_r$ by a Bolt for CASE (1) and CASE (4)

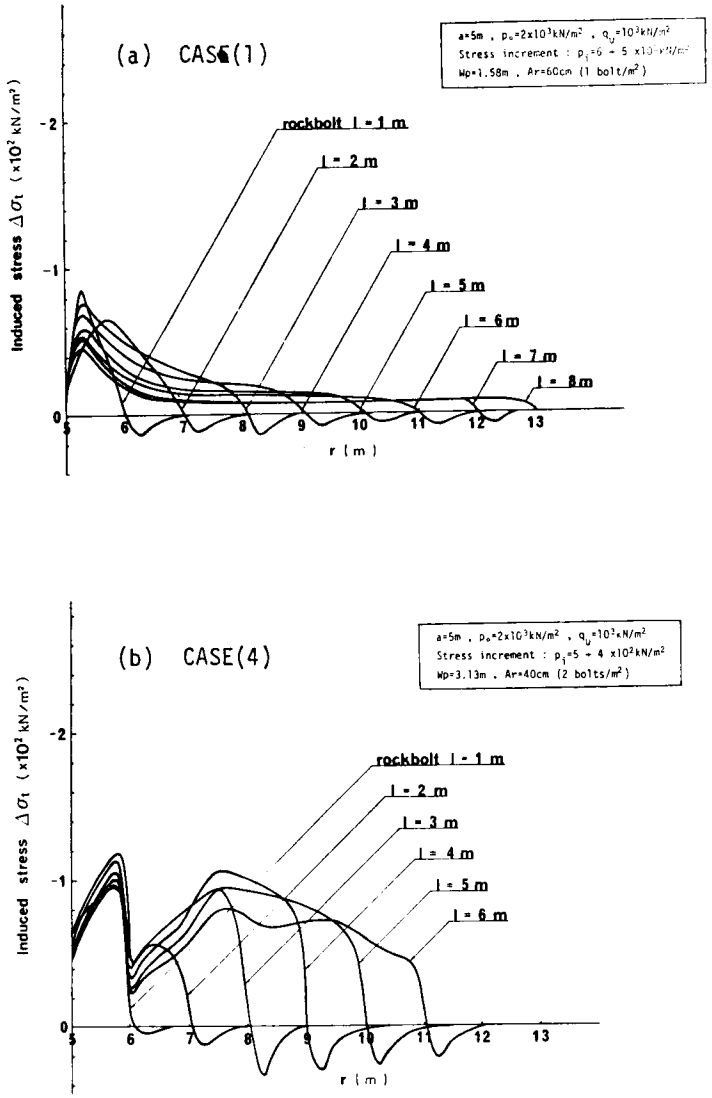

Fig. 9.14 Induced Stress $\Delta\sigma_t$ by a Bolt for CASE (1) and CASE (4)

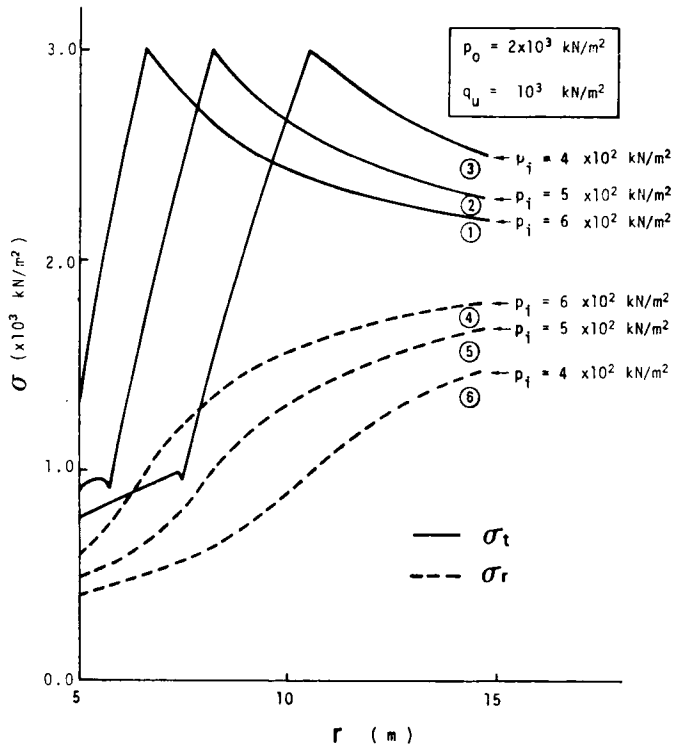

Fig. 9.15 Stress Distribution under $p_i = 6,\ 5$ and 4×10^2 kN/m^2 ($C_f = 0.5$)

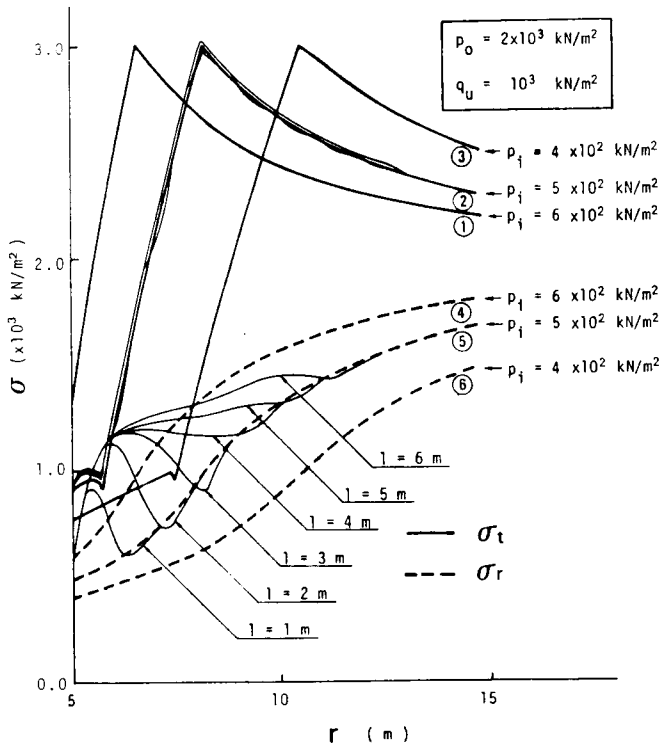

Fig. 9.16

Stress Distribution Induced by Bolts with Various Lengths for CASE (1)

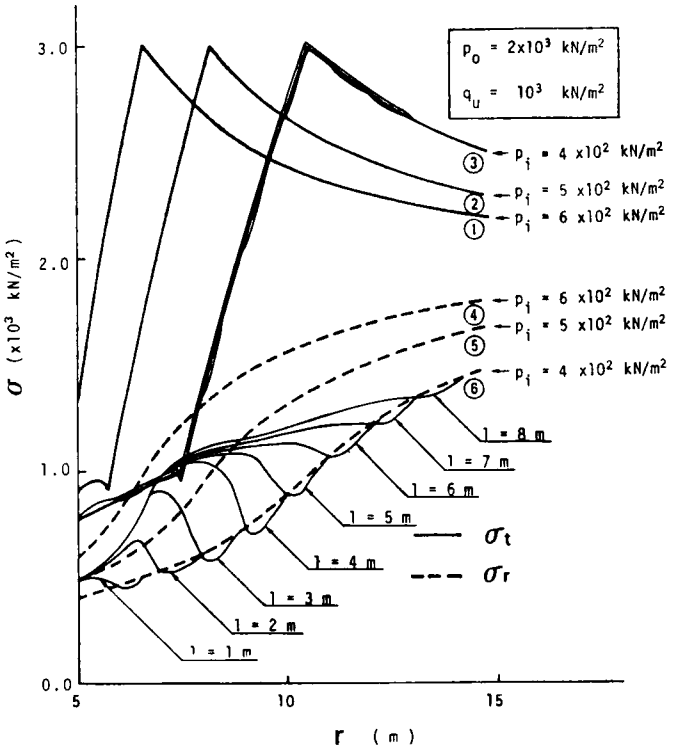

Fig. 9.17

Stress Distribution Induced by Bolts with Various Legnths for CASE (2)

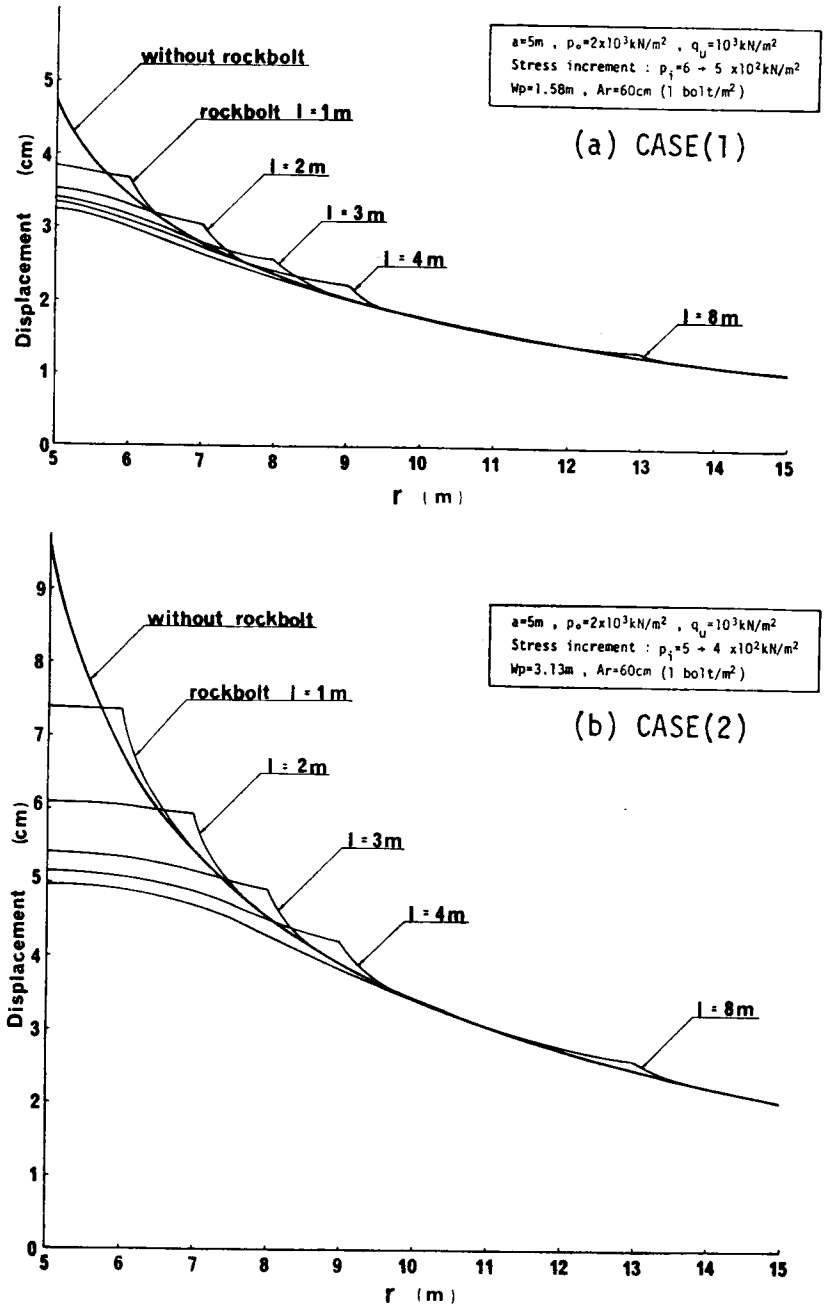

Fig. 9.18 Reduced Displacement Induced by Bolts

where Δp_i : an equivalent inner pressure,

T_o : $(\sigma_t - \sigma_r)$ in the case of no bolt,

ΔT : stress increment $(T - T_o)$,

T : $(\sigma_t - \sigma_r)$ in the case of bolting,

and p_e : increment of excavation force (drag force) on the wall due to the advance of the face.

2) From the reduction of displacement,

$$\Delta p_i = \frac{u_o - u}{u_o} \times \Delta p_e \tag{9.4}$$

where, u_o : displacement in the case of no bolt

and u : displacement with bolting.

Comparing Eq. (9.3) with Eq. (9.4), it might be reasonable, because of its simplicity, to employ Eq. (9.4) as the equivalent inner pressure given by bolts.

In Fig. 9.18, relative displacements corresponding to the increment of excavation force are shown, and Fig. 9.19 shows the state of displacement near the opening under various inner pressures. The two thin straight lines express the boundaries of softening-elastic (ϵ_1 = 1.2%) and flow-softening (ϵ_1 = 2.4%) respectively. The thick dotted curves show absolute displacements caused by bolts with a length of 1 m and 5 m respectively for CASE (4). Comparing the decrease of displacement from the wall, the line corresponding to the flow-softening boundary (ϵ_1 = 2.4%) shows a radical increase of displacement under constant strain, ϵ_t = 2.4%. A similar tendency is recognized in other cases as shown in Fig. 9.20(a) and (b), which were obtained by using Eq. (9.4).

On the assumption that the allowable limit of strain (ϵ_1, that is, ϵ_t) is defined by a magnitude of 2.4%, in the range of $\epsilon_t > 2.4\%$ in Fig. 9.19 and Fig. 9.20, the decreasing rate of displacement which is caused by placing rockbolts becomes larger than the increasing rate of displacement which is expressed by Line A, corresponding to the allowable limit of displacement to be determined by ϵ_t = 2.4%. This means that it is possible to define the magnitude of an equivalent inner pressure given by fully bonded bolts by the magnitude of displacement which occurs on the wall (Uw). The equivalent inner pressure defined by Uw, which is associated with the change of excavation force (p_e) with an increment of 100 kN/m^2, is shown in Fig. 9.21. Judging from the results, with respect to CASE (1) – (4), it is concluded that the equivalent inner pressure given by fully bonded bolts is estimated to be 13 – 27% of the change of excavation force, and double density of bolting makes the equivalent inner pressure 50 – 70% higher than that given by the initial density.

Finally, we should consider the magnitude of axial stress in a bolt. In the discussion up to now, we have not considered the rupture of a bolt or the slip between the rock and the bolt. The strengths of bolts conventionally used in Japan are as follows:

ϕ 25 bolt : yielding strength 1.54×10^5N, ultimate strength 2.25×10^5N

ϕ 30 bolt : yielding strength 2.34×10^5N, ultimate strength 3.41×10^5N

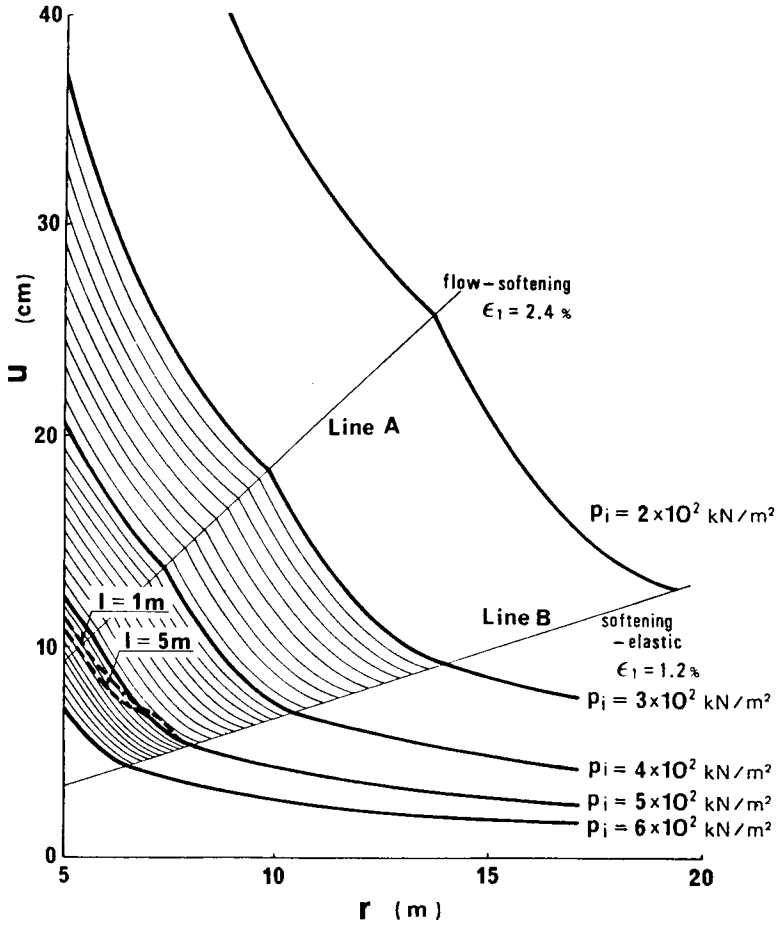

Fig. 9.19 The State of Total Displacement Reduced by Bolts in CASE (4)

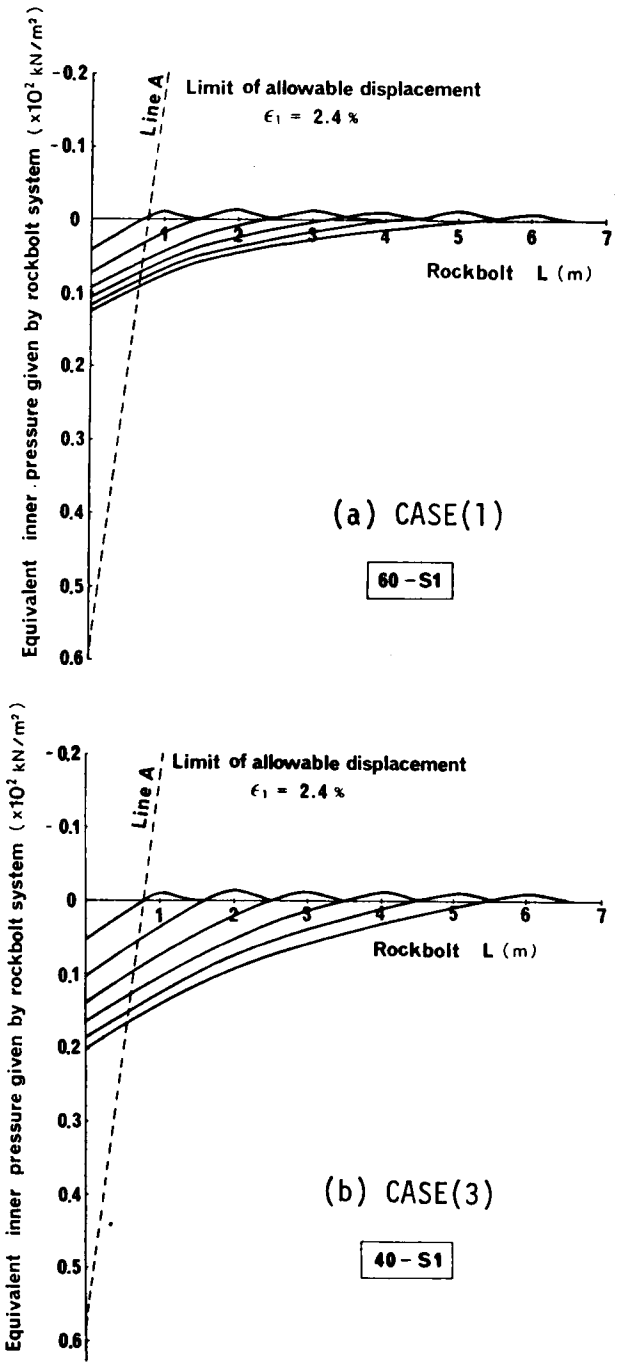

Fig. 9.20 Equivalent Inner Pressure along a Bolt

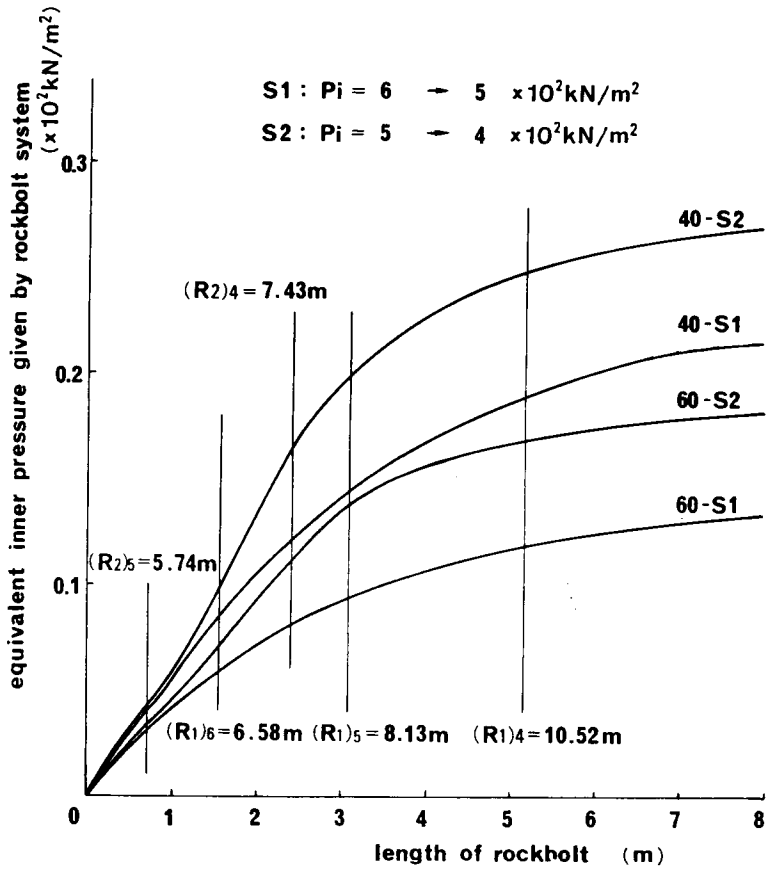

Fig. 9.21 Equivalent Inner Pressure Defined by U_w

The discussion has been conducted using the assumption that a bolt placed in rock deforms with the deformation of the rock, and that there is not slip between the rock and the bolt. However, if we look back to the distribution of axial force as shown in Fig. 9.11, for example, Fig. 9.11 (a) shows 3.3 or 3.4×10^5N at the peak, in the case of a bolt with 25mm in dia, and this value exceeds the ultimate strength of 2.25×10^5N. Actually, of course, this cannot happen. A detailed investigation on the axial force and allowable elongation of a bolt should be carried out with consideration of the magnitude of displacements in rock.

9.5 Conclusion

Concerning tunnel driving with rockbolts in rock which shows strain softening behavior, the following may be concluded.

1) The mining face plays an important role as a temporary support, due to half-dome action, and when advancing the face, it is necessary to place artificial supports, to substitute for the half-dome action, within a span length from the face, so as to mobilize the bearing capacity of the rock mass as fully as possible.

2) As the effects of systematic supports are the mobilizing of confining stress and decreasing of shear stress, a procedure to design supports can be proposed, based on the idea of replacing the effects of supports by an inner pressure acting on the surface of the tunnel wall. By employing this inner pressure as the main parameter, it is possible to calculate the width of the plastic zone, displacement of the wall and plastic strain near the wall.

3) Half-dome action of the face is formed within a range of double the length of the span or the height, in the vicinity of the face.

4) Convergence survey means monitoring the change of radial-normal sttress or extraction force, as well as the displacement of the wall.

5) The peak of the axial stress distribution in a fully bonded bolt shows the boundary between pick-up length and anchor length of a bolt, and it agrees with the boundary between elastic and plastic zones only when the anchor length is longer than the pick-up length.

6) Fully bonded bolts, which are placed only into the plastic zone have some effect, but it is required that bolts should be longer than 1.5 times the width of the plastic zone in order to obtain sufficient effect.

7) The effect of fully bonded bolts, having a length longer than twice the plastic zone, is almost equal to those having twice the length of the plastic zone, and the optimum length of systematic (fully bonded) rockbolts is concluded to be 1.5 to 2.0 times the presumed plastic zone.

8) In field measurement, typical modes of axial force distribution in a fully bonded bolt are classified into five categories. By referring to these modes, it is possible to evaluate the effect of bolting, and to determine a width of plastic zone with some measuring rockbolts having a length longer than twice the width of the presumed plastic zone.

REFERENCES for Chapter 9

[1] Rabcewicz, L.v.: Bolted support for tunnels, Mines and Quarry Engg., March – April, 1955.

[2] Panek, L.A.: Theory of model testing as applied to roof bolting, US Bureau of Mines Report 5154, 1956.

[3] Panek, L.A.: Design of bolting systems to reinforce bedded mine roof, US Bureau of Mines Report 5155, 1956.

[4] Panek, L.A.: Principles of reinforcing bedded mine roof with bolts, US Bureau of Mines Report 5156, 1956.

[5] Panek, L.A.: Anchorage characteristics of roof bolts, Mining Congress J., 43–11, 1957.

[6] Panek, L.A.: The effects of suspension in bolting bedded mine roof, US Burea of Mines Report 6138, 1962.

[7] Panek, L.A.: The combined effects of friction and suspension in bolting mine roof, US Bureau of Mines Report 6139, 1962.

[8] Panek, L.A.: Design for bolting stratified roof, Trans. of SME, 229–2, 1964.

[9] Lang, T.A.: Rock behavior and rock bolt support in large excavation, ASCE, Oct. 1957.

[10] Lang, T.A.: Theory and practice of rock bolting, Trans. SME–AIME, 220, 1961.

[11] Pearse, G.E.: Investigations concerning rock-bolting at Billingham, Bull. Inst. Mining and Met., 69–8, 1960.

[12] Cardon, R., Buisson, R., Chambon, C.: Boulonnage de foit en voie, Revue de l'industrie Minerale, 43–10, 1961.

[13] Stefanco, R.: New Look at long-term Anchorage, Min. Eng., 14–5, May, 1962.

[14] Gaddy, F.L.: Recent developments in drilling and bolting mine roof, Mining Cong. J., 49–8, Aug. 1963.

[15] Thiel, P.S.: Recent development in roof bolting and installation procedure, Can. Mining and Met. Bull, 57–630, Oct. 1964.

[16] Tincelin, E.: Soutenement suspendu tiges d'acier scellees an ciment on a resine polyster dans les mines de Fer de Lorraine, Revue de l'industrie, 47–7, July 1965.

[17] Pralle, G.E., Karol, R.H.: Resin anchored rock reinforcing members, 1st Congress of ISRM, Lisbon, 1966.

[18] Reep, J.J., Ortlepp, W.O.: Grouted bolt for rock stabilization, AIME Int. Min. Conf., July 1969.

[19] McNiven, H.D. et al: Rock bolting of tunnels for structural support, Part 1 and 2, Int. J. Rock Mech. Min. Science, 6–5, 1969.

[20] Kmetz, W.J.: Roof truss support problem strata, Coal Age, Jan. 1970.

[21] Sasaki, Fujimoto, Ito: Fundamental study on support by bonded type roof bolt, J. Mining and Safety, 9–8, 1963. (in Japanese)

[22] Fujimoto, K.: Roof bolt support, Part 1–5, J. Mining and Safety, 6, 1960. (in Japanese)

[23] Standard specification for tunnelling, Japanese Society for Civil Engineers, 1969. (in Japanese)

[24] Misawa, S., Takahashi, A.: Bearing capacity of rockbolt, J. of Tunnels and Underground, 2–5, 1971. (in Japanese)

[25] Misawa, S., Takahashi, A.: Anchoring mechanism of rockbolt, Proc. of 6th Symposium on Rock Mechanics, JSCE, 1970. (in Japanese)

[26] Guide for rockbolting in tunnels, Tunnelling Research Group, Highway Research Association, 1973. (in Japanese)

[27] Freeman, T.J.: The behavior of fully-bonded rockbolts in the Kielder experimental tunnel, Tunnel and Tunnelling, June, 1978.

[28] Farmer, I.W.: Stress distribution along a resin grouted rock anchor, Int. J. of Rock Mechanics and Mining Science, Vol. 12, pp. 347–351, Pergamon Press, 1975.

[29] Bouvard, A.: Contribution to Sympo. on Tunnel Stability by Convergence Confinement Method, French Tunnelling Association, Paris, Oct. 1978. (Tunnels et ouvrages souterrains, AFTES No. 32 Mars–Avril 1979, pp. 122–125, in French.)

Chapter 10

APPLICATION OF SHOTCRETE TO TUNNELLING

10.1 Introduction

Shotcrete is one of the major supporting members in tunnelling by the following reason:

When shotcrete is applied to an erratic rock surface, it will smooth out the surface and help keep the adjacent rock blocks in place through the bond to the rock and through its initial shear strength. As the shotcrete sets up, a composite rock/shotcrete structures is formed. As rock loads develop with time, it is in general the competence of the composite shotcrete/rock structure that is in question. There is not a transfer of load from the rock mass to the shotcrete in a way comparable to the transfer to steel supports. Shotcrete simply helps the rock mass to take care of itself by locking together the immediately adjacent blocks, and thus acts as a reinforcement rather than as a support. [1]

Shotcrete as defined by the American Concrete Institute (ACI 506–66) includes both pneumatically applied mortar and pneumatically applied concrete. In tunnelling practice and literature, the term is most often used for pneumatically applied concrete only, and the term gunite for pneumatically applied mortar. This distinction is used in the dissertation.

According to Brekke's review [1] on the development of shotcrete and gunite use in under ground openings, it is as follows:

Fettweis (1961) points out that the first attempts to use gunite underground were made in Brucetown in 1914 by the Bureau of Mines on the inititative of Chief Engineer George Rice (Rice, 1918). Between the world wars, gunite was extensively used in American mines and was also introduced in other underground openings (e.g. the San Jacinto Tunnel in California).

After the Second World War, machines were developed in Europe for pneumatic application of concrete with aggregate up to 1″ in size. At the same time, the application of shotcrete close to the face as an integrated part of the driving process was initiated (Sonderegger, 1956). This use of shotcrete, often in combination with rock bolts and nets, rapidly spread through the Alpine countries and to the Scandinavian peninsula. Shotcrete and composite reinforcement/support systems that include shotcrete are today very widely used in underground openings in Europe, and have proved to be both efficient and economical in stabilizing a number of types of adverse ground conditions. Shotcrete has also been used successfully in other parts of the world, including South America, Hong Kong and Japan.

The author, in Japan, can pick up the case of Seikan Tunnel, with 54 km long under construction, in which engineering staffs of Japan Railways Construction Authority have been carring out their investigation regarding various problems in shotcrete fundamentally and practically since 1968. Most of items on shotcrete in Japan are dealt with in that long term project. Recently they

developed very excellent shotcreting system, called SEC–system, which yields rebound of 10% approximately, occasionally 10% – 15%, but not more than 15%. Also in the new project, called 2nd Najio Tunnel (3 km long), the author, who has been engaged in the position as the superviser regarding NATM from the academic side, confirmed its noticeable capability of producing well-controlled shotcrete with steady, high strength. This will be discussed in following section.

10.2 Shotcrete and SEC

In general, there are basically two ways of bringing the mix to the nozzle for application, namely as a dry mix or as a wet mix. The most commonly used so far is the dry mix method. Cement, sand, and coarse aggregate are brought to an open dry-mix hopper, where powder accelerator is usually indtroduced through an adjustable feeding mechanism. Via a feed wheel chamber or – in some models – pressure chamber, this mix is fed continuously through a hose to the nozzle under pneumatic pressure. The correct pressure is a function of hose size and length, but is normally around 5 – 6 kgf/cm^2.

The water is added at the nozzle, usually at a pressure of about 4 – 4.5 kgf/cm^2. The amount of water added is controlled by the nozzleman. He therefore has a crucial influence on the quality of the final mix. Experience and good judgement on the part of the nozzleman are obviously important to ensure a good mix. One advantage of his control of the water is that the nozzleman can reduce the water he adds on rock surfaces with seeping water.

It would be proper to name the dry mix method the so called "dry mix method". The sand used normally will contain moisture that may amount to about half of the total water needed. When the powder accelerator is added in the shotcrete machine, this moisture can be sufficient to initiate reactions before the mix reaches the nozzle.

An inherently better approach is to add the accelerator at the nozzle. This is easily done for fluid accelerators, since these can be mixed with the water in a simple mixing pump at a present ratio. Even powder accelerators can be added at the nozzle, but with present devices that is rather complicated to control properly.

The major advantages of the wet mix are that a ready mix can be brough to the site in concrete trucks, and that the water/cement ratio is under full control. (This ratio is normally higher than with the dry mix method to ensure sufficient plasticity for feeding through the hose to the nozzle.) Experience shows that the rebound is lower than with a dry mix, yielding a shotcrete in place that is closer to the original mix.

A major disadvantage at present for wet mixes is the mentioned lock of satisfactory control devices for the addition of powder accelerators at the nozzle. This problem will certainly eventually be solved. In the meantime, wet mix seems more useful under conditions where accelerators are not needed. [1]

Now, let us talk on the results obtained in the application of SEC–system.

The system of SEC has been developed by the Japan Railway Construction Authority and Rib

Concrete Engg., Co. and its name is derived from mortar produced with "Sand Enveloped with Cement". This employment of SEC seems to be quite new in the application of shotcrete to tunnelling.

The production procedure of SEC-mortar is initiated by equalizing the state of water content on the surface of sand particles by means of a centrifugal water separator. This makes cement cover the surface of sand entirely at constant water content and also makes the appearence of void in concrete much less. So, it means that shotcrete produced by SEC–system has more steady and higher strength with the improvement of cohesion to rock surface.

In the Najio Tunnel project, the system as shown in Fig. 10.1 is employed. [2] Sand–controller is located at the portal beside aggregate bin, and sand which passes through is loaded onto the movable hopper with uniform water content. Movable facility is consisted of hoppers for aggregate and cement, mixer for mortar, mortar pump and dry type shotcrete machine. (Photo 10.1) Total quantity of about 2000 m^3 is sprayed by SEC–system, and representative mixing ratio is as shown in Table 10.1.

According to laboratory tests, uniaxial compressive strength of sampled cores regarding SEC is as follows:

at 3 days $\sigma_3 = 120 - 180$ kgf/cm^2 $(1.2 - 1.8 \times 10^4$ kN/$m^2)$

at 28 days $\sigma_{28} = 200 - 300$ kgf/cm^2 $(2 - 3 \times 10^4$ kN/$m^2)$

The rock of Najio Tunnel is medium hard rhyolite, and full face cutting method is employed. Daily rate of advance is approximately 6.0 m in two round. Instead of a nozzleman, robot projector is employed so conveniently because of the operation at high position such as full face cut for double tracked railway. (Photo 10.2)

The sequence of works is as shown in Fig. 10.2.

10.3 Stress Measurement in Shotcrete Lining

In the discussion on the measurement in NATM, J. Golser's comment should be taken note of. [3]

In the following many galleries and tunnels have been executed applying shotcrete and anchors and systematic measurements have been made to control the behavior of the support and the surrounding rock. In the railroad tunnel in Schwaikheim in marls, dolomites and sandstones a very extensive observation programme has been executed in a test gallery and in the tunnel itself. Fig. 10.3 shows the procedure of execution of work from which we can see that it was considered essential to close the invert within the shortest possible time of 25 days and to place the inner concrete ring as late as possible, that is, after equilibrium has been reached by the outer semirigid support. Due to the fact that the forces are deviated through the rock and that only a small share of the tangential forces is taken by the shotcrete lining, this lining can be temporarily undercut on a considerable length. In this tunnel the full mortar embedded SN bolts have been applied for the first time on the Continent.

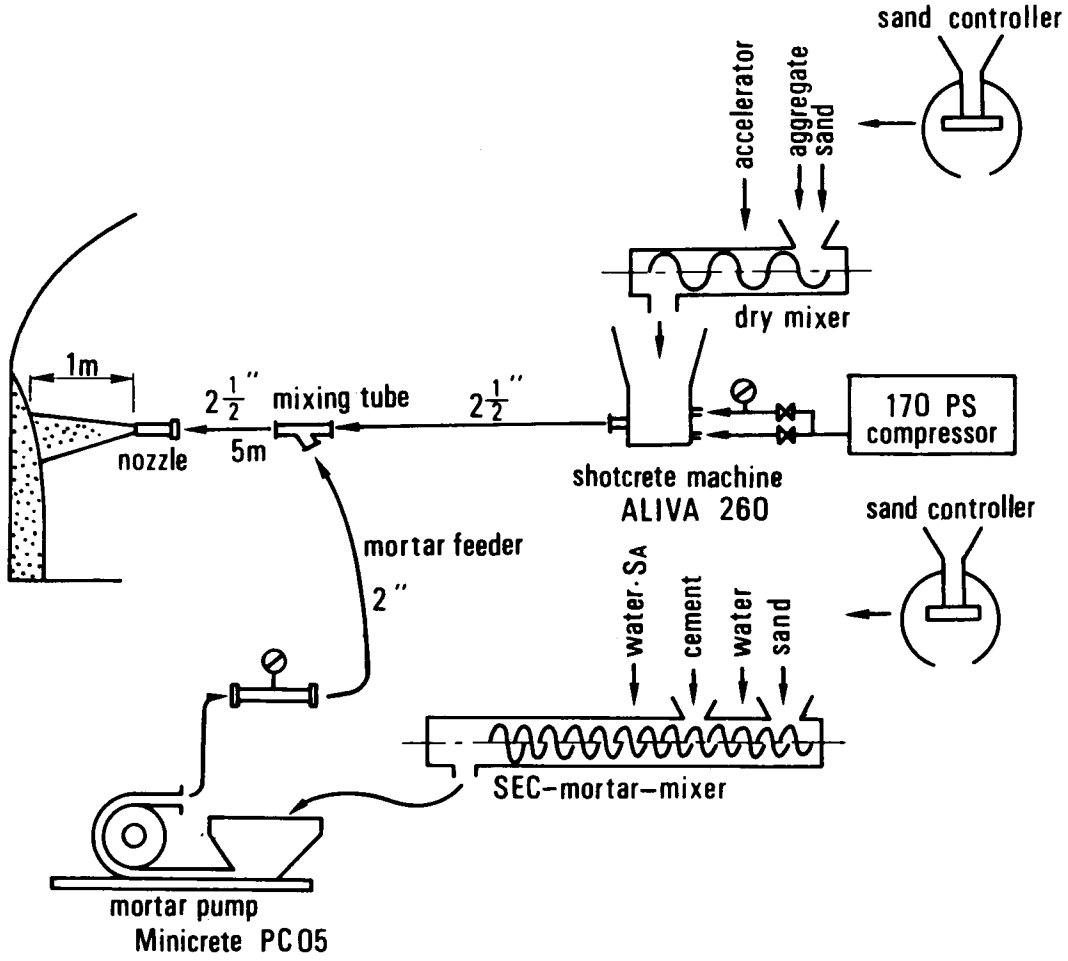

Fig. 10.1 Flow of Shotcrete by SEC–System

Table 10.1 Mixing Ratio of Shotcret (per 1 m^3)

W/C	S/A	unit weight kg				
		cement	sand	aggregate (15 mm)	water	accelerator
49.4 %	69.4 %	350	1273	580	173	C × 5 %

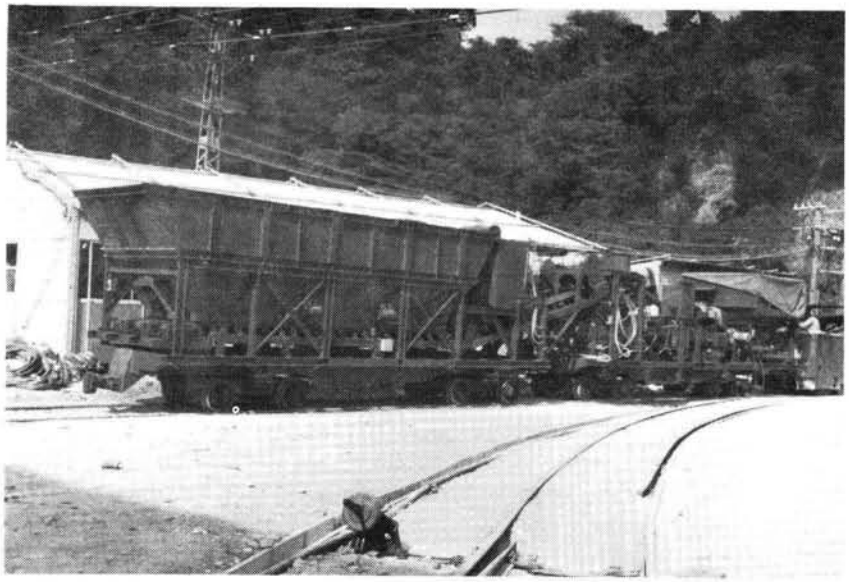

Photo 10.1 SEC Movable Concrete Plant

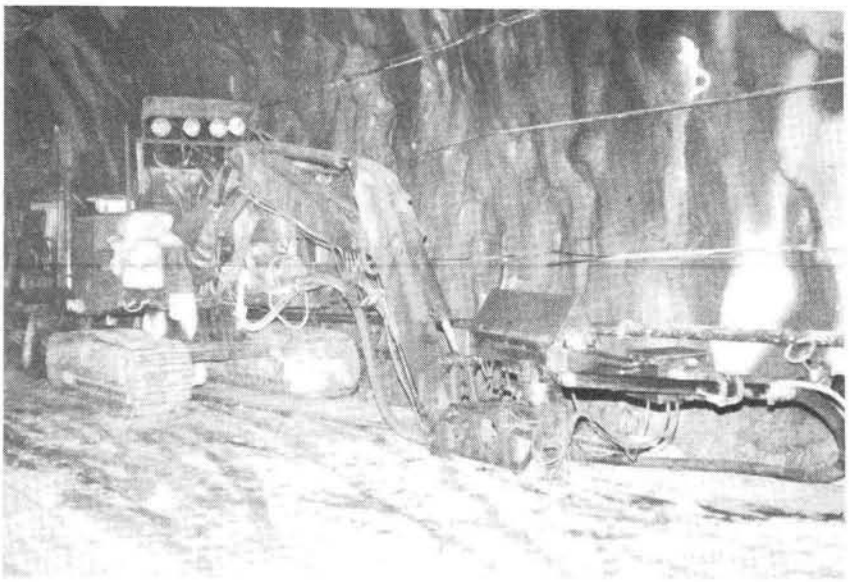

Photo 10.2 Remote-Controlled Nozzle (Robot)

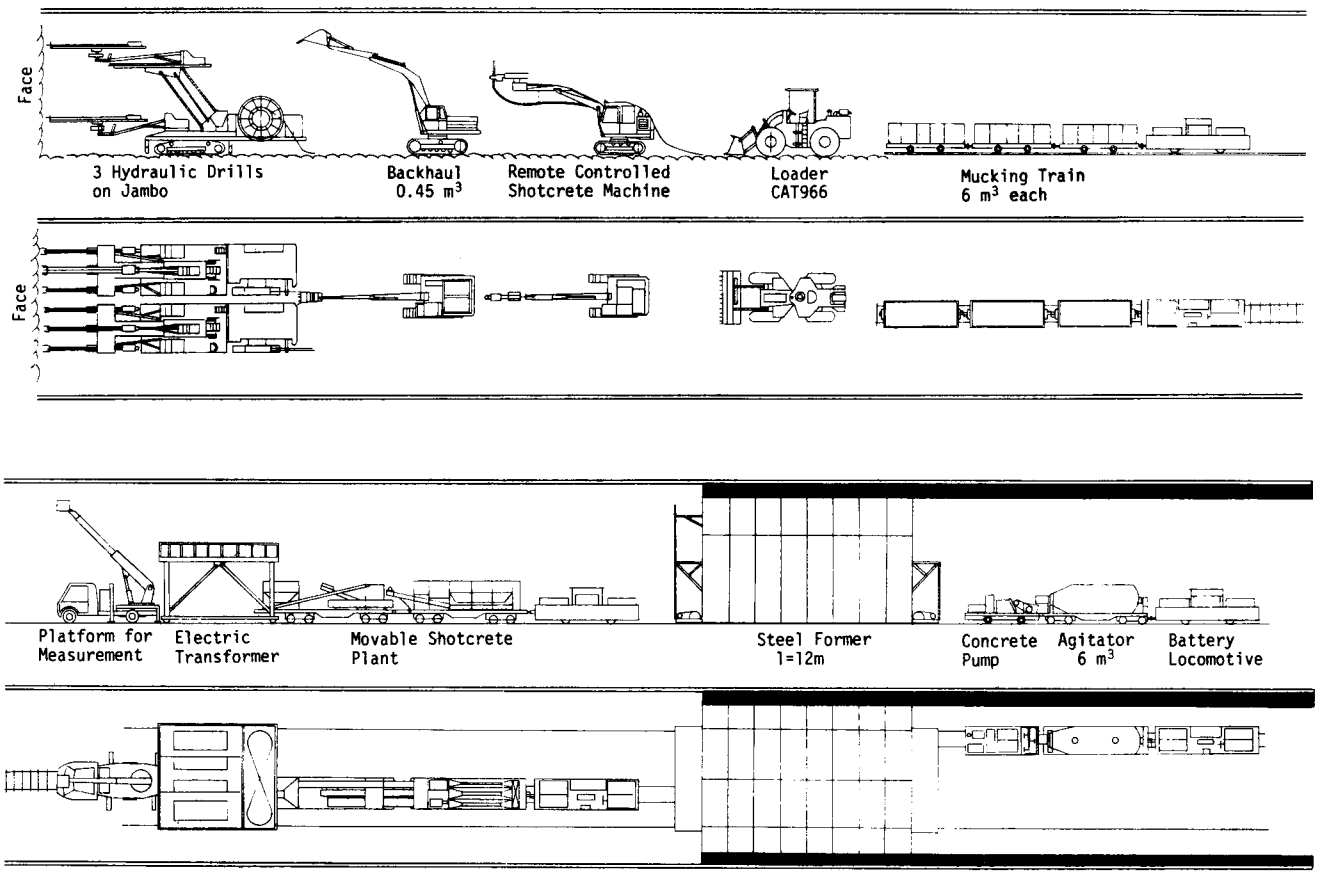

Fig. 10.2 Construction Sequence of Najio Tunnel

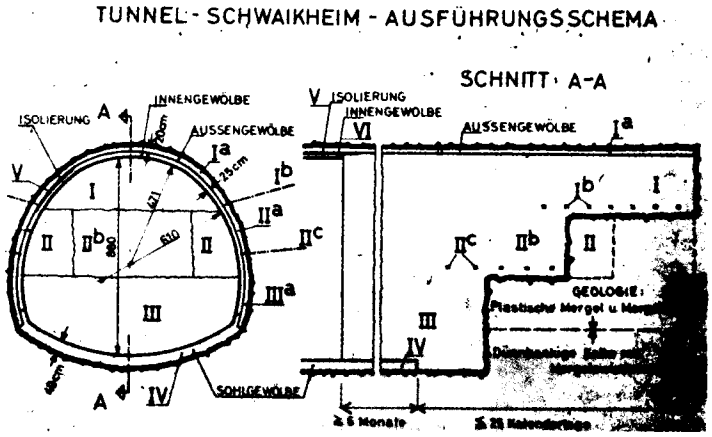

Fig. 10.3 Excavation and Supporting Scheme in Case of Schwaikheim Tunnel [3]

Another very interesting example is the Massenberg–tunnel in Austria. The tunnel has been designed coventionally with a thick concrete ring. The tunnel driving started according to the Belgian Method by applying a greatly overdimensioned shotcrete lining in clay and altered soft graphitic and sericitic schists with considerable water content. The tunnel collapsed when the bench excavation commenced. It has subsequently been redesigned. With a comparatively thin, reinforced shotcrete lining of 20 cm thickness and 4 m long Perfo-bolts, permanent equilibrium has been reached.

From a series of observations in tunnels it has been established as essential law for future dimensioning that the very reason of failure of the lining in voidless contact to the rock mass is not bending as commonly considered hitherto but shear.

Due to the excavation of a cavity the force lines are deviated to both sides and concentrated near the walls, causing wedge shaped bodies to be squeezed out towards the cavity in a right angle to the primary main stress direction. By the release of tangential stresses to both sides of the cavity the span is increased causing the roof and bottom to fail and eventually the typical folding at the roof and at the bottom comes into being. (Fig. 10.4)

The scheme of "impact failure by horizontal compression" as observed by the Corps of Engineers Underground test program corresponds exactly with the above schedule of failure. Also the experiments of Prof. Mohr in argillaceous schist confirm this conception. On the ground of these findings it becomes evident that all computations of tunnel supports, which consider bending

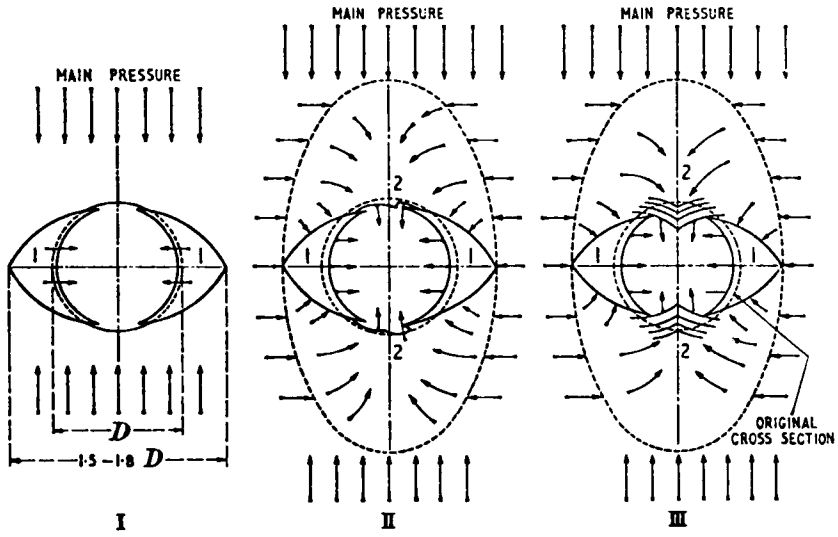

Fig. 10.4 Sketch of Mechanical Process and Sequence of Failure around a Cavity by Stress Rearrangement Pressure [3]

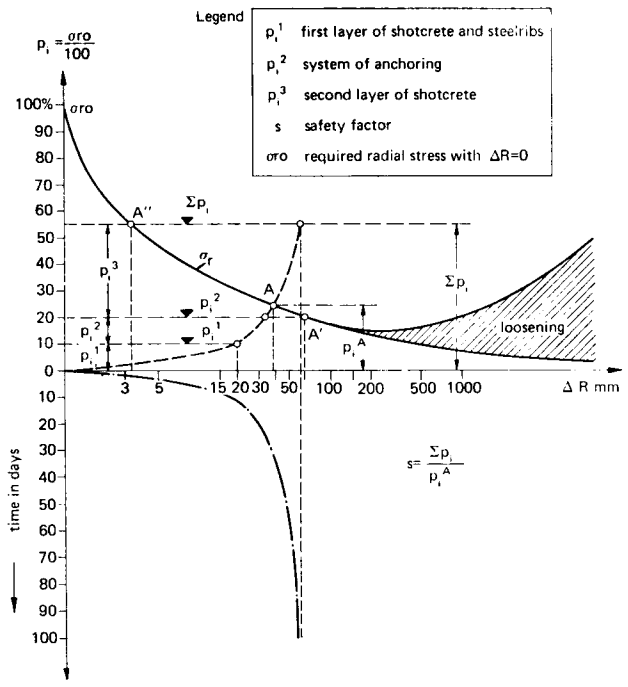

Fig. 10.5 Schematic Representation of the Reciprocal Relationship between σ_r, ΔR, p_i and T (according of Fenner and Pacher [3])

as critical reason of a tunnel collapse are wrong. A tunnel lining in close contact with the rock all around can only fail by shear. Dangerous bending cracks develop without exception due to bad workmanship, leaving cavities behind the lining, an omission which nowadays is not at all acceptable. These practical experiences of shear failures have fully been confirmed by Prof. Sattler's tests made at the Technical University in Graz. A thin concrete ring, 2 cm thick with 1.0 m diameter – corresponding at a scale 1 : 10 to a 20 cm lining with 10 m diameter – has been embedded in a steel frame, filled by sand or clay and subsequently put under stress. In course of these experiments the lining has often been deformed many times greater than ever observed in nature. Then a series of hardly perceptible bending cracks formed with increasing pressure. While the deformation by bending proceeded entirely noiseless and without signs at the instruments, the shear failure which occured eventually was always accompanied by a shotlike report and by a sudden release of the indicating instruments. This means, that bending cracks are of no consequence on the stability of the lining, they are simply joints. The lining is being transformed in a multiple hinged arch, which adjusts itself to the new form developed by the stress rearrangements. The reciprocal effect of decompression stresses required lining resistance and the carrying capacity of a support is shown in the Fenner – Pacher graph. (Fig. 10.5)

The theoretical Fenner curve – which would be valid also in the range of great radial deformations ΔR, if these movements would not cause a reduction of the rockphysical parameters – is to be superposed with the influence of loosening. So a curve comes into being with a certain minimum required lining resistance at a certain radial deformation of the borderzone. While the σ_r curve is descending the semirigid support is placed in form of shotcrete, anchors etc. This support is building up a resistance until at the intersection with the σ_r curve equilibrium is reached. The lining resistance is further increasing to Σp_i and the safety factor is given by $s = \frac{\Sigma p_i}{p_i A}$ Should the lining resistance in any of the cases where the σ_r curve is intersected on the descending branch decrease for any reason, that is, by breaking of anchors, cracking of shotcrete or some other failure nothing serious happens and equilibrium is simply obtained again at a lower point of the σ_r curve. This is a very important feature of the NATM.

Should on the other hand a support characteristic be such that equilibrium is reached beyond the minimum of the σ_r curve, what happens usually with conventional steel supports just the contrary happens. Any further radial displacement causes greater loosening and hence increase of the active forces. Equilibrium can be reached only by immediate suitable strengthening measures, the common experience with conventional methods. For the better understanding of the NATM it becomes almost imperative to add to the original name a short descriptive characteristic by precising the NATM more closely as the method which accomplishes stabilization by "controlled pressure release". Following this principle the surrounding rock is transformed from a charging into a carrying member.

There should of course be no need to emphasize particularly, that the control of the behavior

of the surrounding rock and the support by measurements is an integrant and most important part of the NATM. By means of measurements on the full size section it is possible to recognize within short time if the installed stabilizing means are to be modified to reach an economical optimum. This method of design, the so called "Empirical dimensioning" has thereby been created on an empirical scientific basis. This method is therefore in many aspects superior to highly sophisticated mathematical treatment because implicitely all unknown factors are included by the measuring controls. Mathematical treatments as for instance the finite element method is doubtless very elegant and should be further developed, but the results are only correct if the rock mass is described correctly – which is very seldom the case due to the usual complexity of geological conditions – and if the very important time-factor and the intermediate constructional stages are taken into account appropriately.

The approach in the design is principally as follows: First the support system consisting of a protectional lining and the rock arch is predimensioned by computing its carrying capacity, based on available rock mechanical parameters of the rock in question. Simultaneously the required carrying capacity which is a function of the allowable radial displacements is to be estimated. This can be computed analytically after Lombardi–Amberg, Feder or any other suitable method. The problem, of course, is always to base the computation on rock mechanical parameters which first do not fully describe the rock mechanical behavior because rheological parameters and practicable models are not available and secondly the used parameters vary usually in a wide range. It is therefore evident that this predimensioning can never substitute the empirical dimensioning by in situ measurements.

When the construction starts, measuring sections are placed in suitable distances. The behavior of both, the support and the surrounding rock, the amount of deformation and stresses are being exactly watched by measuring and controled at will. In cases where the deformation velocities are too great and where the stabilizing method have been underdimensioned, possibly resulting in shear cracks, the measuring results indicate in time when and to what extent additional stabilizing method shall be applied. Nothing of any consequence happens when a shear crack occurs, there is no danger for the crew, nor any substantial impediment to the progress of works. It should be noted the adjective "stabilizing" instead of temporary because it is a main principle of the NATM to dimension the structure such as to obtain permanent equilibrium with it.

Stress Measurement by Pressure Cell

Hydraulic stress cells of the Gloetzl type are placed in several pairs around the circumference of the tunnel. The cell at the rock-shotcrete interface is to monitor the contact stress and the one embedded in the shotcrete measures the concrete stress (Fig. 10.6). Pressure and return lines are led to a common switching terminal for each instrumented section, and reading is done by means of a portable manual hydraulic pump with pressure gauges of different range.

Accuracy of readings is 0.01 or 0.05 bar, depending on the cell range. With the use of a leak-

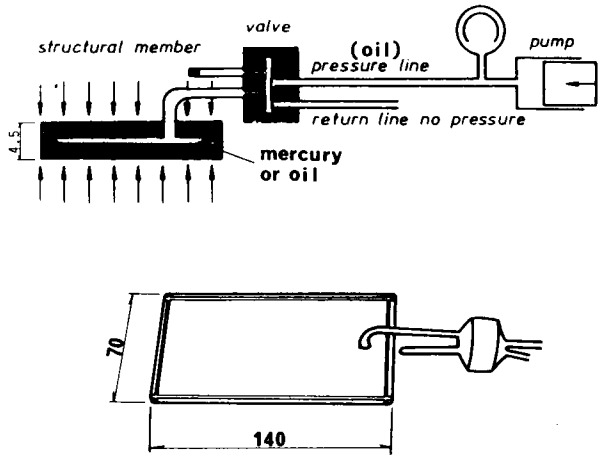

Fig. 10.7 Gloetzl–Type Pressure Cell

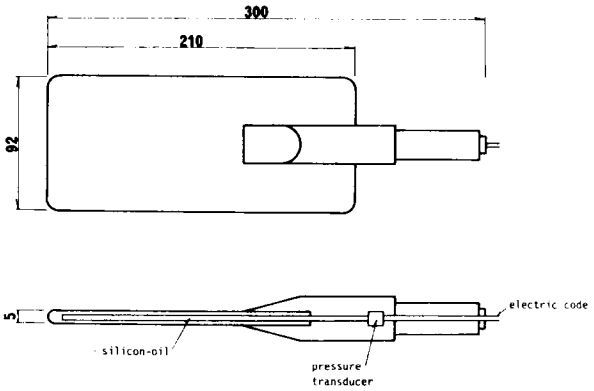

Fig. 10.8 OYO–Total Pressure Cell

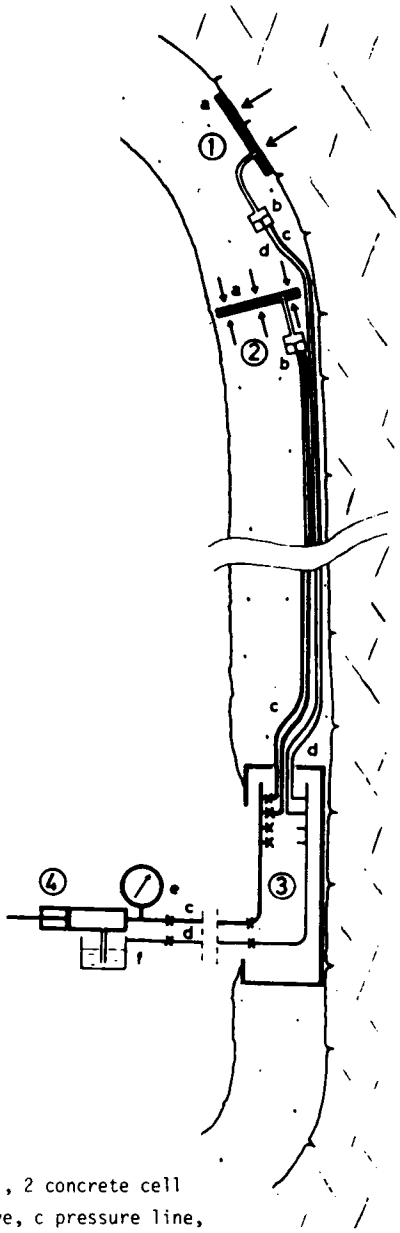

Fig. 10.6 Stress Measurement with Hydraulic Cells [4]

proof connector system the hydraulic lines can be led through the watertight tunnel sealing so measurements can be continued even after the final lining has been applied. [4]

In Japan, in field measurement objecting to NATM, several types of pressure cell are available, and the detecting mechanism of most of them is different from the Gloetzl–type.

As practical engineers are apt to employ them conveniently without any consideration on the difference between mechanical device and electrical one, the author tried to calibrate several types of pressure cell having different measuring mechanism under the equal condition. The Gloetzl cell and Total Pressure Cell were picked up for test as representative cells. Fig. 10.7 and 10.8 show the fundamental mechanisms of Gloetzl cell and Total Pressure Cell, respectively. Each cell set in the block (manufactured with concrete or plaster) with the size of 30 cm x 30 cm x 20 cm as shown in Fig. 10.9. By using conventional loading machine for material test, the relation between known load and indicated load by pressure cell was discussed.

Mechanical properties of blocks are:

Mortar: $E = 1.79 \times 10^5$ kgf/cm^2 (1.79×10^7 kN/m^2), $\nu = 0.23$,
$q_u = 123$ kgf/cm^2 (1.23×10^4 kN/m^2)

Plaster: $E = 4.10 \times 10^4$ kgf/cm^2 (4.10×10^6 kN/m^2), $\nu = 0.27$,
$q_u = 70$ kgf/cm^2 (7×10^3 kN/m^2)

where E, ν and q_u denote Young's modulus, Poisson's ratio and unconfined compressive strength, respectively.

The obtained results are as shown in Fig. 10.10 and Fig. 10.11 corresponding to Gloetzl type cells and Total Pressure Cells, respectively. From these figures it is clear how the respective pressure cell act in concrete block. The choice of type of cell is very important in stress measurement at tunnelling sites, where the space and situation for measurement or monitoring is quite restricted due to narrow, wet and changeable conditions.

The author recommends mechanical measurement more than electric, for reliability with easy handling is more important than high sensitivity.

10.4 Nabetachiyama Tunnel Driven through Expansive Mudstone

People in the Hokuriku region (the north west part of the mainland of Japan) are subjected to complicated topography and heavy snow in winter. For the purpose of securing reliable transportation, the 59.4 km long new railways called Hokuetsu–Hokusen Line is under construction. Nabetachiyama Tunnel, with a length of 9.1 km, the second longest in the line, is considered as one of the most difficult construction sites by reason that the ground, Neogene Tertiary mudstone, which the tunnel is driven through, behaves expansively, and yields combustible methane gas and petroleum at many places. Fig. 10.12 shows the location of the tunnel and the distribution of Tertiary sedimentary rocks and Green-tuff. (after Nakano [5])

Among the Tertiary sedimentary rocks in this region, mudstone and shale of Neogene deposit,

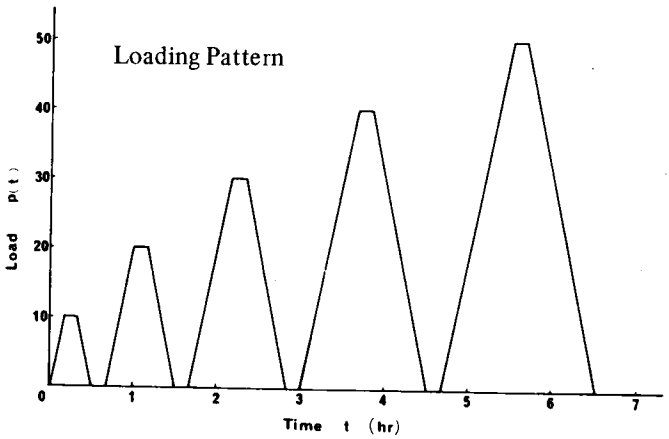

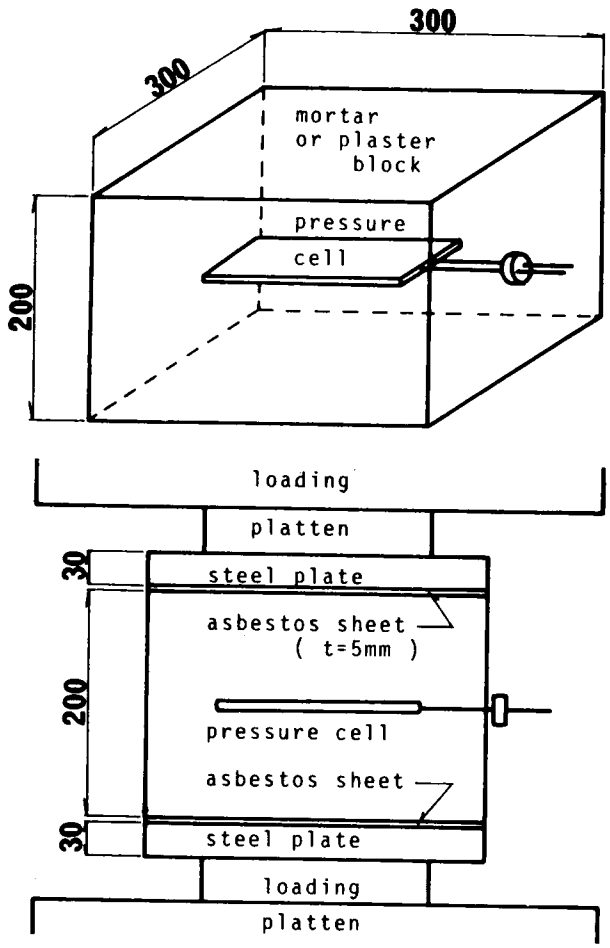

Fig. 10.9 Concept of Test

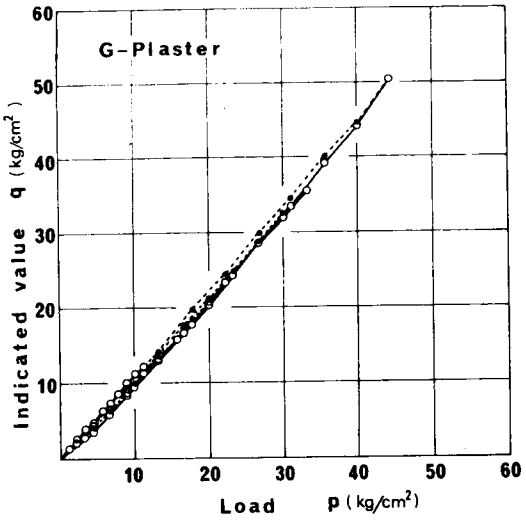

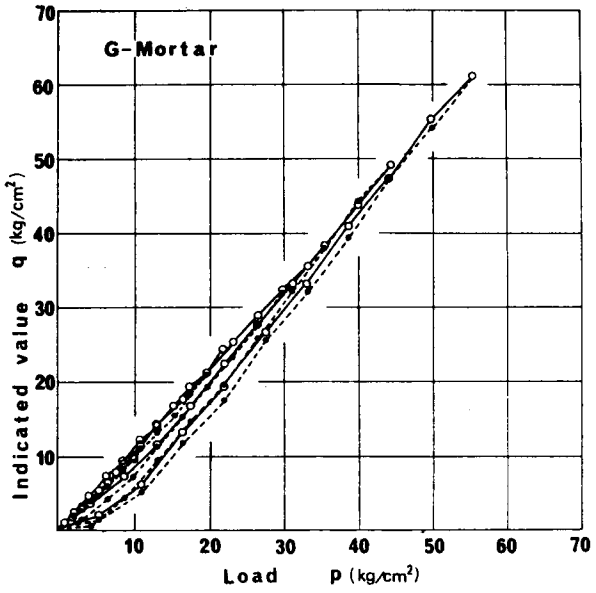

Fig. 10.10 Results of Tests regarding Gloetzl-Type Cell

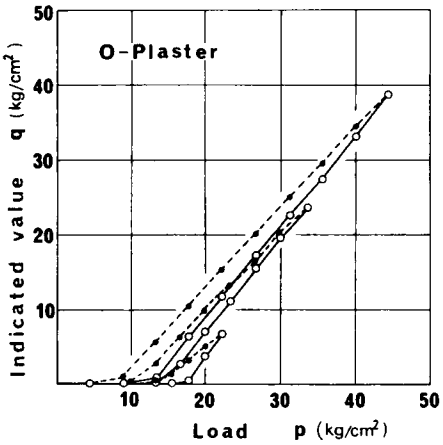

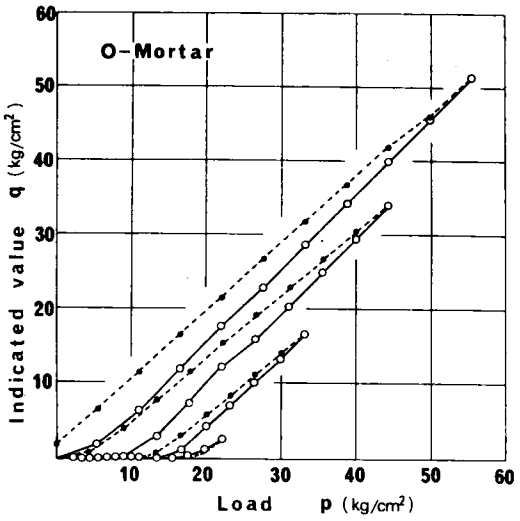

Fig. 10.11 Results of Tests regarding OYO Cell

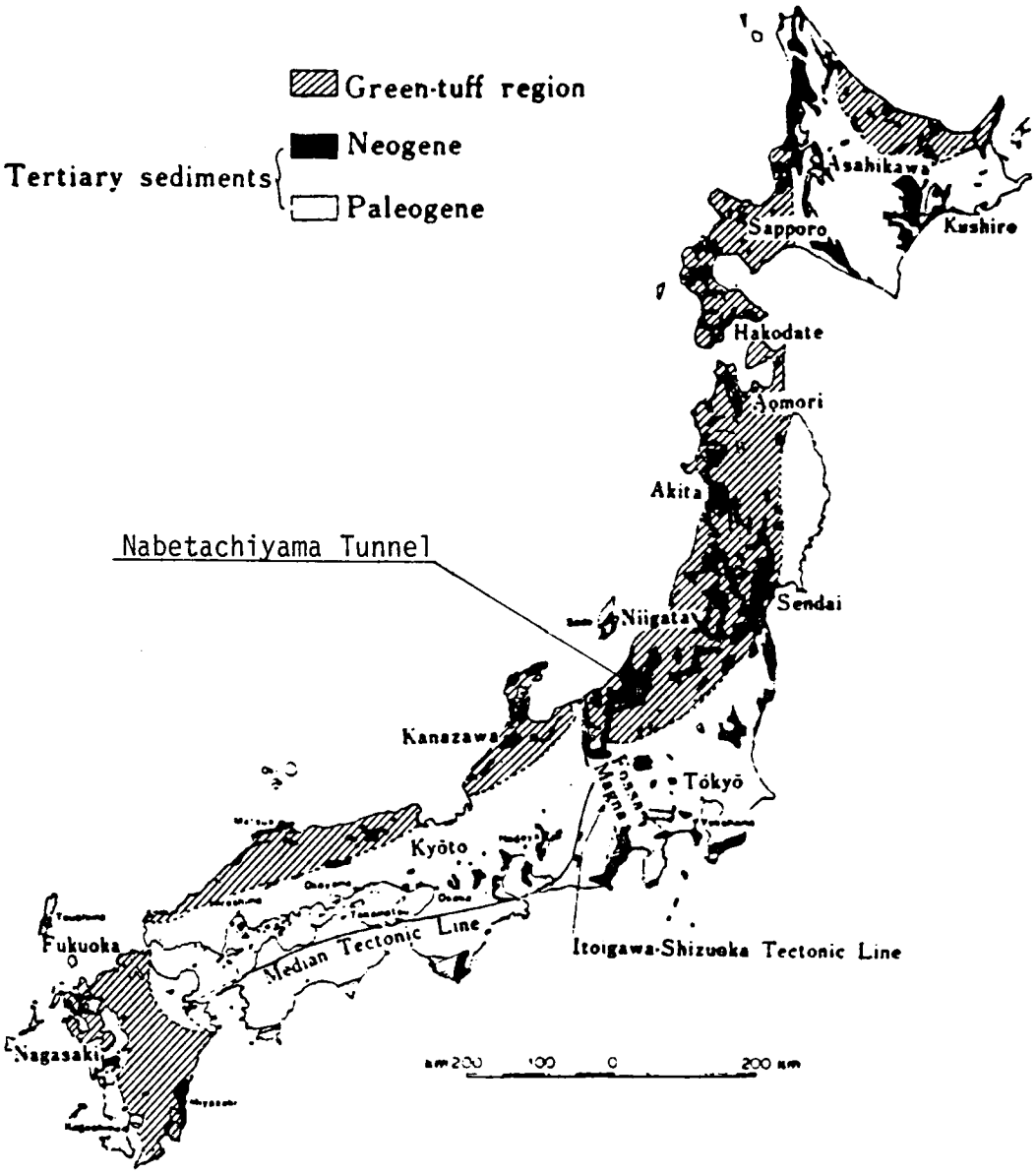

Fig. 10.12 Distribution of Tertiary Sedimentary Rocks and Green-Tuff Region of Japan (after Nakano [5])

known as the petroliferous Teriary formation, often causes troubles in geotechnical engineering, such as landslides in natural slopes and man-made cut, heavy rock pressure in tunnelling, deformation of dam foundations and abutments etc. The author tries to evaluate the effect of rock-bolt support, being based on Nakano's hypothesis that a so-called swelling rock pressure on tunnel supports often experienced in mudstone containing montmorillonite is caused not by the increase in volume of the rock mass due to swelling but by the squeezing of the rock mass which is yielded by concentrated shear stress and whose strength is reduced to a fully softened or critical state [5].

The geology of the ground in the vicinity of Nabetachiyama Tunnel consists of Neogene Tertiary formations called Nishiyama Formation, Shiiya Formation and Teradomari Formation from the top respectively, and the tunnel is driven through two main anticlines, many faults and fractured zones as shown in Fig. 10.13.

The tunnel is divided into three sectors, the East Sector (29.574 – 31.324 km), Middle Sector (31.324 – 34.651 km) and West Sector (34.651 – 38.690 km), and their overburden are 100 – 150 m, 80 – 130 m and 80 – 220 m respectively. Physical properties of rock, where the tunnel has been driven, and the degree of expansion upon tunnelling are described in Table 10.2.

Though the cation exchange capacity (CEC) was considered as the main parameter of expansion in the construction of Akakura Tunnel, with a length of 10.334 km, which was driven through the same kind of ground 17 km east of Nabetachiyama Tunnel [6], Table 10.2 shows that for Nabetachiyama Tunnel the main parameter of expansion is not CEC itself, but a

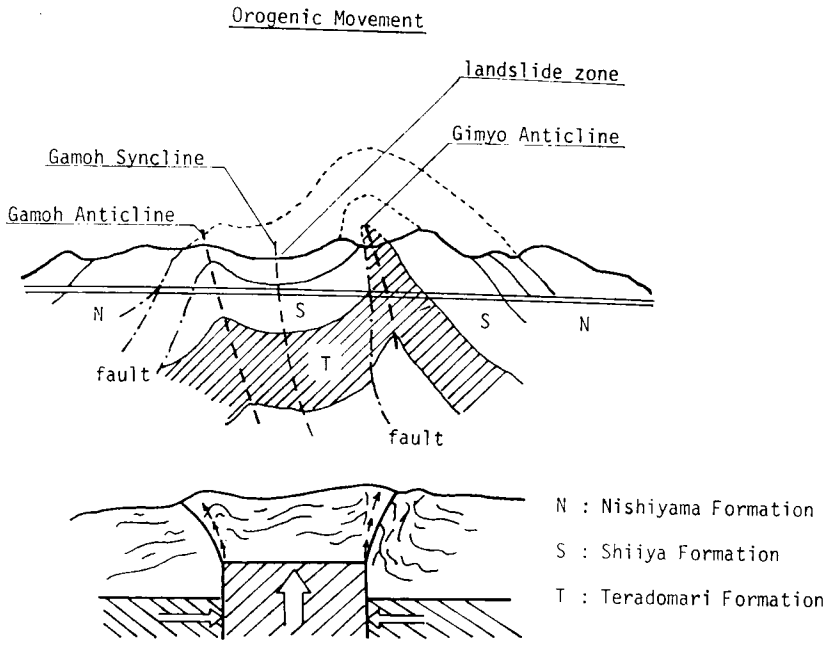

Fig. 10.13 Schematic Profile of Nabetachiyama Tunnel

Table 10.2 Physical Properties of Expansive Mudstone in Hokuriku Region

Name of Tunnel	γ_t (Mg/m^3) Density	w_n(%); Natural Water Content	LL(%); Liquid Limit	I_p; Plastic Index	I_f; Flow Index	ρ(%); Particle under 2μ	q_u (kN / m^2) unconfined compressive strength	E_{50} (kN / m^2) Deformation coefficient	E_x(%); Expansion Ratio	CEC (meq/100q); Cation Exchange Capacity	C_f; Competence Factor	Degree of Expansion
Nabetachiyama T. West Sector	2.05	21.0	147	125	21.5	40.9	3820	760000	2.38	33	1.91	Light - heavy
Nabetachiyama T. Middle Sector (Double tracks sec.)	2.08	21.0	146	124	20.2	35.5	4120	600000	2.10	50	2.06	Heavy
Nabetachiyama T. Middle Sector (Single track sec.)	1.98	23.7	128	105	19.6	39.9	920	130000	4.04	33	0.46	Very heavy
Nabetachiyama T. Middle III Sector	1.78	23.5	168	150			2110	400000	0.99	38	1.06	Heavy
Akakura T. (Shiiya Form.)	2.12	18.1	95	73	22.5	41.3	3680	250000		41	1.84	Light - heavy
Akakura T. (Kaizume Form.)	2.06	19.1	60	32	9.2	20.4	6430	800000		23	3.22	Very light - light

competence factor (C_f). It can be assumed that the expansive behavior of the mudstone ground in Hokuriku Region is associated mainly with a low competence factor and the swelling, the magnitude of which is related to contained montmorillonite (expressed by CEC), is caused by concentrated shear stress. Namely, the squeezing of the rock mass is the prime expansion agent, and the swelling is symptomatic.

CEC is an expression of the number of cation adsorption sites per unit weight of soil. The mudstone mentioned in this paper can be considered as a kind of over-consolidated clay from the point of view of soil mechanics. CEC is defined as the sum total of exchangeable cations adsorbed, expressed in milliequivalents per 100 grams of oven-dry soil. An equivalent is that quantity which is chemically equal to one gram of hydrogen. The number of hydrogen atoms in an equivalent is equal to Avogadro's number (6.02×10^{23}). A milliequivalent is equal to 0.001 gram of hydrogen. If there was one milliequivalent of cation exchange capacity in a teaspoon of soil, it would contain 6.02×10^{20} negatively charged adsorption sites. [7]

The competence factor (C_f) is defined as the ratio of unconfined compressive strength (q_u) to overburden pressure (i.e. $\rho \cdot h$, the product of density ρ and depth h), $qu/(\rho \cdot h.)$ [8] Based on the observed behavior at more than 50 tunnelling sites in Japan, Nakano points out the relation between rock pressure and competence factor as follows:

$C_f > 10$ for slight or no rock pressure,
$4 < C_f \leqq 10$ for loosening rock pressure,
$2 < C_f \leqq 4$ for light ~ large squeezing rock pressure,
$C_f \leqq 2$ for heavy ~ very heavy squeezing – swelling rock pressure

Nabetachiyama Tunnel is planned to be a single track railway tunnel in which an underground station 1010 m long will be located, typical cross sections are shown as Fig. 10.14. The construction has been almost 70% completed (September, 1979). Compared with other sectors, the Middle sector holds the most troublesome conditions, such as low competence factor, main faults, many fractured zones and inflammable gas, and only in a short distance of 280 m, serious collapse have occurred three times and still no effective method to stabilize the face adequately against heavy squeezing (almost in a state of 'flow') has been established at this time. According to several field measurements, laboratory tests and analyses, it was found that the support system consisting of steel ribs, rockbolts, shotcrete lining, pipe struts and concrete lining works good, but widely spread plastic zones (wider than 10 m) and the movement of plasticized ground in the vicinity of the mining face, which happens ahead of the face position (farther than 10 – 15 m), makes the face unstable, and therefore supports near the face are subjected to yielding loads one by one, being associated with backward displacement. This means that the face, which should play a role as a temporary support to mobilize half dome action, loses its bearing capacity due to its quite low competence factor and the only way to make the tunnel stable is prereinforcing the

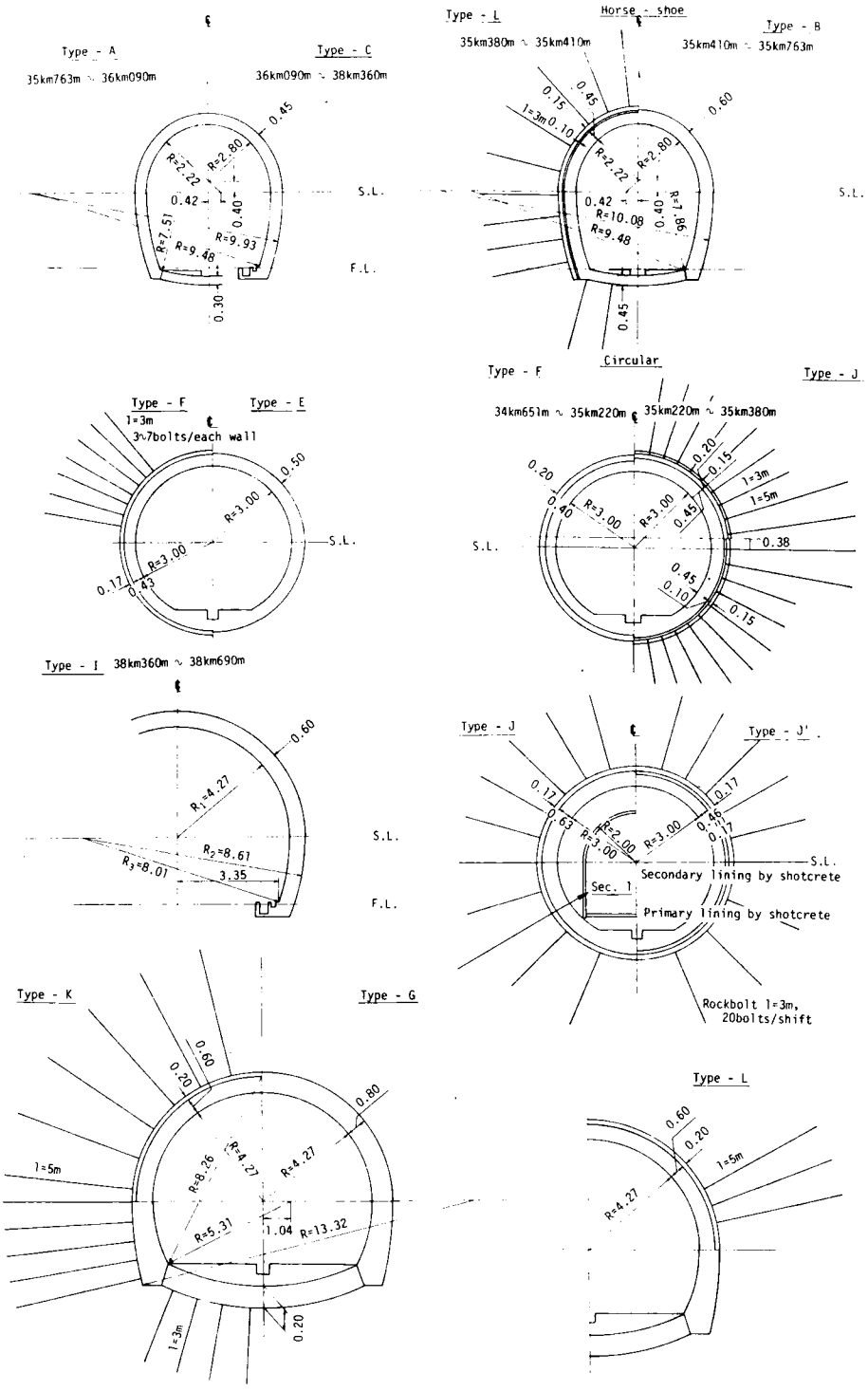

Fig. 10.14 Cross Sections of Nabetachiyama Tunnel

ground ahead of the face.

Spiling rockbolts and face stabilizing rockbolts (made of steel and/or glass fiber) to be set perpendicularly to the face were tried, but successful results were not obtained because drilling for rockbolt was so difficult that, although it took only 10 – 15 minutes in the case of drilling less than 3 m, it took longer than one hour due to the jamming of liquefied debris in the case of drilling over 3 m, whether drilling (or boring) was done with or without water.

The steel ribs which have been used in the construction are as shown in Fig. 10.15. The outline of construction and the deformation of the tunnel with respect to the most troublesome parts of the Middle Sector is summarized in Table 10.3.

Judging from the state of the collapsed support, critical bearing capacity of each support was estimated as follows by calculation.

H–175 rib, ϕ216 pipe support (c–c 0.75 m) —$4 \sim 8 \times 10^2$ kN/m^2
Shotcrete lining of 10 cm thick — $3 \sim 6 \times 10^2$ kN/m^2
Rockbolts of 3 – 5 m long at the density of 2 – 3 bolts/m^2
—$1 \sim 1.5 \times 10^2$ kN/m^2

In the discussion of ground-support interaction curves, the point which gives minimum load to support exists ahead of the face and no displacement should be allowed in the case of Nabetachiyama Tunnel due to quite low competence factor. This means that the more displacement permitted, the higher the rock pressure employed in support action. Photo–3 to 6 give some illustration of the real state of the deformed tunnel. Photo–3 shows the state of the collapsed cross sections in the area of STA. 33.225 – 255 km which were supported by ϕ216 pipes and struts placed at c–c 0.75 m with 17 cm thick shotcrete lining and rockbolt system of 1 bolt/m^2. Excavation was carried by Mini-bench method as shown in Fig. 10.16. Between STA. 33.189 – 226 km, the horseshoe-shaped and circular pilots aiming at strain relief were forwarded because of having caused too large a deformation. Photo–4 shows the state of yielded H–125 steel ribs for the horseshoe shaped pilot around STA. 33.220 km, and also Photo–5 shows rock debris squeezed out from the face in the case of driving a circular pilot. Finally, squeezed ground intruded into the pilot opening and many rockbolts already set around the opening were pulled out from their original positions. Among experienced personnel it is confirmed that the deformation of this kind of ground is apt to be decreased after relieving strains ahead of full face mining, and Nabetachiyama Tunnel behaved in the same manner temporarily, though the magnitude of deformation exceeded conventional experiences by far. However, it is still doubtful whether the effect of strain relief might be good (or not) in the case of the Middle Sector having a competence factor of less than 0.5. Further research on the mechanism of strain relief is required.

10.5 Shotcrete Lining as Support

In most of cases of tunnel driving through rock, the fundamental requirement is how to

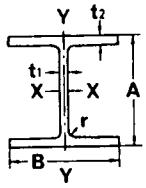

type mm	dimension mm					sectioned area cm²	unit weight kg/m	moment of inertia of area cm⁴		radius of gyration of area cm		section modulus cm³	
	A	B	t_1	t_2	r			Ix	Iy	ix	iy	Zx	Zy
100x100	100	100	6	8	10	21.90	17.2	383	134	4.18	2.47	76.5	26.7
125x125	125	125	6.5	9	10	30.31	23.8	847	293	5.29	3.11	136	47.0
150x150	150	150	7	10	11	40.14	31.5	1640	563	6.39	3.75	219	75.1
175x175	175	175	7.5	11	12	51.21	40.2	2880	984	7.50	4.38	330	112
200x200	200	200	8	12	13	63.53	49.9	4720	1600	8.62	5.02	472	160

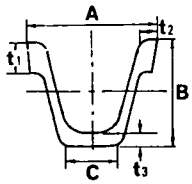

type	dimension mm						sectioned area cm²	unit weight kg/m	moment of inertia of area cm⁴		section modulus cm³	
	A	B	C	t_1	t_2	t_3			Ix	Iy	Zx	Zy
MU29	133.0	120.0	50.7	34.6	19.5	15.7	37.00	29.0	581.0	634.0	97.4	95.8

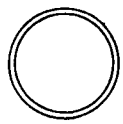

size (A)	outer diameter mm	thickness mm	weight kg/m
200	216.3	5.8	30.1

Fig. 10.15 Steel Ribs used in Construction

Table 10.3 Outline of the Construction and Deformation of the Tunnel between STA. 33.900 km and 33.079 km (Middle Sector)

Division	Section	Support	Thickness of lining (cm) (A) Shotcrete (B) Cast-in-place concrete	Rock-bolt (A) wall (B) face * Number of rock-bolt per 0.75m ** Number of rock-bolt per 1.50m	Driving rate (m/month)	Deformation (cm) (A) Settlement of crown (B) settlement of arch foot (C) Lateral displacement of arch foot	Observation
33km 900m - 517m (L = 383m)	Ⓐ 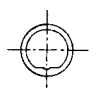	H-175 0.90 c-c 0.75 c-c	(A) Nil (B) t = 50	Nil	51	33km 525m (A) 20 (B) 30 (C) 30	q_u = 4000kN/m² w = 21% slickenside; including sandy tuff; oil saturated. large deformation of arch rib; alterd to pipe supports
33km 517m - 500m (L = 17m)	Ⓑ 	φ 216 0.75 c-c	(A) t = 17 (B) t = 43 (60)	Nil	34	33km 510m (A) 20 (B) 25 (C) 40	q_u = 3000kN/m² w = 21% alternative layers of tuff and mudstone; remarkable heaving; replaced support due to large deforration; bolted to sides
33km 500m - 255m (L = 245m)	Ⓒ 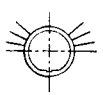	φ 216 0.75 c-c	(A) t = 17 (B) t = 43 (60)	(A) l=3m×6bolt$^{*}_{5}$ (B) Nil	33	33km 335m (A) 35 (B) 45 (C) 55	q_u = 2500kN/m² w = 23% soft mudstone; spalling; face unstable; supplementary bolting was no good; made the ring close earlier
33km 255m - 225m (L = 30m)	Ⓓ 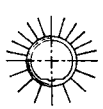	φ 216 + H-175 (suppl.) 0.75 c-c	(A) t_1= 17 t_2= 17 (B) t = 46 (80)	(A) l=3m×20bolt$^{*}_{5}$ (B) Nil	10	33km 230m (A) 25 (B) 45 (C) 50	q_u = 2500kN/m² w = 25% Pipe supports reiforced by hoop straps without shotcrete were collapsed. After replacing pipe supports, rockbolts, H-175 ribs and shotcrete were placed for reinforcement. Deformation decreased.
33km 225m - 218m (L = 7m)	Ⓔ 	Pilot H-125 1.20 c-c Full section φ 216 0.75 c-c	Pilot (A) Nil Full section (A) t = 17 (B) t = 63 (80)	Pilot (A) Nil (B) Nil Full section (A) l=3m×20bolt$^{*}_{5}$ (B) Nil	10 Pilot 31 Full sec.16	33km 220m (A) 10 (B) 15 (C) 15	q_u = 2000kN/m² w = 26% fissured soft mudstone; large expansion; tried strain relief method with a center pilot; advanced only 7m excavation in a pilot impossible; pilot refilled with bubbled mortar.

33km 218m - 186m (L = 32m)	Ⓕ 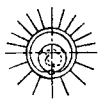	Pilot MU-29 0.80 c-c Full section φ 216 0.75 c-c	Pilot (A) t = 12 Full section (A) t = 17 (B) t = 63 (80)	Pilot (A) l=3m 12bolts* (B) Nil Full section (A) l=3m 20bolts* (B) Nil	10 Pilot 31 Full sec.16	33km 190m (A) 10 (B) 15 (C) 15	q_u = 1000kN/m² w = 28% fissuredsoft mudstone; large expansion; stand-up time of face less than 20minutes; stabilized a face by shotcrete; heavy heaving.
33km 186m - 155m (L = 31m)	Ⓖ 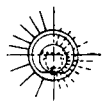	Pilot MU-29 0.80 c-c Full section φ 216 0.75 c-c	Pilot (A) t = 12 Ful section (A) t = 17 (B) t = 63 (80)	Pilot (A) l=4m×8bolts* l=3m×16bolts* (B) Nil Full section (A) l=3m×20bolts* (B) Nil	11 Pilot 30 Full sec.18.5	33km 160m (A) 12 (B) 15 (C) 10	q_u = 1000kN/m² w = 28% checked bearing capacities of MU29, shotcrete and bolts; MU29 yielded heavily
33km 155m - 135m (L = 20m)	Ⓗ 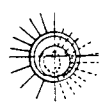	Pilot φ 139 (flexible joint) 0.80 c-c Full section φ 216 0.75 c-c	Pilot (A) t = 12 Full section (A) t = 17 (B) t = 63 (80)	Pilot (A) l=4m×8bolts* l=3m×16bolts* (B) Nil Full section (A) l=3m×20bolts* (B) Nil	10 Pilot 26 Full sec.18.5	33km 140m (A) 7 (B) 8 (C) 8	q_u = 1000kN/m² w = 28% inverts deformed, yielded heavily; flexible joints no good
33km 135m - 115m (L = 20m)	Ⓘ 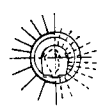	Pilot φ 139 (flexible joint) 0.80 c-c Full section φ 216 0.75 c-c	Pilot (A) t = 12 Full section (A) t = 17 (B) t = 63 (80)	Pilot (A) l=4m×12bolts* l=3m×12bolts* (B) Nil Full section (A) l=3m×20bolts* (B) Nil	11 Pilot 23 Full sec.21	33km 120m (A) 20 (B) 23 (C) 15	q_u = 1000kN/m² w = 29% heavily squeezed from side walls; shotocrete lining failed due to large heaving
33km 115m - 085m (L = 30m)	Ⓙ 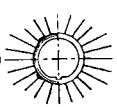	H-175 (flexible joint) + H-150 (suppl.) 0.75 c-c	(A) t_1= 17 t_2= 15 (B) t = 48 (80)	(A) l=4m×10bolts** l=3m×14bolts* (B) l=4m×30bolts**	10	33km 100m (A) 12 (B) 11 (C) 64	q_u = 1000kN/m² w = 29% heavily squeezed from side walls and face; excavation very difficult
33km 085m - 079m (L = 6m)	Ⓚ 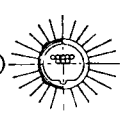	H-175 (flexible joint) + H-150 (suppl.) 0.75 c-c	(A) t_1= 17 t_2= 15 (B) t = 48 (80)	(A) l=4m×10bolts** l=3m×14bolts* (B) l=4m×15bolts* (FRP)	4	33km 082m (A) 36 (B) 20 (C) 150	q_u = 500kN/m² w = 31% strain relief by φ450 boring (l = 4.5m × 7), no good; large expantion of face;
33km 079m - 073m (L = 6m)	Ⓛ 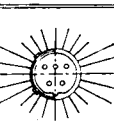	H-175 (flexible joint) + H-150 (suppl.) 0.75 c-c	(A) t_1= 17 t_2= 15 (B) t = 48 (80)	(A) l=8m×10bolts** l=3m×14bolts* (B) l=10m×80bolts per 3.75m	4	33km 075m (A) 20 (B) 35 (C) 90	q_u = 500kN/m² w = 31% strain relief by φ800 boring (l = 10m × 4),no good; heavy squeezing at face; the ground in vicinity of a face was almost in the state of flow
33km 073m -	Ⓜ 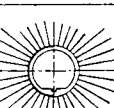	φ 216 0.75 c-c	(A) t = 17 (B) t = 63 (80)	(A) l=8m×18bolts** l=5m×18bolts* (B) l=10m×80bolts per 3.75m			

Photo 10.3 Observed Collapse at STA. 33 km 225 m – 255 m

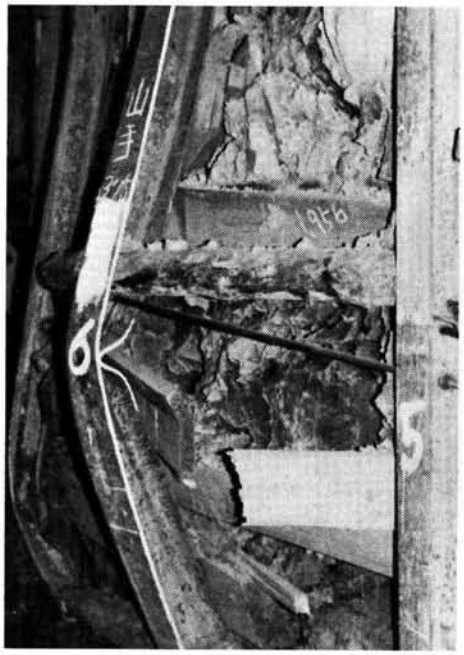

Photo 10.4 The State of Yielded H–125 Steel Ribs at STA. 33 km, 220 m.

Photo 10.5 Squeezing out from the Face at STA. 33 km, 300 m.

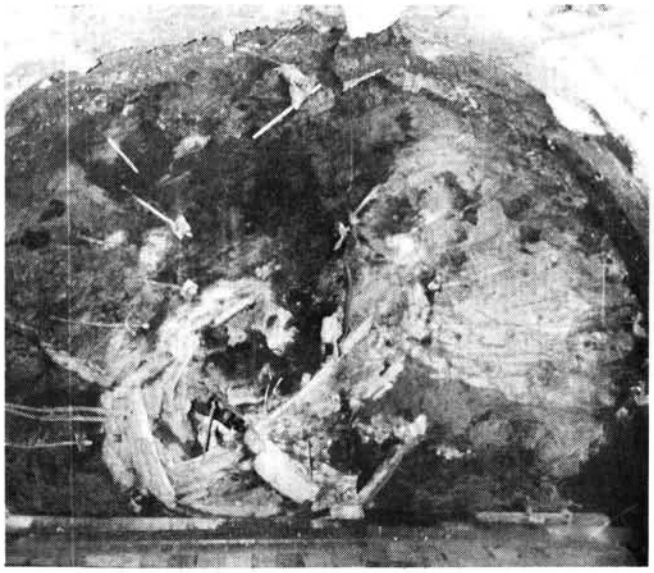

Photo 10.6 Circular Pilot Opening Intruded by Squeezing Ground

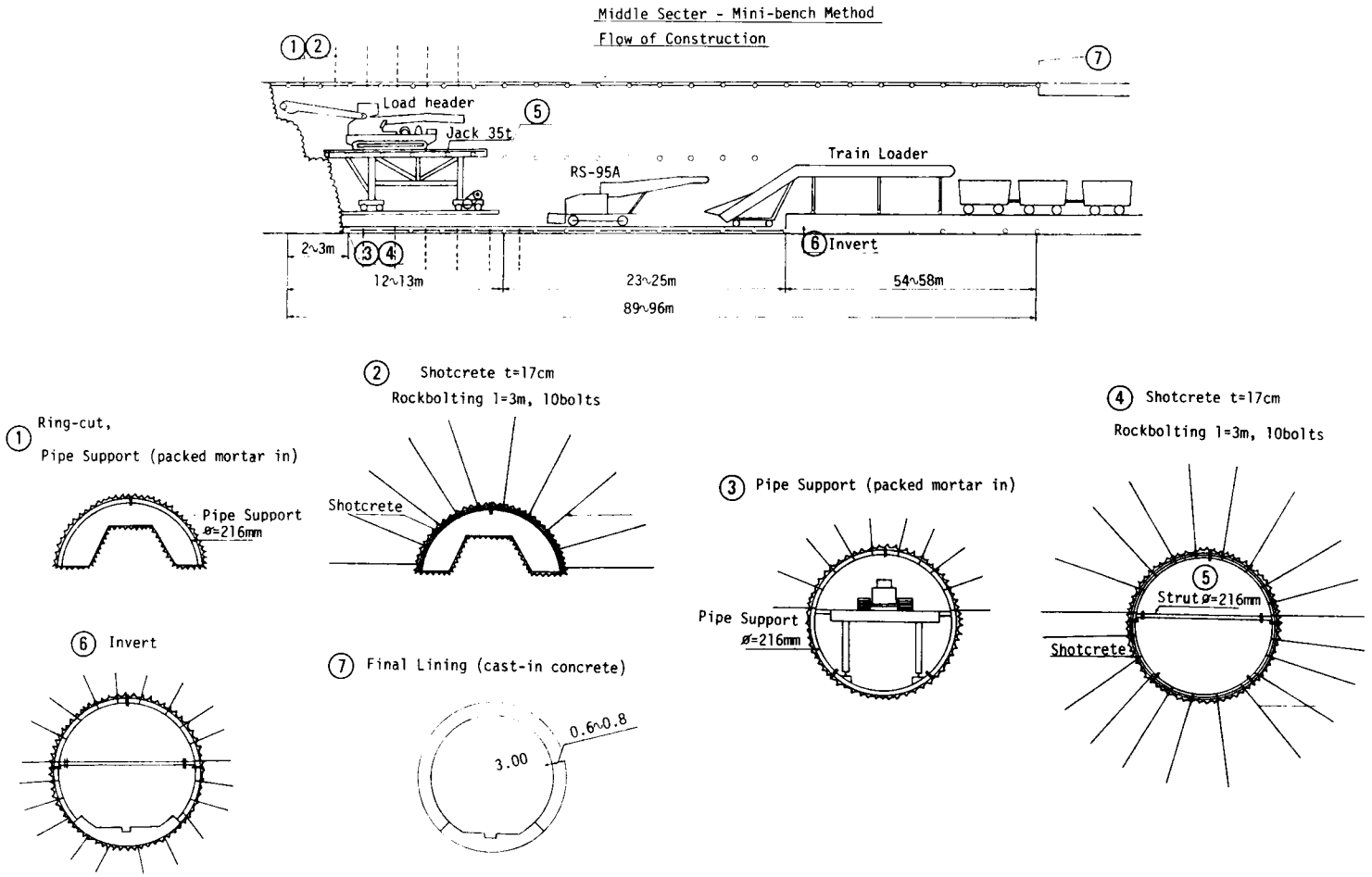

Fig. 10.16 Flow of Construction by Mini-Bench Method

advance the mining face so as to make the original state of the ground as undisturbed as possible, and it can be pointed out (with the exception of seriously creeping ground) that the most predominant deformation occurs in the vicinity of the advancing face and is subjected to positional (geometrical) condition, judging from experience and observations of convergence surveys which showed that the increase of convergence was almost negligible when (the advance of) the face stopped and that the time dependency of deformation depended on the progressive failure of rock, caused by having allowed too much displacement near the opening. This means that the face plays an important role as a temporary support. The rock mass near the face is stabilized by the 'half-dome action' in the profile and the 'ring action' in the cross section. When advancing the face, it is required to place artificial supports to substitute for the half-dome action within a span length from the face, in the driving direction, so as to mobilize the bearing capacity of the rock mass as fully as posible.

The so-called New Austrian Tunnelling Method (NATM), where rockbolting and shotcrete lining are applied, is the latest and most feasible tunnelling method for this purpose, especially from the practical point of view. Such supports as rockbolts, shotcrete lining and steel arch ribs are placed tightly near the face and are subjected to a three dimensional stress field. From the point of view that the effects of systematic supports are 'mobilizing confining stress' and 'decreasing shear stress', a procedure to design supports can be proposed by replacing the effects of supports by the inner pressure acting on the surface of the tuunel wall.

Let us consider on the flexure of shotcrete. In the discussion on excavation sequence, cracking due to flexure becomes serious problems in the application of shotcrete. The fundamental concept of rational tunnelling method such as NATM is based on the principle that thin layer of shotcrete tightly sprayed on rock surface is not subjected noticeable flexure, as its breakage is governed by shear strength which much higher than tensile strength as known well.

Fig. 10.17 shows four cross-sections coming from different sequences of construction.

To assume shotcrete models of unclosed ring and closed ring for stage 1 – 3 and stage 4, respectively, flexure moment and displacement of shotcrete layer were analyzed by FEM. Fig. 10.18 (a) – (d) give the computed results corresponding stage 1 – 4, respectively. Figures on the left and right are the cases for assumed free and fixed conditions at the lower end of shotcrete layer, and half circles on the left and right in each figure show flexure moment and displacement. Unclosed models show unequal distribution of moment, and if tensile strength is not sufficient to load, associated with the excavation, yield or breakage of shotcrete layer must be induced at the feet of unclosed arch of shotcrete. When shotcrete layer is closed as a ring structure at a full section such as Stage 4, flexure moment is almost the same at any point and takes lower value than other stages. Comparing Stage 4 to Stage 1, the magnitude of flexure moment in Stage 4 is 1/10 of Stage 1. This result verifies the principle of NATM.

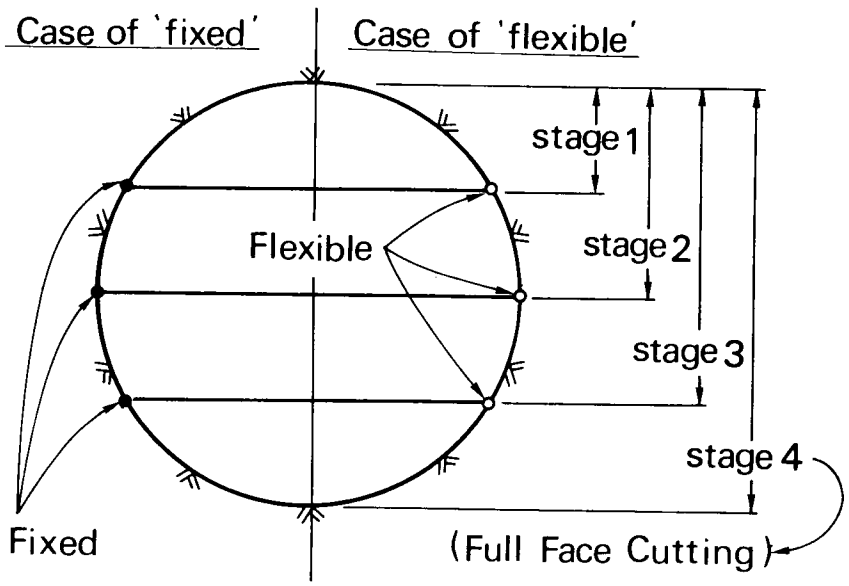

Fig. 10.17 Excavation Stage

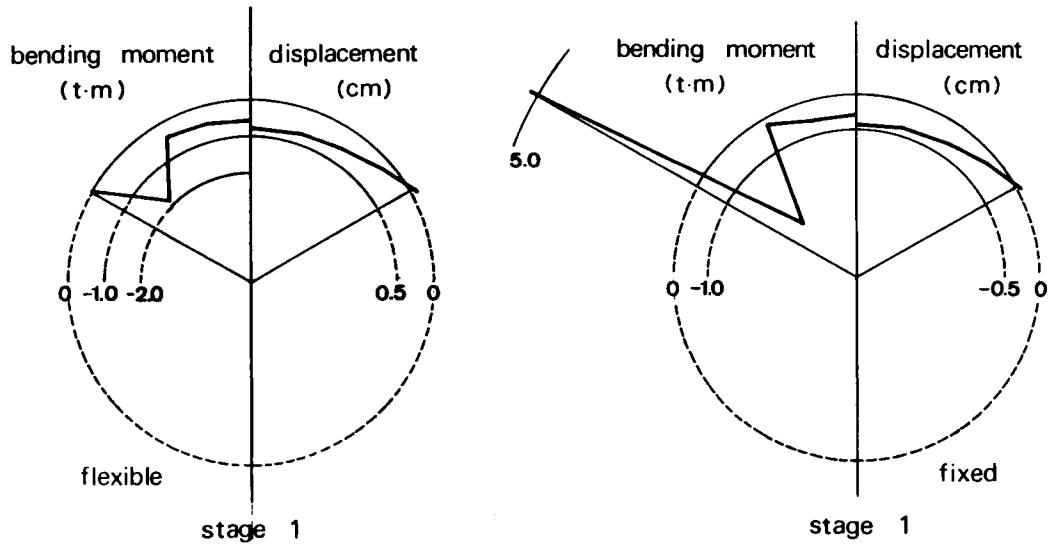

Fig. 10.18 (a) Moment and Displacement for Stage-1

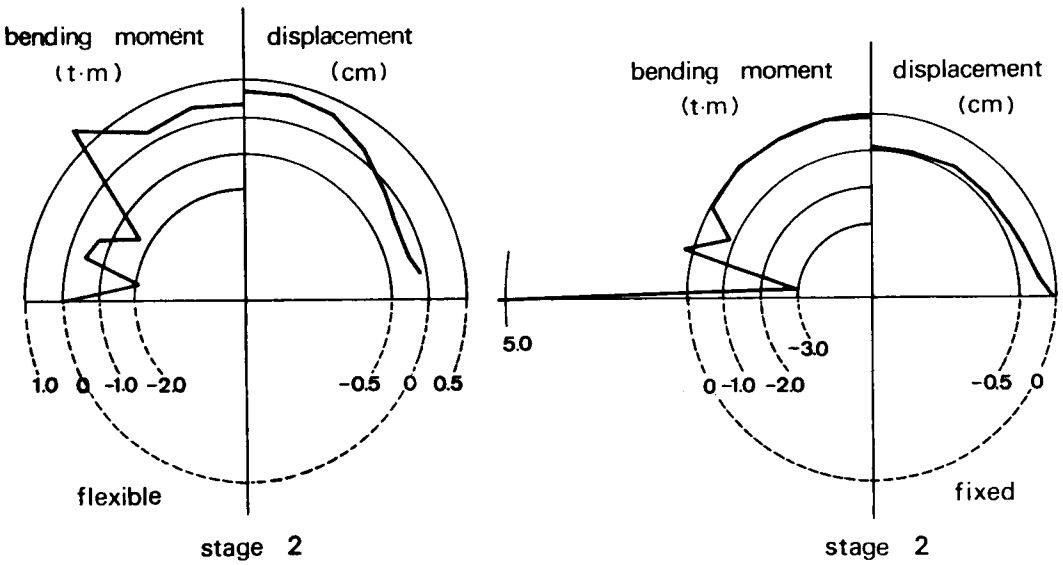

Fig. 10.18 (b) Moment and Displacement for Stage-2

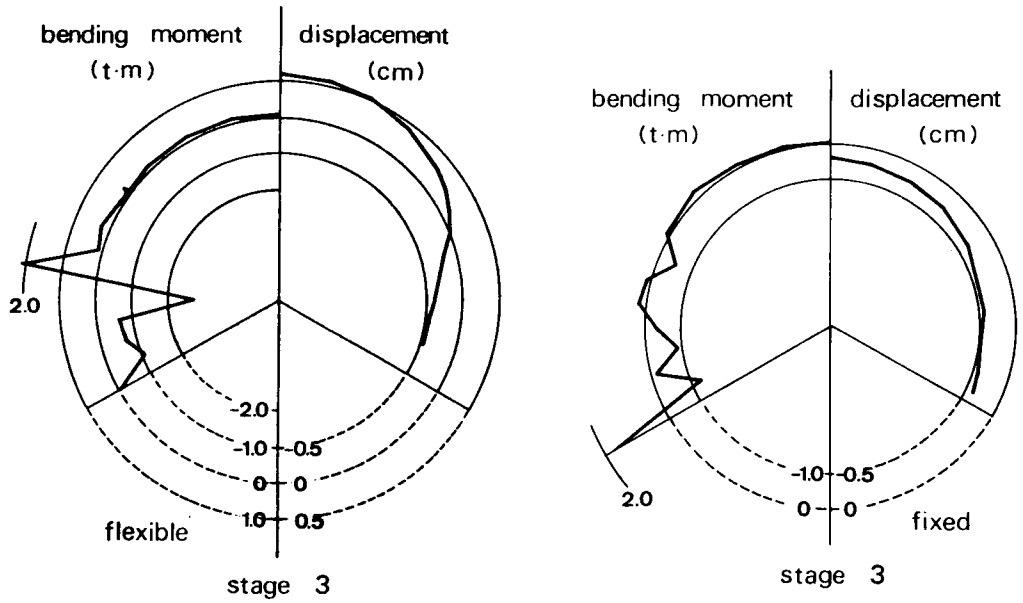

Fig. 10.18 (c) Moment and Displacement for Stage-3

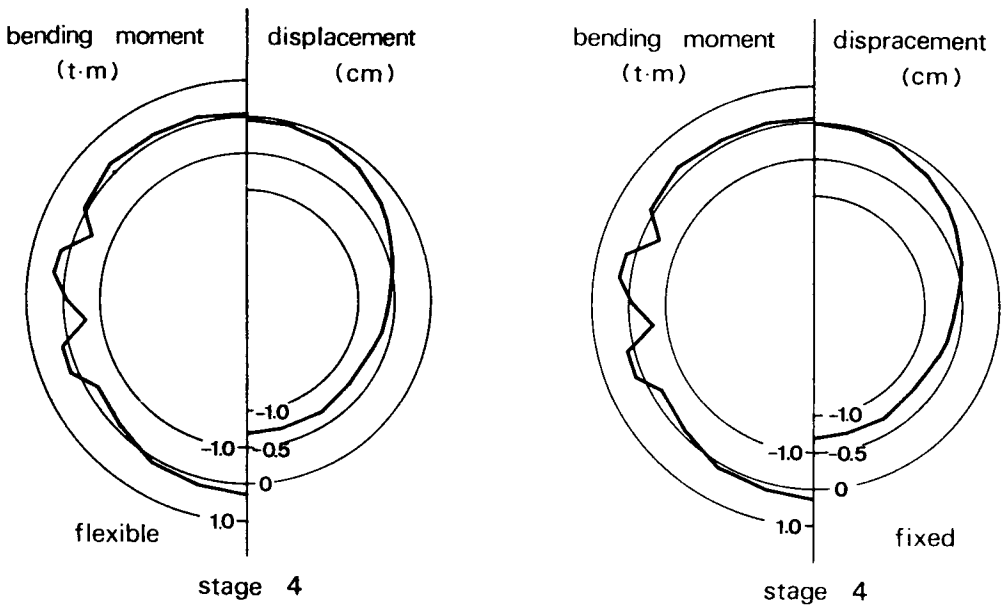

Fig. 10.18 (d) Moment and Displacement for Stage-4

10.6 Conclusion

(1) Shotcrete aims at keeping the adjacent rock blocks in place through the bond to the rock and through its initial shear strength.

(2) Shotcrete helps the rock mass to take care of itself by locking together the immediately adjacent blocks as a reinforcement.

(3) SEC (Sand-enveloped with cement) system give only 10 – 15% rebound, but in other cases rebound is 25 – 35%, and also it was confirmed by laboratory test that the shotcrete has steady strength.

(4) In the calibration of pressure cell, pressure indicated by pressure cell does not always show true value in case of the low stiffness of cell. Mechanically measured cell with high stiffness such as Gloetzl–type one is recommendable.

(5) Ring closure by shotcrete at early stage just after excavation is most essential, and when ring is mobilized adequately, shotcrete layer is subjected to shear force only.

REFERENCES for Chapter 10

[1] Brekke, T.L.: Shotcrete in hard-rock tunnelling, Bulletin of the Association of Engineering Geologists, Vol. IX, No. 3, Summer 1972. pp. 291–264.

[2] Hata, S., Tanimoto, C.: Technical Report, Research on the application of NATM to hard rock, entrusted by Japan National Railways, March 1980. (in Japanese)

[3] Golser, J.: The New Austrian Tunnelling Method (NATM) – Theoretical background and practical experiences, Shotcrete for Ground Support, ACI Publication SP–54, 1977.

[4] Voort, H.B.: Tunnel Instrumentation, Shotcrete for Ground Support, ACI, Publication SP–54, 1977, pp. 718.

[5] Nakano, R.: Geotechnical Properties of Mudstone of Neogene Tertiary in Japan, Proc. Int'l Sympo. on Soil Mechanics, Oaxace, Mexico, Vol. 1, pp. 75–92, 1979.

[6] The Report on the analysis of the expansive behavior of the ground observed through the construction of Akakura Tunnel, Tokyo Office, Japan Railway Construction Authority, 1977. (in Japanese)

[7] Foth, H.O., Turk, L.M.: Fundamentals of Soil Science, 5th Ed. p. 171, John Wiley and Sons, Inc., 1972.

[8] Muirwood, A.M.: Tunnels for road and motorways, The Quarterly J. of Engineering Geology, Vol. 5, No. 1, No. 2, pp. 119–120, 1972.

Chapter 11

CONCLUDING REMARKS

This dissertation has presented the result of investigation on rational design and construction for tunnelling in rock through theoretical analyses, numerical simulations, laboratory tests and field measurements. In this conclusive chapter, the objectives of this study and the main results of foregoing chapters will be reviewed comprehensively to discuss commonly related conclusions with proposals for tunnelling engineers and also in relation to the prospect for future studies to be continued.

It would be the most reasonable way of rational tunnel support designing to drive a tunnel in rock, having many uncertainties, through field measurement or daily monitoring. As the almost mechanical behavior of surrounding rock is reflected to the deformation in the vicinity of mining face, it is essential for practical engineers to understand the relation between resultant deformation and rock properties, and on the other hand, researchers should keep on finding and establishing how to interpret the actual behavior through simplified measurement or monitoring. It should be realized that field measurement is a large scaled experiment and supplies valuable informations. Specially, to speak of the required subject, classification with various quantitative categories as well as well described qualitative evaluation should be pointed out. That is rock mechanics with consideration of discontinuity.

The dissertation have been manuscripted in accordance with the tunnelling procedure from the standing point on construction engineering. So long as engineering is defined by the expression of "Science for Approximation and Economy", theory should not be theory alone. In his research the author have tried to simplify his thinking way as easy as he can. When the mining face is stable at the moment, foregoing effort is only to switch the half-dome action of the face as a temporary support to artificial support such a rockbolts and shotcrete by maintaining bearing capacity of surrounding rock itself.

Conclusions in general regarding **tunnel stability** are as follows:

(1) The mining face plays an important role as a temporary support, due to half-dome action, and when advancing the face, it is necessary to place artificial supports, to substitute for the half-dome action, within a span length from the face, so as to mobilize the bearing capacity of the rock mass as fully as possible.

(2) As the effects of systematic supports are the mobilizing of confining stress and decreasing of shear stress, a procedure to design supports can be proposed, based on the idea of replacing the effects of supports by an inner pressure acting on the surface of the tunnel wall. By employing this inner pressure as the main parameter, it is possible to calculate the width of plastic zone, displacement of the wall and plastic strain near the wall.

(3) Half-dome action of the face is formed within a range of double the length of the span or the height, in the vicinity of the face.

(4) Convergence survey means monitoring the change of radial normal stress or extraction force, as well as the displacement of the wall.

(5) Concerning a tunnel in rock whose competence factor is less than 1.0, it is difficult to evaluate the plastic zone without consideration of strain softening behavior. Equations presented by the author give solutions for stresses, strains and displacements in the case of a circular opening.

(6) The peak of the axial stress distribution in a fully bonded bolt shows the boundary between pick-up length and anchor length of a bolt, and it agrees with the boundary between elastic and plastic zone only when the anchor length is longer than the pick-up length.

(7) Fully bonded bolts, which are placed only into the plastic zone have some effect, but it is required that bolts should be longer than 1.5 times the width of the plastic zone in order to obtain sufficient effect.

(8) The effect of fully bonded bolts, having a length longer than twice the plastic zone, is almost equal to those having twice the length of the plastic zone, and the optimum length of systematic rockbolts is concluded to be 1.5 to 2.0 times the presumed plastic zone.

(9) In field measurement, typical modes of axial force distribution in a fully bonded bolt are classified into five categories. By referring to these modes, it is possible to evaluate the effect of bolting, and to determine a width of plastic zone with some measuring rockbolts having a length longer than twice the width of the presumed plastic zone.

(10) Shotcrete aims at keeping the adjacent rock blocks in place through the bond to the rock and through its initial shear strength.

(11) Shotcrete helps the rock mass to take care of itself by locking together the immediately adjacent blocks as a reinforcement.

(12) SEC (Sand-enveloped with cement) system give only 10 – 15% rebound, but in other cases the rate of rebound is 25 – 35%, and also it was confirmed by the laboratory test that the shotcrete by SEC–System has steady strength.

(13) In the calibration of pressure cell, pressure indicated by pressure cell does not always show true value when a cell has too low stiffness. Mechanically measure cell such as Glötzl-typed one is recommendable.

(14) Ring closure by shotcrete at early stage just after excavation is most essential, and when ring is mobilized adequately, shotcrete layer is subjected to shear force only.

Regarding **blasting**:

(1) Considering the observed changes in the propagation velocity when only a No. 8 cap was detonated at one end of the cylindrical rock specimen, the existence of three regions with different properties for the induced stress wave, plastic, shock and elastic wave zones, was recognized.

(2) According to the obtained attenuation of the stress wave induced in and propagated through the rock specimen, it was concluded that the detonation pressure of a No. 8 cap was about 10 kb and that the attenuation of the stress wave in the rock specimen with increasing distance from the shot point could be expressed by a decreasing exponential function and that its attenuation coefficient was a little different in the three kinds of rock used.

(3) From the observed stress wave shape and the length of the spall created near the free end of the specimen, the dynamic tensile strength of the rock was determined and it was found that the shorter the wave length of the stress pulse induced, the stronger the dynamic tensile strength of the rock, and that the order of the strength in the three rocks used was different from that for static tension.

(4) In order to solve the problems in the actual rock blasting, it seems to be reasonable that 1 – 5 times the strength obtained by the conventional tension test is used for the dynamic tensile strength of the rock. Also, the dynamic compressive strength of rock which was nearly equal to 5 – 7 times the strength obtained by the static conventional compression test, was observed in this experiment.

(5) The peak stress of induced wave shape decreased with increasing distance from shot point, but the attenuation coefficient of the stress wave obtained experimentally was larger than the attenuation coefficient of the stress wave calculated theoretically.

(6) In the stress wave shape obtained experimentally, the behaviour of increasing wave length with the distance from the shot point was recognized, but the theoretical equations used for the stress wave shape was not considered on the increase of the stress wave length.

(7) In the comparison of the actual stress wave, it is considered that the lost stress amplitude of the wave induced in rock was not only due to the energy loss with its propagation, but also due to the increase of the stress wave length. Consequently, in the calculation of the stress induced in the rock, the theory of the elasticity should not be used only, but the theories of the viscosity and the plasticity should be also used, and the exactly theoretical analysis appears to be an interesting problem remaining in future.

(8) The behavior of ground vibration generated by blasting is governed by the following factors: a) distance from the blasted point; b) type of explosive; c) quantity of charge; d) method of initiation; e) drilling pattern; f) tamping condition; g) path of propagation; h) characteristics of ground; and i) state of ground formation.

(9) Differing from earthquake with frequency lower than 10 Hz, blasting generates vibration with the frequency of 30 – 800 Hz. The frequency should be the predominant factor correlated with the magnitude of damages.

(10) In the discussion on the damage of structures and the sensitivity of human body caused by blasting vibration, the particle velocity should be dealt with as the main parameter because the intensity of damage and human sensitivity has the proportional relation with the particle velocity in the case of being subjected to the vibration with frequency over 30 Hz.

(11) For the prediction of blasting vibration, the following propagation equation can be applicable.

$$V = K \cdot L^{2/3} \cdot D^{-2}$$

where V: maximum particle velocity [cm/s],
L: charge weight per delay [kg],
D: distance from blasted point [m],
and K: constant determined by the type of explosive, method of initiation, and geological condition. For example, K=1000 for the case of center cut by initiating gelatine dynamite with instantaneous EB caps.

(12) The raise time of gas pressure induced by explosion correlates much with amplitude of vibration, and this means that explosive with lower detonation velocity generates less vibration. The relative ratios of gelatine dynamite (De), AN–FO (Ao), smokeless powder (Sp) and concrete cracker CCR (Cr) are

De : Ao : Sp : Cr = 1.0 : 0.35 : 0.3 : 0.1

(13) The usage of explosive with higher detonation velocity generates vibration with higher frequency. According to spectrum analyses, the vibration generated by dynamite shows the prominent peaks in the range of 200 – 800 Hz, and others show their prominent peaks on wave records in the range below 300 Hz.

(14) The sensible limit of blasting vibration to human body is considered 0.038 – 0.05 cm/s in particle velocity.

(15) the allowable limit of vibration to buildings can be specified by the particle velocity in the range of 3 – 5 cm/s.

(16) To initiate with the delayed EB–caps reduces the vibration. In general, center cut generates higher vibration than easer cut, and the vibration amplitude in easer cut is 50% – 60% of the amplitude in center cut with Zero-delayed caps. By utilizing the slight scattering of initiation time of delayed EB–caps such as DS–delay caps or MS–delay caps with higher number than MS–4, it is possible to reduce more.

(17) As the duration of the main parts of wave motion showing high peaks is considered as 100 ms approximately, no noticeable superposition of wave motion can happen at the usage of DS–delay cap and MS–delay caps with higher number than MS–4. Consequently, it is verified that the amplitude of vibration can be specified by the quantity of explosive per delay.

(18) Pre-splitting blasting is considered as one of the solutions for reducing vibration to nearby structures and it is necessary to produce considerably wide and thick presplit zone which can cover the whole vicinity of mining face in order to obtain fruitful effect.

(19) In smooth blasting, a decoupled charge is normally used. In this case, the so-called pressure spike which generally appears in the case of the fully coupled charge is considered to disappear by the action of the air gap in the charge hole and the extent of the radial crack caused by

an explosion is decreased with the increase of the degree of decoupling.

(20) Moreover, in smooth blasting the hole space is not so large and the charges loaded in each hole are not initiated quite instantaneously because of the existence of the difference in ignition time between each detonation cap.

(21) Therefore, in many cases, the tangential tensile stresses on the line towards the adjacent hole become larger than those in the other directions because the adjacent holes act as an empty hole to the charge hole.

(22) The crack along the projected plane of breakage may develop much longer than the cracks towards the other directions, and in the case where the hole space is close enough, this crack may reach the adjacent hole.

(23) On the other hand, even in the case where this crack can not reach the adjacent hole, there is a possibility of producing other new cracks from the adjacent hole because of the stress concentration at the two points on this hole which are the closest to and the farthest from the explosion.

(24) Furthermore, as the quasi-static pressure due to the explosion gases in the adjacent hole may act on the hole for a pretty long period of time, the hole must be kept under considerable prestressed conditions.

(25) Thus, in smooth blasting, the cracks along the projected plane of breakage can develop extremely and the quasi-static pressure in the hole acts to force the growth of these cracks and makes them as open ones. The growth of cracks towards the other directions is repressed to a considerable extent by the action of the rarefaction wave from the main crack mentioned above and cracks can not grow as open ones. In this way, a smooth wall along the projected plane of breakage can be procuced finally.